

https://dspace.org/

The Upper Critical and Lower Main Zones of the eastern Bushveld Complex

Seabrook, Charlotte

2006-11-15T12:20:00Z
http://hdl.handle.net/10539/1742

Downloaded from a DSpace repository. https://dspace.org/

The Upper Critical and Lower Main Zones of the eastern Bushveld Complex

By

Charlotte L. Seabrook

Submitted in fulfilment of the requirements for the degree of Doctor of Philosophy,

in the Department of Geosciences, University of the Witwatersrand,

Johannesburg, South Africa

2005

Declaration

I, *Charlotte Louise Seabrook*, hereby state that all work contained in this thesis is the original work of the author, except where specific acknowledgements is made to the work of others. I further declare that no part of this thesis has been, or is concurrently being submitted for a degree or other qualification at any other university or educational institution.

Signed:

Charlotte L. Seabrook

School of Geosciences

University of the Witwatersrand

Johannesburg

April 2005

Acknowledgements

Anglo Platinum, Impala Platinum and Lonplats generously provided financial support for this project. Their contributions and assistance are gratefully acknowledged. Anglo Platinum and Impala Platinum are thanked for allowing access to core and permission to publish.

I am indebted to my supervisor, Prof. R. Grant Cawthorn for all the help he has given me over the years, particularly his patience in reviewing early chapters. My most sincere thanks also go to Dr Paul Nex and Prof. Judith Kinnaird who have given me unfailing support, advice and discussion throughout. Prof. Johan Kruger is thanked for his extensive assistance and discussions on the Sr isotope work and many other aspects of this project. Sharon Turner is gratefully acknowledged for her perseverance in dealing with all my XRF samples. Many thanks also to Trevor Richardson for his assistance in obtaining samples. C. Harris and J. R. Wilson are thanked for their constructive reviews.

Abstract

This project focuses on the Upper Critical and Lower Main Zones in the eastern Bushveld Complex, South Africa. Lithological and stratigraphic information show that there are distinct differences at this level between the eastern and western limbs of the complex. Geochemical studies are centred on the Merensky and Bastard Cyclic Units in which the platiniferous Merensky Reef occurs.

A major geochemical hiatus occurs in the Bushveld Complex at the level of the platiniferous Merensky Reef, close to the Critical/Main Zone boundary. The origin of this hiatus and its relation to mineralisation has not been fully resolved. Geochemical parameters are investigated that allow minerals in the Merensky and Bastard Cyclic Units to be classified as originating from either Critical or Main Zone magmas. Modelling of element ratios (Ni/Y, Cr/Ni, Cr/Co, Y/Co, Cr/V, Co/V and Cr/MgO) demonstrates the varying reliability of using ratios as geochemcial tools to constrain magma influxes within a chamber. However, it is shown that the Cr/MgO ratio is effective in determining real differences across the Critical/Main Zone boundary that are independent of lithology. In addition, initial Sr isotope ratios for plagioclase are significantly different in Critical and Main Zone rocks. Geochemical data through the Merensky and Bastard Cyclic Units indicate that orthopyroxene that originated from magma with composition like that of the Critical Zone magma sometimes occurs together with plagioclase that originated from Main Zone magma. In detail, in the pyroxenite at the base of the Merensky Unit, both plagioclase and orthopyroxene display Critical Zone signatures, but in the overlying part of the Merensky Cyclic Unit, plagioclase increasingly shows a Main Zone signature, whereas orthopyroxene continues to display a Critical Zone signature. Similarly, in the Bastard pyroxenite, Sr isotopes and absolute Sr in plagioclase display a range of values from Main Zone to Critical Zone, but orthopyroxene consistently displays Critical Zone affinity. These observations of mineral disequilibrium clearly show that the two major minerals in the Merensky and Bastard Cyclic Units were formed from two different, but coexisting, magmas. A model that accounts for this disequilibrium is proposed here. It invokes the influx of Main Zone magma at the level of the base of the Merensky unit that dispalced the Critical Zone magma upward, but the two magmas did not mix. The latter continued to crystallise orthopyroxene which sank through the Main Zone influx, due to its density contrast. These crystals collected on the crystal pile to form the Merensky pyroxenite. The Main Zone magma, into which the cumulus Critical Zone orthopyroxene accumulated, crystallised interstitial plagioclase that had a Main Zone Sr isotopic ratio.

Whole-rock, major element geochemical data show that a variable proportion of the plagioclase in both the Merensky and Bastard pyroxenites is cumulus. It is inferred to have accumulated with orthopyroxene and has a Critical Zone initial Sr isotope ratio. Thus the two pyroxenites now yield a mixed Sr isotopic signature of Critical Zone cumulus and Main Zone intercumulus and possibly cumulus plagioclase that varies along strike. Above the two pyroxenites, the Sr signature of the norites and anorthosites of both cyclic units is dominated by cumulus plagioclase from the Main Zone magma. It is concluded that the variations in initial Sr isotope ratios do not result from mixing of magmas, but result from accumulation of orthopyroxene and plagioclase from a higher, isotopically distinct layer of magma into an underlying layer. The Merensky and Bastard Cyclic Units therefore display features of Critical or Main Zone magma characteristics depending upon which chemical parameter is considered. These cycles are therefore classified as a Transitional Unit.

Contents

		PAGE NUMBER
Chapter 1 - Introduction		1
1.1	The Marginal and Lower Zones	4
1.2	The Critical Zone	4
1.3	The Main Zone	5
1.4	The Upper Zone	5
1.5	Mineralisation	5
1.6	Potholes	6
1.7	Replacement pegmatoids	7
1.8	The eastern Bushveld Complex	7
1.9	The subdivisions of the eastern limb	9
	1.9.1 The southern sector	10
	1.9.2 The central sector	10
	1.9.3 The western sector	11
1.10	Terminology	11
	1.10.1 Rock type classification	11
	1.10.2 Zones and their boundaries	12
1.11	The extent and aims of the project	13
Chapter 2 - The stratigraphic succession of the sampled cores		14
2.1	Richmond (RM15)	16
2.2	Kennedy's Vale (KV5854)	20
2.3	Eerste Geluk (EG5)	22
2.4	Klipfontein (KF35)	25
2.5	Summary	26

Chapter 3 -
Stratigraphic comparisons across the Bushveld Complex 28

3.1 North and south of the Steelpoort lineament 28
3.1.1 The Upper Critical Zone 30
3.1.2 The Lower Main Zone 33
3.2 Comparisons between the eastern and western limbs 35
3.2.1 The Upper Critical Zone 35
3.2.2 The Giant Mottled Anorthosite 38
3.2.3 The Lower Main Zone 41
3.3 Summary and implications of lithological variations 43

Chapter 4 - Petrology 47

4.1 Nomenclature 47
4.2 Anorthosite 49
4.3 Norite 51
4.4 Feldspathic pyroxenite 52
4.5 Chromitites and chromite 53
4.6 Recrystallisation processes 53

Chapter 5 - Geochemistry 55

5.1 Whole-rock chemistry 58
5.1.1 Major element variations 58
5.1.2 Trace element variations 64
5.2 Orthopyroxene mineral separates 69
5.3 Plagioclase mineral separates 75
5.4 Strontium isotopes 82
5.5 Sulphide concentration in the Merensky Reef 88

Chapter 6 - Some geochemical investigation techniques 91

6.1 Element ratio modelling in the Upper Critical and Main Zones 91
6.1.1 Trace element ratios 91
6.1.2 Cr/MgO ratios in orthopyroxene and whole-rock 97
6.2 Cumulus an intercumulus minerals 99
6.2.1 Trapped liquid estimation 100
6.2.2 Testing the reliability of incompatible elements 100
6.2.3 Estimating cumulus plagioclase content in the Merensky and Bastard pyroxenites 105
6.3 Sr isotopes and their application to layered intrusions 109
6.3.1 Background information 109
6.3.2 Crustal contamination 110
6.3.3 Magma mixing 112

Chapter 7 - The Critical / Main Zone boundary 115

7.1 The placing of boundaries 115
7.2 The Critical/Main Zone transition 116
7.3 The boundary based on the appearance of clinopyroxene 118
7.4 Chemical criteria to define the Critical and Main Zones 121
7.4.1 Initial Sr isotope ratios 121
7.4.2 Sr and An# in plagioclase 122
7.4.3 MgO and Cr in orthopyroxene 126
7.4.4 Cr/MgO in whole-rock 129
7.5 The nature of the Critical and Main Zone magmas 132
7.5.1 Temperature and density of Critical and Main Zone magmas 133
7.6 The Merensky and Bastard cyclic units in light of new information of the Critical and Main Zone magmas 134
7.7 Fractionation in the Critical Zone 138
7.8 Implications for the positioning of the boundary 139

Chapter 8 –
The origin of the Merensky and Bastard cyclic units 141

8.1 A model for the formation of the Merensky and Bastard cyclic units 140
8.2 Processes within the magma chamber 147
8.2.1 Sinking crystals 147
8.2.2 Intermittent sinking of plagioclase 151
8.2.3 The mechanics of layering 152
8.2.4 The thickness of the Critical and Main Zone magmas 155
8.3 Comparison with other models 156
8.3.1 Magma mixing 156
8.3.2 Repeated magma injection 157
8.3.3 Temperature and density considerations of the injected magma 158
8.3.4 Mineral disequilibrium 159
8.3.5 Crystal settling 160
8.3.6 Plagioclase suspension 162
8.3.7 Fluids 165
8.4 Variations between profiles 166
8.5 Summary 167

Chapter 9 - The origin of PGE in the Merensky Reef 168

9.1 PGE concentration in an immiscible sulphide liquid 168
9.1.1 The partitioning of PGE and the Merensky Reef 168
9.1.2 Sulphur-saturation models 170
9.1.3 S, Ni and Cu in the Merensky Reef at Richmond and Kennedy's Vale 171
9.2 PGE concentration by fluids 177
9.3 PGE as discrete grains 181
9.4 The source of the PGE 182
9.5 The crystal settling model and its implications for PGE mineralisation 184

Chapter 10 - Summary and conclusions 190

10.1 Stratigraphic variations 190
10.2 Geochemical investigations 190
10.3 Mineral disequilibrium and the formation of the Merensky and Bastard cyclic units 192

References 194

Appendices I - VII 212

List of Figures

		PAGE NUMBER
1.1	Map of the Bushveld Complex	2
1.2	Stratigraphic column of the Bushveld Complex	3
1.3	Locations of farms in the central sector of the eastern Bushveld Complex	8
1.4	Locations of farms in the southern sector of the eastern Bushveld Complex	9
2.1	Stratigraphic logs of the four studied cores, from Richmond, Kennedy's Vale, Eerste Geluk and Klipfontein	15
3.1	Stratigraphic cores of logs in the eastern Bushveld	29
3.2	Section through the eastern Bushveld, demonstrating changes in thickness of the UG2 – Merensky Reef unit	32
3.3	Stratigraphic comparison of the Main Zone in eastern Bushveld cores	34
3.4	Correlation of cores in the western Bushveld Complex	37
3.5	Stratigraphic comparison of the GMA between the eastern and western Bushveld.	40
3.6	Schematic diagram showing A) the Steelpoort lineament acting as a barrier to magma flow, B) the merging of the UG3 with the UG2, the thinning of the UG2 – Merensky package and the Merensky Reef over the Steelpoort lineament	45
4.1	Graph of whole-rock Al_2O_3 plotted against MgO showing modal ranges for rock types in this study	48
4.2	Photomicrographs of (a) poikilitic orthopyroxene (b) typical norite, (c) orthopyroxene enclosing a small, equant plagioclase grain in pyroxenite, (d) Plagioclase-filled embayment in orthopyroxene in norite, (e) pyroxenite, (f) chromite grains.	50
5.1	Graph showing extent of variation of Cr_2O_3 content in single orthopyroxene grains	56
5.2	Harker diagrams of major element oxides plotted against MgO for RM15 whole-rock samples	60

5.3	Harker diagrams of major element oxides plotted against MgO for KV5854 whole-rock samples	61
5.4	Harker diagrams of major element oxides plotted against MgO for EG5 whole-rock samples	62
5.5	Harker diagrams of major element oxides plotted against MgO for KF35 whole-rock samples	63
5.6	Trace elements plotted against height for RM15 whole-rock samples	64
5.7	Trace elements plotted against height for KV5854 whole-rock samples	66
5.8	Trace elements plotted against height for EG5 whole-rock samples	67
5.9	Trace elements plotted against height for KF35 whole-rock samples	68
5.10	Mg# in orthopyroxene plotted against height for (a) Richmond, (b) Kennedy's Vale, (c) Eerste Geluk and (d) Klipfontein	70
5.11	Trace elements plotted against height for RM15 orthopyroxene separates	71
5.12	Trace elements plotted against height for KV5854 orthopyroxene separates	72
5.13	Trace elements plotted against height for EG5 orthopyroxene separates	73
5.14	Trace elements plotted against height for KF35 orthopyroxene separates	74
5.15	An# in plagioclase plotted against height for (a) Richmond, (b) Kennedy's Vale, (c) Eerste Geluk and (d) Klipfontein	76
5.16	Trace elements plotted against height for RM15 plagioclase separates	77
5.17	Trace elements plotted against height for KV5854 plagioclase separates	78
5.18	Trace elements plotted against height for EG5 plagioclase separates	79
5.19	Trace elements plotted against height for KF35 plagioclase separates	80
5.20	Plots of Mg# versus An# for KV5854, EG5, RM15 and KF35	81
5.21	Sr isotope initial ratios plotted against height for (a) RM15 and (b) KF35	85

5.22	Sr isotopes plotted against height in the Merensky and Bastard cyclic units for (a) RM15 and (b) KF35	87
5.22	S, Cu and Ni plotted against stratigraphic height through the Merensky interval for (a) RM15 and (b) KF35	89
5.23	Cu vs. S in RM15 showing the positive correlation between these two elements	90
6.1	Calculated trace element ratios with varying trapped liquid proportions, based on Main Zone and Critical Zone parental magmas	94
6.2	Calculated absolute Cr and V composition compared with observed Cr and V by Eales *et al.* (1986) and calculated Cr/V ratios for Main Zone and Critical Zone rocks	96
6.3	Plot of Cr against MgO, from Cawthorn (1999b), showing the positive linear relationship between these two elements in orthopyroxene	97
6.4	Calculated Cr/MgO in orthopyroxene at varying MgO content at 10% and 20% trapped liquid content, showing that the Cr/MgO remains constant with variations in lithology	99
6.5	Whole-rock P_2O_5 (a), K_2O (b) and Zr (c) in core RM15 plotted against height. These graphs show that there is little correlation between these elements	102
6.6	Whole-rock P_2O_5 (a) and Zr (b) plotted against K_2O and Zr plotted against P_2O_5 (c) for core RM15, showing little correlation	103
6.7	Diagram of whole-rock Al_2O_3 plotted against MgO and compositions of plagioclase and orthopyroxene mineral separates showing the proportion of cumulus plagioclase present in the Merensky and Bastard pyroxenites	106
6.8	Proportion of cumulus plagioclase plotted against Zr ppm showing slightly higher incompatible element content where the proportion of cumulus plagioclase has been determined as low	107
6.9	Diagram of a) whole-rock Al_2O_3 against MgO showing estimated proportions of trapped liquid in the Merensky and Bastard pyroxenites and b) trapped liquid % against Zr ppm for those samples	108
6.10	Sr isotopes, Sr, Rb and K_2O plotted against height for cores (a) RM15 and (b) KF35	111

6.11	Rb in plagioclase plotted against Sr isotope ratios for RM15	111
6.12	$^{87}Sr/^{86}Sr$ initial ratios plotted against stratigraphic height for different profiles discussed in the text	113
7.1	Diagram of whole-rock Al_2O_3 plotted against CaO and compositions of plagioclase and orthopyroxene mineral separates	120
7.2	Sr content of plagioclase (a) and An# of plagioclase (b) plotted against height for cores RM15, KV5854, EG5 and KF35	123
7.3	Plot of whole-rock Sr vs. MgO for RM15 (a) and KF35 (b)	124
7.4	Plot of Sr isotope initial ratio vs. $1/^{86}Sr$ in plagioclase for RM15 (a) and KF35 (b)	125
7.5	Cr content of orthopyroxene (a) and Mg# of orthopyroxene (b) plotted against height for cores RM15, KV5854, EG5 and KF35.	127
7.6	Cr/MgO in orthopyroxene plotted against height for cores RM15 (a), KV5854 (b), EG5 (c) and KF35 (d)	128
7.7	Whole-rock Cr/MgO plotted against height for cores RM15 (a), KV5854 (b), EG5 (c) and KF35 (d), indicating similar variations to those observed in Cr/MgO in orthopyroxene	129
7.8	Cr/MgO values plotted against stratigraphic height for the different profiles discussed in the text	131
7.9	Comparison between Sr isotopes and Sr content of plagioclase and Cr/MgO in orthopyroxene for (a) RM15 and (b) KF53.	136
8.1	Schematic diagrams illustrating the development of the Merensky and Bastard cyclic units	143
8.2	Graph of Sr isotope initial ratio plotted against Sr in plagioclase, showing mixing of plagioclase grains	148
8.3	Schematic representation of potholing in the Merensky Reef that may contribute to the remobilisation of plagioclase-rich footwall.	163
9.1	Plot of whole-rock MgO *versus* Ni, showing positive correlation and Ni/MgO ratio of approximately 23	172
9.2	Plot of Ni/MgO in orthopyroxene plotted against height.	173
9.3	Ternary diagram of Cu, Ni and S ratios of sulphide-rich samples from the Merensky Reef at Richmond	175

9.4 a) S and Zr plotted against stratigraphic height, and b) S, Zr, Y, V and TiO_2 plotted against stratigraphic height through the Merensky Reef 180

9.5 a) PGE content plotted against height and b) PGE content plotted against Cu for core and two deflections in RM15 186

List of Tables

		PAGE NUMBER
3.1	Thickness of units in the central and southern sectors of the eastern Bushveld Complex	31
3.2	Thicknesses of units in the western Bushveld Complex	38
4.1	Modal proportions of plagioclase and orthopyroxene and corresponding MgO and Al_2O_3 content	48
5.1	Average probe and XRF separates data from the Merensky and Bastard pyroxenites, showing that the two methods give comparable results.	57
5.2	Isotope data from plagioclase separates in core RM15	83
5.3	Isotope data from plagioclase separates in core KF35	84
6.1	Determination of trace element compositions of Critical and Main Zone magmas	93
6.2	Determination of liquid composition for Critical and Main Zone magmas based on the composition of orthopyroxene in this study	98
6.3	Repeat analyses of K_2O wt% and P_2O_5 wt%	101
6.4	Estimations of trapped liquid content based on parental magmas and the composition of rocks in this study.	103
7.1	Summary of geochemical parameters that can be used to distinguish between minerals that originated from Critical and Main Zone magmas.	132
7.2	Composition, temperature and density of Main Zone and Critical Zone magmas.	134
7.3	Summary of mineral affinities to Critical or Main Zone magma within the Merensky and Bastard cyclic units, for numerous locations around the Bushveld Complex.	137

Chapter 1

Introduction

The Bushveld Complex is an igneous intrusion that covers nearly 70,000 km^2 in the Republic of South Africa (Figure 1.1) and is by far the largest intrusion of this type on Earth. Similar layers crop out for more than 100 km in each of two separate arcs within the ultramafic and mafic layered sequence of the Rustenburg Layered Suite (RLS). This sequence transgressively intruded the epicrustal felsic lavas of the Rooiberg Group and sedimentary rocks of the Transvaal Supergroup (Eales & Cawthorn 1996). The latter consists of a 12 km thick succession of clastic and chemical sediments, deposited in the Transvaal Basin. The term "Bushveld Complex" will be used for the mafic layered rocks, as this is the terms most widely in use. The Bushveld Complex varies between 7000 and 9000 m in thickness and outcrops in five main localities, which are known as the western, eastern, far-western, southern and northern/Potgietersrus limbs. Gravity data support a model where the mafic rocks are continuous at depth, beneath the felsic cover in the centre (Cawthorn *et al.* 1998) and that the Moho is also depressed and the crust thickened (Wright *et al.* 2003). The age of the Bushveld Complex is considered to be around 2.05 Ga (2061 ± 27 Ma, Walraven *et al.* 1990, 2058.9 ± 0.8 Ma, Buick *et al.* 2001), with the whole complex being intruded in a relatively short period of time (<75000 years) (Cawthorn & Walraven 1998). Generally, the layers dip inwards, towards the centre of the intrusion, but it has been proposed that layers were near horizontal at the time of their formation (Gough & van Niekerk 1959 and Kruger *in press*), which has been interpreted to indicate that the whole intrusion is a lobate, interconnected, wide and shallow, sill-like intrusion.

The Bushveld Complex has been stratigraphically subdivided into a number of zones, based on lithological and geochemical parameters. These are Marginal, Lower, Critical, Main and Upper Zones (Hall 1932). A late plutonic phase [2054 ± 2 Ma, Hattingh & Walraven (1993)], represented by the Bushveld Granites (Lebowa Granite Suite), occurred after intrusion of the Bushveld Complex. A stratigraphic column of the Bushveld Complex is given in Figure 1.2. Floor rocks to the complex are the mainly sedimentary Palaeoproterozoic Transvaal Supergroup and precursor Rooiberg Group

volcanics. The complex is overlain by the granites of the Lebowa Granite Suite and remnants of Transvaal/Rooiberg successions.

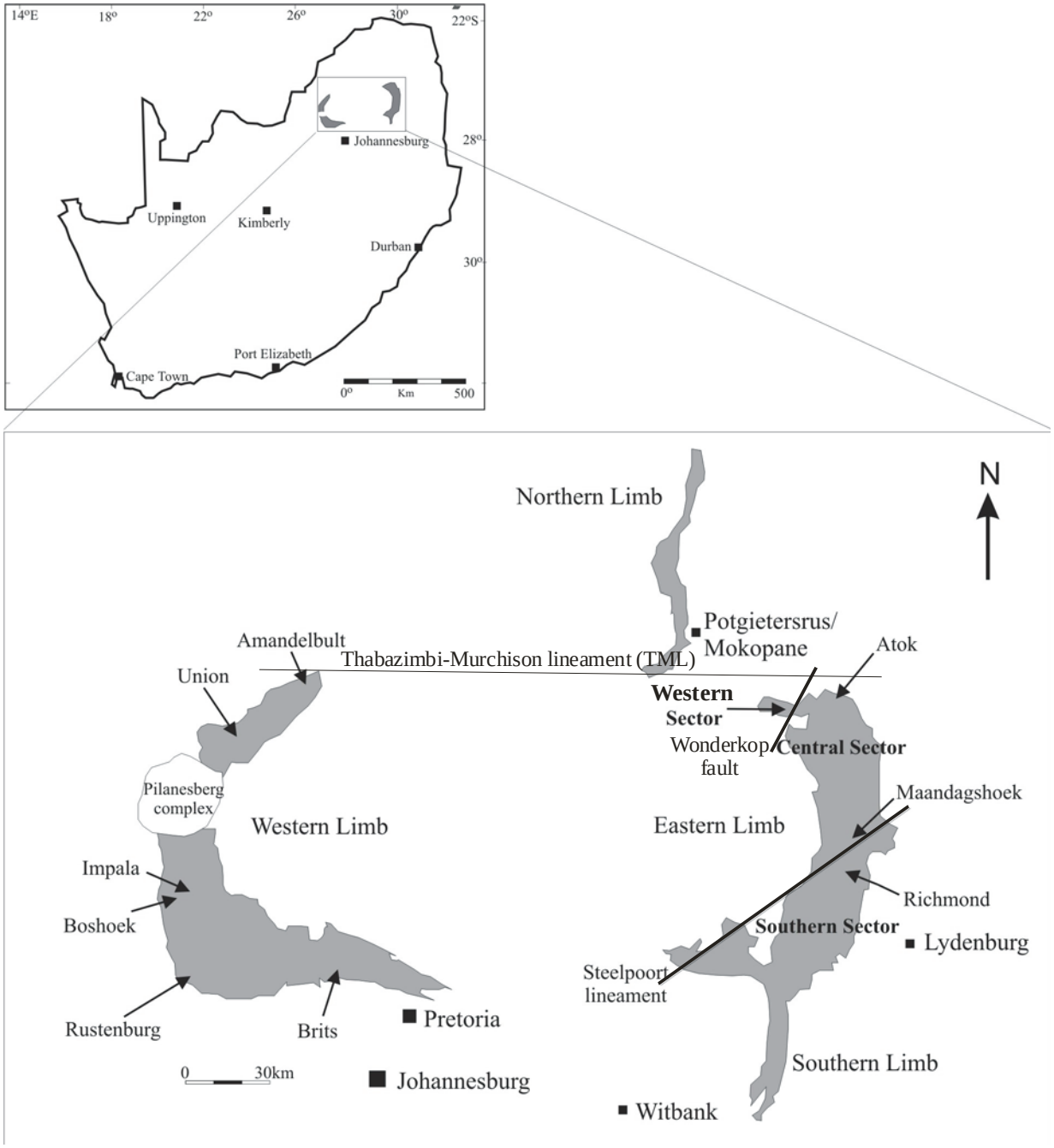


FIGURE 1.1 Map of the Bushveld Complex in South Africa showing the four main limbs and location of the study areas and other areas discussed in the text

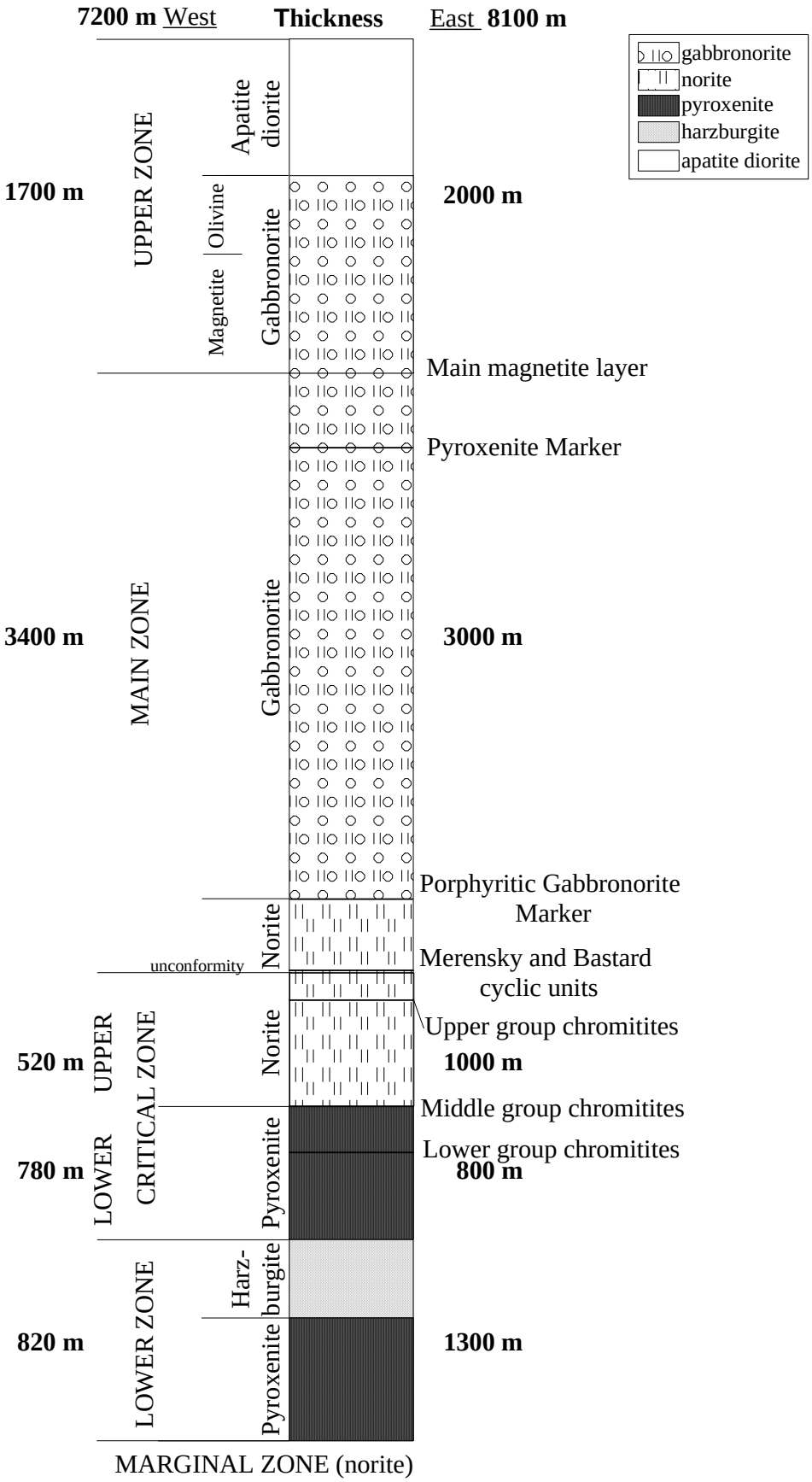


FIGURE 1.2 Stratigraphic column of the Bushveld Complex, showing comparative thicknesses of the eastern and western limbs (based on Eales & Cawthorn 1996).

1.1 The Marginal and Lower Zones

The Marginal Zone is between 100-250 m thick and comprises interlayered fine-grained norites, pyroxenites and olivine-rich cumulates that intrude the Pretoria Group (Harmer & Sharpe 1985). These rocks are intruded by numerous sills (Sharpe 1981) and show evidence of crustal assimilation (Cawthorn & Walraven 1998). Early interpretations suggested that the norites represent the parental magma of the complex, but cumulus textures and igneous layering contradict this (Eales & Cawthorn 1996).

The Lower Zone is largely ultramafic and consists of a sequence of pyroxenites, harzburgites and dunites with minor norites. The layering occurs on varying scales, from <1 m to hundreds of meters, through out the 1600 m thick zone. Teigler & Eales (1996) described the type section for Lower Zone in the western Bushveld. Cameron (1978) described this sequence in the eastern limb.

1.2 The Critical Zone

The Critical Zone is between 900 and 1500 m thick and includes all of the intensively mined chromitite horizons that have been subdivided into Lower Group (LG), Middle Group (MG) and Upper Group (UG) chromitites (Hatton & von Gruenewaldt 1987). Of the seven LG chromitites, the LG6 is the most prominent and consistent layer. The Lower Critical Zone rocks are dominantly pyroxenite and harzburgite, whereas the Upper Critical Zone comprises mainly norite, pyroxenite and anorthosite (Eales & Cawthorn 1996). The boundary between the Lower and Upper Critical Zones is set by the first appearance of cumulus plagioclase (Cameron 1980, 1982, Cawthorn & Walraven 1998). The Critical Zone can be further subdivided by defining cyclic units based on the underlying chromitite, e.g. the UG1 Cyclic Unit, consisting of chromitite, pyroxenite, norite and anorthosite. The Merensky and Bastard Units are the uppermost cyclic units and the former hosts the Merensky Reef, which contains significant platinum-group element (PGE) mineralisation. However, there is some discussion as to whether the Merensky and Bastard Cyclic Units should be considered part of the Critical Zone or the Main Zone and this aspect will be discussed in detail later.

1.3 The Main Zone

This zone can be up to 4400 m thick and consists of anorthosites, norites, gabbronorites and minor pyroxenites. There is a noticeable absence of chromite and olivine through the sequence. The first appearance of cumulus clinopyroxene occurs within the Lower Main Zone at the Porphyritic Gabbronorite Marker that comprises distinctly coarse-grained clinopyroxene, approximately 200-400 m above the Merensky pyroxenite (Figure 1.2). The Main Zone has been subdivided into various units (von Gruenewaldt 1973, SACS 1980, Mitchell 1990 and Nex *et al.* 1998), largely defined by marker horizons such as the Pyroxenite Marker and the Main magnetite layer. These divisions will be discussed in greater detail in section 3.1. The Main Zone forms characteristic "pyramid hills" in both the western and eastern Bushveld. These features are the result of a resistant textural relationship, where primary pigeonite underwent inversion to orthopyroxene during slow cooling and annealed into large poikioblastic grains and produced a mechanically strong cement.

1.4 The Upper Zone

The Upper Zone is about 2000 m thick and comprises gabbros, gabbronorites, norites, anorthosites and ferrodiorites, with the proportion of orthopyroxene decreasing upwards in the sequence. It hosts the economically important magnetitite layers, all of which are vanadiferous. The Upper Zone has been divided into four subzones by Molyneaux (1970) and von Gruenewaldt (1973). The basal subzone A is marked the first appearance of magnetite, subzone B refers to the olivine-free lithologies above the main magnetite layer, the base of subzone C is marked by the reappearance of cumulus olivine and subzone D by the appearance of cumulus apatite.

1.5 Mineralisation

The Bushveld Complex hosts more the half of the world's PGEs (Cawthorn 1999a). The Merensky Reef and UG2 chromitite contain the highest concentrations, up to 10 g/t, although all the chromitite layers contain some PGE. The Merensky Reef generally refers to the mineralised section, centred on a feldspathic pyroxenite that is laterally consistent throughout much of the complex, although its thickness can vary from a few centimetres to 4 m (Lee 1996). The mineralised section frequently

includes some of the footwall and hangingwall to the pyroxenite. The base of the Merensky Cyclic Unit, comprises a thin basal chromitite typically 1-20 mm thick (Vermaak, 1976), overlain by pyroxenite, norite and anorthosite. Commonly, a pegmatitic feldspathic pyroxenite occurs within the Merensky Reef (Leeb-du Toit 1986, Viljoen *et al.* 1986a, 1986b, Viljoen & Hieber 1986) and in some localities in the western Bushveld the entire pyroxenite is pegmatoidal (Vermaak 1976). The Merensky Reef typically contains some 3% base metal sulphides with associated platinum-group minerals (PGM) and mineralisation frequently extends into the hangingwall and footwall rocks, particularly in thinner reef variants (Kinloch 1982). An unconformity occurs at the base of the Merensky pyroxenite, characterised by potholes. Overlying the Merensky Cyclic Unit is the Bastard pyroxenite, so called because it does not contain economic amounts of PGE.

The Platreef is a PGE mineralised zone that occurs in the northern limb of the Bushveld Complex (White 1994). It varies in thickness from several meters to over 150 m (Cawthorn *et al.* 2002b). Here, the Critical Zone is not developed and Main Zone gabbronorites onlap onto sedimentary or granitic floor rocks. The Platreef occurs at the contact (Lee 1996), along some 35 km of strike (Cawthorn *et al.* 2002b). The host lithology is generally a coarse-grained feldspathic pyroxenite and has been considered to represent the lateral continuation of the Merensky Reef (Lee 1996), although this remains in dispute.

1.6 Potholes

Potholes are features in which one layer of the Bushveld Complex transgresses its footwall and forms a basin-shaped depression (Balhaus 1988, Carr *et al*. 1994, 1999, Lomberg *et al.* 1999). Potholing is common in the Merensky pyroxenite and UG2 and occurs on varying scales, from large regional potholes (hundreds of meters across), to small circular areas of less than 10m in diameter. The Merensky pyroxenite plunges into the depressions, frequently lining the sides and creating anomalously thick, irregular reef along the base. Potholes transgress Merensky footwall and are often seen to terminate in a specific melanoritic layer. These features can frequently disrupt mining.

1.7 Replacement pegmatites

Replacement pegmatites are Fe or Mg-rich pyroxenite bodies or pipe-like features and are common within the Bushveld Complex. The largest is 1.5 km in diameter (Eales & Cawthorn 1996). Viljoen & Scoon (1985) classified them in three groups: Iron-rich pegmatite, non-platiniferous magnesian dunite and platiniferous ultramafic pipes, and a fourth group for other types such as orthopyroxenite pegmatite, anorthosite and granite pegmatite. There are only three economic Pt-bearing pipes, where the Pt generally occurred in a central Fe-rich core within a magnesian dunite, but these have been largely mined out.

1.8 The eastern Bushveld Complex

The Critical/Main Zone boundary interval of the eastern Bushveld is of primary interest in this study. Little work has been done on the uppermost Critical Zone and Lower Main Zone in the eastern Bushveld in comparison with the well-documented western limb, although the Lower, Main and Upper Zones are better described in the east. However, a great deal of exploration, of predominantly the UG2, is currently being undertaken in the area, which is dotted with adits that were initially put in by Hans Merensky soon after the discovery of the Merensky Reef. Wagner (1929) documented these exposures of the reef at outcrop. Cameron (1963) described the structure and rock sequences of the eastern Bushveld Complex. In 1964 he documented a large section of the same region, including a description of the Critical Zone, based on mapping observations, from Winterveld farm, across the Steelpoort lineament (Figure 1.1) to Grootboom and south through Tweefontein, Dwars River and Thorncliffe (Figures 1.3 and 1.4). This description is mainly documentation of the occurrence and distribution of the chromitite layers where they outcrop in the Critical Zone. Cousins (1964a) provided a more detailed stratigraphic succession, using data from three boreholes that were drilled on Helena and Thorncliffe between 1959 and 1961, including the MG and LG chromitite seams as well as the UG chromitites. He also describes the Merensky Reef on Thorncliffe and went on to compare the chromitite layers of the eastern and western Bushveld. Cameron (1980) described Lower Critical Zone chromitite deposits in the central sector of the eastern Bushveld. Cameron (1982) undertook mapping of the Upper Critical Zone on numerous farms including Jagdlust, Winterveld and Hendriksplaats. Gain (1985) described the

UG1, 2 and 3 Cyclic Units on Maandagshoek and Mossom (1986) described the Upper Critical Zone at Atok platinum mine, detailing the UG chromitites and the Merensky and Bastard Cyclic Units. Lee & Tredoux (1986) investigated PGE in the Lower and Lower Critical Zones on Clapham. Hatton & von Gruenewaldt (1987) described and discussed the origin of chromitite layers on Doornvlei, Jagdlust, Clapham, Winterveld and Tweefontein in the eastern Bushveld.

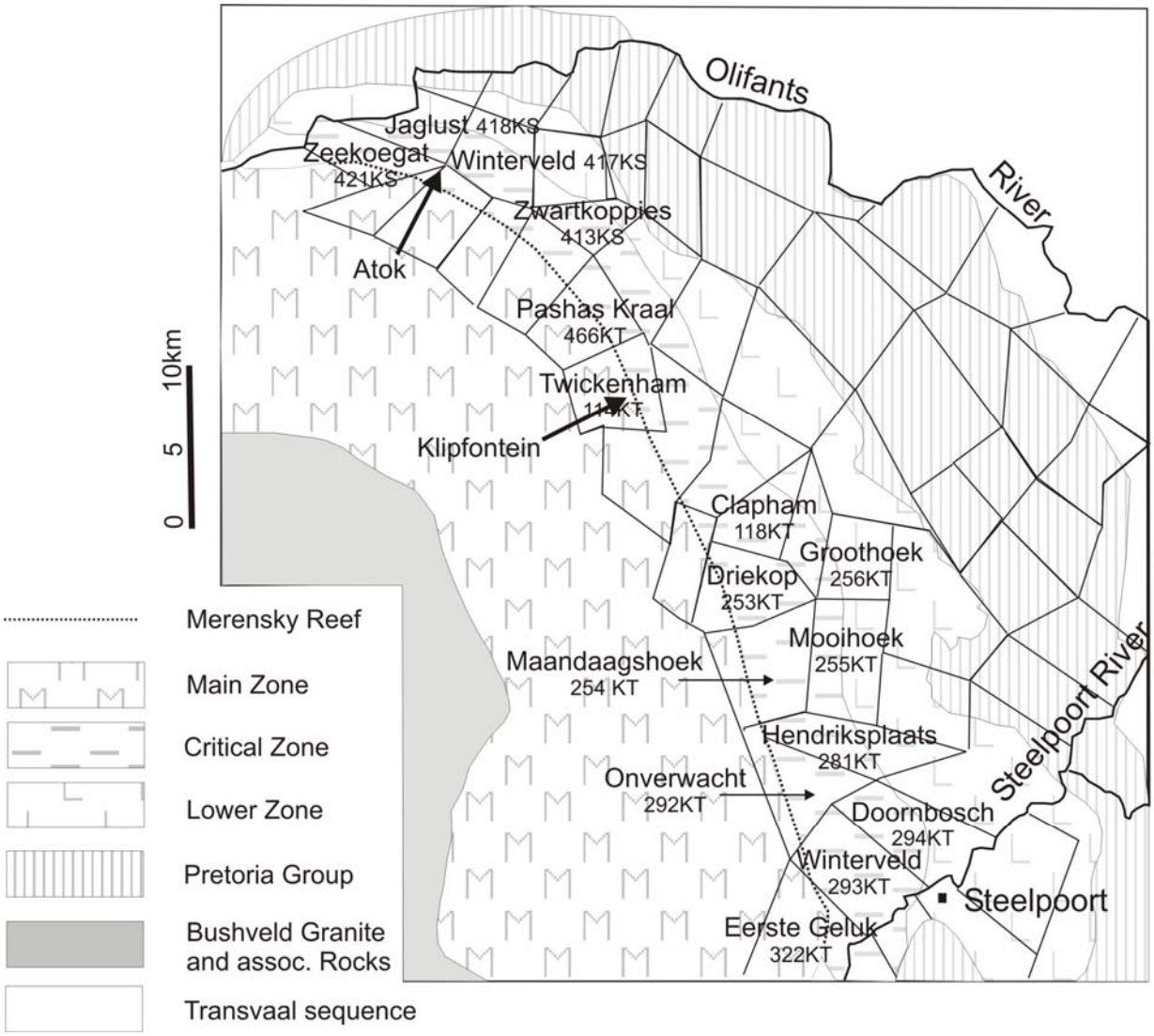


FIGURE 1.3 Locations of farms in the central sector of the eastern Bushveld Complex (Klipfontein lies within the Twickenham farm).

1.9 The subdivisions of the eastern limb

The eastern limb of the Bushveld Complex has been subdivided into three areas: the western, central and southern sectors (Hatton & von Gruenewaldt 1987) that are separated by major structural features, across which, lithostratigraphical changes occur (Scoon & Teigler 1995, Lea 1996). The Wonderkop and Stofpoort faults divide the western and central sectors, while the Steelpoort lineament divides the central and southern sectors (Figure 1.1) (Lea 1996). The latter feature is nearly 3 km wide, and is widely regarded as a fault, downthrown to the west. However, variations in thickness of stratigraphic sequences occur across it (Lea 1996). The Merensky Reef is discontinuous in this area of the lineament.

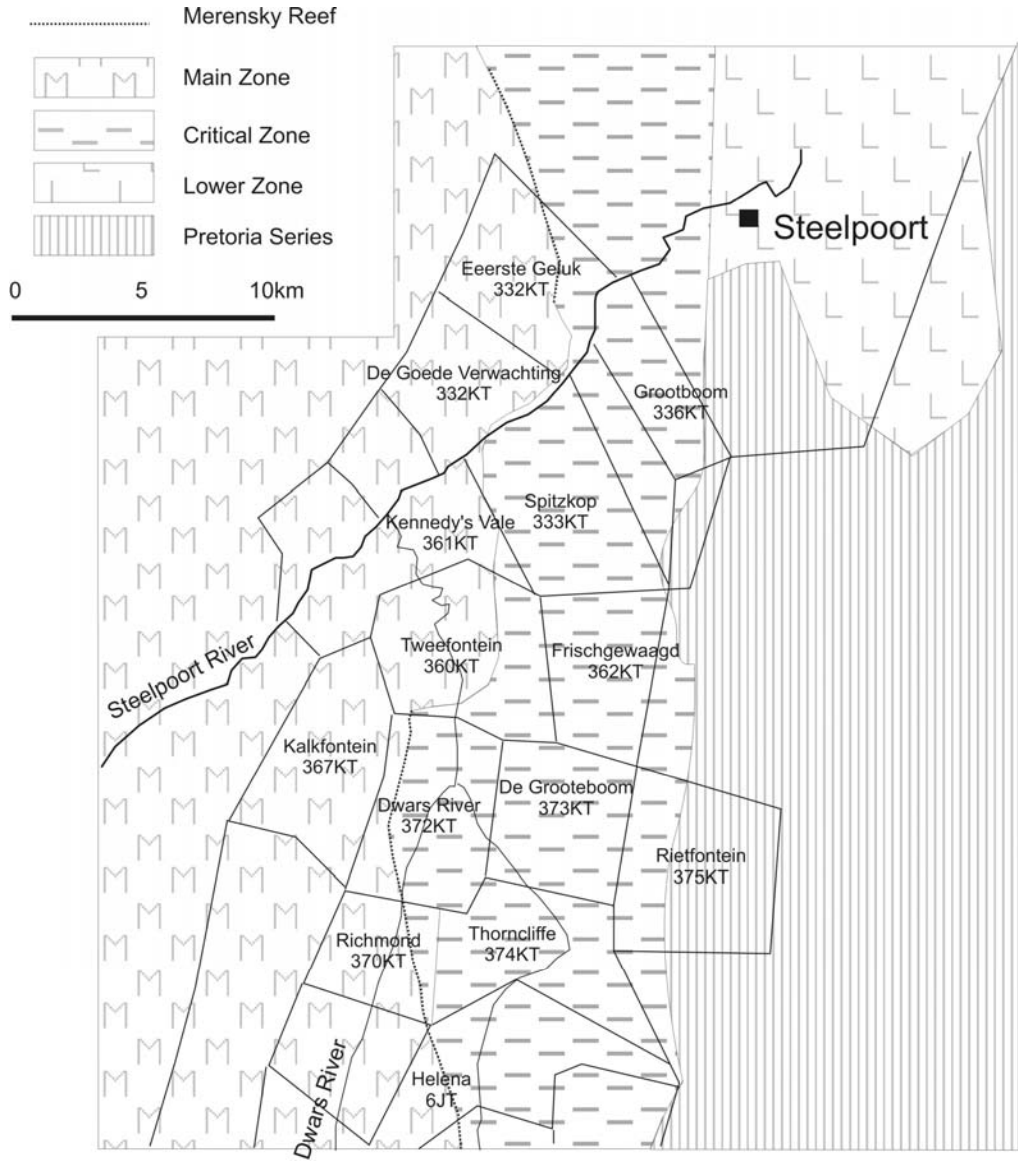


FIGURE 1.4 Locations of farms in the southern sector of the eastern Bushveld Complex.

1.9.1 The southern sector

The southern sector of the eastern Bushveld Complex is taken as that area of the complex lying to the south of the Steelpoort lineament. Here, layering dips at 10-15^{o} to the west and the Lower Zone is entirely absent (Scoon & Teigler 1995). Attenuation of the Lower Zone is abrupt across the Steelpoort lineament to the north. Cousins (1964a) described Lower Critical Zone chromitites grading into chrome-rich pyroxenites towards the south. MG chromitites are thicker than their equivalent in the central sector (Scoon & Teigler 1995). Structurally, the south-eastern Bushveld is reflected in the geomorphology of the area. Hill slopes occur parallel to igneous layering, with breaks in slope and incised valleys resulting from the intrusion of dolerite dykes and faulting. Two dyke sets are apparent, striking NNE and WNW. Faulting and the intrusion of dykes are believed to result from the break-up of the eastern margin of the super continent Gondwanaland. Von Gruenewaldt (1973) provided detailed descriptions of the Main and Upper Zone rocks in the Roossenekal area. He calculated the Main Zone thickness at about 3940 m and estimates the Upper Zone to be 2270 m thick.

1.9.2 The central sector

The central sector is the most widely studied area in the eastern Bushveld. This area dips approximately 10^{o} to the west (Gain 1985), but increases northwards up to 45^{o} in the Olifants River area (Mossom 1986). Trough-like features occur in the Lower Zone (Cameron 1978) at the Olifants River, Clapham and Bugersfort-Winterveld. This is in contrast to the southern and northern sectors in which the Lower Zone is entirely absent. The LG chromitites are well developed on Eerste Geluk, but the MG chromitites are thin and discontinuous in the central sector (Scoon & Teigler 1995). The Lower Critical Zone is largely restricted to this sector. The UG1 and UG2 are present, as well as a UG3/UG3a chromitite. A detailed stratigraphic description of the UG2 on Maandagshoek is given by Gain (1985) and Cameron (1982) described the Upper Critical Zone on Jagdlust/Winterveld. Molyneux (1974) mapped and described Main and Upper Zone rocks in the central sector, estimating thicknesses of 2860 m and 1790 m respectively. Quadling & Cawthorn (1994) also described the layered gabbronorites of

the Main Zone in the central sector and Mossom (1986) gave a detailed description of the Upper Critical Zone at Atok mine in the northern part of the central sector.

Dunite pipes occur in this sector, significantly the Mooihoek, Onverwacht and Driekop pipes, in which Hans Merensky discovered the first PGE from the Bushveld Complex in the 1920's.

1.9.3 The western sector

This sector is relatively poorly known, but the Lower Zone is thought to be absent (Scoon & Teigler 1995). Although the Critical Zone is developed, its total thickness is approximately 250 m, much thinner than both the central and southern sectors, which are 1500 and 600 m thick respectively (Lea 1996). Dip increases substantially to approximately 50-60^{o} and the Merensky Reef is displaced by 10 km between the western and central sectors (Lea 1996).

1.10 Terminology

This section attempts to explain terminology used for rock types and zones in the Bushveld Complex. Frequently, a number of definitions can be in use as mine staff often have their own specific terminology for various units.

1.10.1 Rock type classification

Noritic, gabbroic and ultramafic rocks can be classified using the IUGS system (Streckeisen 1974, Le Maitre *et al.* 1989), which is based on modal proportions of minerals in the rock, regardless of whether they are cumulus or intercumulus. Cumulates are classified after Wager *et al.* (1960), according to the amount of intercumulus material present. Orthocumulates, mesocumulates and adcumulates contain >25, 7-25 and <7 vol.% intercumulus phases respectively. However, since modal proportions in Bushveld rocks do not readily correspond to the triangular model of Streckeisen (1974), rock type divisions in this study are based on modal proportions of the studied interval. This is discussed in more detail in section 4.1. Informal terminology, in common use by local mining companies will be used in this study, in particular those terms relating to anorthosites. Therefore, based on suggestions by Irvine

(1982) and Kruger & Marsh (1985), the term "spotted anorthosite" will be used for rocks containing minor intercumulus orthopyroxene and leuconorite will be used to define rocks containing minor cumulus orthopyroxene. Anorthosites containing large patches of intercumulus orthopyroxene are referred to as "mottled anorthosites". In addition, the term "varitextured" anorthosite may be used to refer to anorthositic rocks where both cumulus and intercumulus orthopyroxene is present. The term "leopard" anorthosite is sometimes used by mining and exploration companies instead of varitextured, but will not be used here. Feldspathic orthopyroxenite contains up to 30% plagioclase, but for simplicity, this lithology is referred to as pyroxenite in this study. "Giant Mottled Anorthosite" (GMA) is used extensively for the mottled anorthosite unit at the top of the Bastard Cyclic Unit, where unusually large orthopyroxene mottles occur and the plagioclase often takes on a distinctly pink hue.

The term layer is used to describe laterally persistent "beds" of invariably a single rock type. Unit names are frequently attached, such as the UG2 chromitite (layer) and the Bastard pyroxenite (layer). "Units" are series of linked layers, composing a distinct package of rocks that are laterally continuous, as in the Merensky Cyclic Unit. "Reef" is predominantly a mining term and is used to describe the portion of a unit or layer that is economically defined in terms of grade and thickness (Kruger 1990). Hence, the Merensky Reef is used to describe the layer within the Merensky Cyclic Unit that is PGE enriched. This unit may contain more than one rock type, but is normally centred on the Merensky pyroxenite. Since the term reef can be confusing, although widely used, in this study, layers of the cyclic units are referred to by their rock type. The Merensky pyroxenite is frequently underlain by a pegmatitic feldspathic olivine pyroxenite, commonly known as pegmatoid. The term pegmatoid will be used in this study as it is in much more common usage among local mining and exploration companies. The term "marker" is used to refer to a particularly distinctive mappable layer of rock that is laterally persistent and can be used as a stratigraphic marker.

1.10.2 Zones and their boundaries

The stratigraphy of the Bushveld Complex is well recorded. However, nomenclature used for defining stratigraphic subdivisions has often been under dispute. Wager & Brown (1968) defined a zone as "a thickness of layered rocks developed while a specific cumulus or assemblage of cumulus minerals was

forming". In 1980, the South African Committee for Stratigraphy (SACS) published a compilation of the lithostratigraphy of the Bushveld Complex that included proposals of formal divisions. However, these recommendations were based solely on lithological and mineralogical features and geochemical and structural features such as unconformities were ignored. The SACS definitions are largely ignored in industry and academia. Specific controversies surrounding zone boundaries will be discussed in full at appropriate locations in the text

1.11 The extent and aims of the project

This study focuses on the Upper Critical and Lower Main Zone of the eastern Bushveld Complex. The eastern Bushveld has been studied far less than the western Bushveld, as the latter has been the focus of the mining industry for many years. Consequently, detailed studies of petrology, geochemistry and mineralogy of the eastern Bushveld are uncommon, making comparison with the western limb difficult. Conversely, exposure is better in the east and extensive mapping and stratigraphic studies have been undertaken (Cameron 1964, 1978, 1982, von Gruenewaldt 1973 and Molyneux 1970). Emphasis is placed on the nature of the boundary between the Critical and Main Zones, which has some significance for exploration since the Main Zone, in contrast to the Critical Zone, is virtually unmineralised. The stratigraphic interval covered in the studied profiles extends from the UG2 footwall to the first appearance of the Porphyritic Gabbronorite Marker in the Main Zone (Figure 1.2), approximately 350 m above the Merensky pyroxenite in this study. The Merensky pyroxenite and Cyclic Unit is investigated in detail, but attention is also paid to the Bastard Cyclic Unit. These foci provide three main aims for this study:

- To contribute to the detailed documentation of the Upper Critical and Lower Main Zones in the eastern Bushveld and make a stratigraphic comparison with the western limb
- To place further constraints on the nature and positioning of the Critical/Main Zone boundary
- To investigate the origin of the Merensky and Bastard Cyclic Units

Chapter 2

The stratigraphic succession of the sampled cores

Samples were taken from 4 boreholes in the eastern Bushveld, located on Richmond, Kennedy's Vale, Eerste Geluk and Klipfontein (Figures 1.3 and 1.4). The first two farms lie in the sector south of the Steelpoort lineament and the latter two lie to the north of that feature. The core from Kennedy's Vale lies very close to the lineament itself. This section describes the stratigraphy in each of the cores. The descriptions are in stratigraphically ascending order. Drilling in all areas only persisted as deep as the UG2 footwall, which is the base of the sampled section, so this description will not include the lower section of the Upper Critical Zone. Stratigraphic logs for each of the sections are given in Figure 2.1 and a summary of each core is given in Appendix I. Correlation with standard units and informal zonal subdivisions are established. All thicknesses are given as intersected, no correction for dip has been applied. Inspection of other adjacent cores shows that thickness of layers varies and so no major importance is attached to any of the thicknesses recorded from a single borehole. No single borehole ever included the entire section that was to be studied and was devoid of alteration, faulting, dykes, granitic pegmatites and had typical thicknesses of all layers when compared with adjacent cores. Hence, it was necessary to produce composites of more than one borehole to obtain the required, complete, fresh sections for this study.

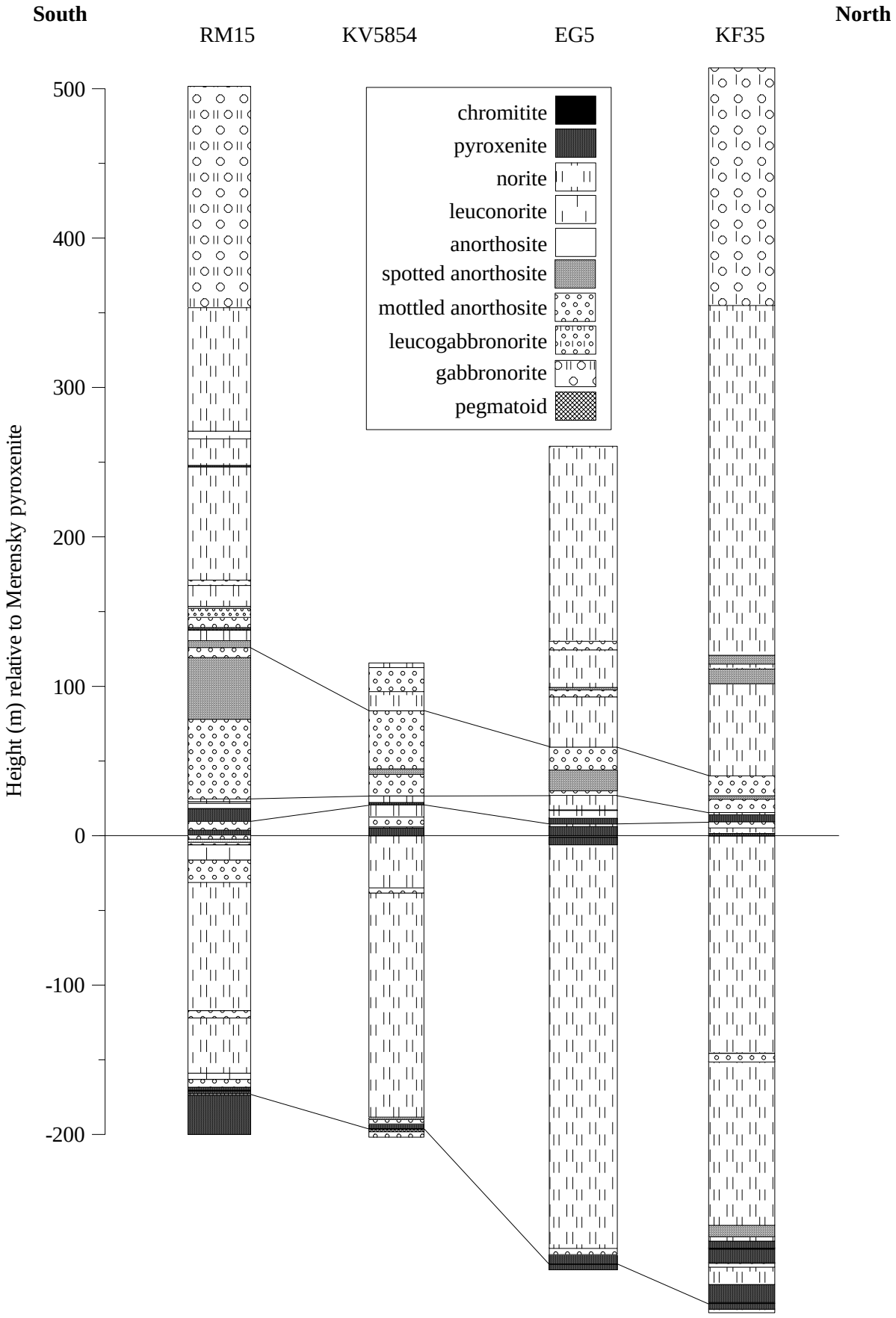


FIGURE 2.1 Stratigraphic logs of the four studied cores, from Richmond, Kennedy's Vale, Eerste Geluk and Klipfontein.

2.1 Richmond (RM15)

RM15 was collared in the Lower Main Zone and extends to just below the UG2. The mother hole contained an abnormally thin Merensky pyroxenite so one of the deflections (deflection 5) that branched off from the main hole just above the Merensky pyroxenite was used to take pyroxenite samples. This deflection contained a thicker, more representative section of pyroxenite. For the purposes of this study, deflection 5 was incorporated as if part of the main core, to simplify logs. Similarly, RM17 was used to allow more of the Lower Main Zone to be sampled, as well as hand samples. RM17 and hand samples have also been added to the logs for simplicity. All contacts are sharp unless otherwise stated.

The UG2 unit

The lowest lithology of the sampled section consists of 1.31 m of pegmatoidal feldspathic pyroxenite (Figure 2.1). Overlying this is the UG2 chromitite layer that is split by a 0.54 m thick norite parting that is pegmatoidal in its upper 10 cm. The basal chromitite is 10 cm thick and the main UG2 above the parting is 44 cm thick. The overlying pyroxenite is 1.29 m thick and is succeeded by a 6 cm thick chromitite leader and a further 24 cm of pyroxenite. A 2 mm thick chromitite occurs at the base of the overlying olivine- and sulphide-bearing pegmatoid, which is 52 cm thick. The main UG2 pyroxenite overlies the pegmatoid and is 2.42 m thick. This is overlain by 8.07 m of mottled anorthosite that grades into a medium-grained leuconorite. There is a sharp contact with the overlying homogeneous norite that is about 34 m thick and gradually grades into a mottled anorthosite, which is overlain by a further 82 m of homogeneous norite. Overlying the norite unit is a mottled anorthosite, 14.38 m thick, with a few noritic intervals (up to 70 cm thick) and is succeeded by 9.48 m of norite that includes a few anorthosite intervals. The norite gradually becomes more leucocratic and grades into a mottled anorthosite that is 1.03 m thick. A 1.6 m thick leuconorite, with a gradational basal contact completes the UG2 Cyclic Unit.

The Merensky Cyclic Unit

The underlying leuconorite has a sharp contact to the Merensky chromitite (no bleaching of the norite occurs at the contact, a common feature in other parts of the complex). The chromitite is 3-4 mm thick, with sharp contacts and overlain by the Merensky pyroxenite. The pyroxenite is feldspathic and contains poikilitic clinopyroxene and minor sulphides. The pyroxenite is only 28 cm thick in the mother hole, which is abnormally thin for this area so deflection 5, where the pyroxenite is 2.52 m thick (a more typical thickness), was sampled for analyses. Overlying this is 6 m of mottled anorthosite that includes some porphyritic orthopyroxene spots in the upper section of the anorthosite. Euhedral orthopyroxene frequently displays a plagioclase rim and sulphides (mainly chalcopyrite) are present as ovoid inclusions in plagioclase. A thin layer of chromitite, consistently one grain thick occurs at the upper contact of the anorthosite.

The Bastard Cyclic Unit

The Bastard pyroxenite overlies the upper anorthosite of the Merensky unit and is 6.97 m thick. The Bastard pyroxenite has a high felsic content and is variable in composition. An ultramafic base (about 15 cm thick) grades into a feldspathic central section of the pyroxenite and the upper section is of a more ultramafic composition. There is a sharp contact to the overlying anorthosite (~2 m thick), which is not typically mottled, but includes some irregular interstitial pyroxene. A thin (~1 m) overlying leuconorite grades into heterogeneous norite that is over 12 m thick. The GMA can be divided into three sections; Lower GMA, the Giant Mottled Middling (GMM) and the Upper GMA (this is discussed further in section3.2.2) The overlying mottled anorthosite is a distinct unit comprising unusually large mottles, ~10 cm in size, and the plagioclase takes on a slightly pink-tint. This is the LGMA and it is 15.88 m thick. Overlying the LGMA is a 5.16 m thick heterogeneous spotted anorthosite (GMM), containing subhedral porphyritic orthopyroxene. Some thin sections of this unit contain finer-grained orthopyroxene (leuconorites) and infrequent mottling also occurs. There is a gradational upper contact to the overlying mottled anorthosite that contains smaller, slightly faint mottles. This is the UGMA and is 26.81 m thick. The overlying GMA comprises a distinct lower unit (Lower GMA), which is densely mottled at the base, becoming more leucocratic, until a pure

anorthosite section is attained, at about 28 m above the base of the Merensky pyroxenite. Plagioclase in this unit is tinted pink. A spotted anorthosite overlies the LGMA that includes some leuconorites with finer-grained orthopyroxene. This is the Middle GMA and is 5.18 m thick. The Upper GMA is 27.11 m thick and contains smaller, sometimes faint mottles.

Deflection 5

For complete documentation, the details of deflection 5 are given here because material from the Merensky unit is used in this study.

Deflection 5 ends in leuconorite of the Merensky Reef footwall. A one-grain thick chromitite layer marks the sharp contact to the Merensky pyroxenite. This pyroxenite is 2.52 m thick (Figure 2.1), feldspathic and has a poikilitic texture. The contact to the overlying leuconorite (1.05 m thick) is undulating. Above this, the deflection returns to the mottled anorthosite that forms the Bastard footwall in the mother hole.

The Lower Main Zone

The base of the Main Zone, defined in this section as above the GMA (the exact position of the Critical/Main Zone boundary is discussed in Chapter 7), is characterised by consecutive sequences of mottled anorthosite and norite. Overlying the UGMA is a spotted anorthosite that contains porphyritic orthopyroxene and includes a slightly mottled section, between 104-98.3 m above the Merensky pyroxenite, with highly gradational upper and lower contacts. This is overlain by 6.88 m of homogeneous medium-grained norite that has a sharp upper contact with a thin (0.67 m) melanorite. This melanorite has a sharp contact with the overlying spotted anorthosite (12.73 m thick), which is overlain by an homogeneous medium-grained norite (1.06 m) that has a sharp contact with another thin (34 cm) melanorite. This is overlain by 34 cm medium-grained norite that marks the top of the unweathered core in RM15.

From this point (129.8 m above the Merensky pyroxenite) RM17 was used to extend the section from Richmond further into the Lower Main Zone. RM17 was sampled from the top of the GMA. The upper contact of the GMA grades into a varitextured anorthosite, with subhedral porphyritic

orthopyroxene and some “blotchy” orthopyroxene and clinopyroxene mottles and extends for 20.48 m. However, this unit can be divided into three sections, based on the appearance of blotchy clinopyroxene patches, and simultaneous reduction in the number of orthopyroxene patches, after 4.21 m. This is followed by a reversal to larger orthopyroxene patches and big clinopyroxene mottles for 17.61 m. Overlying the varitextured unit is a noritic unit, 9.29 m thick. At the base, this section is leuconoritic, but becomes increasingly mafic upwards. This is overlain by a spotted anorthosite containing porphyritic orthopyroxene. This is 5.46 m thick and is overlain by 0.46 m of mottled anorthosite. A spotted unit (6.32 m thick) overlies this and contains a few clinopyroxene mottles, and porphyritic orthopyroxene spots. A 5.58 m thick mottled anorthosite, with both orthopyroxene and clinopyroxene mottles overlies this. A significant decrease in the size of the mottles occurs after 3.74 m. Between 115.15 and 114.91 m (above the base of the Merensky pyroxenite) is a mafic dyke. Overlying the mottled anorthosite is a medium-grained leuconorite that grades into a norite over 3.72 m. This is overlain by a fine-grained norite, comprising small crystals of densely packed orthopyroxene, which grades upwards into a medium-grained leuconorite. The norite is 3.49 m thick and the leuconorite is 5.89 m thick. Overlying the leuconorite is an anorthosite (1.3 m thick) with a few clinopyroxene mottles, which grades upwards into a mottled anorthosite (3.79 m thick) as mottles become more common. In this unit clinopyroxene mottles display rims of plagioclase overgrowths. In the overlying norite mottles gradually start to disappear and orthopyroxene becomes porphyritic, so that a varitextured texture is developed over 8.9 m. Overlying this is a 7.77 m thick homogeneous norite with some mottles at the base. It has a sharp upper contact with a leuconorite (3.63 m thick) that contains some clinopyroxene mottles towards the top of the unit. Overlying this is a fine-grained norite, 63.22 m thick. The upper 40 m of this norite includes some thin (2-5 cm) anorthosite sections. The norite itself is not homogeneous, containing some small clinopyroxene mottles. A mafic dyke occurs between 168.99 and 172.8 m above the Merensky pyroxenite. An overlying medium-grained norite is 6.88 m thick and is overlain by a thin (0.25 m) medium-grained feldspathic pyroxenite. A medium-grained norite, 14.94 m thick, becomes increasingly more feldspathic and gradually grades into a leuconorite, which persists for 4.62 m, before returning to a norite that continues to the top of the borehole (11.37 m).

Continuing up the hill above the RM17 collar, it was possible to continue this section further into the Lower Main Zone by taking hand samples from outcrop. A further seven samples were taken. These samples consist of gabbronorites and porphyritic gabbronorites that contain large (up to 5 mm), euhedral clinopyroxene grains. The latter represent the highest level in the sequence that was sampled and consist of relatively coarse-grained clinopyroxene and orthopyroxene in a fine-grained plagioclase matrix. This is a common and noticeable lithology throughout the Bushveld and is known as the Porphyritic Gabbronorite Marker horizon. Samples 3a and 3b are from the same outcrop, where a coarse-grained and a fine-grained gabbronorite occur directly adjacent to one another in outcrop.

2.2 Kennedy's Vale (KV5854)

Core KV5854 was sampled on the Kennedy's Vale (Figure 1.1). This core is near the Steelpoort lineament and contains some alteration, most notable as a green colouration of plagioclase, and small scale faulting and fracturing.

The UG2 unit

The bottom of this unit is represented by a coarse olivine-bearing pegmatoidal feldspathic pyroxenite layer of 2 m in thickness. Sulphides are also present and the upper 30 cm of the pegmatoid are more ultramafic. Overlying this pegmatoid is the UG2 chromitite, which is 0.71 m thick and includes two pegmatoidal feldspathic pyroxenite internal partings. The chromitite layer has a sharp contact with the overlying pegmatoid. This pegmatoid is 20 cm thick and overlain by a chromitite leader that is 8 cm thick. Another thin 18 cm sulphide-bearing pegmatoid is overlain by the UG2 pyroxenite, which is 1.95 m thick and includes two more chromitite leaders. The lower stringer is 5 mm thick and occurs 3 cm above the base of the pyroxenite and the upper leader is 3 mm and occurs 40 cm below the top of the pyroxenite. Overlying the UG2 pyroxenite layer is a 2.86 m thick mottled anorthosite. There is a sharp upper contact with the overlying medium-grained leuconorite (3.23 m thick) which grades into medium-grained norite (2.38 m thick). This norite becomes increasingly more felsic and grades into a 2.73 m thick leuconorite. There is a gradational contact with the overlying 13.67 m thick norite, which also grades into a thin leuconorite. Overlying this is 116.45 m of homogeneous medium-grained norite.

This norite becomes gradually more melanoritic and there is a sharp contact with the overlying norite, which displays some felsic layering. This norite also becomes more mafic and has a sharp upper contact with a 2.68 m thick mottled anorthosite. This anorthosite typically contains clinopyroxene mottles and some cumulus porphyritic orthopyroxene grains. There is a gradational, but distinct contact with the overlying leuconorite. This leuconorite becomes more feldspathic upwards and is 5.22 m thick. There is a sharp upper contact with the overlying norite, which is 31.48m thick and becomes a little more felsic in the upper few centimetres.

The Merensky Cyclic Unit

There is no basal chromitite. At the base of the Merensky unit is a 7 cm thick pegmatoidal feldspathic pyroxenite. Along the contact with the overlying pyroxenite is a thin chromitite layer of a few mm in thickness. The Merensky pyroxenite is a medium-grained feldspathic pyroxenite and is 4.33 m thick. There is a slightly gradational contact with the overlying norite, which is 72 cm thick. This norite grades into a 1.79 m thick mottled anorthosite. It has a sharp upper contact with a 0.54 m thick anorthosite, in which some faint mottles are apparent. Mottles are much more distinct in the overlying anorthosite which is 5.51 m thick.

The Bastard Cyclic Unit

A thin (3 cm) pyroxenite is present with sharp upper and lower contacts and overlies anorthosite. There is no chromitite layer at the base of the Bastard pyroxenite. As the first occurrence of pyroxenite above the Merensky pyroxenite it can be classified as the Bastard pyroxenite. However, a second, thicker pyroxenite does occur above it in the stratigraphy so this thinner unit will be called the lower Bastard pyroxenite. Overlying the lower pyroxenite is 7.33 m of homogeneous medium-grained norite. The medium-grained feldspathic upper Bastard pyroxenite is 1.85 m thick and has a slightly gradational contact with the overlying norite. This norite unit is 4.1 m thick and is overlain by the GMA. This distinctive layer comprises 14.95 m of anorthosite with large orthopyroxene mottles. Within this unit is a patch of disseminated sulphides, approximately 5 cm thick.

The Lower Main Zone

Overlying the GMA is varitextured anorthosite. Mottles in this unit are distinctly smaller than those of the underlying unit and are largely clinopyroxene mottles, with fewer orthopyroxene mottles. Overlying this is 40.52 m of mottled anorthosite. In this unit, mottles become increasingly smaller than those in the units below and are denser in their distribution. This unit has a gradational upper contact with the overlying norite, which is 13.6 m thick and gradually becomes mottled. These mottles are very small and there is a distinct but gradational contact with an overlying section containing larger mottles. This mottled anorthosite unit is 14.71 m thick in total. There is a sharp contact with the overlying norite, which is 4.74 m thick and terminates at the top of the borehole. No other boreholes were sampled to continue this section to higher levels in the Main Zone.

2.3 Eerste Geluk (EG5)

The UG2 unit

The basal part of the UG2 unit consists of 2.35 m of poikilitic feldspathic pyroxenite, which contains small amounts of base metal sulphides. Overlying this is the UG2 chromitite layer, which is 0.29 m thick. Several chromitite leaders of 1-5 mm thick are overlying in the base of the UG2 pyroxenite, which is 2.06 m thick. This is a medium-grained feldspathic pyroxenite, which becomes pegmatoidal and more feldspathic towards the top. Overlying this is a feldspathic chromitite leader layer, 9 cm thick. A thin, 36 cm fine-grained harzburgite containing highly serpentinised olivine overlies this chromitite. Overlying this is a 4.37 m thick coarse feldspathic pyroxenite that also becomes pegmatoidal towards its upper contact. A package of thinly interlayered medium-grained norites and mottled anorthosites, with sharp boundaries, overlies the pyroxenite. In the uppermost mottled anorthosite are numerous mm-thick chromitite layers. This is overlain by a 77.67 m thick norite that includes some thin, 1-5 cm, but distinct anorthosite layers and grades into a melanorite for 1.62 m. There is a sharp contact to a 64.32 m thick homogenous norite. At the upper contact of this norite is a 2 mm thick chromitite layer, which while thin, may represent the UG3 chromitite, although it has norite above and below and is not part of a typical cyclic unit. Overlying this is a norite, but it is distinctly finer grained that the norite beneath it and the contact between them is abrupt. The fine-grained norite is 35.66 m thick and grades into a

coarser norite that contains large amounts of interstitial clinopyroxene and patches where little orthopyroxene is present, giving it a blotchy appearance. This coarser norite is 8.94 m thick and it has a sharp upper contact with a 28.54 m thick norite of normal grain size. Overlying this is a 3.28 m thick melanorite, which abruptly changes to a thin 16 cm leuconorite and back to a melanorite. This is overlain by a medium-grained norite that is 14.5 m thick and becomes increasing finer-grained towards its upper contact with a sulphide-bearing pegmatoid that is 1.64 m thick. A thin 7 cm norite layer has a gradational boundary with a feldspathic pyroxenite layer that is 2.43 m thick. Overlying this is another pegmatoid, 1.43 m in thickness. A thin, 9 cm thick feldspathic pyroxenite is overlain by 4 cm of anorthosite that contains disseminated chromite. There is a sharp contact with the base of the Merensky pyroxenite.

The Merensky Cyclic Unit

The Merensky feldspathic pyroxenite is 8.37 m thick, medium-grained, but becomes slightly pegmatitic towards the top. This is overlain by a disseminated chromite layer, 3 cm thick. Overlying this is 11 cm of norite, which is overlain by 79 cm of pyroxenite that becomes increasingly feldspathic and grades into medium-grained norite. The footwall to the Bastard pyroxenite is 3.15 m of mottled anorthosite.

The Bastard Cyclic Unit

A Lower Bastard feldspathic pyroxenite occurs and is 40 cm thick, medium-grained and has a sharp upper contact with 5.64 m of homogeneous medium-grained norite. This is overlain by a 77 cm thick layer of feldspathic pyroxenite at the top of which is a 1 cm thick chromitite. A thin 7 cm norite is overlying, succeeded by 81 cm of pegmatoid. This is overlain by a 99 cm thick coarse-grained, feldspathic pyroxenite and followed by a coarse-grained norite, which is 3.23 m thick and contains some patchy pegmatoid. A 3.37 m thick unit of pegmatoid overlies this. The GMA is 25.8 m thick.

The Lower Main Zone

The GMA is overlain by 4.34 m of leuconorite that includes orthopyroxene phenocrysts. There is an overlying layer of mottled anorthosite which grades into a leuconorite. This unit is 2.93 m thick and is

overlain by a 19 cm thick anorthosite layer that contains a 1mm chromitite layer 4 cm below its upper contact with a pegmatoid. This is overlain by a mottled anorthosite that contains distinctly smaller mottles that is typical and is 9.85 m thick. This anorthosite has a very gradational upper contact with the overlying norite, which is 4.34 m thick. This is overlain by a 78 cm pegmatoid that has a 1 cm chromitite and 1 mm stringer, at 4 cm above its base. This is overlain by 3.95 m of norite, followed by 4.94 m of pegmatoid. The overlying norite grades into leuconorite after 10.59 m. The leuconorite is 8.68 m thick and has a sharp contact with the overlying norite, which gradually becomes mottled. Overlying this is another norite (1.65 m thick) that also grades into a mottled anorthosite. Overlying this is a thick succession of norite, leuconorite and few melanorites, extending 161.56 m to the top of the borehole.

EG6

Due to the presence of relatively high amounts of pegmatoid in EG5, samples from the GMA were taken from EG6. The mottled anorthosite in this section can be divided into four sections, based on the size of the mottles. Overlying a norite is a coarse mottled anorthosite, approximately 12 m thick. This is overlain by an anorthosite with small mottles, approximately 8 m thick, which then reverts to the coarse mottle-type for approximately 10 m. The upper section of the GMA comprises approximately 6 m with small mottles. Samples from EG6 were substituted into the section of GMA in EG5 for the purposes of this study.

2.4 Klipfontein (KF35)

KF35 on Klipfontein (Figure 1.1) has been sampled by Blumberg (2002) as part of his honours thesis. He performed XRF and Sr isotope analyses on the section between the UG2 and the top of the Bastard Cyclic Unit. KF35 has been relogged in this study, and sampling continued from the top of the Bastard Cyclic Unit into the Lower Main Zone.

The UG2 unit

The 0.63 m thick UG2 chromitite overlies harzburgite. Its hangingwall consists of 9.55 m of medium-grained feldspathic pyroxenite, overlain by a 11.5 m thick medium-grained melanorite. Overlying this is a medium-grained norite that grades into a mottled anorthosite. The UG3 chromitite lies 24 m above the UG2 and is 0.17 m thick. It is overlain by 18.09 m of porphyritic feldspathic pyroxenite. Within the pyroxenite there is a 1.85 m thick harzburgite that occurs 11.83 cm above the basal chromitite and includes the UG3a (3 cm) and UG3b (1 cm). A 270 m thick package of predominantly homogeneous noritic rocks and some pegmatoid succeeds this pyroxenite. The noritic rocks are interlayered with leuconorites, melanorites and some mottled and leuconorites. Four pegmatoidal bodies also occur between the UG3 and the Merensky Reef.

The Merensky Cyclic Unit

The immediate footwall to the Merensky Cyclic Unit is a norite (0.9 m thick). The Merensky feldspathic pyroxenite is medium-grained and 1.38 m thick, with no basal chromitite. The upper 20 cm of the pyroxenite is pegmatoidal. Succeeding this is a medium-grained leuconorite (6.1 m), which is overlain by mottled anorthosite (3.2 m thick).

The Bastard Cyclic Units

The Bastard pyroxenite overlies the mottled anorthosite, with a sharp contact, and comprises a medium-grained feldspathic pyroxenite and is 4.64 m thick. A pegmatoidal feldspathic pyroxenite is also developed in the upper 40 cm of the Bastard pyroxenite. This is overlain by 1.5 m thick leuconorite.

The overlying GMA is approximately 10 m thick, but does not comprise the large mottles that typify this section in other cores.

The Lower Main Zone

Overlying the GMA is a spotted anorthosite (2 m thick), with subhedral porphyritic orthopyroxene and some mottles. This is overlain by a spotted anorthosite that has no mottles developed and is 14 m thick. There is a sharp contact to the overlying medium-grained, 61.5 m thick norite, which has been intruded by a dolerite dyke. The norite is succeeded by a leuconorite (9.5 m thick) that is overlain by a more mafic norite (2 m thick). Overlying this is 7 m of leuconorite. Above this, there is 191 m of fine-grained norite. Within this norite a very distinct needle-like texture is developed over approximately 10 m. This comprises elongate (±5 mm) lathes of orthopyroxene. The norite has a very gradational upper contact with leuconorite (23 m thick). This leuconorite grades gradually back into a norite, which is 21 m thick. Overlying this is a 1 m thick leuconorite that is in turn overlain by 160.7 m of porphyritic gabbronorite. This is the Porphyritic Gabbronorite Marker and it extends to the top of the hole.

2.5 Summary

These boreholes comprise a complete section from the UG2 Cyclic Unit to the Porphyritic Gabbronorite Marker, documenting the Critical/Main Zone boundary in the eastern Bushveld. While each core is different, similarities exist that allows effective correlation with detailed sections from both the eastern and western Bushveld.

The UG2 – Merensky pyroxenite interval is dominated by a thick sequence of homogenous norite (82 m, 116 m, 64 m and 270 m in RM15, KV5854, EG5 and KF35 respectively). Within the Merensky Cyclic Unit, rocks follow a clearly defined sequence from pyroxenite at the base, an overlying norite or leuconorite (except in RM15 where norite is absent) to a mottled anorthosite at the top. The thickness of each of these lithologies is variable. Only in KF35 was pegmatoidal pyroxenite observed. The Bastard Cyclic Unit has similar characteristics to the Merensky Cyclic Unit. The Bastard pyroxenite sometimes displays varying feldspathic component and in KV5854 and EG5, a lower pyroxenite is present. The Bastard pyroxenite in KF35 is pegmatoidal in its upper section. The

pyroxenite is overlain by norite in all cores except in RM15 where a thin anorthosite is present. The upper section of the cyclic unit is characterised by the distinct GMA. The Lower Main Zone is characterised by interlayered norites and spotted and mottled anorthosites in each core. Gabbronorites are only present in cores RM17 and KF35.

An accurate assessment of the thickness of various units can be made allowing precise regional correlation within each sector and across the Steelpoort lineament. Furthermore, this stratigraphic information can be compared with sections in the western Bushveld. This database provides a reference point for detailed studies of the Merensky and Bastard Cyclic Units.

Chapter 3

Stratigraphic comparisons across the Bushveld Complex

Stratigraphic comparisons are an integral part of studies into the nature of the Bushveld Complex. These studies are an attempt to constrain the mechanisms that formed such a vast intrusion. Assessing similarities or differences across the complex may indicate factors such as the origin of layering, whether the limbs are linked at depth, whether mineralisation events occurred simultaneously throughout the chamber(s) and the location of potential feeders. This section examines the profiles used in this study and shows how they compare with other sections of the eastern limb and the western limb. Each of the locations mentioned in the text is given in Figures 1.3 and 1.4.

3.1 North and south of the Steelpoort lineament

The Steelpoort lineament is one of the most obvious features in the eastern Bushveld and is clearly noticeable on aerial photographs. Cameron (1964) showed that stratigraphy varies significantly across this feature and that layers cannot be matched on either side. This has led to the conclusion that the lineament is not a simple fault (Scoon & Teigler 1995, Schürmann *et al*. 1998) as had been previously supposed. This has led some (Cawthorn *pers. comm.* 2003) to suggest that it acted as a feeder to the Bushveld and fed separate chambers in the eastern limb and thus may have important ramifications for stratigraphy. Teigler *et al*. (1992) suggested that tectonic features, such as the Spruitfontein upfold, might have impeded the flow of magma pulses into the chamber and it is possible that the Steelpoort lineament may have acted as a similar barrier. Scoon & Teigler (1995) indicated that the Eerste Geluk dome, near the Steelpoort lineament in the eastern Bushveld, was responsible for lithostratigraphic differences in the Critical Zone sequence between the central and southern sectors. In this section, stratigraphic variations across the Steelpoort lineament are discussed.

Overall, the southern sector is much thinner than the central sector. The Lower Zone is entirely absent in the south, with only a thin, partially developed Lower Critical Zone. In terms of the chromitites, the LG chromitites are thin or absent in the south, but well developed in the central sector, whereas the MG and UG chromitites are much thicker in the southern sector. UG3 and UG3a chromitite

layers are developed above the UG2 in the central sector, but not in the south. Cawthorn (2004) indicated that the UG3 probably terminates slightly to the north of the Steelpoort lineament.

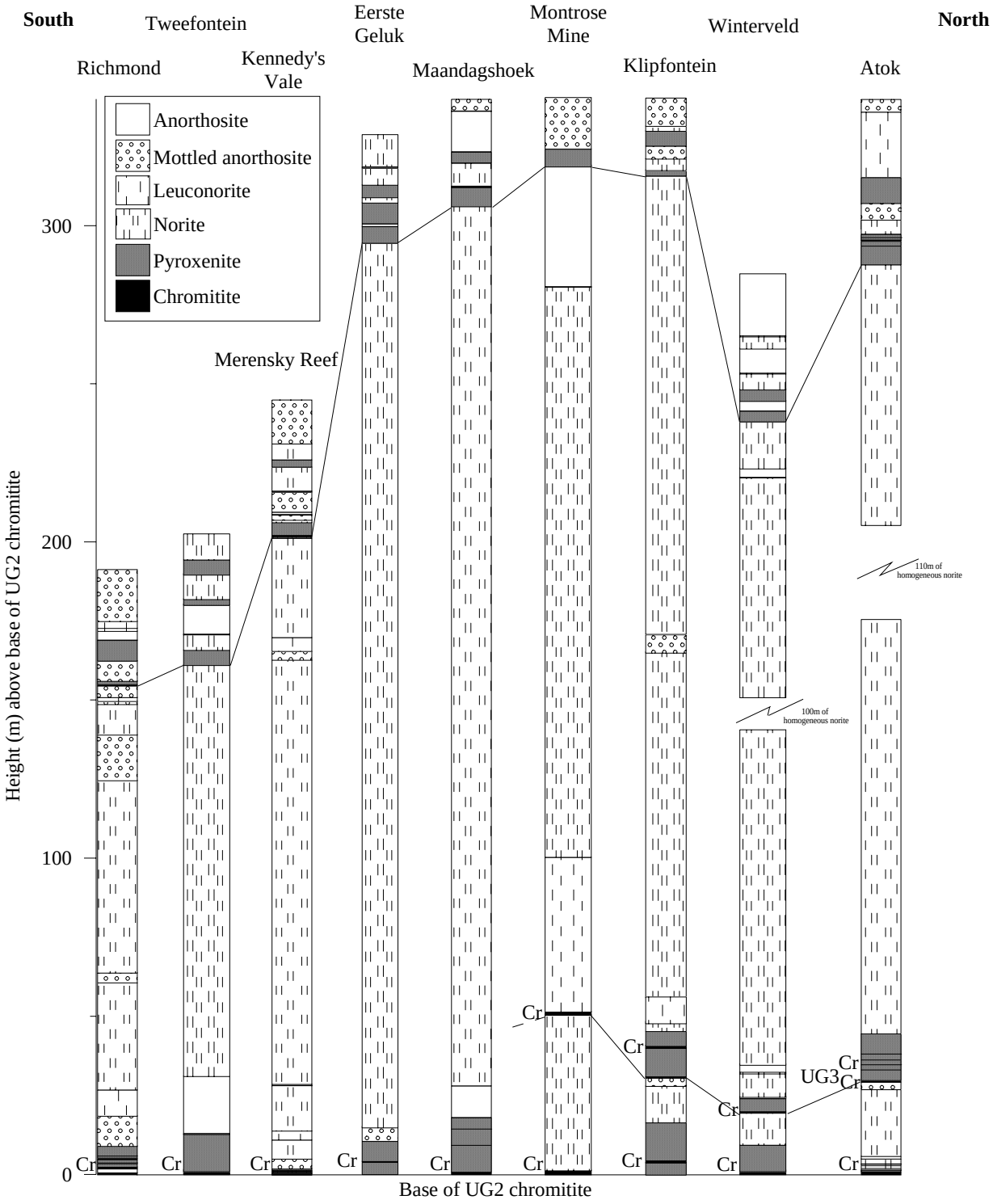


FIGURE 3.1 Stratigraphic logs of cores from the eastern Bushveld, from the UG2 to the top of the Bastard Cyclic Unit. [1] – This study, [2] – Cameron (1963), [3] – Worst (1986), [4] – Cameron (1982), [5] – Mossom (1986).

3.1.1 The Upper Critical Zone

Variations in stratigraphy occur on a local scale all over the Bushveld Complex. For example in RM15 the Merensky pyroxenite hangingwall is norite, whereas in KV5854 it is a mottled anorthosite. These can be considered minor differences that are the result of changes in modal proportion. Of greater significance however, are the differences between the "marker layers". In the Upper Critical Zone, these are the UG2 and the Merensky pyroxenite, which are of substantial economic importance, and will thus be described in more detail. The Upper Critical Zone (which will include the Merensky and Bastard Cyclic Units for the purposes of this study) that has been documented in the eastern Bushveld is given in Figure 3.1. In the central sector, stratigraphic profiles from Atok (Mossom 1986), Klipfontein (this study), Maandagshoek (Gain 1985), Montrose Mine (Worst 1986), Winterveld (Cameron 1982) and Eerste Geluk (this study) (from north to south) are considered, and in the southern sector, Kennedy's Vale (this study), Tweefontein (Cameron 1963) and Richmond (this study) are examined.

The thickness of the UG2 chromitite does not vary significantly between the central and southern sectors (table 3.1). The occurrence of the UG3 chromitite appears to be restricted to the central sector, where it is present in all but one core in this comparison. The exception is on Eerste Geuluk, where only a thin 2 mm chromitite occurs at the boundary between a coarser and finer grained norite. This is not considered to represent the UG3 as it is too thin, has norite above and below it and does not occur at the top or at the base of a cyclic unit. The UG3 is not recorded at all in the southern sector. In each sector, the overlying interval, up to the Merensky pyroxenite generally comprises norites, leuconorites and mottled anorthosites, in varying proportions, but in most cases there is a thick, homogenous noritic unit. Only at Atok does this section seem to show a distinctly more feldspathic stratigraphy, with Mossom (1986) recording a thick leuconorite.

The footwall to the Merensky pyroxenite also varies. At Atok in the northern sector it is a layered norite, as it is at Klipfontein, Maandagshoek and Winterveld. At Montrose and Eerste Geluk, the immediate footwall is anorthosite. In the southern sector the footwalls at Kennedy's Vale and Tweefontein are norites and at Richmond it is a mottled anorthosite. A pegmatoid is present in the Atok and Kennedy's Vale cores only.

Location	Ref	UG2 chromitite thickness (m)	UG2 - Merensky thickness (m)	Merensky pyroxenite thickness (m)	Bastard pyroxenite thickness (m)
Central Sector					
Atok	4	0.71 + 6 leader	390	11	3-5
Winterveld	2	0.7	370	~6	-
Klipfontein	5	0.63	310	1.18	4.6
Maandagshoek	3	0.7 + 5 leader	335	~18(?)	~6
Eerste Geluk	5	0.29 + UG3	285	8.37	0.4
Southern Sector					
Kennedys Vale	5	0.68 + 1 leader	200	4.2	1.85
Tweefontein	1	0.8	200	2.4	-
Richmond	5	0.43 + 3 stringers	170	2.1 (Def 5) / 0.25 (motherhole)	6.97

TABLE 3.1 Thickness of units in the central and southern sectors of the eastern Bushveld Complex.
1 – Cameron (1963), 2 – Cameron (1982), 3 – Gain (1985), 4 - Mossom (1986), 5 – This study.

The most indicative feature that the Steelpoort lineament is not a fault is the change in the thickness of corresponding units across the lineament. Figure 3.2 shows how the thickness of succession between the UG2 and the Merensky pyroxenite varies in the eastern Bushveld. At Atok, this thickness is approximately 390 m, which is similar to the thicknesses recorded on Maandagshoek, 350 m, Montrose, 300 m, and on Winterveld. In this study, the thickness between the UG2 and Merensky Reef on Klipfontein is approximately 310 m and 285 m on Eerste Geluk. South of the lineament however, there is only 200m between the UG2 and the Merensky pyroxenite on Tweefontein (Scoon & Teigler 1995 and references therein), which is comparable to that at Kennedy's Vale, and at Richmond it is about 170 m (this study) (table 3.1). Figure 3.2 clearly shows this relationship, that the UG2 / Merensky pyroxenite separation is thicker in the central sector than the southern sector. This change in thickness may suggest that the Steelpoort lineament had some form of control over lithological variation in the eastern Bushveld Complex.

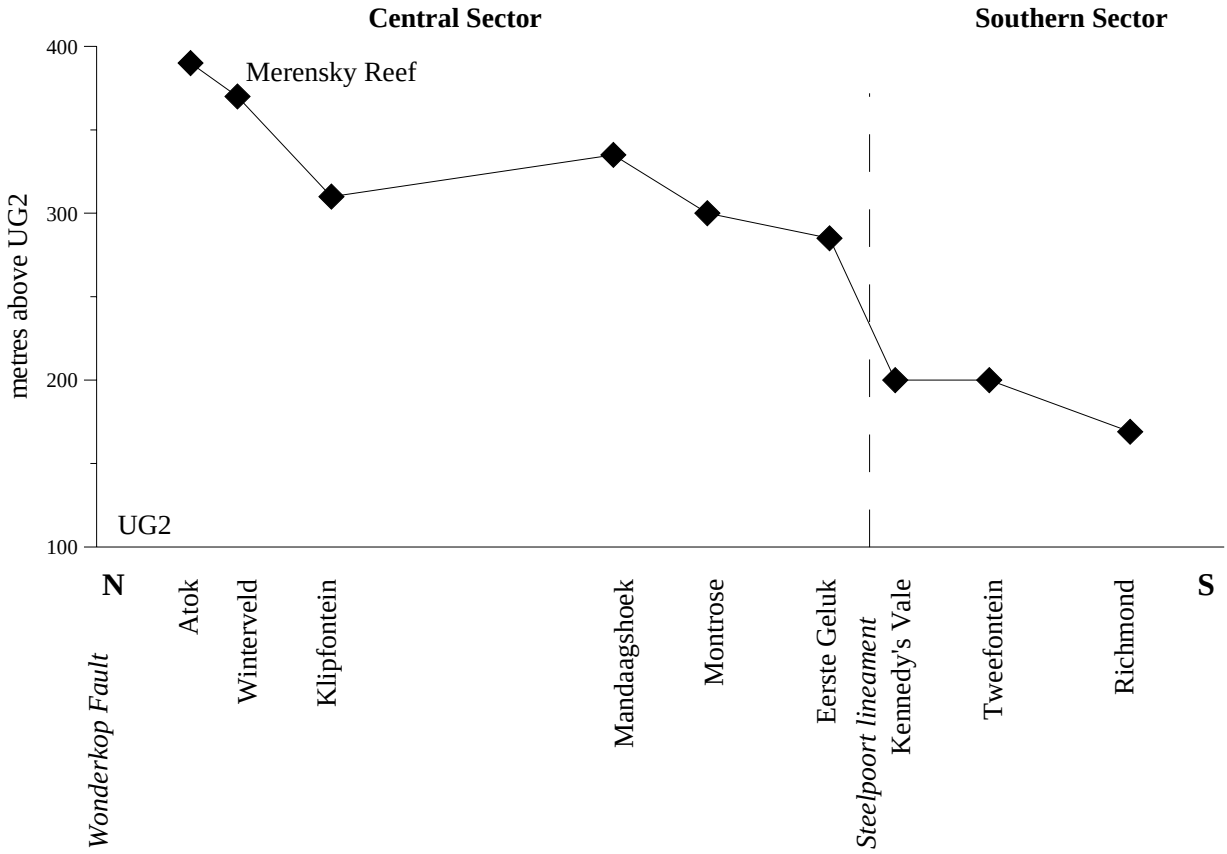


FIGURE 3.2 Section through the eastern Bushveld (N-S), demonstrating changes in thickness of the UG2 to Merensky Reef unit.

Thicknesses of the Merensky pyroxenite are also recorded in table 3.1. These vary more considerably than the UG2. In the central sector, the thickness of the Merensky pyroxenite varies between 1.18 and 18 m but it is much thinner, between 0.25 and 4.3 m, in the southern sector, although it is seen to increase in thickness southwards on Richmond, reaching up to 20 m in thickness (T. Richardson *pers. comm*. 2004). There appears to be no relationship between the relative thickness of the UG2 and Merensky pyroxenite. There is some variation in thickness in the Merensky Cyclic Unit. At Klipfontein it is 10.6 m, at Eerste Geluk it is 12.57 m, at Kennedy's Vale it is 8.56 m and at Richmond it is 6.06 m. At Maandagshoek however, it is thicker, at about 20 m. It is noted that there appears to be a correlation between the thickness of the Merensky and Bastard pyroxenites. The Merensky pyroxenite is comparatively thinner in cores where the Bastard pyroxenite is thicker and vice-versa. The overlying cyclic unit comprises norites and anorthosites. The GMA also displays variations in thickness. It is

thinner in the central sector, EG5 – 33 m and KF35 – 26 m thick, than in the southern sector, KV5854 – 58 m and RM15 – 48 m thick.

3.1.2 The Lower Main Zone

Layering in the Main Zone is far less distinct than it is in the Critical Zone. Nevertheless, variations in lithology are laterally consistent enough for subdivisions to have been proposed (von Gruenewaldt 1973, SACS 1980, Mitchell 1990 and Nex *et al.* 1998). There are distinctive marker layers throughout the Main Zone, e.g. the pyroxenite marker and zebra marker in the western Bushveld, but in this study only the lowest section is considered, up to the Porphyritic Gabbronorite Marker. This section of the Main Zone has been poorly documented in the eastern Bushveld, limited to description of the Roossenekal area by von Gruenewaldt (1973) and the Sekukhuneland area by Molyneux (1974). The stratigraphy of the Main Zone in cores from this study is given in Figure 3.3.

A noritic succession overlies the GMA, which is generally homogenous with some mottled and varitextured anorthosite layers. The first appearance of cumulus clinopyroxene (the Porphyritic Gabbronorite Marker) occurs at 350 m above the Merensky pyroxenite on Richmond, 350 m at Klipfontein and 300 m in Sekhukuneland (Molyneux 1974). The cores on Eerste Geluk and Kennedy's Vale were collared too low in the stratigraphy to record the Porphyritic Gabbronorite Marker, but the spacing must exceed 115 m and 260 m respectively.

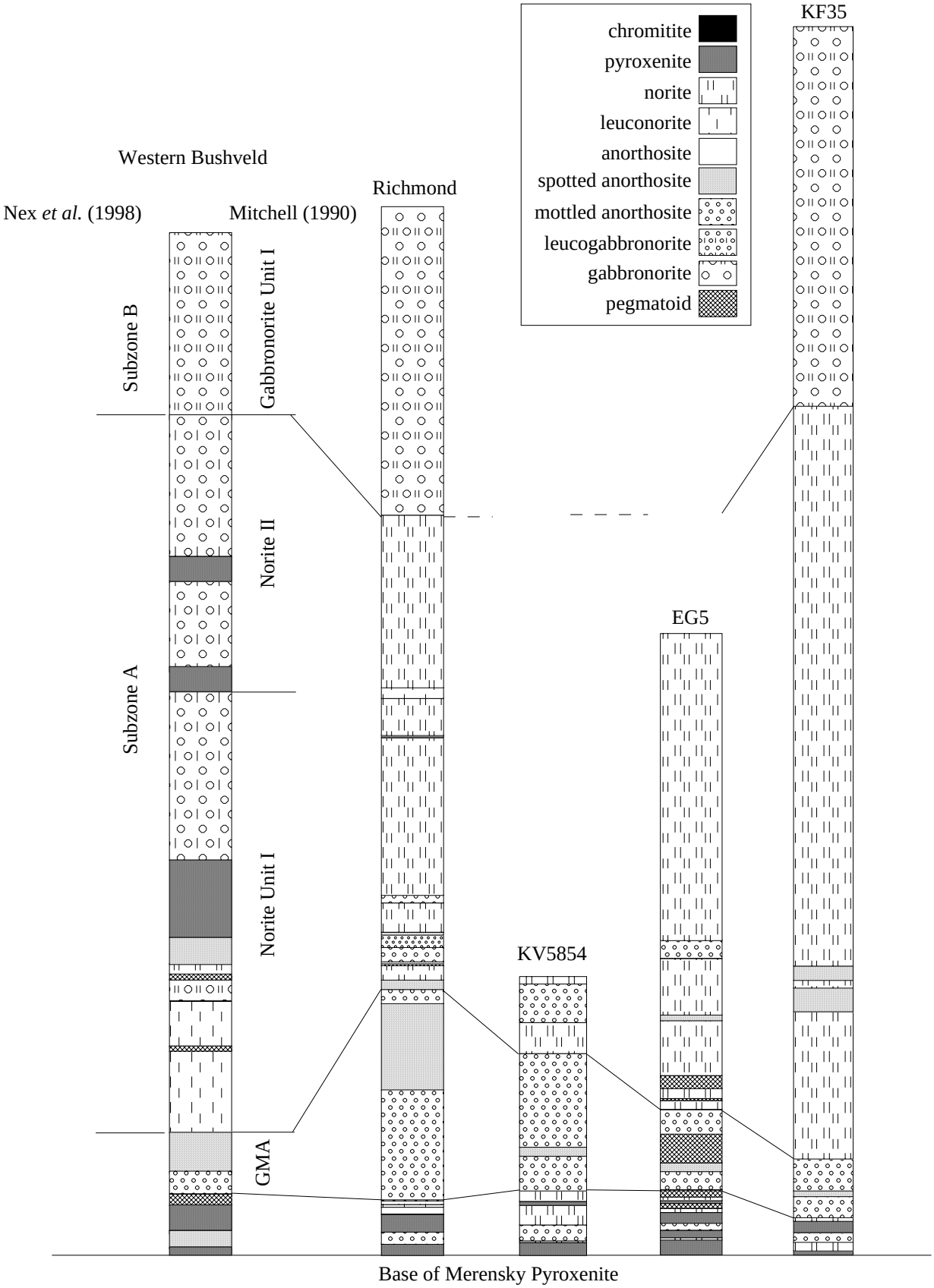


FIGURE 3.3 Stratigraphic comparison of the Main Zone in eastern Bushveld cores with those described by Mitchell (1990) and Nex *et al*. (1998) in the western Bushveld.

3.2 Comparisons between the eastern and western limbs

In the western Bushveld Complex, lithological and geochemical variations have been more clearly identified, due to the intensity of the mining operations that have allowed better access to the rocks, particularly those of the Upper Critical Zone. It should be noted that a much vaster database exists, in which detailed investigations into the mineralised succession have been recorded. Thus, there may be similar changes and patterns occurring in the eastern Bushveld, but are unnoticed as yet due to the paucity of information.

3.2.1 The Upper Critical Zone

Figure 3.4 shows typical stratigraphy of the Upper Critical Zone (including the Merensky and Bastard Cyclic Units) at locations in the western Bushveld. Harzburgitic layers are common and are known as pseudoreefs. At Amandelbult in the north-western Bushveld, two harzburgite layers are present (the Lower and Upper Pseudoreefs) and both are associated with thin chromitites. These are also present at Union Section in the north-western Bushveld. Gain (1985) describes harzburgites associated with the UG2 chromitites in the eastern Bushveld and a thin harzburgite layer is present at Richmond, as a parting in the UG2 pyroxenite. At Rustenburg Section and Impala distinct mottled anorthosite units are present in the UG2 Cyclic Unit, such as the Pioneer and Brakspruit markers at Rustenburg (Viljoen & Hieber 1986). In the eastern Bushveld, a thin anorthosite is present Kennedy's Vale, at approximately 160 m above the UG2, and the Richmond core includes four thin mottled anorthosites in the UG2 Cyclic Unit. However, elsewhere in the east, mottled anorthosites are largely absent from the UG2 to Merensky sequence.

Comparative thicknesses of units have been summarised in the northern and southern sectors of the western limb (table 3.2). The thickness of the UG2 in the western Bushveld is generally consistent, varying between 0.7 and 1.5 m thick. In all cases up to 3 thinner chromitite leaders are present. Three thin leaders are also present at Richmond in the eastern Bushveld, four at Atok (Mosson 1986), five to ten on Eerste Geluk, two on Maandagshoek (Gain 1985) and Kennedy's Vale, and one at Winterveld (Cameron 1982). The thicknesses of the UG2 chromitite in the western Bushveld are comparable with thicknesses recorded in the eastern Bushveld.

The thickness of the Merensky pyroxenite in the western Bushveld is both regionally and locally variable on a scale of a few centimetres to a few meters. It should be noted however, that the extent of potholing makes the thickness of the Merensky pyroxenite very irregular in many locations e.g. in the south-western Bushveld (Viljoen 1999), where rapid thinning of the pyroxenite occurs towards the edges of potholes (Viljoen *et al.* 1986a). Nevertheless, distinct changes in thickness of the Merensky pyroxenite do occur on a regional scale, whether potholing occurs or not (Viljoen 1999). Viljoen & Hieber (1986) described variations in thickness at Rustenburg Section, in the southern part of the western limb and noted that changes in thickness can occur laterally over short distances of a few meters. In the Paaderkraal area the widening of the pyroxenite to 1.5 m (Viljoen 1999) occurs much more steadily, over 3.5 km. Thickening of the pyroxenite also occurs towards the east (Brakspruit Section) of the mine and Viljoen & Hieber (1986) attributed this to part of a regional pattern of thickening towards the east, where the pyroxenite can be up to 12 m thick at Brits, 35 km away. However, Davey (1992) recorded a thickness of only 1-2 m at Marikana, between Rustenburg and Brits. Viljoen *et al.* 1986a discussed thickness variations of the pyroxenite at Union Section, in the northern part of the western limb. Here, the pyroxenite is approximately 1-2 m thick in the north-eastern part of the mine and becomes thicker, to over 7 m, in the south-eastern part. This is a distance of over 5 km. Davey (1992) also recorded a systematic variation in thickness of the pyroxenite, from 0.3 m in the northwest to 5.0 m in the southeast on Rooikoppies, in the Marikana area. Overall, the thicknesses of the Merensky pyroxenite in the western limb are comparable with those in the eastern limb. However, much variation is observed in both limbs. Insufficient data is available from the eastern Bushveld to determine whether systematic variations in thickness occur on a local scale. There appears to be little consistency in these variations in terms of geographic positions (tables 3.1 and 3.2).

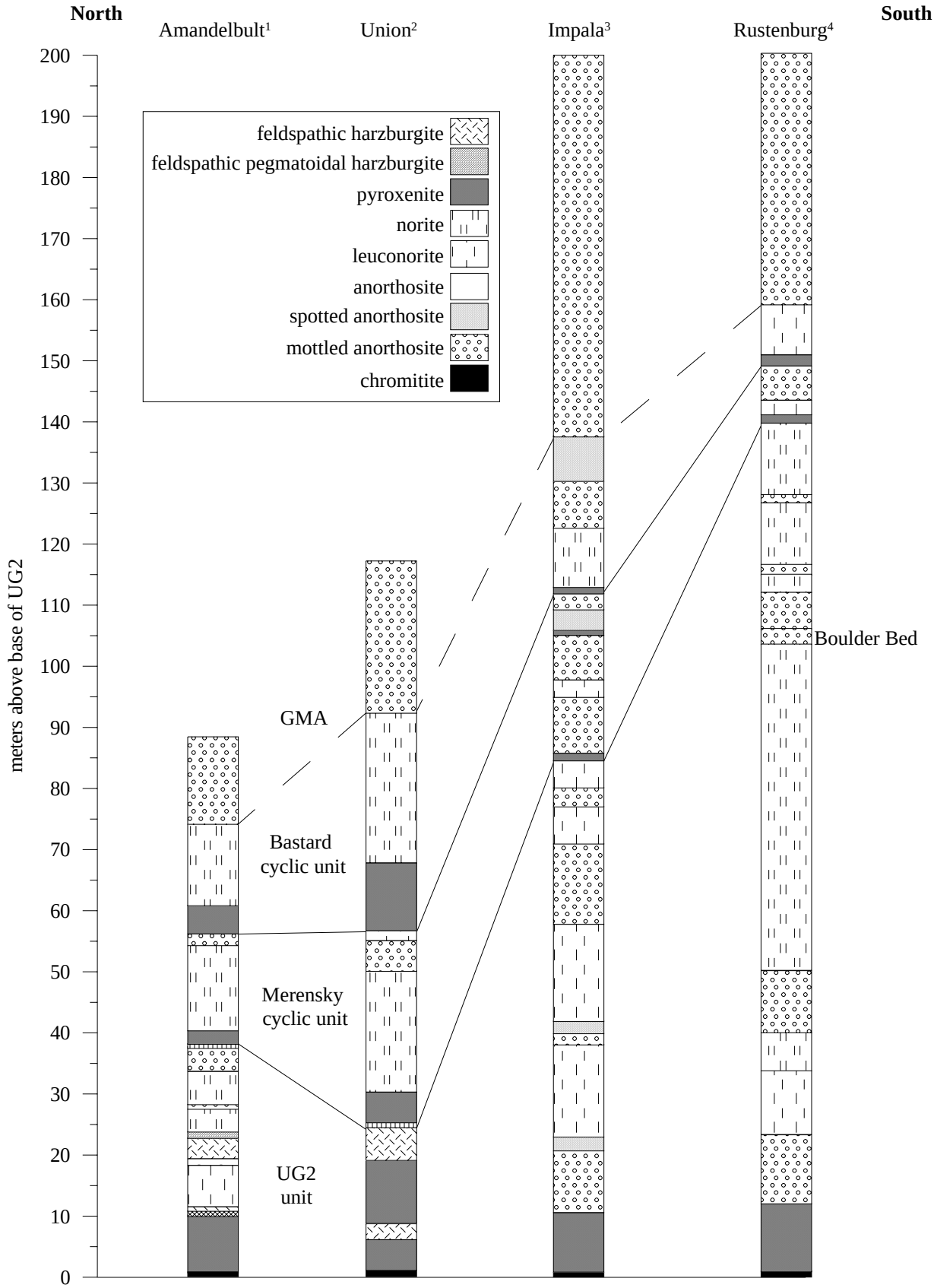


FIGURE 3.4 Correlation of cores in the western Bushveld Complex. [1] – Viljoen *et al.* (1986b), [2] – Viljoen *et al.* (1986a), [3] – Leeb-du Toit (1986), [4] – Viljoen & Hieber (1986)

Location	UG2 chromitite Thickness (m) (ref)	Merensky pyroxenite thickness (m) (ref)	UG2-Merensky thickness (m) (ref)
North			
Amandelbult	1.0 (4)	0-5.0 (4)	38 (4)
Union	0.78 (3)	≈1.0 – 7.0 (3,5)	≈20-30 (3,5)
Bafokeng Rasimone	0.3-1.4 (8)	1.2 (8)	-
Impala	0.8 (7,1)	1.4 (1)	100 (1)
Rustenburg	0.7 (2)	0-4.0 (2)	140 (2)
Marikana	0.8-1.5 (6)	1.0 – 2.0 (6)	95 -176 (5)
Brits	1.3 (7)	12.0 (2)	-
South			

TABLE 3.2 Thicknesses of units in the western Bushveld Complex.

1 - Leeb-du Toit (1986), 2 - Viljoen & Hieber (1986), 3 – Viljoen *et al.* (1986a), 4 – Viljoen *et al.* (1986b), 5 - de Klerk (1991), 6 – Davey (1992), 7 – Maier & Teigler (1995), 8 – Lomberg *et al.* (2004)

In the eastern Bushveld, the distance between the UG2 and the Merensky pyroxenite was shown to vary significantly across the Steelpoort lineament (Figure 3.2), being thicker in the central sector and thinner in the southern sector. In the western Bushveld, this sequence seems to become thicker towards the south. Table 3.2 shows that the UG2 – Merensky pyroxenite sequence is much thinner at Amandelbult and Union Section, 38 and 20-30 m respectively, than at Impala, Rustenburg and Marikana, where this interval is over 100 m. Most significantly however, the interval between the UG2 and the Merensky pyroxenite is, overall, much thicker in the eastern limb than the western limb. The average thickness in the east is 286 m and in the west it is 95 m (based on tables 3.1 and 3.2 respectively).

3.2.2 The Giant Mottled Anorthosite

The GMA has been studied in the western Bushveld. In this study, an attempt is made to correlate its detailed stratigraphy with the GMA in the eastern Bushveld. De Klerk (1995) subdivided the GMA in the western limb into three distinct parts. The Lower Giant Mottled Anorthosite (LGMA) is a mottled anorthosite with large, diffuse mottles. The Giant Mottled Middling (GMM) is a zone of mixed lithologies, comprising leuconorites and varitextured anorthosites. Some leuconorites may display subdued mottling. The Upper Giant Mottled Anorthosite (UGMA) is a layer in which the mottles are smaller and less distinct than those in the LGMA. Logs of the GMA are given in Figure 3.5 and show the correlation between cores from this study in the eastern Bushveld and a representative stratigraphic

column from the western Bushveld (de Klerk 1995). This diagram shows that there is a generally good correlation between eastern and western Bushveld, based on de Klerk's subdivision of the GMA. All of the four eastern Bushveld cores show three distinct units within the GMA. In each case, the bottom unit is a mottled anorthosite, which was noted to comprise larger mottles in RM15 and KV5854. This is consistent with the LGMA in the western Bushveld. Overlying this is a unit that comprises leuconorites, which sometimes also have mottles. This lithology is commonly known as varitextured. A few thin anorthosites are also present in this unit. This unit represents the lithologies of the GMM. The overlying unit is in almost every case another mottled anorthosite, in which mottles were recorded to be smaller in EG5 and KV5854. This agrees with de Klerk's observations of the UGMA in the west. However, in the KF35 core, this upper unit is a leuconorite, in which mottles are not present. Apart from this one exception, it is shown that the subdivisions of the GMA laid out by de Klerk (1995) can be readily correlated in the eastern Bushveld.

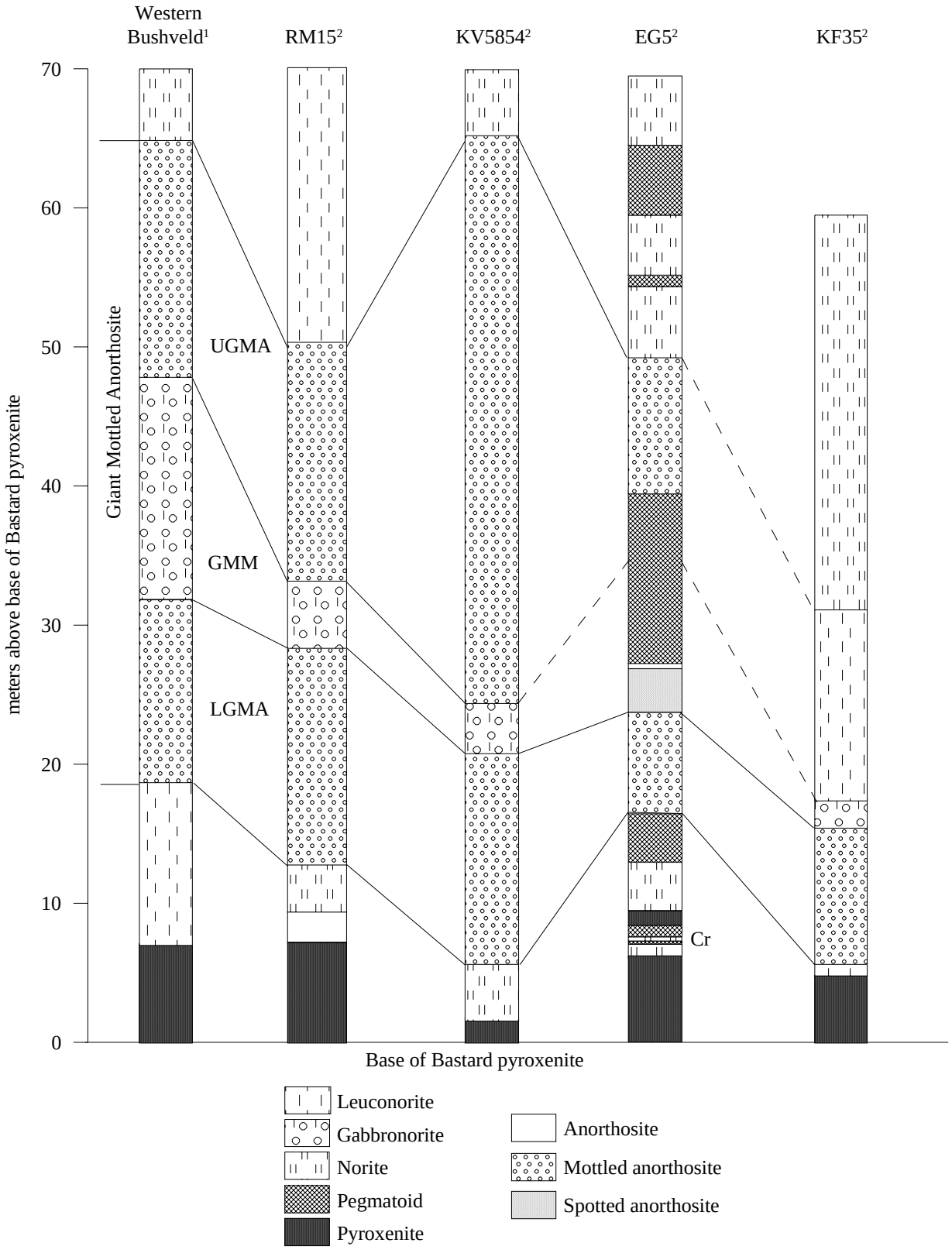


FIGURE 3.5 Stratigraphic comparison of the Giant Mottled Anorthosite between the western and eastern Bushveld. [1] – de Klerk (1995), [2] – This study.

3.2.3 The Lower Main Zone

The Main Zone in the western Bushveld has been studied more than in the east. This has led to the development of various classifications for rocks in the western Main Zone (Nex *et al*. 1998, Mitchell 1990) and it remains unclear as to whether these classifications can be correlated effectively with rocks in the eastern Bushveld Complex. The overall subdivisions of the Lower Main Zone are of interest in this study.

Although more investigations into Main Zone stratigraphy have been made in the western Bushveld, an early attempt at subdividing the Zone in the east was made by von Gruenewaldt (1973). He divided the Zone into subzones A, B and C. Subzone A being lowermost and comprising norites towards its base, but becoming predominantly gabbroic upwards, with pyroxenite and spotted and mottled anorthosites. He estimated this unit to be approximately 1,200 m thick. The South African Committee for Stratigraphy (SACS 1980) divided the Main Zone based on local lithologies and these units varied between the eastern and western Bushveld. Subsequent researchers have largely ignored these subdivisions. Mitchell (1990) described the lithologies of the Lower Main Zone at Union Section in the western Bushveld. He divided the Lower Main Zone into six units, based on lithology (Figure 3.3). Only the lower three of these, Norite Unit I, Norite Unit II and Gabbronorite Unit I will be discussed here, since they include the studied section. Mitchell described Norite Unit I as leuconoritic, with a general spotted appearance. Norite Unit II is 102 m thick and comprises norite with two coarse-grained feldspathic pyroxenite layers. Gabbronorite Unit I essentially comprises the Porphyritic Gabbronorite Marker, which grades upwards into a more equigranular fine- to medium-grained gabbronorite. Nex *et al.* (1998) revised these divisions creating a subzone A that essentially combined the Norite Units I and II of Mitchell and a subzone B that combined Mitchell's Gabbronorite Units I, II and III (Figure 3.3). Nex *et al*.'s divisions are based on the cumulus minerals present, with a cumulus mineralogy of plagioclase and orthopyroxene in subzone A and plagioclase, orthopyroxene and clinopyroxene in subzone B.

Figure 3.3 shows the logs of the boreholes in the eastern Bushveld from this study, as well as the log that Mitchell (1990) used to define his Main Zone units. This diagram shows that it is difficult to correlate the lowermost section of the Main Zone in the western Bushveld with that in the east, based

on Mitchell's classification. The section above the GMA in the eastern Bushveld is generally less homogeneous than Mitchell's section, with interlayering of mottled and varitextured anorthosites. Gabbronorites do not generally appear until higher up in the succession in the eastern Bushveld. The base of Norite Unit II is marked by the appearance of feldspathic pyroxenite. Pyroxenites are not common occurrences in the Main Zone, especially not ones as thick as those described by Mitchell (5.5 and 10 m thick). However, a 25 cm pyroxenite is present in RM15, and could potentially be correlated with the Lower Main Zone pyroxenites in the west, but it is more likely a local occurrence. Although Mitchell notes the occurrence of melanorites at this height from other areas of the Bushveld Complex, it is felt that these are not distinct enough in the eastern Bushveld to constitute a marker horizon. In this study, thin melanorites occur in RM15 (0.67 and 0.32 m thick) and in KF35 (2 m thick), but are completely absent at Eerste Geluk and Kennedy's Vale. This suggests that the pyroxenite/melanorite layer is not laterally consistent in the eastern Bushveld and should thus not be used as a boundary marker. Using subzone A of Nex *et al.* (1998), by combining Norite Units I and II, means that the presence of a pyroxenite marker layer is unnecessary. However, the base of Gabbronorite Unit I coincides with the first appearance of clinopyroxene at the Porphyritic Gabbronorite Marker layer. This can be correlated easily in the eastern Bushveld and in this study is identified on Richmond and Klipfontein. This is also the location of the base of Nex *et al.*'s subzone B. It is clear that the lithologies of the Lower Main Zone in the eastern Bushveld are easier to correlate with the western Bushveld (and each other) using the subdivisions of Nex *et al*. Identification of position in stratigraphy is made easier by the use of mineralogy to classify zones, making location in the field much easier.

3.3 Summary and implications of lithological variations

In summary the key differences between the central and southern sectors in the eastern Bushveld are as follows:

- The thicker UG2 – Merensky pyroxenite sequence in the central sector
- The presence of the UG3 in the central sector only
- The thicker Merensky pyroxenite in the central sector
- The thinner GMA in the central sector

In addition, there may be a relationship between the thickness of the Merensky pyroxenite and the Bastard pyroxenite whereby one is thinner where the other is thicker.

The main points of comparison in the Upper Critical and Lower Main Zones between the eastern and western Bushveld are:

- The similar thicknesses of both the UG2 chromitite and the Merensky pyroxenite
- The thicker interval between the UG2 and Merensky pyroxenite in the eastern Bushveld
- The three-fold subdivision of the GMA (de Klerk 1995) can be applied in the eastern Bushveld as well as the west
- The Lower Main Zone of the eastern Bushveld can be subdivided into subzones A and B, based on Nex *et al*. (1998)

The interval UG2 to Merensky pyroxenite in the central sector of the eastern Bushveld clearly contains a greater volume of rock than the southern sector. One of two possible conclusions can be drawn to explain this. Either more magma was intruded into the central sector at this height in the Complex, or magma or rock was removed from the southern sector. If the former is true, then this might imply that the Steelpoort lineament acted as a structural control on magma chamber dynamics by restricting magma movement between the central and southern sectors. If the latter is true, a mechanism to explain

this preferential erosion in the southern sector would have to be determined. The unconformity at the base of the Merensky pyroxenite is a well-known feature (e.g. Vermaak 1976, Viljoen *et al*. 1986a, 1986b, Viljoen & Heiber 1986, Leeb-du Toit, 1986, Mossom 1986, Eales *et al*. 1988) and some erosion is thought to have occurred throughout the Bushveld Complex (Kruger 1990). It is possible that the extent of this unconformity was far greater in the southern sector of the eastern Bushveld than in the central sector.

Kruger (*in press*) proposed that the Bushveld magmas entered the chamber at different locations and from different directions. The increased thickness of the Upper Critical Zone magma immediately to the south of the Thabazimbi-Murchison Lineament (TML) (Figure 1.1) has led Kruger (*in press*) to conclude that this magma was intruded at or close to the TML, which formed half-graben geometry. Cawthorn (2002) also indicated that plagioclase grains were transported laterally towards the southeast in the western limb. Stratigraphic relationships, such as the Critical Zone extending over the Lower Zone and onlapping onto the floor in the southern sector of the eastern Bushveld, imply that this magma intruded southwards. These observations are supported by the stratigraphic comparisons made in this study, where the Upper Critical Zone rocks, from the level of the UG2, are much thicker in the central sector than in the southern sector of the eastern Bushveld. The Steelpoort lineament may have acted as a barrier that impeded flow of magma flowing southwards, as suggested by the thinner UG2-Merensky pyroxenite sequence in the southern sector (Figure 3.6A).

In addition, the UG3 Cyclic Unit, that may represent an additional pulse of magma, is only present in the central sector. This might indicate that this additional magma influx was intruded from the north did not reach the southern limb, either because it was blocked by the Steelpoort lineament, or there was not sufficient magma to travel further south (Figure 3.6A). However, since the UG3 is not found in the western Bushveld, it would suggest that an additional magma impulse only occurred in the north-eastern sector. However, Hornsey (2004) described the UG2 at Two Rivers, near Dwars River, south of the Steelpoort lineament. He recorded that the UG2 was characterised by intraformational discontinuities with locally preserved remnants of silicate sequences. In addition, he showed that metallogeny, total PGE grade and host silicate stratigraphy indicates that the upper section of the UG2 correlates directly with the UG3 north of the Steelpoort lineament. Cawthorn (2004) proposed that the

UG3 merged with the UG2 in the south eastern sector and that the UG3-forming event occurred everywhere in the Bushveld (Figure 3.6B). He attributed the merging of the UG3 and UG2 to either non-deposition of the intervening silicates in the southeast or to erosion of that unit.

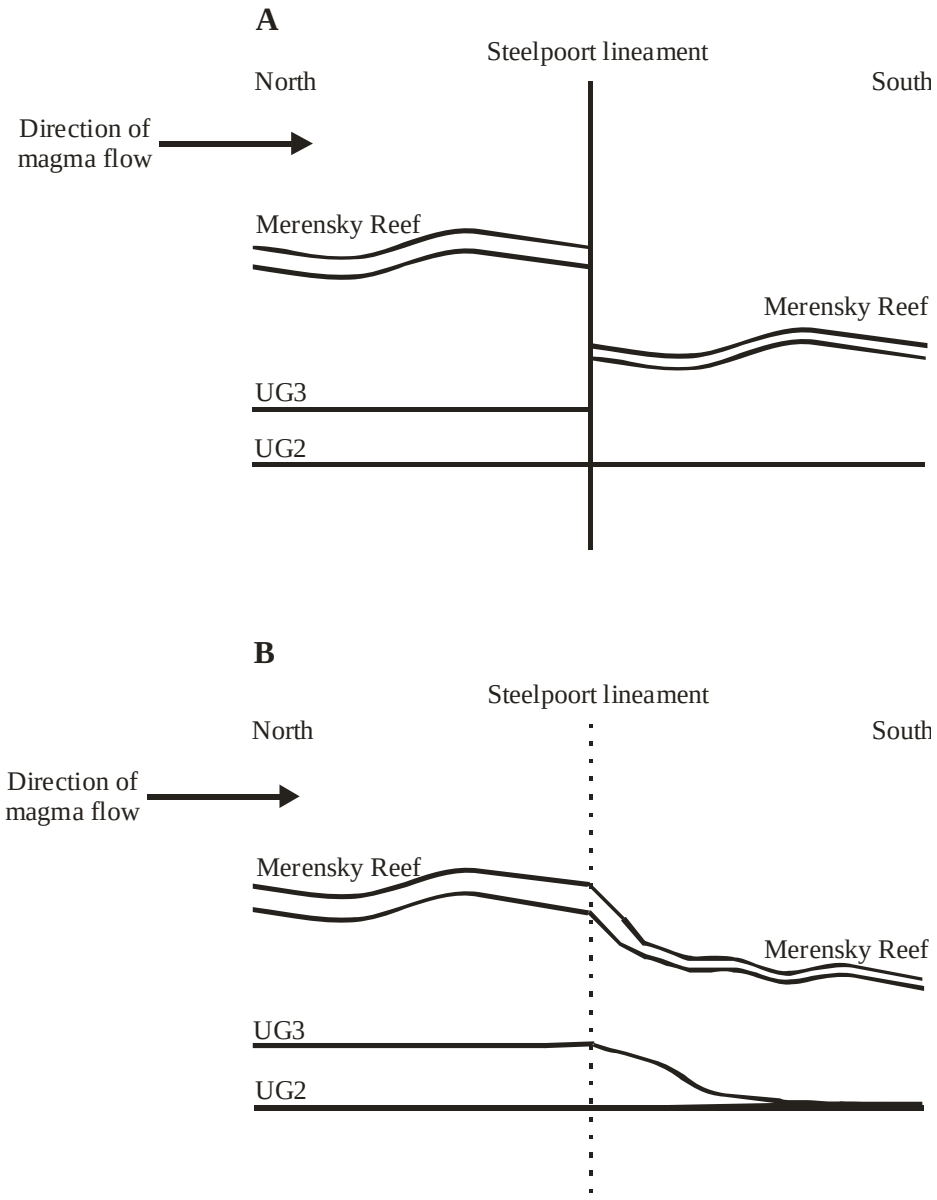


FIGURE 3.6 Schematic diagram (not to scale) showing A) the Steelpoort lineament acting as a barrier to magma flow, resulting in no deposition of the UG3 in the southern sector of the eastern Bushveld Complex and a thinner UG2 – Merensky package and B) the merging of the UG3 with the UG2 and the thinning of the UG2 – Merensky package and the Merensky Reef over the Steelpoort lineament.

Cawthorn (2004) indicated that erosion was unlikely due to the extent of the necessary erosion and that the UG2 is apparently undisturbed. However, he accepted that extensive non-deposition, where huge sections of the magma chamber undergo no crystallisation while accumulation is occurring elsewhere,

is not easy to explain either. The merging of the UG3 with the UG2 in the south-eastern sector also correlates with the thinner UG2-Merensky sequence in this sector. Whether the Steelpoort lineament had any control over the non-deposition and bifurcation of these layers it not apparent from this stratigraphic analysis, but it remains clear that variations across it are not consistent with it being a simple fault system

Eales *et al*. (1988) suggested the distance from a feeder influences lithological and geochemical differences in the western Bushveld. They proposed that where fewer plagioclase cumulates are present in the Upper Critical Zone, it represents a "proximal" facies e.g. at Union Section, and where the cumulates are thicker it is a "distal" facies. Scoon & Teigler (1995) correlated the central sector of the eastern limb with the proximal facies of Eales *et al*. (1988) and correlated the southern sector with the distal facies and also suggested that magma flow was from the central towards the southern sector in the eastern Bushveld. Maier & Teigler (1995) described ultramafic and chromitite-rich cumulates from the western Bushveld that have geochemistry typical of a more primitive magma. These cumulates should be more abundant in proximal facies. If the central sector represents proximal facies in the eastern Bushveld (Scoon & Teigler 1995) then these cumulates should contain more chromitite than the distal, southern sector. This is not supported in the southern sector of the eastern Bushveld, where the Upper Critical Zone has more chromitites than in the central sector. Thus, the facies model appears to be incompatible in the eastern Bushveld.

Chapter 4

Petrography

Processes that operated subsequent to crystallisation of minerals from the melt are likely to have affected individual grains so that interpretations based on textural features alone may be inaccurate. Nevertheless, textural features can be very informative and distinctive throughout the Bushveld Complex, both laterally and stratigraphically. Thus, petrographic descriptions can be used to distinguish layers and units and aid stratigraphic comparisons. Previous petrographic examinations of the studied stratigraphy have focused largely on the Merensky Reef. Leeb-du Toit (1986), Cawthorn (1999a) and Barnes & Maier (2002) provided detailed petrographic descriptions of the Merensky Reef at Impala Platinum Mines. Kruger & Marsh (1985) described the petrography of the Boulder unit and the Merensky Cyclic Unit at Rustenburg, whereas Nicholson & Mathez (1991) focused on the Merensky Reef in that area. Mitchell (1990) and Mitchell *et al.* (1998) provided petrographic descriptions of rocks from the Main Zone and de Klerk (1995) described textures in the Giant Mottled Anorthosite of the western Bushveld.

4.1 Nomenclature

The majority of the rock types analysed and discussed in this study comprise variable proportions of orthopyroxene, plagioclase and clinopyroxene. Estimates of mode at low abundances may be inaccurate due to heterogeneity in the rock. A thin section made from a piece of core may not reflect the true distribution of the minerals, which makes visual estimates of mineral proportions unreliable. Instead, chemical analyses can be used. Thus, the linear variation between orthopyroxenite and anorthosite can be subdivided based on the proportions of Al_2O_3 and MgO in the rock (Eales *et al*. 1988). The modal ranges encompassed for the different rock types, as used in this study, are shown in Figure 4.1. For the purposes of this study approximate subdivisions are summarised in table 4.1. These ranges are shown on Figure 4.1. Gabbronorites plot below the orthopyroxene-plagioclase tie-line, towards clinopyroxene.

Rock type	Approximate modal proportions		% MgO	% Al_2O_3
	% plagioclase	% orthopyroxene		
Anorthosite	90-100	0-10	<4	>27
Leuconorite	80-90	10-20	2.5-7	24-27
Norite	40-80	20-60	7-17	16-24
Gabbronorite	55-75	25-45 (opx+cpx)	6-10	16-24
Melanorite	30-40	60-70	17-20	10-13
Feldspathic pyroxenite	10-30	70-100	>20	3-10

TABLE 4.1 Modal proportions of plagioclase and orthopyroxene and corresponding MgO and Al_2O_3 content

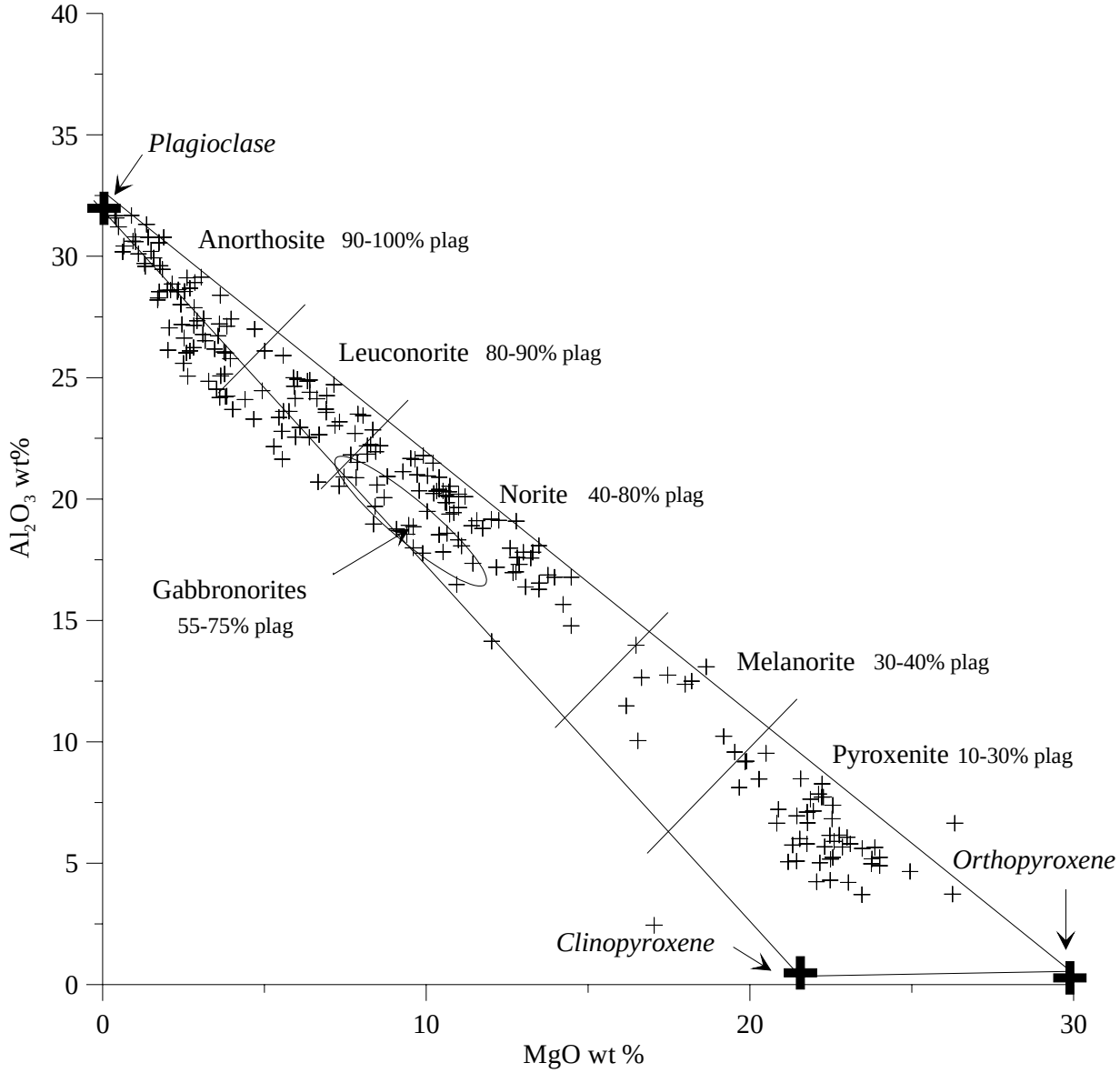


FIGURE 4.1 Graph of whole-rock Al_2O_3 plotted against MgO for all cores analysed showing modal ranges for rock types used in this study.

4.2 Anorthosite

Anorthosites containing 100% plagioclase are uncommon in the Upper Critical and Lower Main Zones where they normally display “mottles” and/or “spots” of orthopyroxene. Plagioclase is typically subhedral-anhedral and 0.5-2 mm in size, although some grains can be up to 4 mm in size, and generally displays a granular, interlocking texture. Some crystals have serrated edges where grains boundaries interdigitate. Grains of subhedral plagioclase infill spaces between larger grains. In addition, in some areas, polygonal grains shapes are present. No zoning of plagioclase is observed. Small grains of intercumulus clinopyroxene are rarely present.

Mottled anorthosites contain approximately 90% plagioclase with the remaining 10% comprising interstitial, optically continuous (over distances of up to 10 cm in the GMA) orthopyroxene and/or clinopyroxene that give rise to the mottled texture. These poikilitic mottles (Figure 4.2a) range in size, smaller mottles are typically 0.5-1.5 cm, but mottles that are 10 cm or larger are found in the GMA. The plagioclase chadacrysts are generally smaller (<1 mm) than grains that are not enclosed and are predominantly euhedral. Plagioclase inclusions do not display any preferred orientation. Orthopyroxene mottles frequently contain augite exsolution lamellae.

Spotted anorthosites contain euhedral orthopyroxene “spots” (typically 0.5-2 mm) that occur as single isolated intercumulus grains between plagioclase. This texture and can be confused with leuconorites, where orthopyroxene is cumulus, but spotted anorthosites generally contain less orthopyroxene. Varitextured anorthosites contain 10-20% euhedral orthopyroxene and intercumulus orthopyroxene mottles.

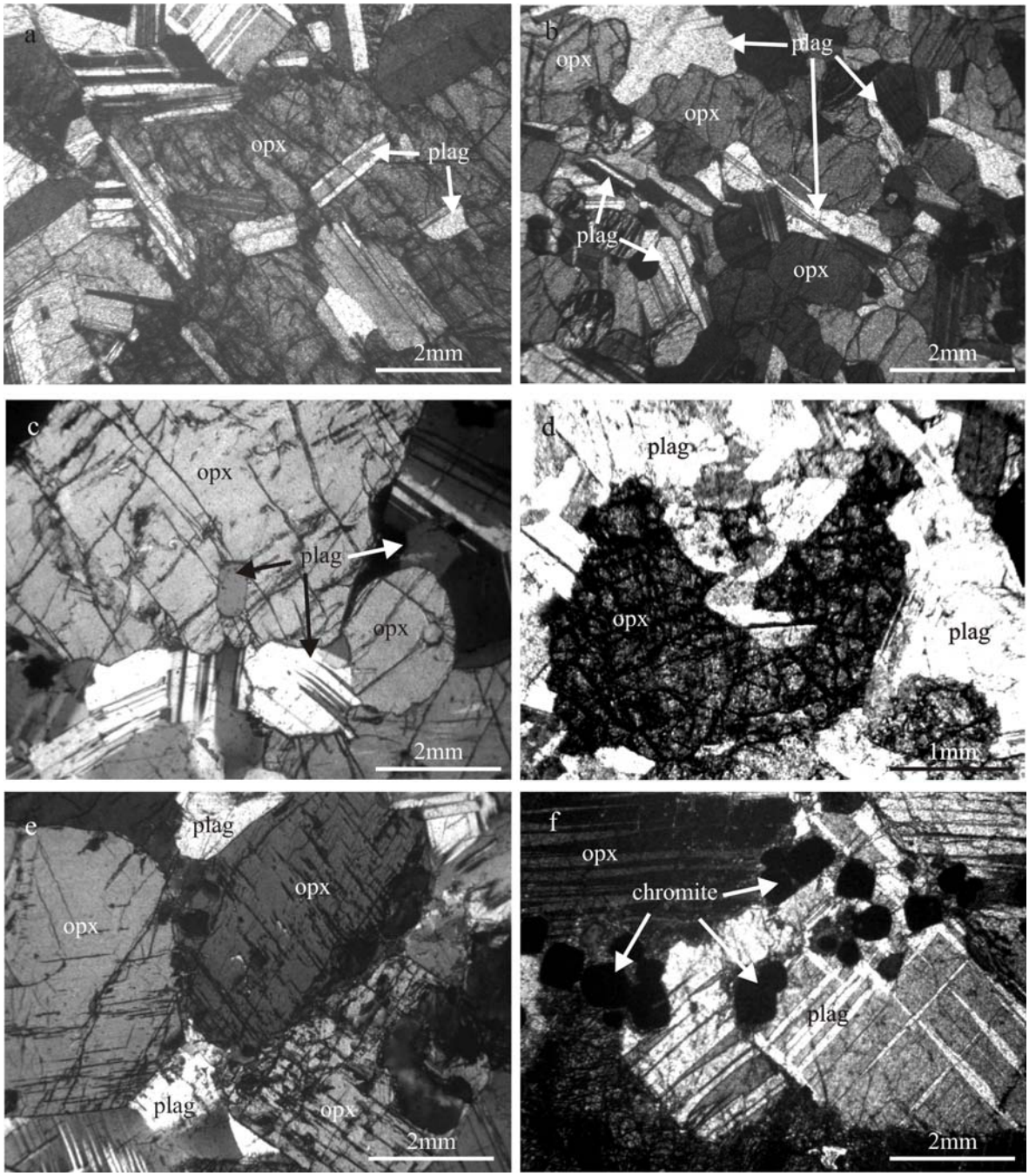


FIGURE 4.2 Photomicrographs in crossed polarised light of (a) poikilitic orthopyroxene enclosing plagioclase grains in mottled anorthosite, (b) typical norite showing rounded orthopyroxene and subhedral plagioclase, (c) orthopyroxene grain with euhedral plagioclase inclusion and subhedral plagioclase grains, (d) Plagioclase-filled embayment in orthopyroxene in norite, (e) euhedral orthopyroxene in orthopyroxenite, (f) small disseminated grains of chromite at the base of the Merensky pyroxenite.
opx – orthopyroxene, plag – plagioclase.

4.3 Norite

Norites and leuconorites consist of plagioclase and orthopyroxene, with minor clinopyroxene and accessory biotite typically comprising less than 1% of the rock. Figure 4.2b shows the texture of a typical norite. Plagioclase varies texturally, but is predominantly subhedral and <2 mm in length. Some grains are unusually elongate and can extend up to 5 mm in length. Small (<0.5 mm) rounded grains are also apparent. No zoning was observed. Plagioclase also displays interstitial textures, growing around euhedral orthopyroxene grains and as small (<0.5 mm) crystals with highly irregular boundaries. Some plagioclase grains show extensive crystal overgrowths. In addition, bending of plagioclase twins suggests some post-crystallisation deformation.

In this study, rocks described as fine-grained norites contain orthopyroxene grains that are <1 mm in size. Medium-grained norites typically comprise orthopyroxene grains of 2-6 mm. In both fine- and medium-grained norites, plagioclase can comprise a range of sizes. In coarse-grained rocks, only observed here as pegmatoidal units, grain-size of both plagioclase and orthopyroxene is typically >10 mm. Few rocks contain orthopyroxene grains that fall in the 6-10 mm size range.

The majority of norites are medium-grained, where orthopyroxene typically occurs as subhedral grains, approximately 2-6 mm in size and sometimes contains thin exsolution lamellae of augite. Inclusions of one or two small (<0.5 mm) grains of equant plagioclase are common (Figure 4.2c), but poikilitic textures as observed in anorthosites do not occur. No preferential orientation of these inclusions is apparent. Some small, touching orthopyroxene crystals appear to have been recrystallised and joined together to form one optically continuous crystal in which the original grains are still apparent. Embayments are also common in orthopyroxene (Figure 4.2d). Clinopyroxene is present as small, irregularly shaped grains.

Fine-grained norites contain small orthopyroxene grains (<1 mm in size) and slightly larger plagioclase grains of <2 mm in size, but plagioclase phenocrysts can be as large as 6 mm.

Gabbronorites contain euhedral medium-grained plagioclase (1 mm), but some grains can be up to 3 mm. Subhedral orthopyroxene is 1-3 mm in size and clinopyroxene occurs as either smaller (0.5-2 mm) subhedral grains, elongate lath-like porphyritic grains (3-8 mm long) or infrequently, as small interstitial grains with highly irregular boundaries. Rarely, elongate clinopyroxene grains develop an

indistinct fabric. Typically, the Porphyritic Gabbronorite Marker contains 60% plagioclase, 20% orthopyroxene and 20% clinopyroxene. Approximately half of the clinopyroxene grains are elongated and porphyritic, with the other half comprising small interstitial grains. Orthopyroxene is medium-grained and phenocrysts that are observed in this layer in other parts of the intrusion (Mitchell *et al.* 1998, Leeb-du Toit 1986, Eales & Cawthorn 1996) are not seen here. However, only the lowermost few meters were sampled, and Leeb-du Toit (1986) recorded that phenocrysts are smaller, around 3 mm, in this lower section of the unit.

4.4 Feldspathic orthopyroxenite

The modal proportions of plagioclase and orthopyroxene in feldspathic orthopyroxenite are shown in table 4.1. Minor clinopyroxene, chromite and sulphides (<1%) are also present. Feldspathic orthopyroxenites consist of granular subhedral-euhedral orthopyroxene of grain size 1-6 mm (Figure 4.2e). Orthopyroxene grains frequently enclose small, 1 mm equant plagioclase grains, some of which are occasionally rimmed by clinopyroxene. Orthopyroxene commonly contains exsolution lamellae of augite. Plagioclase occurs as irregular grains that are typically 1-4 mm in size, but can be up to 12 mm. The large central areas of these larger grains may represent overgrowth of plagioclase around a cumulus core. Interstitial clinopyroxene occurs as large (5-8 mm) anhedral oikocrysts, with small (1-2 mm) inclusions of subhedral plagioclase. Some smaller (1-3 mm) grains of interstitial clinopyroxene also occur. Sulphides mainly occur interstitial to the silicates. Small amounts of sulphides occur as highly irregular-shaped inclusions in the interstitial plagioclase.

The Merensky feldspathic orthopyroxenite is typically medium-grained, but in some cores a pegmoidal part of the pyroxenite is present at the base. This coarse-grained feldspathic orthopyroxenite contains euhedral orthopyroxene grains of approximately 1 cm in size and irregular anhedral plagioclase that frequently exceed 1 cm. The Bastard feldspathic pyroxenite is not generally associated with any pegmatoidal material.

4.5 Chromitites and chromite

Visual estimation of modal proportion of chromitites indicates that they comprise approximately 90% cumulus chromite and 10% poikilitic orthopyroxene (in the Merensky chromitite) or plagioclase (in the UG2 chromitite). Chromite grains are small (<0.5 mm) subhedral and densely packed. Triple-point junctions are common and occur within larger chromite grains (>1 mm) where polygonal grains shapes are perfectly developed. Orthopyroxene grains are subhedral, approximately 1-2 mm in size and contain inclusions of small chromite grains. Some interstitial plagioclase also occurs.

Chromite also occurs in the sampled sequence as disseminated and thin layers of only one or two grains thick. In each case, the chromite grains are small (<0.5 mm) and rounded (Figure 4.2f). Thin chromite layers often occur at boundaries between footwall norite/anorthosite and the Merensky and Bastard pyroxenites e.g. in core RM15 or at the upper contact of the Merensky pyroxenite e.g. in core KV5854 and disseminated chromite grains often occur in the pyroxenite as inclusions in orthopyroxene and plagioclase (Figure 4.2f). Chromite grains also occur at grain boundaries, surrounding a specific crystal.

4.6 Recrystallisation processes

Recrystallisation, for example by annealing, results in textural equilibration and changes in grain shape (Hunter 1996) and thus post-cumulus processes become superimposed on initial textural features. McBirney & Hunter (1995) suggested that the terms *adcumulate* and *orthocumulate* should not be applied to a rock that has crystallised in an open-system where non-cumulus processes might have occurred, such as the Merensky and Bastard Cyclic Units in the Bushveld Complex. As well as contamination from wall/roof rocks which would not prevent the formation of adcumulates, these processes include percolation of residual liquid or metasomatic processes that might have involved extensive modification and even complete replacement of textures. With specific reference to the Merensky and Bastard pyroxenites, Mathez *et al.* (1997) suggested that textures (and mineral compositions) indicated hydration partial melting and recrystallisation of the two pyroxenites. This was based on the presence of pegmatoidal material, phlogopite and hornblende which they interpreted to indicate the accumulation of hydrated interstitial melt and irregular, discontinuous masses of Cr which

is stabilised relative to other phases by the introduction of water. McBirney & Hunter (1995) suggested that the origins of these rocks cannot be established using only textural features, a fact that was reiterated by Morse (1998). The cumulus and interstitial nature of minerals in some layers is discussed in Chapter 6.

Some of the textures described in this chapter suggest that post-cumulus recrystallisation has been a significant process in the Upper Critical and Lower Main Zones of the Bushveld Complex. Polygonal grains shapes in anorthosites and the development of triple-point junctions, such as those in chromitites, indicate that annealing has occurred and granular textures in plagioclase suggest textural equilibration. Annealing textures are indicative of extensive recrystallisation, which makes it impossible to base interpretations of these rocks on textural features alone. However, a number of features may be more indicative of original textures prior to recrystallisation. For example, Teigler & Eales (1996) observed that chromite grains encapsulated in orthopyroxene oikocrysts occurred as small euhedral crystals and were not annealed, thus they suggested that this encapsulation protected the grains from post-cumulus annealing processes. Eales *et al.* (1991) suggested that the enclosure of bladed or lath-like plagioclase crystals in orthopyroxene implies early crystallisation of plagioclase within the melt, or cotectic crystallisation with pyroxene, although the embayed plagioclase inclusions in orthopyroxene that Eales *et al.* described are not observed here. Thus, inclusions of plagioclase within poikilitic pyroxenes may represent original cumulus grains that have not been recrystallised. In this case, original grain sizes would have been much smaller than the typical grain size observed in the rocks now.

Chapter 5

Geochemistry

207 core samples, typically 20 cm in length, listed in appendix I, were analysed for whole-rock major and trace element composition by X-ray fluorescence spectrometry (XRF) using facilities at the School of Geosciences, University of the Witwatersrand, Johannesburg. Instrument information and analytical techniques are given in appendix II. Samples were analysed for the following oxides and elements:

Major element oxides (wt%): SiO_2, TiO_2, Al_2O_3, total Fe as Fe_2O_3, MnO, MgO, CaO, Na_2O, K_2O, P_2O_5 and Loss on Ignition (LOI).

Trace elements (ppm): Rb, Sr, Y, Zr, Nb, Co, Ni, Cu, Zn, V, Cr and Ba

Mineral separates of plagioclase, orthopyroxene and clinopyroxene were obtained from all samples where modal proportions allowed. Separation was performed using a Franz magnetic separator at the School of Geosciences, University of the Witwatersrand, based on the varying magnetic susceptibilities of the constituent minerals. Further details of the process are given in appendix II. The mineral separates were analysed by XRF for major element oxides and trace elements. In order to obtain greater precision on the Cr and Ni contents of orthopyroxene than possible by electron microprobe, we have prepared mineral separates and analysed Cr and Ni as a trace element, yielding a precision of better than 12 ppm. Lower detection limits are also given in Appendix II. Electron microprobe data from Schürmann (1993) shows that there is considerable random variation of Cr content in single grains of orthopyroxene (Figure 5.1). Multiple analyses of individual grains showed that a wide range of results were obtainable for Cr_2O_3. Typical results show variations of 0.14 wt% Cr_2O_3 within a single orthopyroxene, but variations of up to 0.28 wt% were also recorded (sample IWS10, 0.22 - 0.50 wt% Cr_2O_3). Thus, using bulk orthopyroxene separates from individual layers gives a much better indication of orthopyroxene composition in that layer,

by averaging the inconsistencies observed in probe data. However, it is possible that the orthopyroxene separates contain chromite inclusions, which would affect the apparent Cr contents. For further comparison, table 5.1 shows average probe data from the Merensky and Bastard pyroxenites (Kruger & Marsh, 1985). This is compared with the average XRF data obtained from orthopyroxene separates in this study from the same layers. It shows that Cr/MgO ratios are similar, which suggests that there is no Cr enrichment in the separates. Where there are inclusions of chromite within orthopyroxene grains, these samples are immediately recognised by their anomalous Cr content e.g. in the Merensky pyroxenite (appendix IV), and are excluded from calculations and interpretations. Cr/MgO ratios will be discussed in detail later. There are relatively few probe and mineral separate data of orthopyroxene, compared to whole-rock data, available from the Bushveld Complex as a whole.

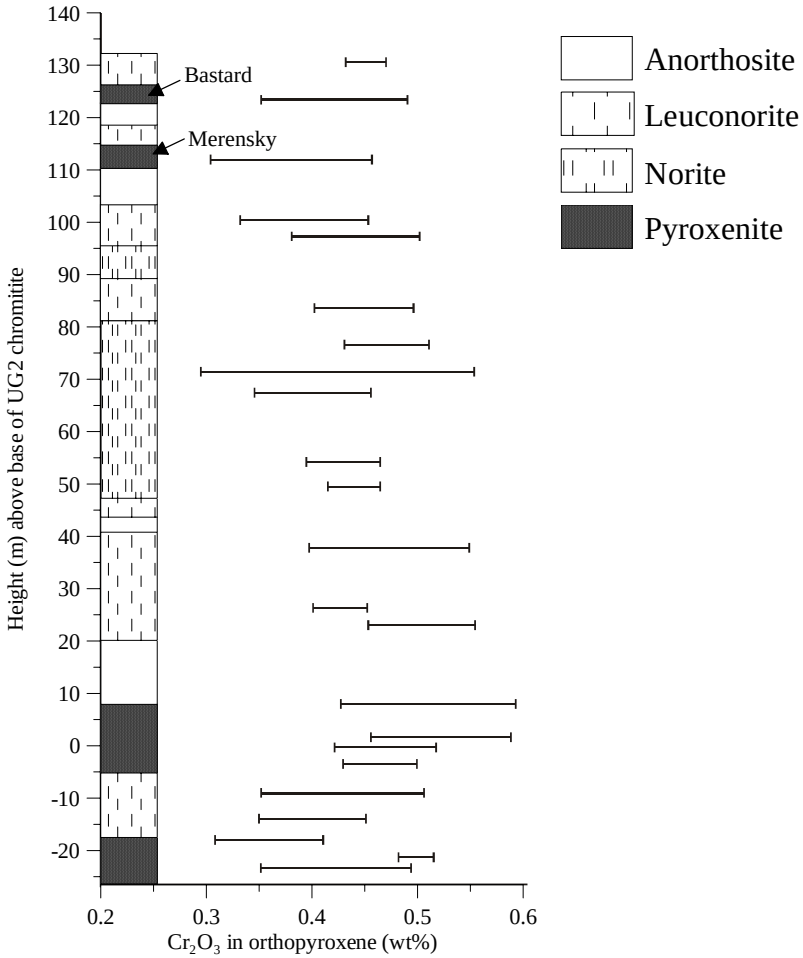


FIGURE 5.1 Graph showing extent of variation of Cr_2O_3 content in single orthopyroxene grains, based on analyses by Schürmann (1993).

Method	Merensky pyroxenite			Bastard pyroxenite		
	Cr (ppm)	MgO (wt%)	Cr/MgO	Cr (ppm)	MgO (wt%)	Cr/MgO
Probe*	3100	27.13	114	2870	28.67	100
XRF Separates†	3385	28.65	118	2940	27.67	106

TABLE 5.1 Average probe and XRF separates data from the Merensky and Bastard pyroxenites, showing that the two methods give comparable results.

* Average data from Kruger & Marsh (1985),

† Average data from this study excluding samples containing Cr inclusions shown by elevated Cr

Strontium isotope analyses by mass spectrometry were performed on plagioclase mineral separates from two profiles (RM15 and KF35) through the Upper Critical Zone into the lower Main Zone, with detailed studies of the Merensky and Bastard Cyclic Units. Analyses were performed on a total of 43 samples of pure hand-picked plagioclase from bulk mineral separates consisting of approximately 20 cm sections. 1 sample of clinopyroxene was also analysed. All samples are back corrected for an initial age of 2050 ± 25 Ma (Walraven *et al.* 1990). Details of this method and calculations are given in appendix II.

Sulphur (wt%) was determined from a total of 40 samples through the Merensky pyroxenite from the cores RM15 (19 samples) and KV5854 (21 samples). Sulphur analyses were conducted using a Leco infrared sulphur analyser at the School of Geosciences, University of the Witwatersrand (appendix II).

5.1 Whole-rock chemistry

Whole-rock major element oxides and trace elements data are presented in appendix III.

5.1.1 Major element variations

In this study, whole-rock major element variations are controlled by modal proportion of minerals in the rock. This is demonstrated by plotting major element oxides against MgO and is shown in Figures 5.2, 5.3, 5.4 and 5.5, for samples from Richmond, Kennedy's Vale, Eerste Geluk and Klipfontein respectively. In the latter profile, data from Blumberg's honours thesis (Blumberg 2002) has been combined with data obtained in this study. In general, positive correlations with MgO are observed for SiO_2, Fe_2O_3, TiO_2 and MnO and negative correlations for Al_2O_3, CaO, Na_2O and K_2O. Negative correlations with MgO are controlled by the abundance and chemical composition of plagioclase in the rock. Pyroxenites and anorthosites plot at the endpoints, plagioclase at 0% MgO and 30% Al_2O_3 and orthopyroxene at 1% Al_2O_3 and 30% MgO. Similarly, the partitioning of trace elements into orthopyroxene controls positive correlations. Variations in modal proportion of plagioclase and orthopyroxene define a line between anorthosite and pyroxenite. A notable break (MgO 12 – 17 wt %) between norites and pyroxenites occurs in each core (Figure 4.1) which reflects the lack of melanorites in the studied sections. TiO_2 and K_2O are only found in low concentrations in the rocks. They have low partition coefficients into the major cumulus minerals and thus largely reflect accessory phases. TiO_2 does occur in trace amounts in orthopyroxene [partition coefficient (D) of Ti = 0.1, and 0.4 for clinopyroxene (Rollinson 1993, and references therein)]. K_2O has a small partition coefficient into plagioclase, but elevated concentrations of this element (>0.11 wt%) might represent the presence of small quantities of orthoclase in the rock, or possible effects of trapped liquid.

Differences in major element geochemistry are apparent between Critical and Main Zone samples. There are no rocks with >17% MgO in the Main Zone, which reflects the absence of pyroxenites. Element ratios are different between the two zones. This is most obvious in Figure 5.2, where the Main Zone has been more densely sampled. At a given MgO content, the Main Zone samples contain generally higher

SiO_2, Fe_2O_3, TiO_2 and MnO, and slightly lower Al_2O_3 and CaO content than the Critical Zone samples. For Na_2O and K_2O, Main Zone samples have slightly higher concentrations. Major elements have not been plotted against stratigraphic height as these diagrams only reflect the gross mineralogy of the rock types.

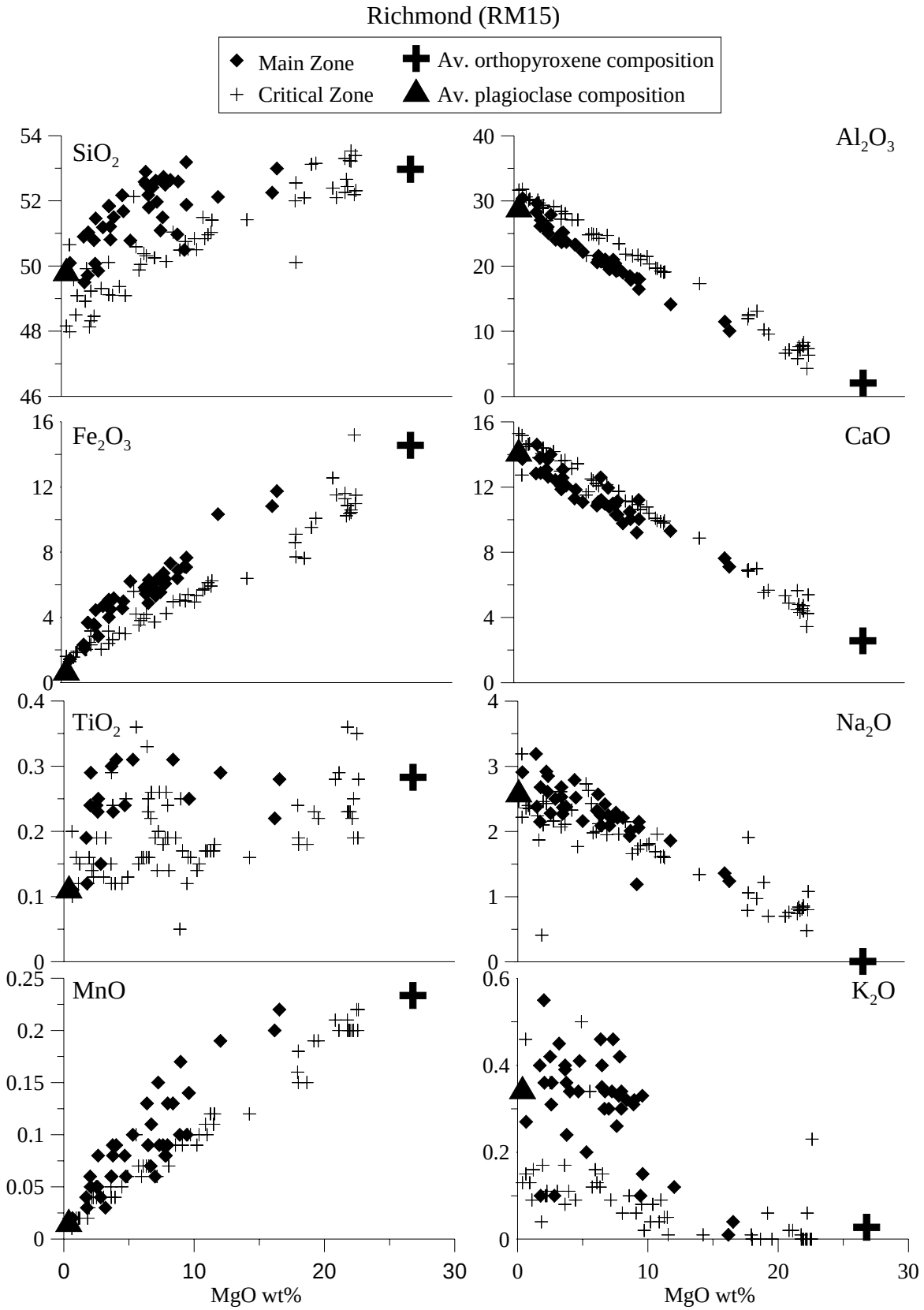


FIGURE 5.2 Harker diagrams of major element oxides plotted against MgO for RM15 whole-rock samples.

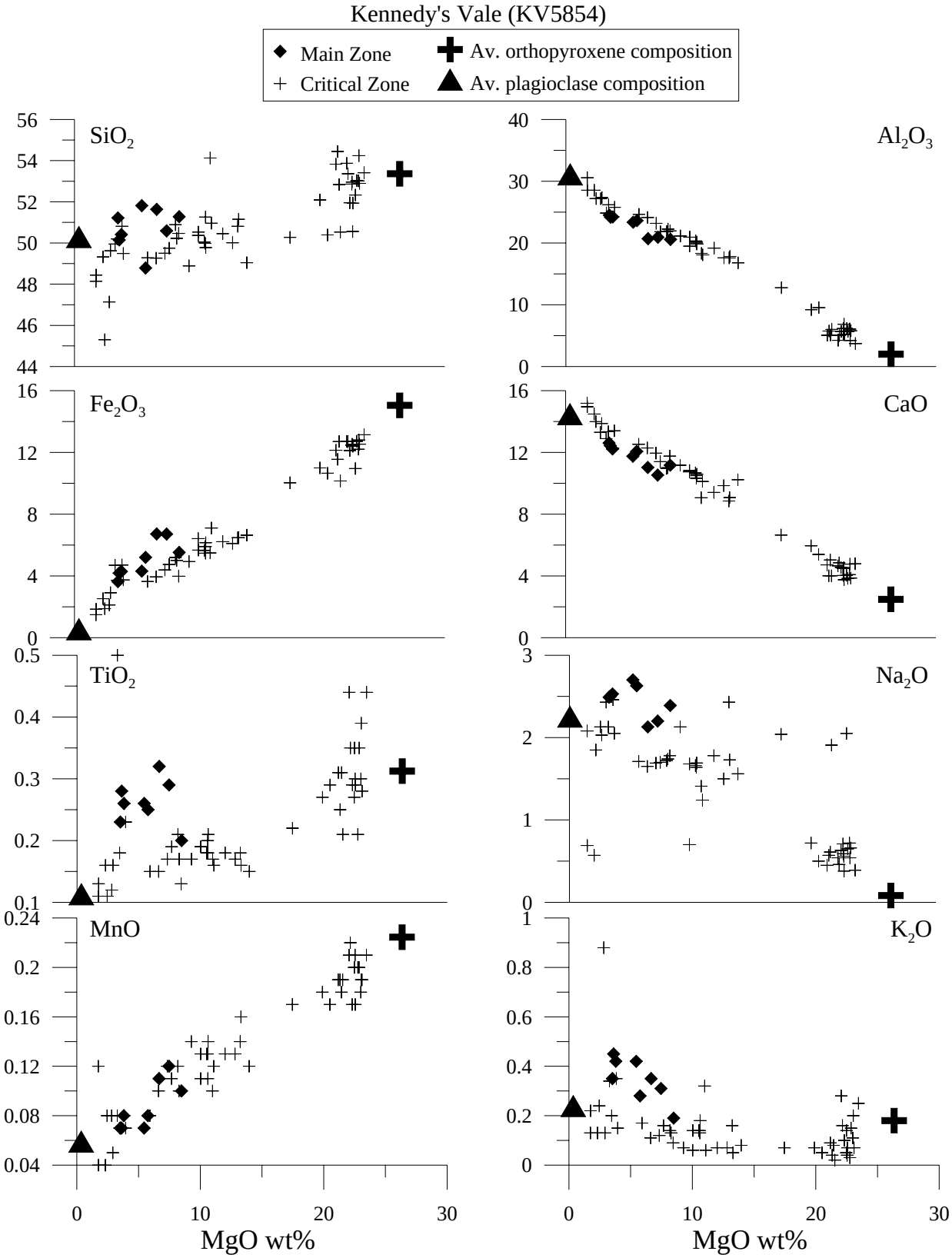


FIGURE 5.3 Harker diagrams of major element oxides plotted against MgO for KV5854 whole-rock samples.

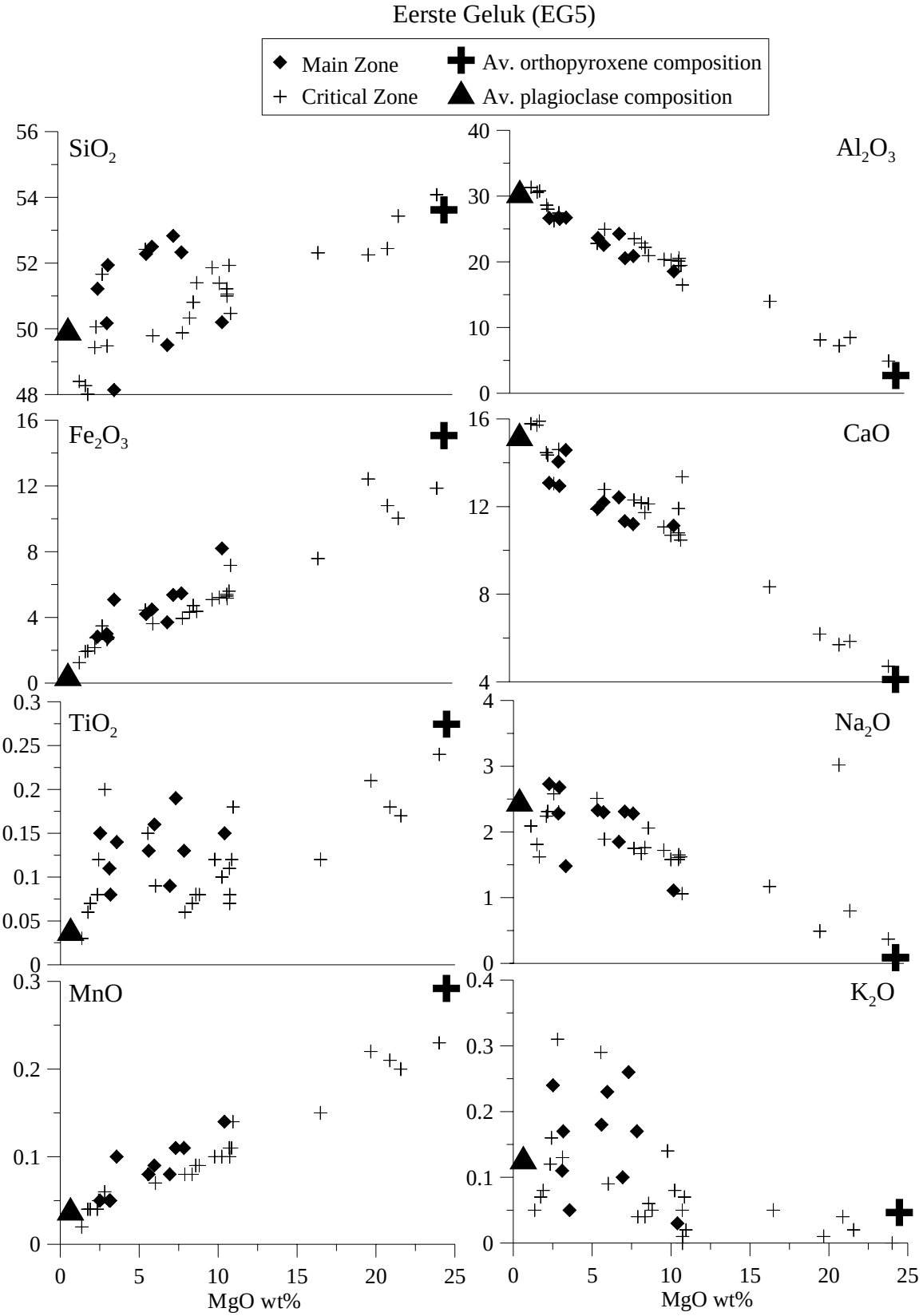


FIGURE 5.4 Harker diagrams of major element oxides plotted against MgO for EG5 whole-rock samples.

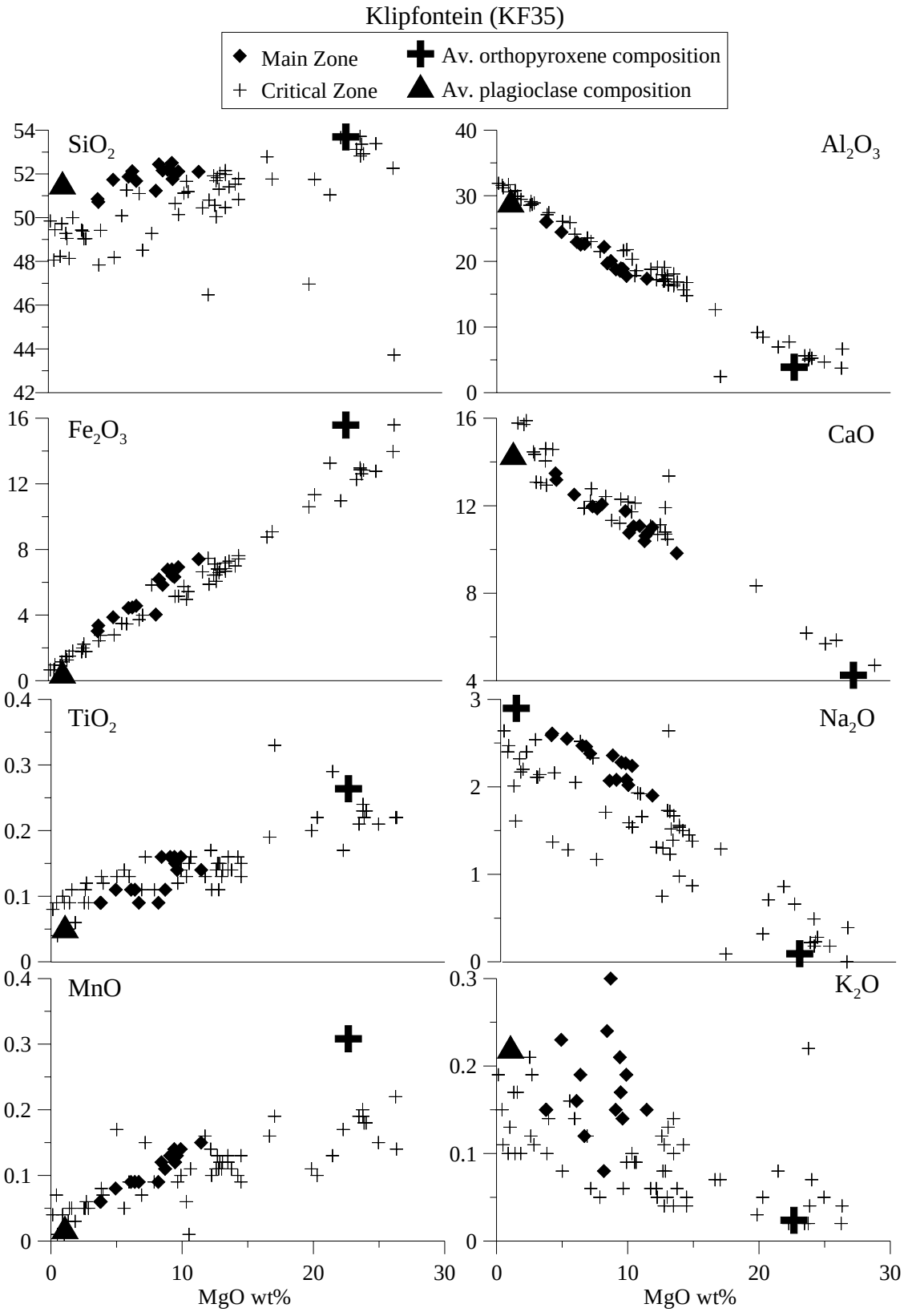


FIGURE 5.5 Harker diagrams of major element oxides plotted against MgO for KF35 whole-rock samples.

5.1.2 Trace element variations

Whole-rock trace element concentrations are given in appendix III. Trace element concentrations are controlled by the partition coefficient of the element into the minerals present in the rock, which is reliant upon the size, charge and orbital shape of the ions relative to the site(s) available in the minerals in question. Consequently, the presence of different minerals will control the abundance of trace elements. The elements Co, Cu, Ni, Zn, V and Cr are generally compatible into the crystal lattice of orthopyroxene and are thus largely controlled by the abundance of this mineral. Sr is highly compatible with plagioclase, substituting for Ca in the crystal lattice. Ni, Cu and Co sulphides form and where S has not been assayed, Cu can be used as an indication of sulphide content based on this relationship. Ni is less reliable as a measure of sulphide content due to its compatibility with orthopyroxene. Cr and V are highly compatible with chromite, resulting in extremely high values of these elements where chromite is present. Elements Zr, Ba and Rb have low partition coefficients into plagioclase and orthopyroxene and therefore concentrate in the residual liquid and are thus contained mainly in accessory phases and not influenced by cumulus modal proportion. Trace elements and K_2O are plotted against height are given in Figures 5.6, 5.7, 5.8 and 5.9. Note that the graphs of Cr, Cu and Ni are on a logarithmic scale. Generally, the graphs of Sr and Zn reflect the lithologies of each profile, where higher Sr indicates norites and anorthosites and higher Zn indicates pyroxenites. Notably, extreme concentrations of Cu, Ni, Cr, Co and to a lesser degree, V and TiO_2 occur at the level of the Merensky Reef, controlled by the presence of sulphide and chromite in the reef. Overall, concentrations of Zr, Ba, Rb and K_2O are slightly higher in Main Zone rocks. Specifically, an increase in Zr, Ba, K_2O and TiO_2 occurs within the GMA, usually the upper section, GMM and UGMA. This is the same location that Mitchell & Manthree (2002) noticed an increase in both TiO_2 and K_2O in core from Impala Platinum Mine. Notably, Cr ppm is significantly lower in Main Zone rocks than in Critical Zone rocks.

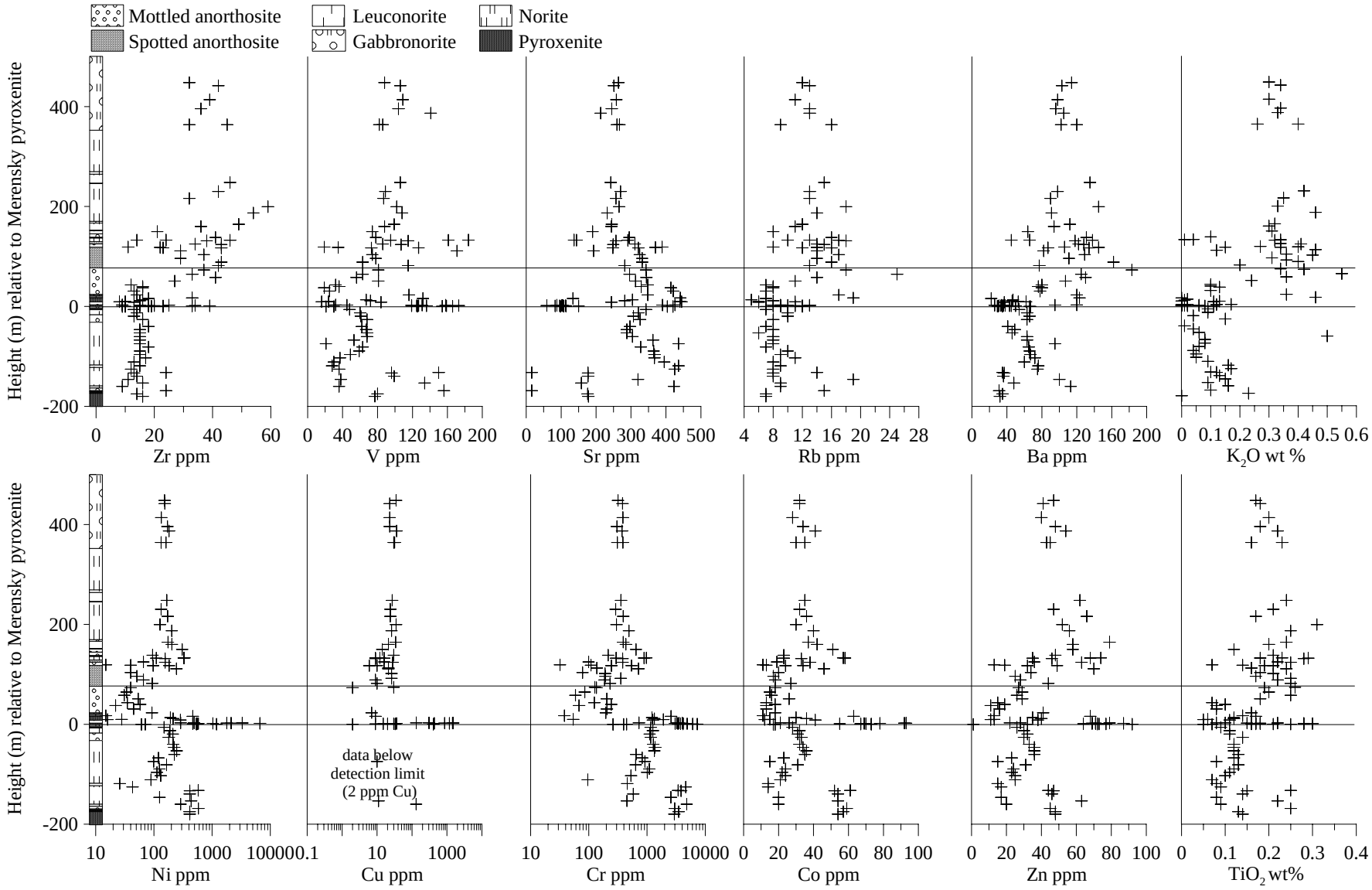


FIGURE 5.6 Trace element and K_2O abundances plotted against height for RM15 whole-rock samples. Lines mark base of Merensky pyroxenite and top of LGMA.

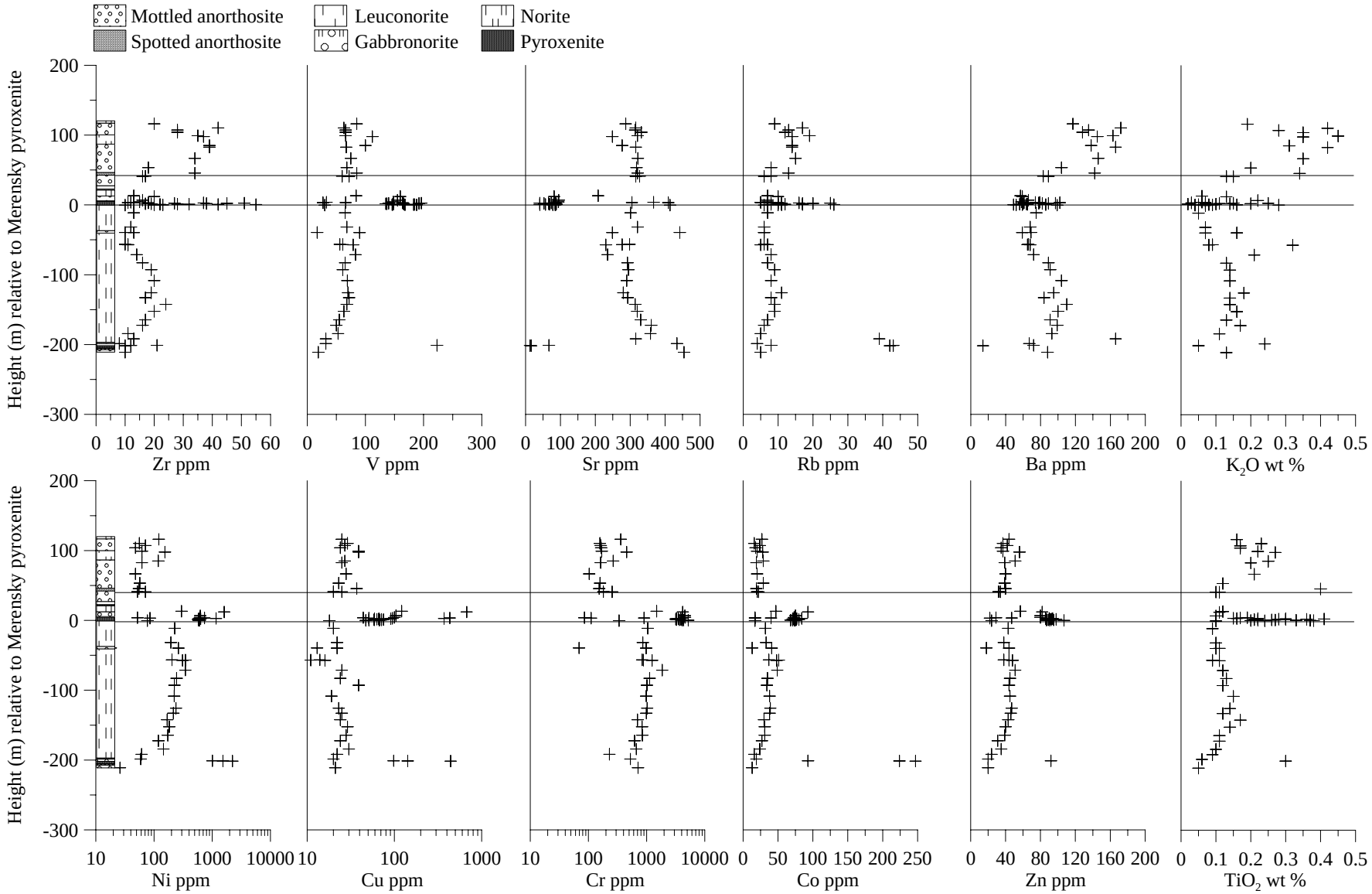


FIGURE 5.7 Trace element and K_2O abundances plotted against height for KV5854 whole-rock samples. Lines mark base of Merensky pyroxenite and top of LGMA.

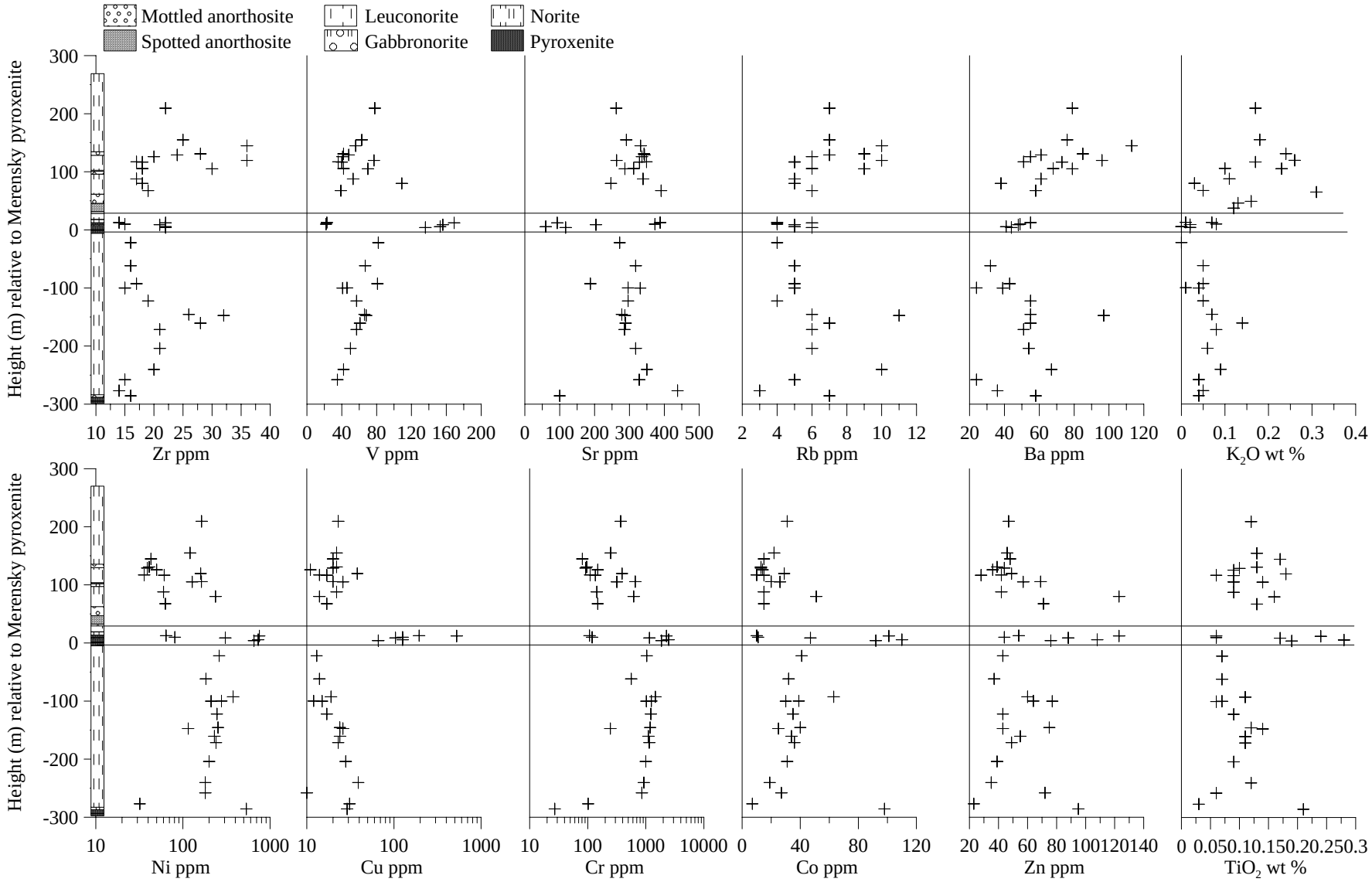


FIGURE 5.8 Trace element and K_2O abundances plotted against height for EG5 whole-rock samples. Lines mark base of Merensky pyroxenite and top of LGMA.

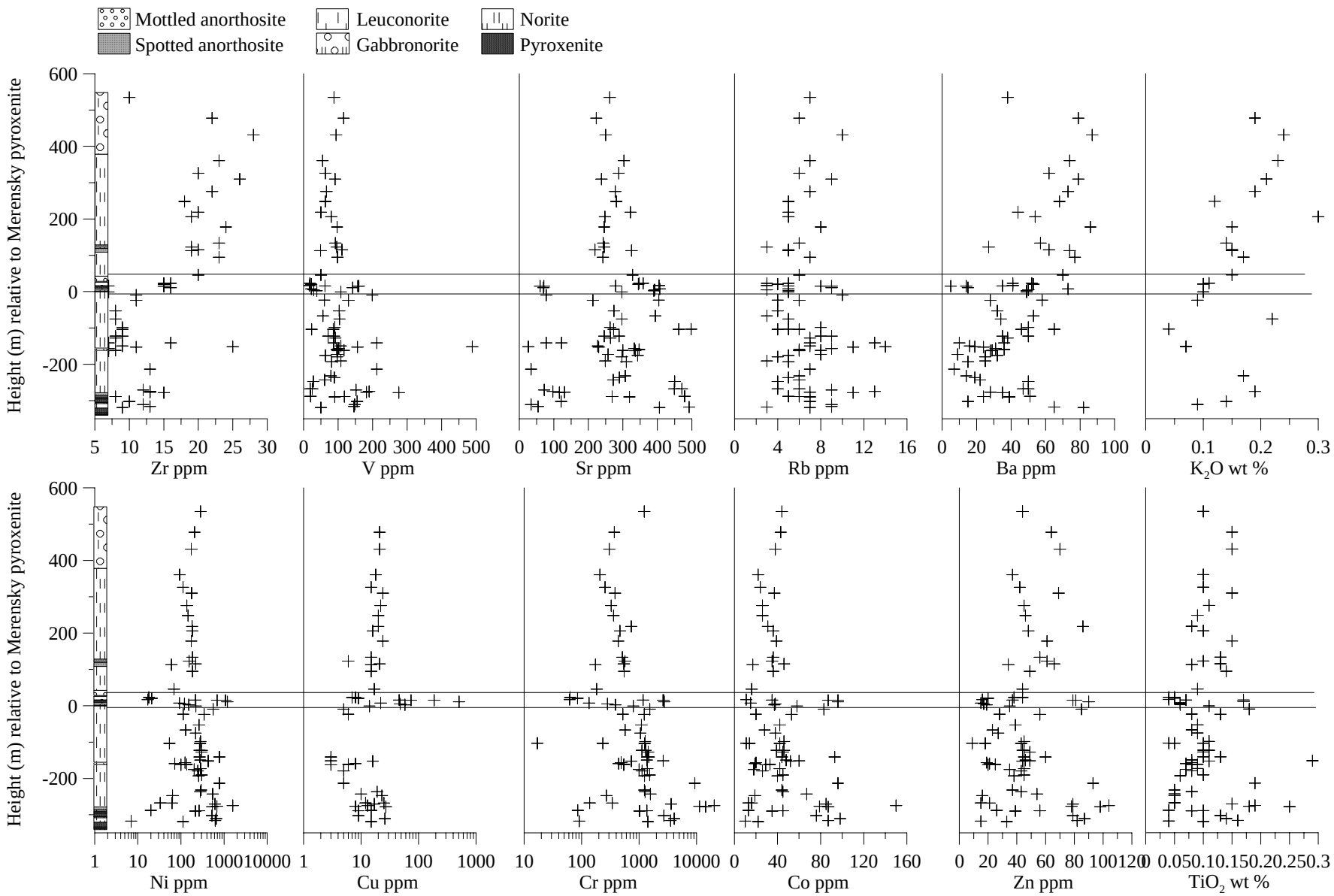


FIGURE 5.9 Trace element and K_2O abundances plotted against height for KF35 whole-rock samples. Lines mark base of Merensky pyroxenite and top of LGMA.

5.2 Orthopyroxene mineral separates

Major and trace element data for orthopyroxene mineral separate are given in appendix IV. In total, 161 samples of orthopyroxene separates were analysed. Compositional variations of orthopyroxene can be represented using the cation ratio 100*((%MgO/40.3)/((%MgO/40.3)+((%Fe_2O_3/158.69)*2))) (Mg#). Fe_2O_3 was converted to Fe^{2+} and Fe_2O_3 assumed to be zero. While there will be some Fe_2O_3, which will lower the absolute value of Mg#, the main use of Mg# in this study is nowhere an issue of absolute value, but focuses on making comparisons between Critical and Main Zone orthopyroxene (section 7.4.3). Mg# decreases with increasing fractionation and Mg# in orthopyroxene plotted against stratigraphic height, for each profile, is given in Figure 5.10. Each profile follows a broadly similar trend whereby Critical Zone samples have higher Mg#, approximately 75-80 and Main Zone samples have consistently lower Mg# of approximately 70-75. However, some variation is observed. In RM15 a decrease to Mg# <70 occurs in the GMA, but this increases to typical Main Zone values in the overlying norites. KV5854 also shows Mg# <70 in the GMA. In each profile, Mg# does not show significant decrease over large vertical distances as predicted by differentiation.

Trace element contents in orthopyroxene were also determined (appendix IV) and these are plotted against stratigraphic height for each profile in Figures 5.11, 5.12, 5.13 and 5.14. Elements reflect their compatibility with orthopyroxene. Low concentrations of Zr, Sr, Rb, Ba and Zn are recorded, as these are incompatible with orthopyroxene, whereas V, Ni, Cr and Co are high. Elevated Cu values are observed where there are sulphide inclusions within the orthopyroxene grains. In general, incompatible elements have lower values in the Critical Zone than the Main Zone and are more tightly constrained. In the Main Zone, these elements show much more scatter and overall, concentrations notably increase upward in all sections. Overall, Ni in orthopyroxene is higher in the Critical Zone and Co and V are lower, compared to the Main Zone. The compatible element Cr shows a very distinct variation between the Critical and Main Zones, with concentrations of approximately 2000-3000 ppm in the Critical Zone and approximately 1000 ppm in the Main Zone. The gradual decrease in Cr ppm through the Critical Zone of the KF35 profile is

discussed in section 7.7, along with other geochemical variations that occur simultaneously in KF35. Values of Sr greater than about 10 ppm reflect the presence of plagioclase (possibly as inclusions in orthopyroxene).

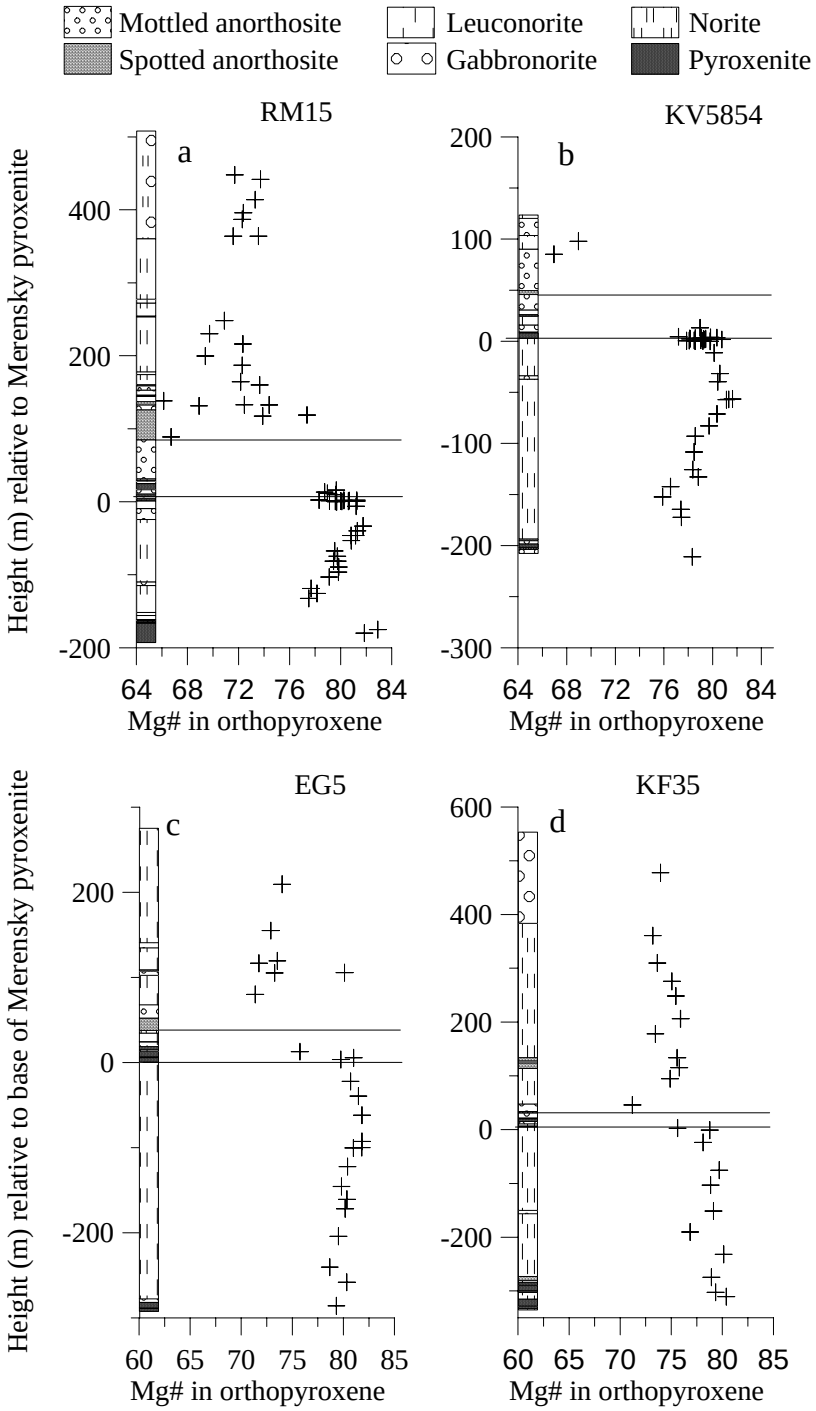


FIGURE 5.10 Mg# in orthopyroxene plotted against height for (a) Richmond, (b) Kennedy's Vale, (c) Eerste Geluk and (d) Klipfontein. Lines mark base of Merensky pyroxenite and top of GMA.

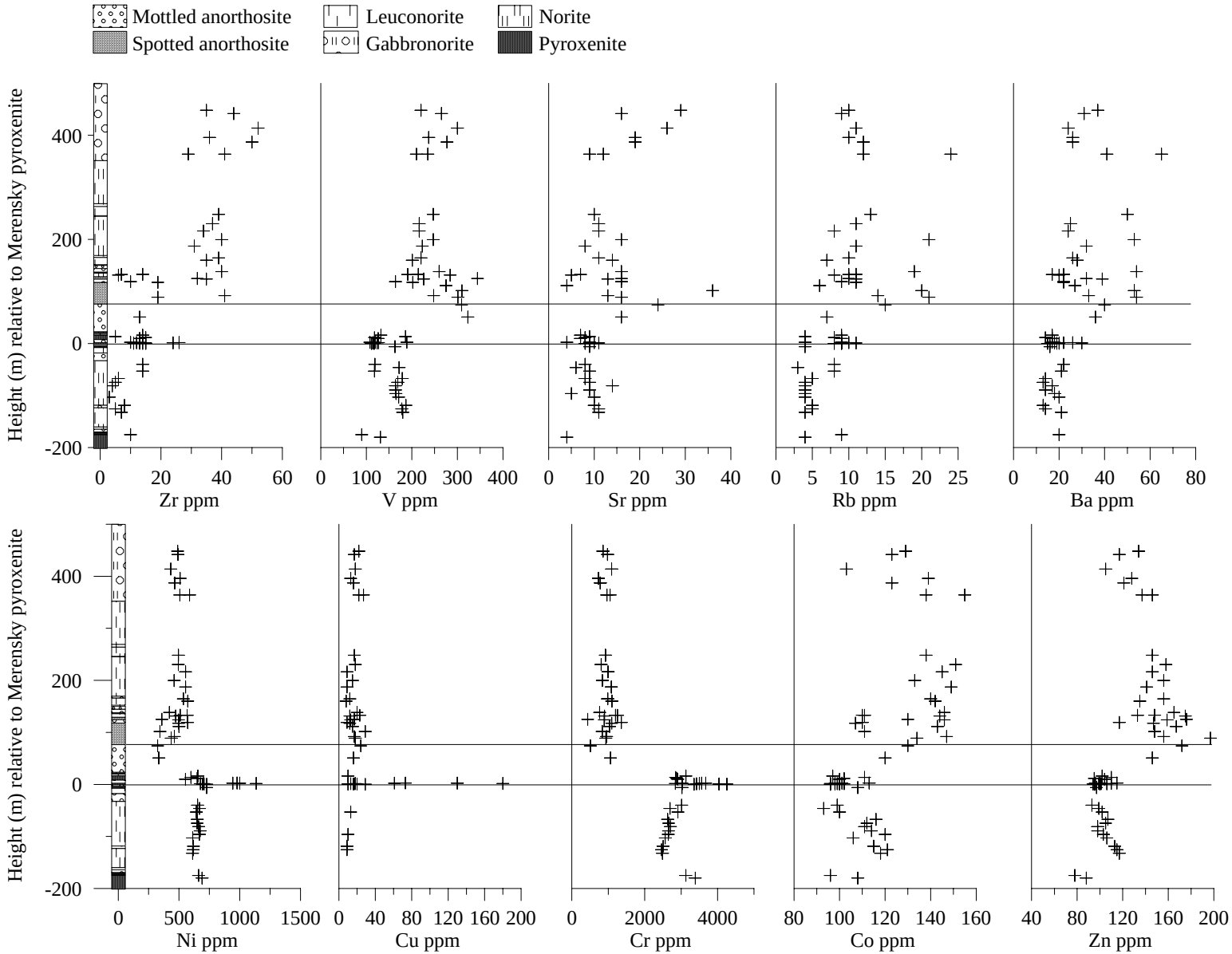


FIGURE 5.11 Trace element abundances plotted against height for RM15 orthopyroxene separates. Lines mark base of Merensky pyroxenite and top of GMA.

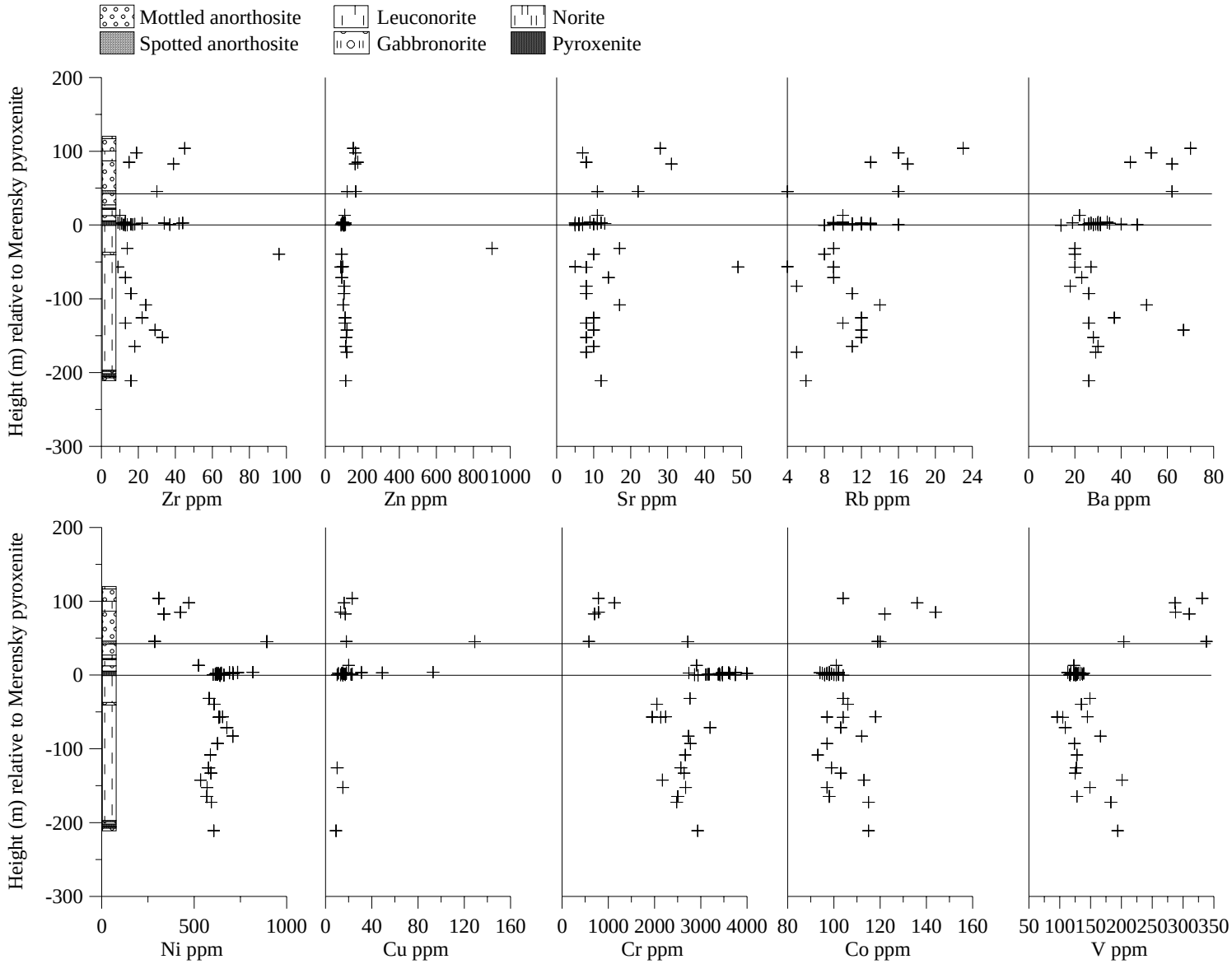


FIGURE 5.12 Trace element abundances plotted against height for KV5854 orthopyroxene separates. Lines mark base of Merensky pyroxenite and top of GMA.

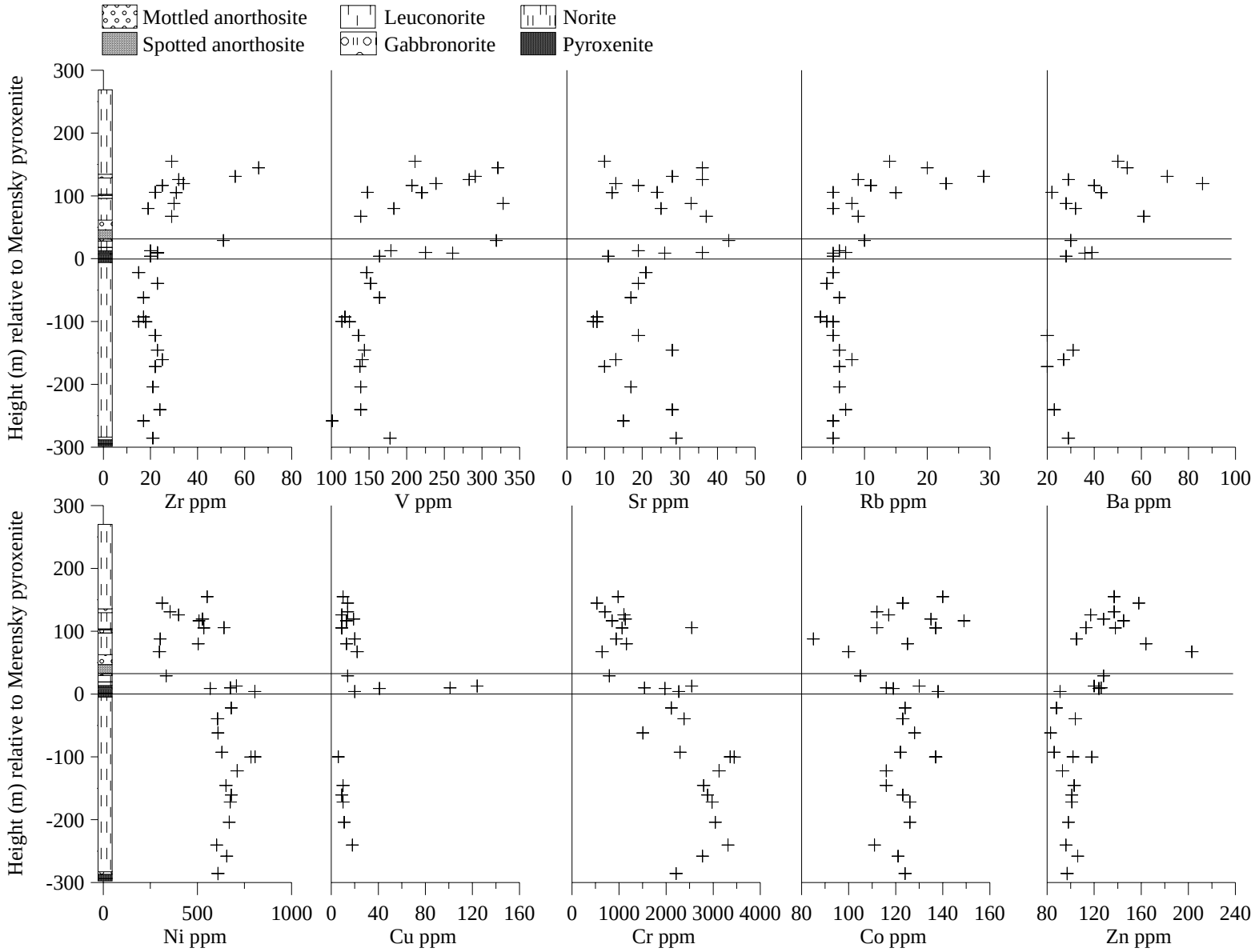


FIGURE 5.13 Trace element abundances plotted against height for EG5 orthopyroxene separates. Lines mark base of Merensky pyroxenite and top of GMA.

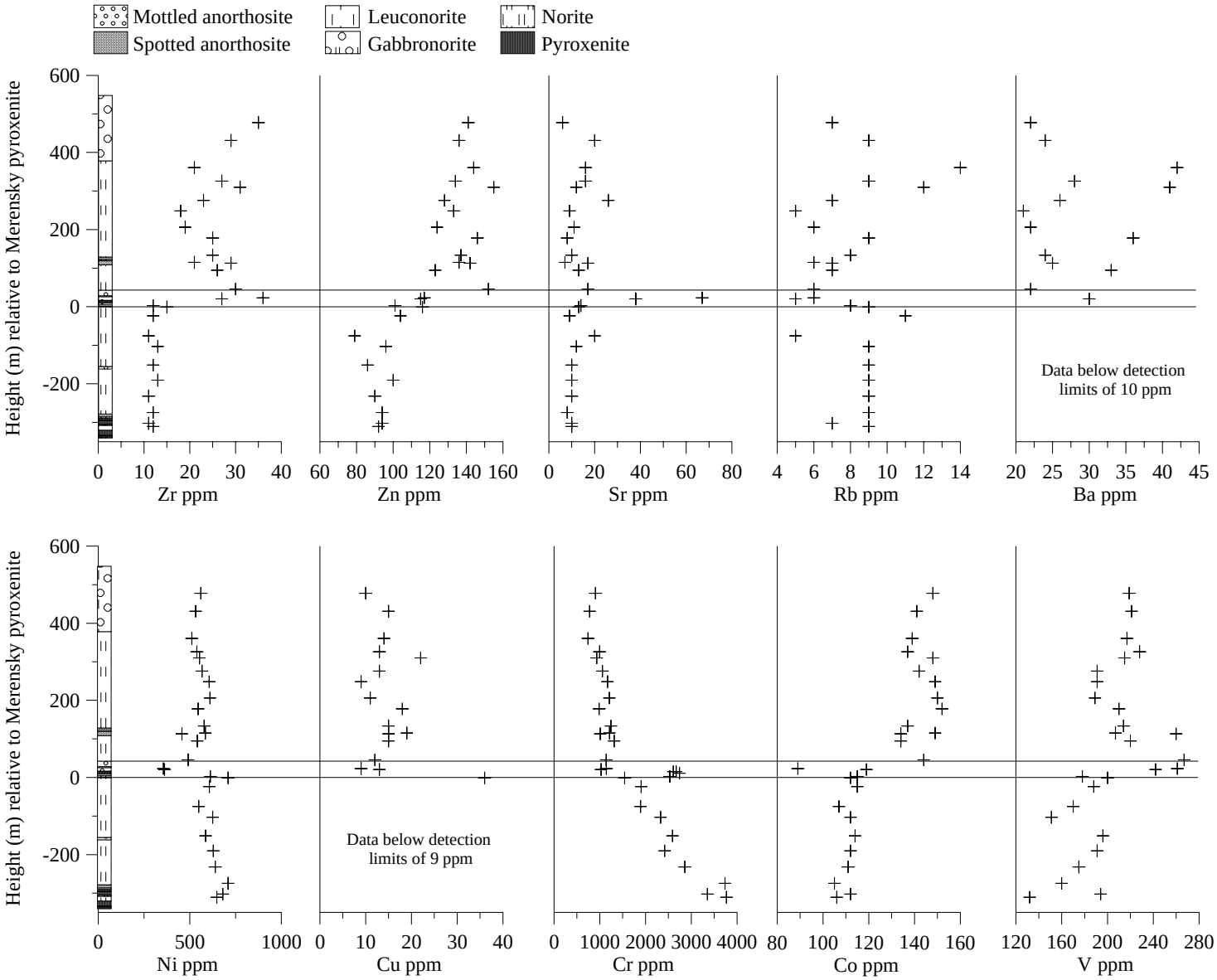


FIGURE 5.14 Trace element abundances plotted against height for KF35 orthopyroxene separates. Lines mark base of Merensky pyroxenite and top of GMA.

5.3 Plagioclase mineral separates

Plagioclase mineral separate data are given in appendix V. In total, 167 plagioclase separates were analysed. The cation ratio 100*((%CaO/56.08)/((%CaO56.08)+((%Na_2O/61.98)*2))) (An#) plotted against stratigraphic height for each profile is shown in Figure 5.15. An# also displays variations between Main Zone and Critical Zone rocks. In general, Critical Zone rocks have An# between 75 and 80. In the Main Zone, An# is overall slightly lower, at approximately 70. However, both KF35 and EG5 show values of 80-85 within and above the Merensky and Bastard Cyclic Units and in all profiles there is no distinct break between typical Critical Zone and typical Main Zone values.

Minor element variations in plagioclase are plotted against stratigraphic height and shown in Figures 5.16, 5.17, 5.18 and 5.19. Due to their very low partition coefficients into plagioclase, V, Ni and Co have been excluded as values are below detection limits. Rb has also been excluded as values are close to or below detection limits. Although Zr has been included, values are frequently at detection limits. As for orthopyroxene, trace elements Zr and Ba display lower more constrained values in the Critical Zone, but much more scattered, generally higher values in the Critical Zone. Sr, which is highly compatible with plagioclase, shows systematically higher values in the Critical Zone of approximately 440-480 ppm and lower values in the Main Zone, of approximately 360-400 ppm. Cu, Zr and Cr do not enter the crystal structure of plagioclase and anomalously high values represent the presence of sulphide, zircon and chromite respectively as microinclusions within the plagioclase.

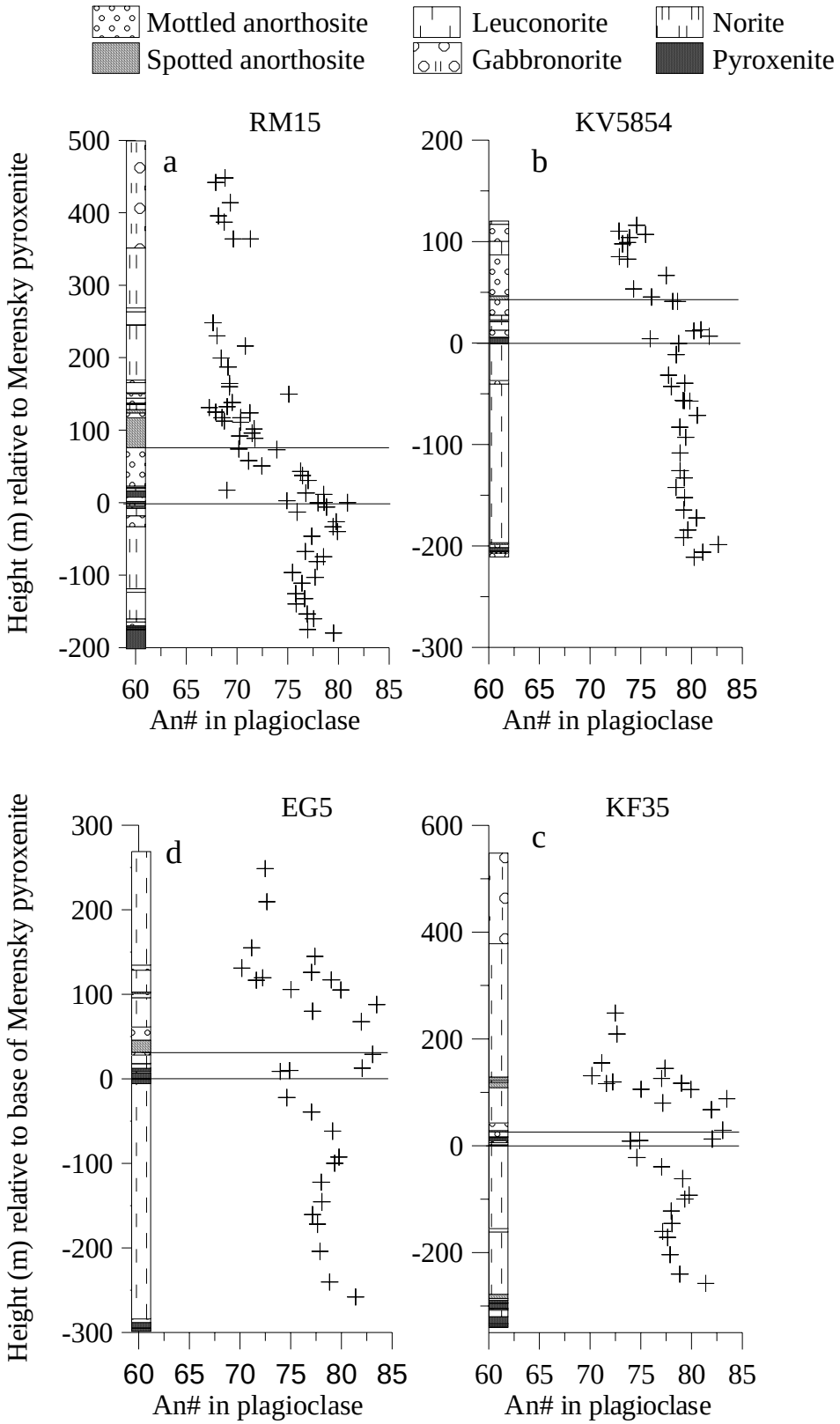


FIGURE 5.15 An# in plagioclase plotted against height for (a) Richmond, (b) Kennedy's Vale, (c) Eerste Geluk and (d) Klipfontein. Lines mark base of Merensky pyroxenite and top of GMA.

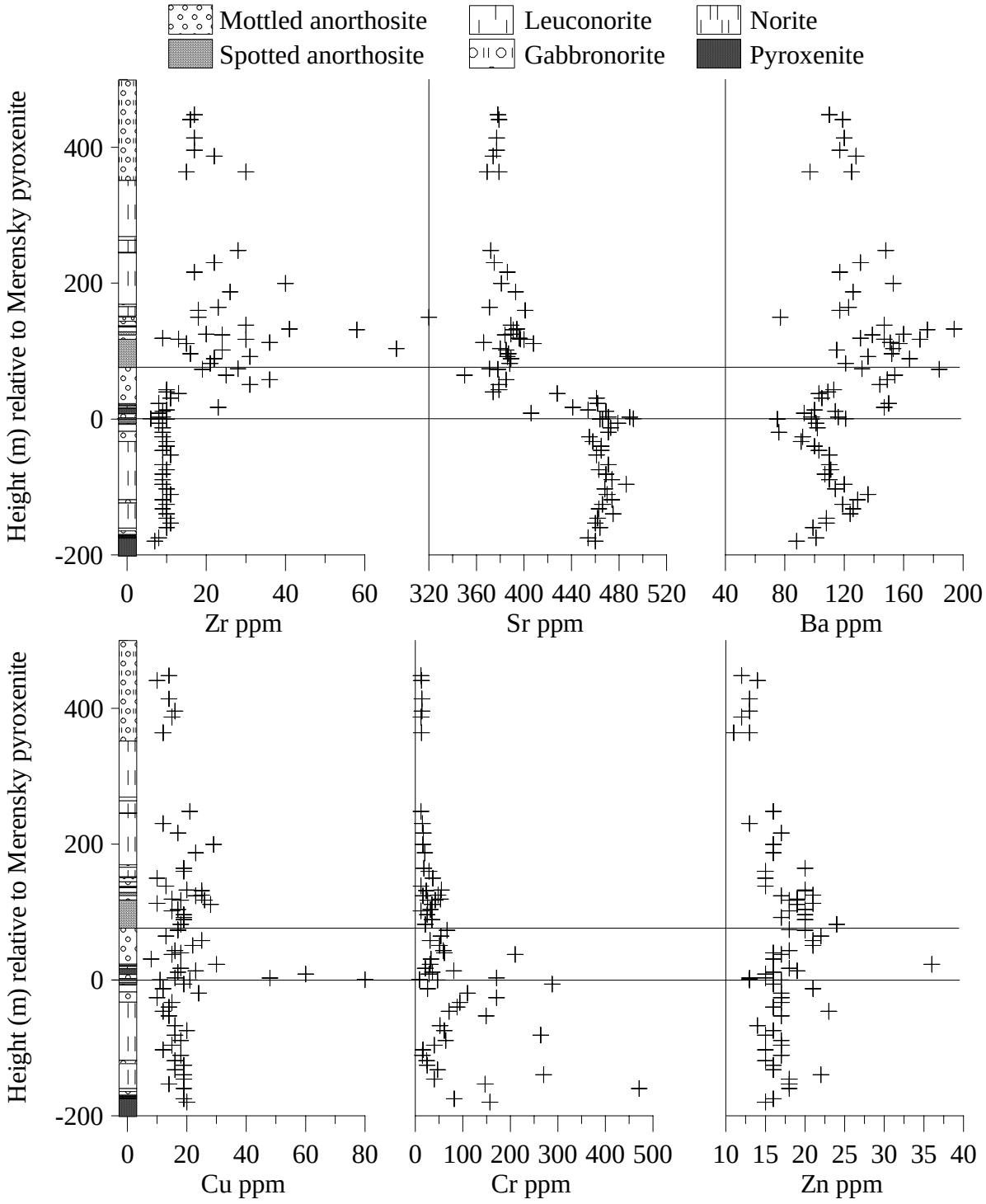


FIGURE 5.16 Trace element abundances plotted against height for RM15 plagioclase separates. Lines mark base of Merensky pyroxenite and top of GMA.

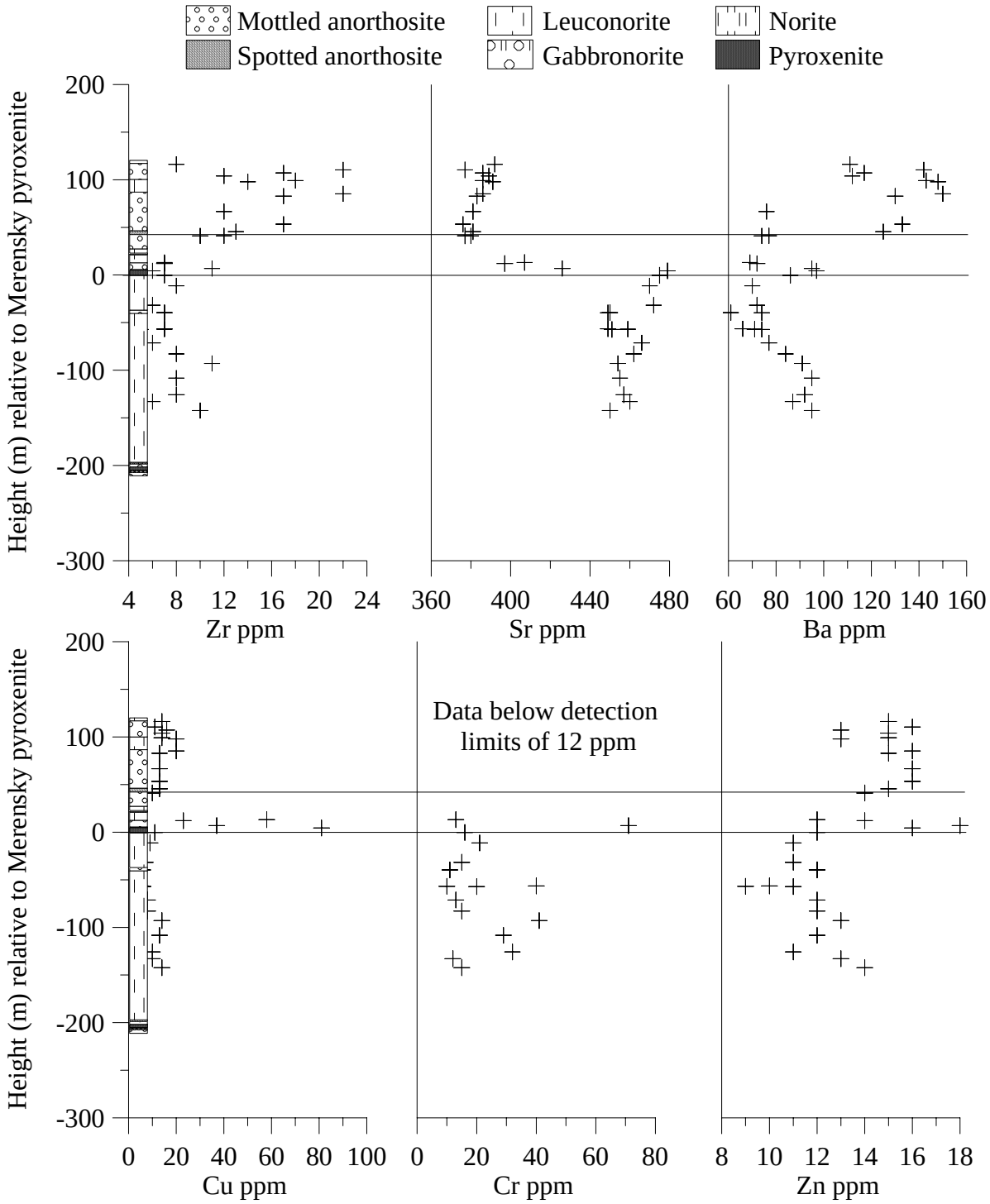


FIGURE 5.17 Trace element abundances plotted against height for KV5854 plagioclase separates. Lines mark base of Merensky pyroxenite and top of GMA.

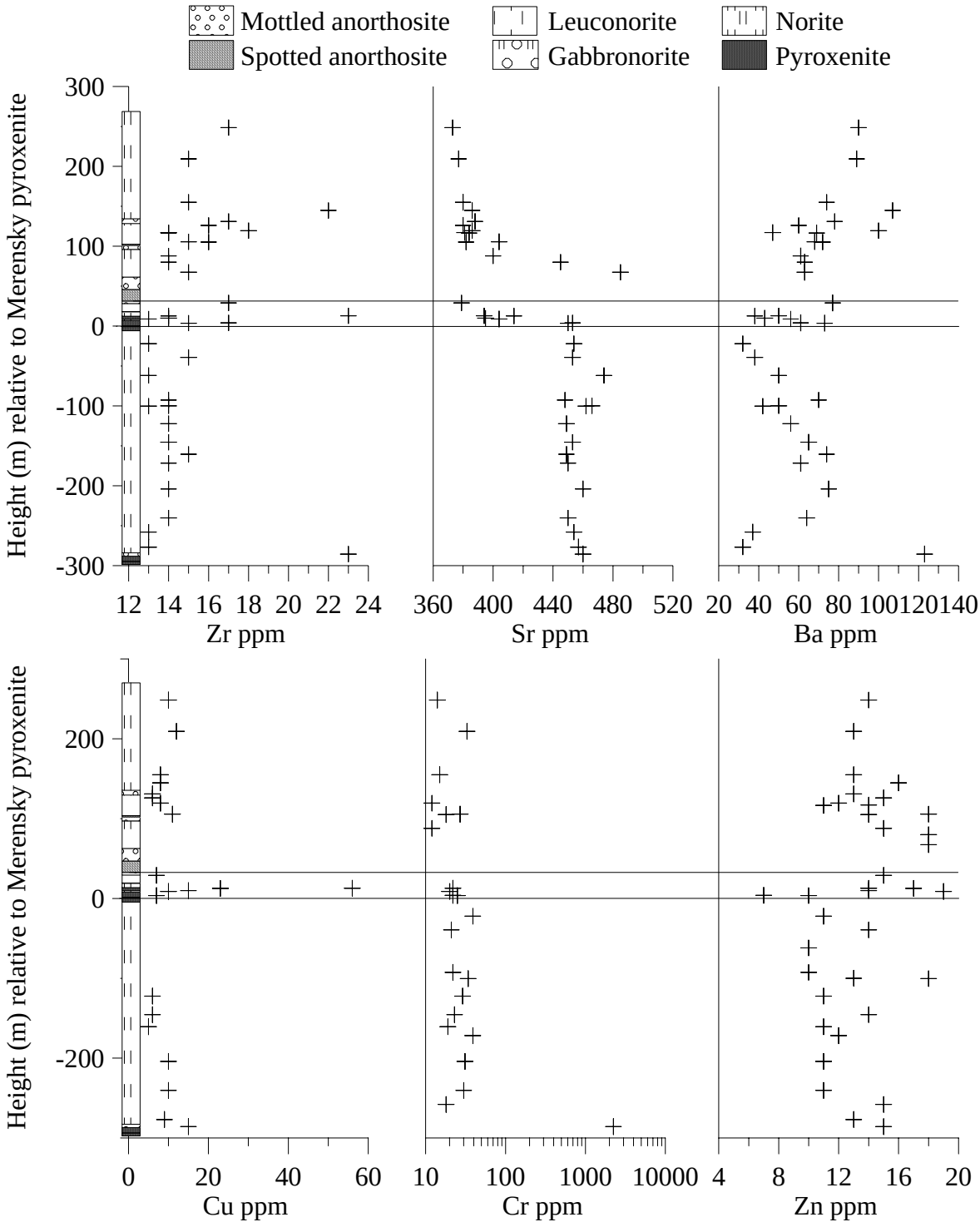


FIGURE 5.18 Trace element abundances plotted against height for EG5 plagioclase separates. Lines mark base of Merensky pyroxenite and top of GMA.

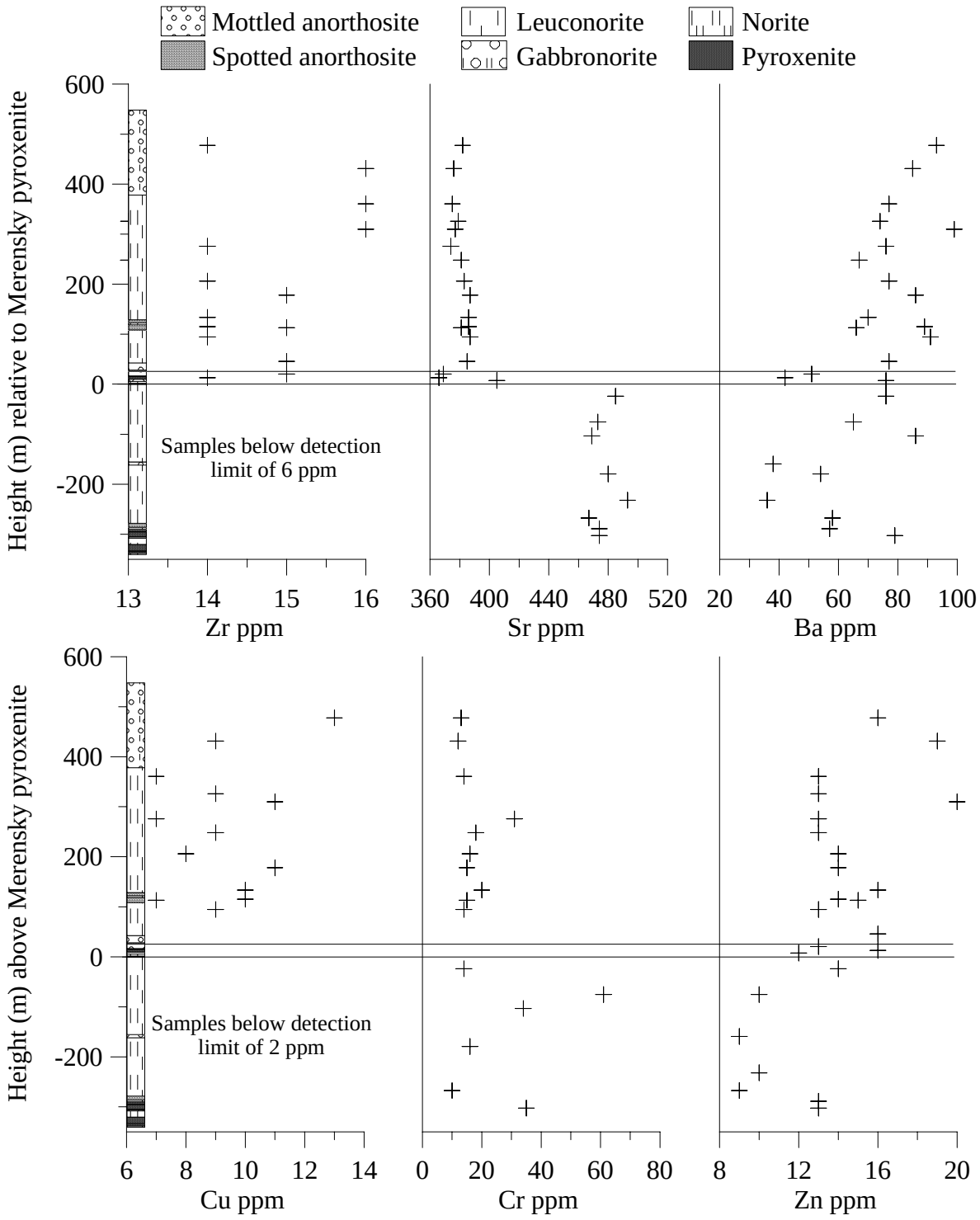


FIGURE 5.19 Trace element abundances plotted against height for KF35 plagioclase separates. Lines mark base of Merensky pyroxenite and top of GMA.

In addition, Mg# was plotted against An# (Figure 5.20) for each core sampled. These plots show clearly the difference between Critical and Main Zone samples, with lower An# and Mg# in the Main Zone samples. The expected fractionation trend is not observed and the spread of Critical Zone samples, seen most clearly in the plots of EG5 and KF35, from approximately An 74 – 82, reflects cumulus and intercumulus minerals.

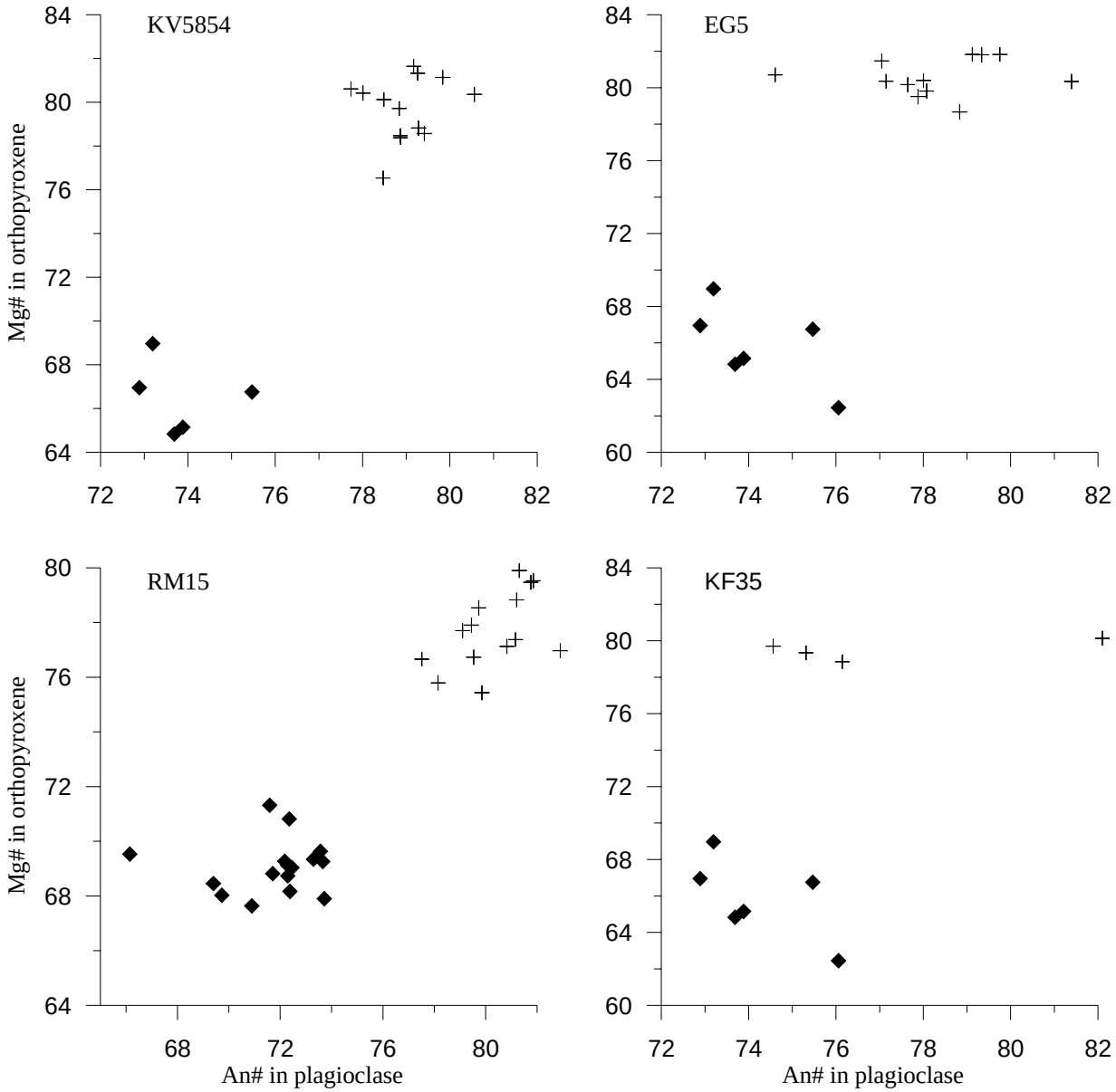


FIGURE 5.20 Plots of Mg# *versus* An# for KV5854, EG5, RM15 and KF35.

5.4 Strontium Isotopes

43 samples were selected for isotopic analysis from the RM15 and KF35 cores (one north and one south of the Steelpoort lineament) on the basis of previous work and lithology in the Upper Critical and the Lower Main Zones. For the purposes of this study, KF35 data have been combined with data collected by Blumberg (2002) from the same core. Blumberg sampled the UG2 – Merensky interval, thus the compilation of the two sets produces an entire sequence through the Main Zone/Critical Zone interval. Sr, Rb, present day $^{87}Sr/^{86}Sr$ ratios and initial isotope ratios at 2050 Ma (Sr_i) are given in Tables 5.2 and 5.3. These data give a minimum initial ratio of 0.70609 and a maximum ratio of 0.70863 for RM15 and a minimum of 0.70601 and a maximum of 0.70868 for KF35.

The variation in the initial isotope ratio with stratigraphic height for RM15 and KF35 is given in Figure 5.21a and b respectively. This diagram clearly shows that samples below the level of the Merensky pyroxenite generally have lower values (0.706-0.707) than those above the Merensky Cyclic Unit (0.707-0.708). In addition, those samples above the level of the Merensky Cyclic Unit show a gradual increase in initial ratio with height. Sample RM15 316.43 (153.4 m below the Merensky pyroxenite) shows an apparently anomalously low value of 0.70342 and is excluded.

TABLE 5.2 Isotope data from plagioclase separates in core RM15

Sample Number	Height (m) relative to base of Merensky pyroxenite	Lithology	Mineral	Rb ppm	Sr ppm	^{87}Rb	^{86}Sr	$^{87}Rb/^{86}Sr$	$^{87}Sr/^{86}Sr(p)$	±	2 se	Initial @ 2050	±	2 sigma
Main Zone														
RM15 5	448.17	gabbronorite	plagioclase	7.0	381	1.9611	36.8827	0.0526	0.709913	±	24	0.70836	±	0.00016
RM15 3	441.87	gabbronorite	plagioclase	11.1	384	3.1247	37.0747	0.0833	0.710683	±	23	0.70822	±	0.00017
RM15 1	387	gabbronorite	plagioclase	10.0	387	2.8009	37.4094	0.0740	0.710813	±	23	0.70863	±	0.00016
RM15 6a	364	gabbronorite	plagioclase	8.6	376	2.4295	36.3142	0.0661	0.710124	±	21	0.70817	±	0.00016
RM15 6b	364	gabbronorite	plagioclase	4.4	386	1.2369	37.2919	0.0328	0.709329	±	15	0.70836	±	0.00015
Bastard Cyclic Unit														
RM15 30.28	132.75	melanorite	plagioclase	2.0	381	0.5655	36.88	0.0152	0.709078	±	20	0.70863	±	0.00015
RM15 45.57	117.46	norite	plagioclase	4.9	380	1.3674	35.9902	0.0376	0.709053	±	18	0.70794	±	0.00015
RM15 59.35	103.68	mottled anorthosite	plagioclase	10.3	381	2.8958	36.8527	0.0777	0.709959	±	27	0.70766	±	0.00017
RM15 81.18	81.85	leuconorite	plagioclase	6.2	397	1.7397	38.4315	0.0447	0.709292	±	18	0.70797	±	0.00016
RM15 105.04	57.99	mottled anorthosite	plagioclase	10.1	398	2.8489	38.5075	0.0731	0.709933	±	32	0.70777	±	0.00016
RM15 123.24	39.79	spotted anorthosite	plagioclase	3.0	374	0.8336	36.21	0.0228	0.708650	±	29	0.70798	±	0.00015
RM15 125.52	37.51	spotted anorthosite	plagioclase	3.4	425	0.9482	41.1442	0.0228	0.707807	±	44	0.70713	±	0.00015
RM15 132.23	30.8	mottled anorthosite	plagioclase	3.0	4656	0.8578	45.0195	0.0188	0.707226	±	16	0.70667	±	0.00015
RM15 140	23.03	mottled anorthosite	plagioclase	15.0	462	4.2238	52.2362	0.0799	0.708882	±	21	0.70652	±	0.00017
RM15 140	23.03	mottled anorthosite	clinopyroxene	1.4	51	0.3828	4.9135	0.0770	0.709450	±	23	0.70718	±	0.00016
RM15 145.76	17.27	anorthosite	plagioclase	14.9	443	4.1879	42.8628	0.0966	0.709497	±	132	0.70664	±	0.00017
RM15 146.90	16.13	melanorite	plagioclase	0.8	441	0.2356	42.6016	0.0055	0.707500	±	19	0.70734	±	0.00014
RM15 149.62	13.41	leuconorite	plagioclase	1.6	456	0.4445	44.108	0.0010	0.706993	±	37	0.70670	±	0.00014
RM15 151.13	11.5	norite	plagioclase	1.6	465	0.4451	44.9408	0.0010	0.706911	±	78	0.70662	±	0.00014
RM15 153.20	9.83	melanorite	plagioclase	1.1	451	0.3207	43.5695	0.0073	0.706974	±	25	0.70676	±	0.00014
RM15 153.46	9.57	melanorite	plagioclase	1.0	450	0.2804	43.5543	0.0064	0.707065	±	27	0.70688	±	0.00014
RM15 153.55	9.48	melanorite	plagioclase	2.9	402	0.8101	38.9133	0.0206	0.708107	±	67	0.70750	±	0.00015
Merensky Cyclic Unit														
RM15 153.61	9.42	mottled anorthosite	plagioclase	2.5	399	0.7055	38.6132	0.0181	0.707903	±	44	0.70737	±	0.00015
RM15 154.37	8.66	mottled anorthosite	plagioclase	1.86	395	0.4938	38.2339	0.0128	0.707754	±	14	0.70738	±	0.00015
RM15 155.57	7.33	mottled anorthosite	plagioclase	3.4	362	0.9612	28.1182	0.0338	0.707503	±	15	0.70650	±	0.00016
RM15 156.66	6.24	mottled anorthosite	plagioclase	3.0	394	0.8439	33.6692	0.0248	0.707541	±	24	0.70681	±	0.00026
RM15 158.54	4.36	mottled anorthosite	plagioclase	1.1	398	0.3050	32.0642	0.0094	0.706668	±	17	0.70639	±	0.00021
RM15 160.09	2.94	mottled anorthosite	plagioclase	2.8	491	0.7907	47.4407	0.0165	0.706708	±	13	0.70622	±	0.00015
RM15 160.28	2.75	mottled anorthosite	plagioclase	1.8	490	0.5132	47.3523	0.0107	0.706604	±	42	0.70629	±	0.00014
RM15 160.28 Rb repeat		mottled anorthosite	plagioclase	1.9		0.5361				±			±	
RM15 160.48	2.55	pyroxenite	plagioclase	0.5	458	0.1451	44.2512	0.0032	0.706436	±	14	0.70634	±	0.00014
RM15 161.62	1.41	pyroxenite	plagioclase	1.0	457	0.2708	44.1563	0.0061	0.706579	±	19	0.70640	±	0.00014
Critical Zone														
RM15 162.98	-0.03	anorthosite	plagioclase	2.5	468	0.7151	45.2244	0.0156	0.706953	±	12	0.70649	±	0.00015
RM15 169.10	-6.07	leuconorite	plagioclase	1.5	475	0.4183	45.8958	0.0090	0.706683	±	33	0.70642	±	0.00014
RM15 169.10 Rb repeat		leuconorite	plagioclase	1.5		0.4292				±			±	
RM15 216.10	-53.07	norite	plagioclase	3.4	458	0.9704	44.2807	0.0217	0.707083	±	17	0.70644	±	0.00015
RM15 259.27	-96.24	norite	plagioclase	3.4	490	0.9694	29.13	0.0329	0.707989	±	17	0.70702	±	0.00015
RM15 295.29	-132.26	norite	plagioclase	4.6	453	1.2932	43.8097	0.02918	0.707174	±	23	0.70631	±	0.00015
RM15 338.00	-174.97	pyroxenite	plagioclase	0.3	459	0.0911	44.4323	0.00202	0.706151	±	16	0.70609	±	0.00014

TABLE 5.3 Isotope data from plagioclase separates in core KF35

Sample Number	Height (m) relative to base of Merensky pyroxenite	Lithology	Mineral	Rb ppm	Sr ppm	^{87}Rb	^{86}Sr	$^{87}Rb/^{86}Sr$	$^{87}Sr/^{86}Sr(p)$	±	2 se	Initial @ 2050	±	2 sigma
Main Zone														
KF35 118.41	431.29	gabbronorite	plagioclase	3.6	384	1.0153	37.0926	0.0271	0.70948	±	26	0.708681	±	0.00015
KF35 223.77	325.93	norite	plagioclase	1.7	382	0.4708	36.9449	0.0198	0.708983	±	12	0.708397	±	0.00015
KF35 239.66	310.04	norite	plagioclase	2.6	394	0.7411	38.0872	0.0192	0.709166	±	18	0.708598	±	0.00015
KF35 371.68	178.02	norite	plagioclase	2.5	373	0.6978	36.0913	0.0191	0.708458	±	36	0.707893	±	0.00015
KF35 436.84	112.86	spotted anorthosite	plagioclase	1.5	390	0.4362	37.7313	0.0114	0.708152	±	19	0.707814	±	0.00015
KF35 455.20	94.5	norite	plagioclase	3.2	396	0.9151	38.2447	0.0237	0.708603	±	21	0.707904	±	0.00015
KF35 503.96	45.74	norite	plagioclase	2.5	396	0.7018	38.3195	0.0181	0.708362	±	15	0.707827	±	0.00015
Bastard Cyclic Unit														
KF35 532.6*	17.1	mottled anorthosite	plagioclase	0.6	370	0.1742	35.74	0.0048	0.707780	±		0.707638	±	0.00014
KF35 534.65*	15.05	pyroxenite	plagioclase	0.4	403	0.1248	38.93	0.0032	0.707771	±		0.707677	±	0.00014
KF35 538.8*	10.9	pyroxenite	plagioclase	1.0	446	0.2707	43.17	0.0061	0.707685	±		0.707502	±	0.00014
Merensky Cyclic Unit														
KF35 542.25*	7.45	mottled anorthosite	plagioclase	0.8	408	0.2131	39.45	0.0053	0.707494	±		0.707336	±	0.00014
KF35 547.06*	2.46	spotted anorthosite	plagioclase	0.9	404	0.2385	39.04	0.0060	0.707418	±		0.707240	±	0.00014
Critical Zone														
KF35 550.6*	-0.9	norite	plagioclase	1.5	468	0.4174	45.25	0.0091	0.706712	±		0.706443	±	0.00014
KF35 573.55*	-23.85	melanorite	plagioclase	3.7	479	1.0461	46.31	0.0223	0.706669	±		0.706009	±	0.00015
KF35 653.1*	-103.4	norite	plagioclase	1.4	469	0.3943	39.07	0.0100	0.706684	±		0.706389	±	0.00014
KF35 781.7*	-232	norite	plagioclase	0.4	493	0.105	40.45	0.0026	0.706478	±		0.706402	±	0.00014
KF35 838.69*	-288.99	norite	plagioclase	0.9	478	0.2547	46.24	0.0054	0.706254	±		0.706093	±	0.00014

* Blumberg (2002) 2 se was not recorded by Blumberg in his thesis.

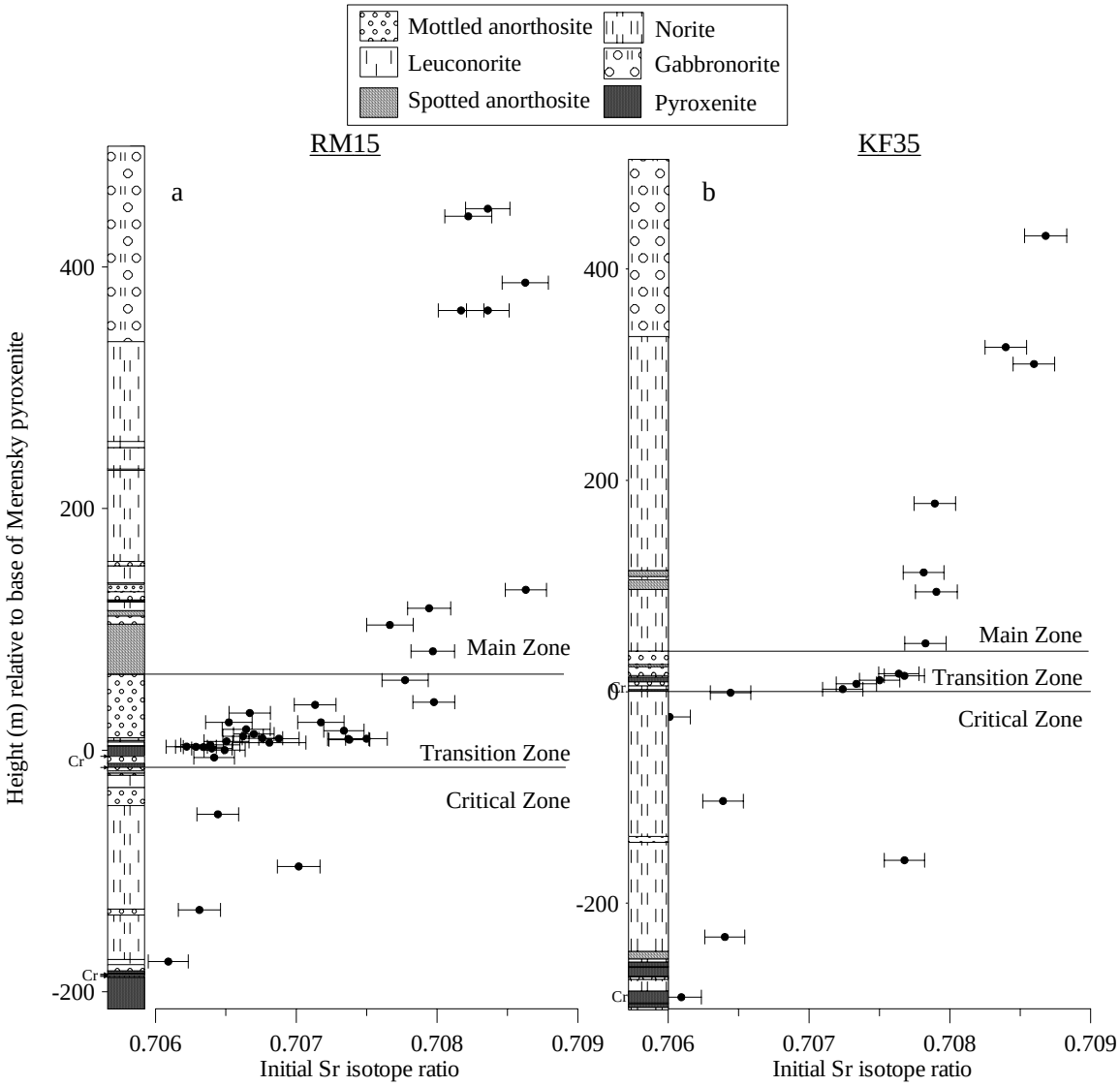


FIGURE 5.21 Sr isotope initial ratios plotted against height for (a) RM15 and (b) KF35. Error bars represent 2 sigma on the calculated initial ratio.

Although grossly similar, the two profiles in this study do show some variation. Figure 5.22 shows the interval from the Merensky pyroxenite footwall to the Bastard pyroxenite hangingwall. The RM15 profile shows a slight, but significant decrease in Sr isotope ratio through the Merensky pyroxenite (Figure 5.22a). The overlying norites display an overall increase in Sr isotope ratio, but this is not a systematic increase. However, Sr isotopes in the Bastard pyroxenite in RM15 are distinctly lower than that sample in the Bastard pyroxenite in KF35. At the Bastard footwall the value in KF35 is similar to that in the RM15 profile. At the very base of the pyroxenite there are high values, which are followed immediately by a

significant decrease to Critical Zone values (<0.707). However, these values are slightly higher than those below the Merensky Reef. Initial ratio values continue to decrease through the Bastard pyroxenite and into the overlying anorthosite. A single higher value occurs, but decreases again to values comparable with those in the Bastard pyroxenite. From about 25 m above the Merensky reef, the initial Sr isotope ratio begins to increase, until typical Main Zone (0.7076 – 0.708) values are obtained at about 40 m above the Merensky pyroxenite. These Main Zone values persist to the top of the core. Although KF35 has not been sampled in the Merensky pyroxenite itself, it is clear that the initial ratio increases through the Merensky Cyclic Unit and continues to increase into the Main Zone (Figure 5.22b). In KF35 Sr isotope ratio increases from the Merensky footwall into the hangingwall and continues to increase through the Bastard pyroxenite and into the Lower Main Zone. KF35 shows no reversal in values at the Bastard pyroxenite and initial ratio steadily increases to Main Zone values, which are reached at a height of approximately 15 m above the base of the Merensky pyroxenite.

Another feature that should be noted is the two anomalously high Sr isotope ratios at –96.24 m below the Merensky pyroxenite in RM15 and –159.4 m in KF35. Both these samples have Sr isotope ratios of over 0.707, which is not usually observed until the Main Zone. Interestingly, the RM15 sample has anomalously high absolute Sr content in plagioclase (490 ppm), while the KF35 sample has a value slightly lower (392 ppm) than typical for this level in the stratigraphy. An# of both samples is not significantly different to other samples in the Critical Zone, neither is the Cr content of orthopyroxene from the same level.

One clinopyroxene separate was analysed (sample RM15 140, 23.03 m above the base of the Merensky pyroxenite) and gives a result of 0.70718, which is significantly higher than the plagioclase analysed from the same height in the stratigraphy (Figure 5.22). This might imply that the cumulus and intercumulus phases originated from different magmas and this has been discussed in more detail in section 8.1.

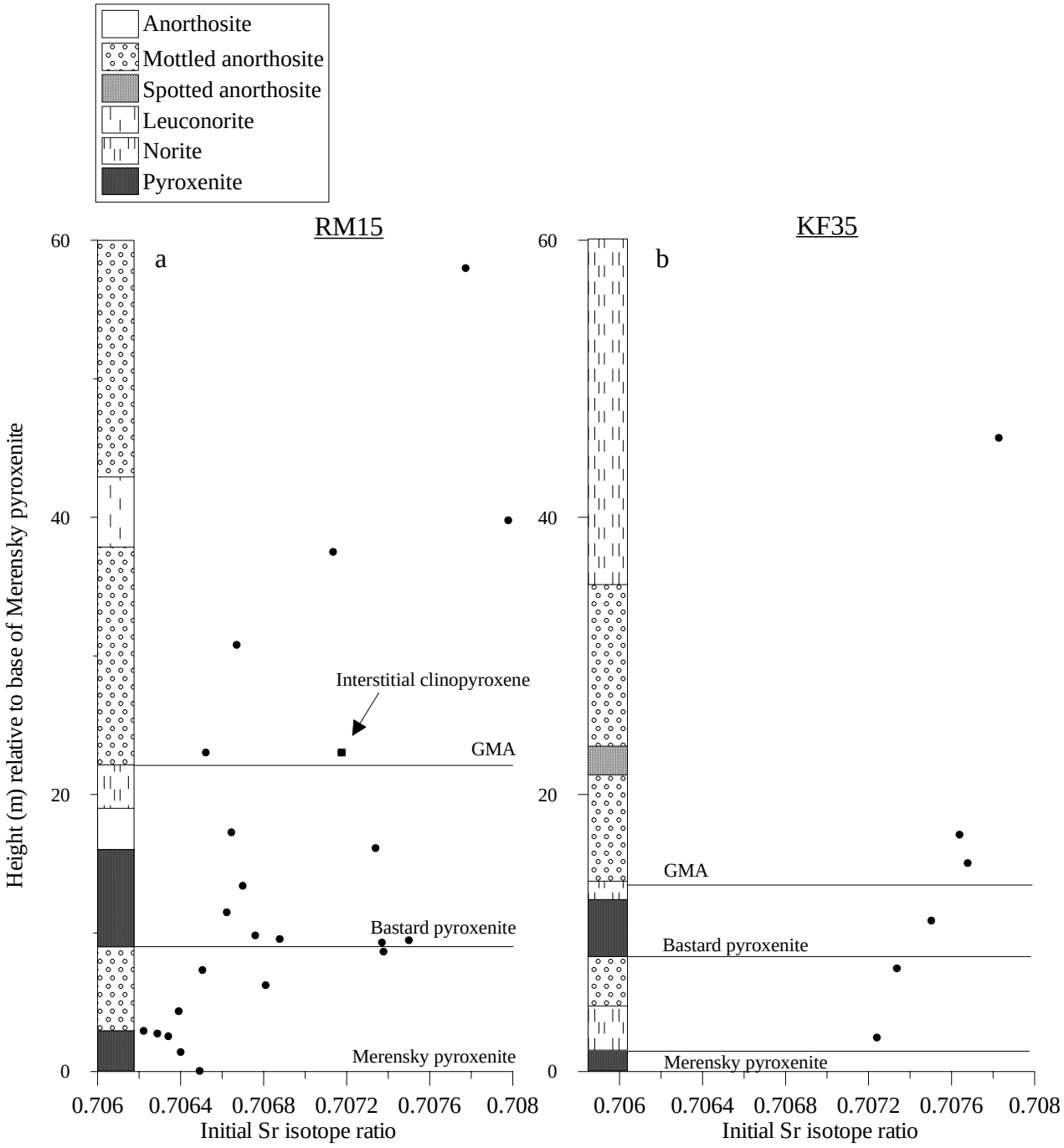


FIGURE 5.22 Sr isotopes plotted against height in the Merensky and Bastard Cyclic Units for (a) RM15 and (b) KF35.

5.5 Sulphide concentration in the Merensky Reef

The abundance of sulphur present in the Merensky pyroxenite and its hangingwall and footwall at Richmond and Kennedy's Vale is given in appendix VI. Figure 5.23 shows these values plotted against height. Samples with values below the detection limit have been included in the graphs in order to show that minimal sulphur values are present. In RM15 (Figure 5.23a), the footwall sample contains very minimal sulphur, below the detection limits (0.001 wt %, appendix II). There is some variation of sulphur content within the pyroxenite itself. The sample at the base of the pyroxenite has a S content below detection limits, but the sample 20 cm above this shows a sharp increase to 0.263 % S, which is followed by a decrease to 0.00105 %. Values remain low and constant until approximately a 50 cm below the top of the pyroxenite. There is a second sharp increase at this point to 1.8 %, four orders of magnitude greater than the sample below it. High values are observed through the uppermost section of the pyroxenite. There is a decrease to approximately 0.1 % S in the two samples from the overlying anorthosite.

Sulphur contents in the Merensky pyroxenite in KV5854 (Figure 5.23b) follow a similar trend to that in RM15. Low values (below detection limits) occur at the base of the pyroxenite. 3 m above the base of the pyroxenite there is a sharp increase to 0.208 % S, which is followed by a subsequent decrease in sulphur content to values similar to those in the lower portion. The uppermost sample in the pyroxenite in KV5854 shows a second sharp increase to 0.432 % S. The overlying sample from the Merensky anorthosite in the hangingwall is also relatively high, 0.173 % S, and this decreases upwards to below the detection limit. Cu and Ni are also plotted in Figure 5.23 and these values correlate well with S. Figure 5.24 shows a plot of Cu vs. S, that demonstrates the positive correlation between these two elements.

Unpublishable PGE data (restricted by confidentiality considerations) are available from Richmond and have been used qualitatively in Chapter 9.

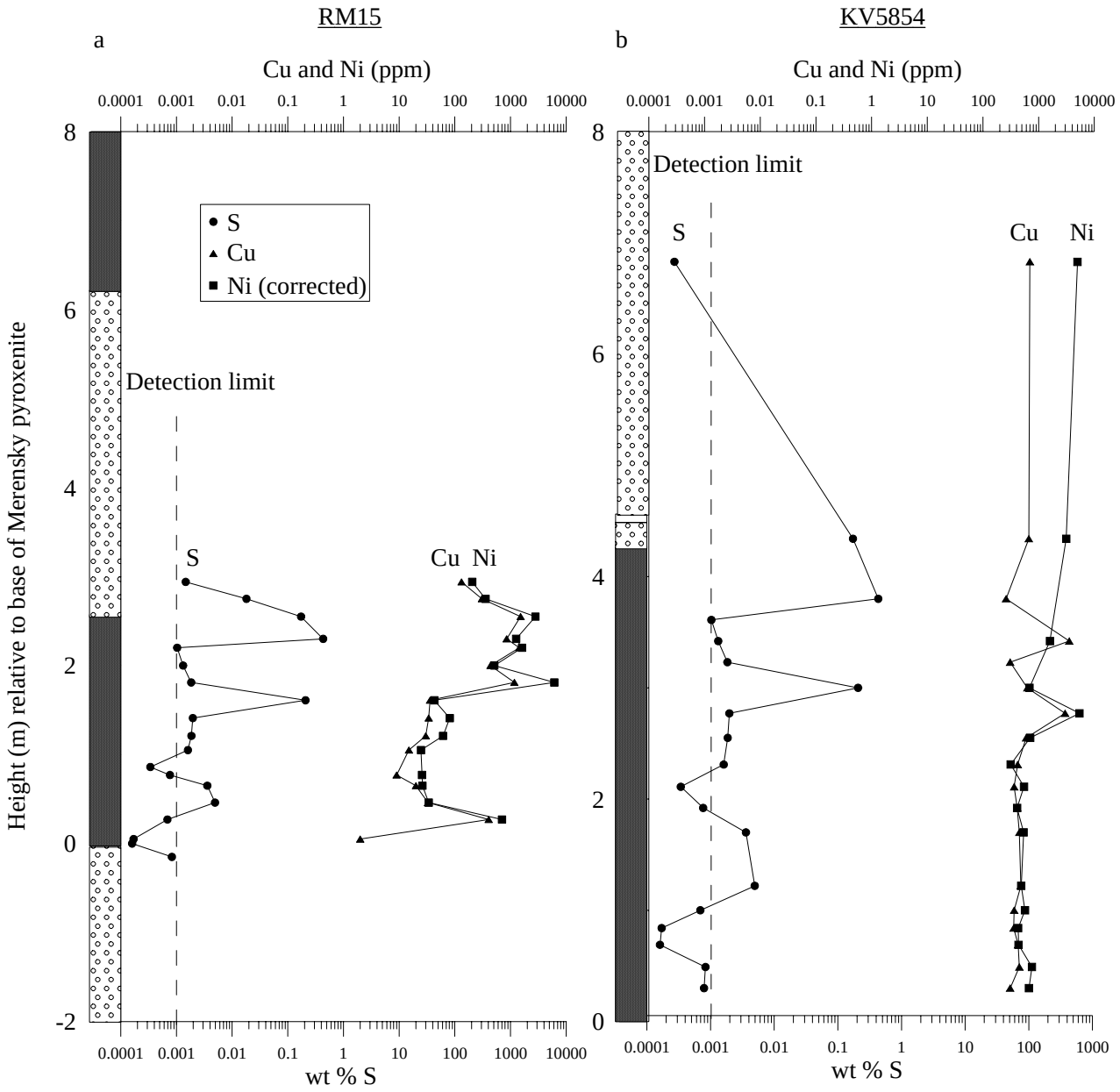


FIGURE 5.23 S, Cu and Ni plotted against stratigraphic height through the Merensky interval for (a) RM15 and (b) KF35. (See section 9.1.3 for details of correction factor for Ni.)

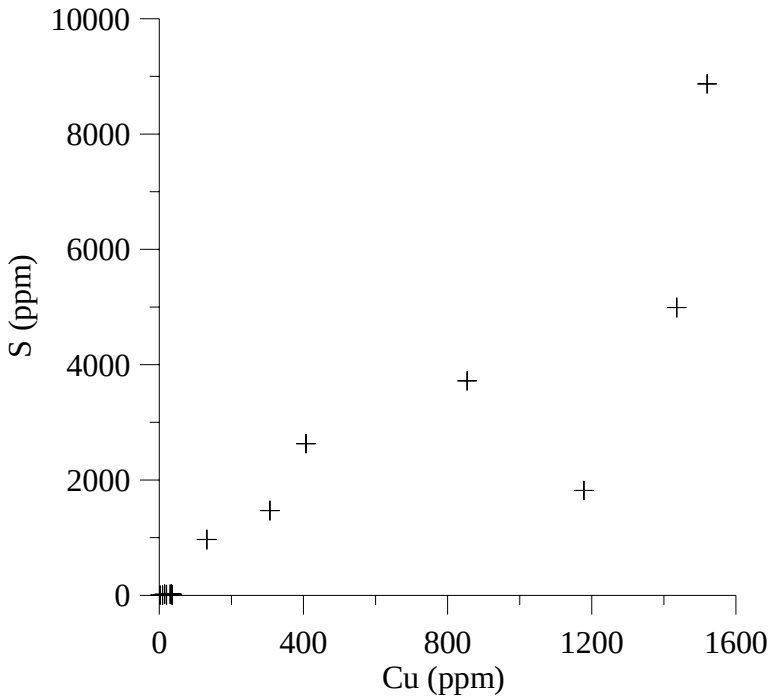


FIGURE 5.24 Cu vs. S in RM15 showing the positive correlation between these two elements.

Chapter 6

Some geochemical investigation techniques

In this section, the use of geochemical data in the study of layered intrusions is discussed. Geochemistry has a wide range of applications that can be used to demonstrate fundamental geological processes, such as those that take place in magma chambers. However, interpretations of geochemical data are often based on assumptions and incompletely considered implications. As a result of this, conclusions can be frequently misleading and inaccurate. This section attempts to clarify the application of geochemical modelling in this study.

6.1 Element ratio modelling in the Upper Critical and Main Zones

Concentrations of single elements in the Bushveld Complex are lithologically controlled. Their compatibility into the minerals present (plagioclase, orthopyroxene or clinopyroxene at the level in this study) is reflected in whole-rock analyses (section 5.1). Elements that are highly compatible with plagioclase will have higher concentrations in anorthosites whereas elements compatible with orthopyroxene show higher concentrations in pyroxenites. Elements that are completely incompatible with both plagioclase and orthopyroxene will have a very low concentration in both anorthosites and pyroxenites, but this is also dependent on the proportions of trapped liquid present. Where elevated amounts of trapped liquid were present, higher concentrations of incompatible elements are observed in the rock.

6.1.1 Trace element ratios

Trace elements can be used to demonstrate fractional crystallisation and evolution of a magma. In rocks accumulated from magma that has undergone fractional crystallisation, it has been assumed that ratios of trace elements in the cumulates do not vary. This theory has been used to propose the influx of fresh batches of magma at certain levels throughout the Upper Critical and Lower Main Zones and to define cyclic units (Eales *et al*. 1986). Specifically, Eales *et al*. used the ratios Co/V and Cr/V, stating that although a single element will show progressive increase or decrease through a cyclic unit as a result of

modal controls, ratios of elements would be independent of modal proportions. Consequently, they concluded that a progressive change in element ratios demonstrated fractional crystallisation and thus sharp increases indicated new magma influxes, which developed the cyclic units. However, the fact that element concentrations will vary according to the proportion of minerals present in the rock and are dependent upon the partition coefficient, as well as proportion of trapped liquid, indicates that element ratios will also vary with a change in these parameters. Thus it is incorrect to assume that element ratios are independent of modal proportions, if D values do not change. In order to demonstrate this principle, a series of theoretical calculations are undertaken and compared with Main Zone and Critical Zone data, taken from RM15 and KV5854.

The behaviour of the trace elements V, Cr, Ni, Co, Y and Zr, and various trace element ratios in whole-rock and in plagioclase, orthopyroxene and clinopyroxene are modelled using average mineral separate analyses obtained from the section under study. Whilst Y and Zr are incompatible elements and should only be controlled by the proportion of trapped liquid, these elements are included for comparison with Eales *et al.* (1986). Partition coefficients were used to determine the composition of the coexisting liquid using the equation:

$D = C_{mineral} / C_L$ which can be rearranged as $C_L = C_{mineral} / D$,

where D = partition coefficient of the mineral, $C_{mineral}$ = composition of the mineral (averages from XRF mineral separates data from Richmond and Kennedy's Vale) and C_L = composition of the liquid from which the minerals formed. It is assumed to be the composition of the liquid trapped after the cumulus grains have accumulated. Whereas this statement may appear self-evident, a number of situations will be discussed in chapters 7 and 8 where it may not be correct.

Table 6.1 was constructed using D values from literature and orthopyroxene and clinopyroxene compositions from this study. Cumulus clinopyroxene did not occur in sufficient quantities to sample in the Critical Zone samples. $D^V_{opx} = 2.6$ (White 2001) was used as this seems much more reasonable than the value of 0.3 (Bédard 1994). This gives a liquid composition that is, when used in the calculations

discussed below, more consistent with observed element values in samples. $D^{Cr}_{cpx} = 10$ was used as it is in agreement with data from Wilson (1992) that shows that the concentration of Cr in clinopyroxene is 1.78 times greater than that in orthopyroxene in the Great Dyke, Zimbabwe (limited studies of clinopyroxene in the Bushveld Complex are available). Thus $D^{Cr}_{cpx} = 10$ and $D^{Cr}_{opx} = 6.5$ used in this study give Cr concentrations closer to those in the study of Wilson (1992) and $D^{Cr}_{cpx} = 34$ (Rollinson 1993) is considered inaccurate. D values for trace elements in table 6.1 into plagioclase are very low (<0.05) and many element concentrations are below detection limits in plagioclase. Thus, attempting to use these values to determine a liquid composition is highly inaccurate and has been excluded in this table. Liquid compositions were calculated using the above equation for both orthopyroxene and clinopyroxene (Main Zone only) and an average taken.

	C_{opx} (ppm)		D_{opx}	C_{liquid} (ppm)		C_{cpx} (ppm)		D_{cpx}	C_{liquid} (ppm)		Av. Liquid compositions	
	MZ	CZ		MZ	CZ	MZ	CZ		MZ	CZ	MZ	CZ
	n=16	n=16		(opx)		n=1	-		(cpx)			
V	246	169	2.6[1]	95	65	385	-	3.1[3]	124	-	110	65
Cr	938	2608	6.5[2]	144	401	1298	-	10[4]	130	-	137	401
Ni	485	649	5[3]	97	130	310	-	3[3]	103	-	100	130
Y	14	7	0.17[3]	82	41	33	-	0.47[3]	70	-	76	41
Co	132	110	2[3]	66	55	52	-	1.2[3]	43	-	55	55
Zr	35	8	0.16[†]	219	50	19	-	0.12[†]	158	-	189	50

TABLE 6.1 Determination of trace element compositions of Critical and Main Zone magmas

[1] White (2001), [2] Bédard (1994) table 1 and references therein, [3] Barnes (1986), [4] Cox *et al.* (1981).

MZ – Main Zone, CZ – Critical Zone, opx – orthopyroxene, cpx – clinopyroxene

Using table 6.1 it is possible to predict the total content of each element in a variety of rock types, based on modal proportions. Consequently, models can be constructed in which the proportions of plagioclase, orthopyroxene and clinopyroxene can be changed methodically to create a range of rock types, from pyroxenite to anorthosite. In addition, the proportion of trapped liquid can also be varied for each rock type. For example, to determine the amount of Ni (ppm) in a Main Zone norite (50% plagioclase and 50% orthopyroxene) (0.5*0.1)+(0.5*485) = 243 ppm. Minimal values for Ni

concentration in plagioclase are used. In the same rock that had 10% trapped liquid (0.45*485)+(0.45*0.1)+(0.1*100) = 228 ppm Ni. Similarly, for Y (0.5*14)+(0.5*0) = 7 ppm in norite where there is no trapped liquid present and (0.45*0)+(0.45*14)+(0.1*76) = 14 ppm where 10% trapped liquid is present. These calculations give a Ni/Y value of 35 with no trapped liquid and 16 with 10% trapped liquid. Another Main Zone rock with 100% orthopyroxene would contain 485 ppm Ni (1*485) and 14 ppm Y (1*14). With 10% trapped liquid the rock would contain (0.9*485)+(0.1*100) = 447 ppm Ni and (0.9*14)+(0.1*76) = 20 ppm Y. Therefore, calculated Ni/Y ratios for this pyroxenite are 35 and 22 where there is 0% and 10% trapped liquid respectively.

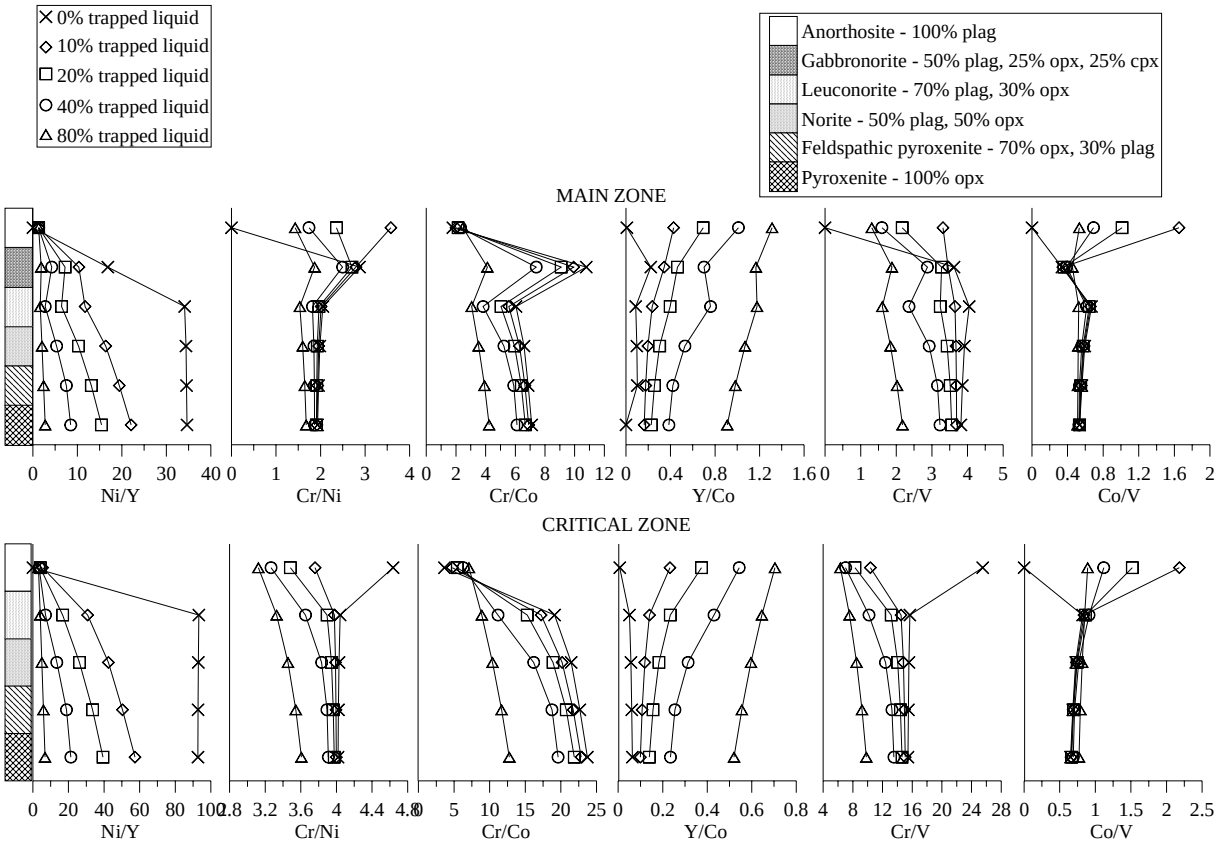


FIGURE 6.1 Calculated trace element ratios with varying trapped liquid proportions, based on Main Zone and Critical Zone parental magmas. These graphs show that variations in trace element ratios are solely dependent on lithological variations.

Using these data, calculated element ratios can be plotted against hypothetical logs that mimic cyclic units within the Critical and Main Zones. Figure 6.1 shows the range of values achieved from modelling some trace element ratios, some of which have been used to demonstrate cyclicity (e.g.

Co/V, Cr/V Eales *et al.* 1986, Eales *et al*. 1990). The hypothetical logs are typical of the succession found in the Critical and Main Zones. It is clear that a range of values is obtainable for each ratio, based solely on changes in mode, even though all rocks have formed from the same magma composition. In addition, there are distinct variations in ratios with changes in the proportion of trapped liquid, which can vary randomly in a vertical succession. It is stressed that in these calculations the composition of the magma is taken as a constant.

For comparison, absolute values for V and Cr are plotted using data from Eales *et al*. and the calculated data obtained in this study, in order to demonstrate appropriate correspondence between them (Figure 6.2). Most notably, it can be seen that both Cr and V ppm decrease significantly with increasing plagioclase content in both the calculated and observed profiles. Trends exist whereby a significant decrease in Cr/V occurs as plagioclase content increases. The most dramatic decrease is observed for anorthosites. In addition, due to the higher partition coefficient of Cr into clinopyroxene than Cr into orthopyroxene, there is an increase of any ratio Cr/x in a gabbronorite layer. This is also seen in the data of Eales *et al.* (1986) where Cr/Co increases in the Porphyritic Gabbro Marker. The modelling undertaken here shows that this increase is the result of different partition coefficients of Cr between minerals and not the result of an influx of new magma. Thus it is shown that it is not necessarily fractional crystallisation of magma that causes changes in these ratios, but changes in the proportions of accumulating phases and trapped liquid content.

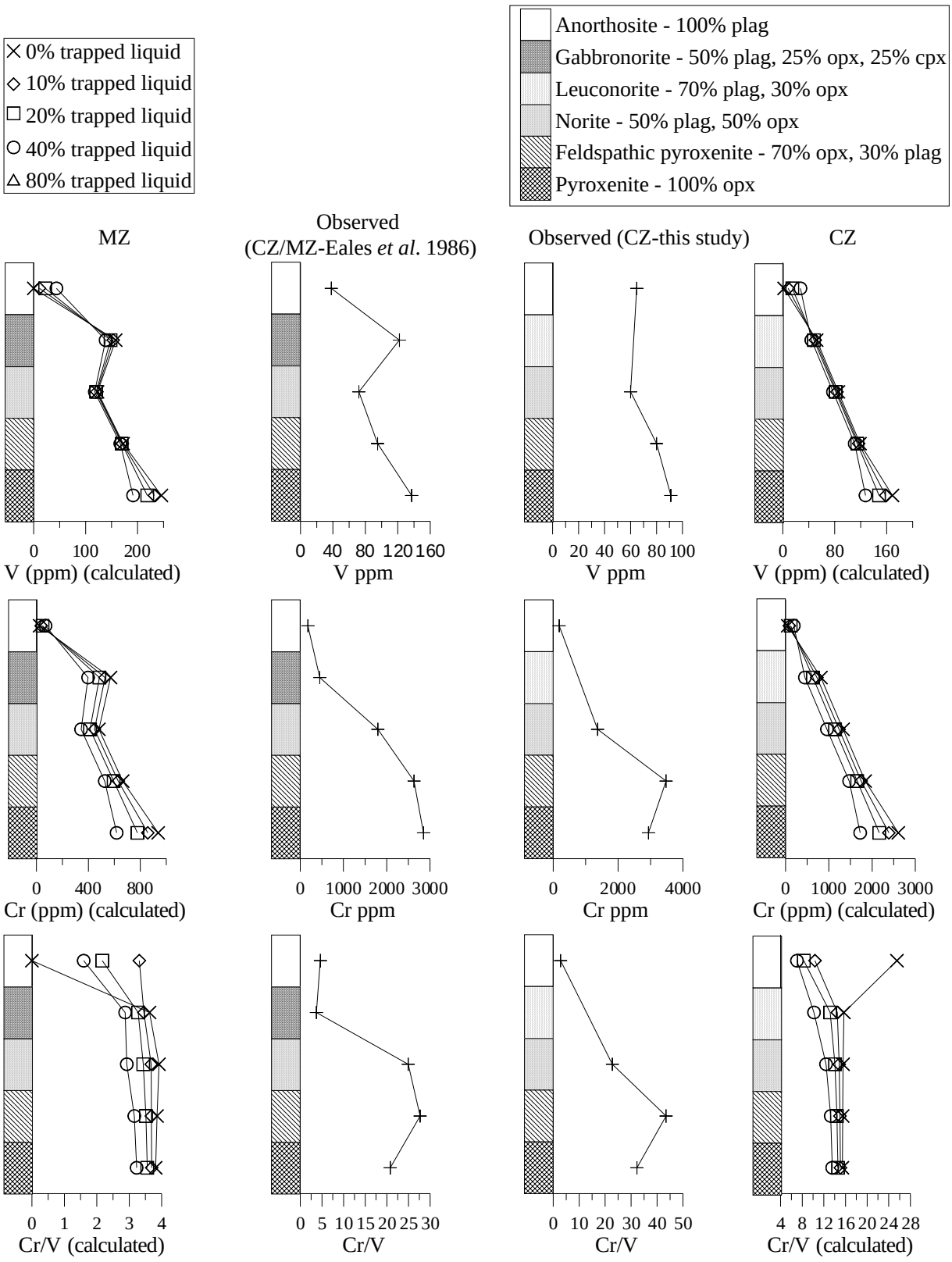


FIGURE 6.2 Calculated absolute Cr and V composition compared with observed Cr and V by Eales *et al.* (1986) and calculated Cr/V ratios for Main Zone and Critical Zone rocks. These graphs demonstrate that the Cr/V ratio varies with lithology and thus new magma additions are not required to show cyclic variations. CZ – Critical Zone, MZ – Main Zone

6.1.2 Cr/MgO ratios in orthopyroxene and whole-rock

Cawthorn (1999a) demonstrated the relationship between Cr and MgO in the Upper Critical Zone. He showed that Cr content in samples from the Upper Critical zone at Impala Platinum Mines increases with increasing wt% MgO and that samples plot in a triangle defined by the compositions of orthopyroxene, plagioclase and trapped liquid (Figure 6.3). The positive linear correlation on this diagram makes it possible to predict the Cr/MgO ratio for these rocks at about 130. The average Cr/MgO of Critical Zone rocks in RM15 and KF35 is 130, but closer to 100 in EG5 and KV5854. Nevertheless, the constant relationship between Cr and MgO regardless of modal proportion may be a useful tool for determining position in the Complex. To this end, it is necessary to model the theoretical Cr and MgO content and thus Cr/MgO of orthopyroxene at different heights in the stratigraphy. Eales (2000) emphasised the fundamental difference between the Cr content of orthopyroxene in the Critical and Main Zones, so distinct differences in Cr/MgO ratios are likely over this boundary. This section demonstrates that Cr/MgO values in orthopyroxene and whole-rock (as both Cr and MgO are highly compatible in orthopyroxene) should be predictable in Critical and Main Zone rocks. Orthopyroxene grains that have chromite inclusions have anomalously high Cr contents (>3500) and have been excluded from calculations and graphs.

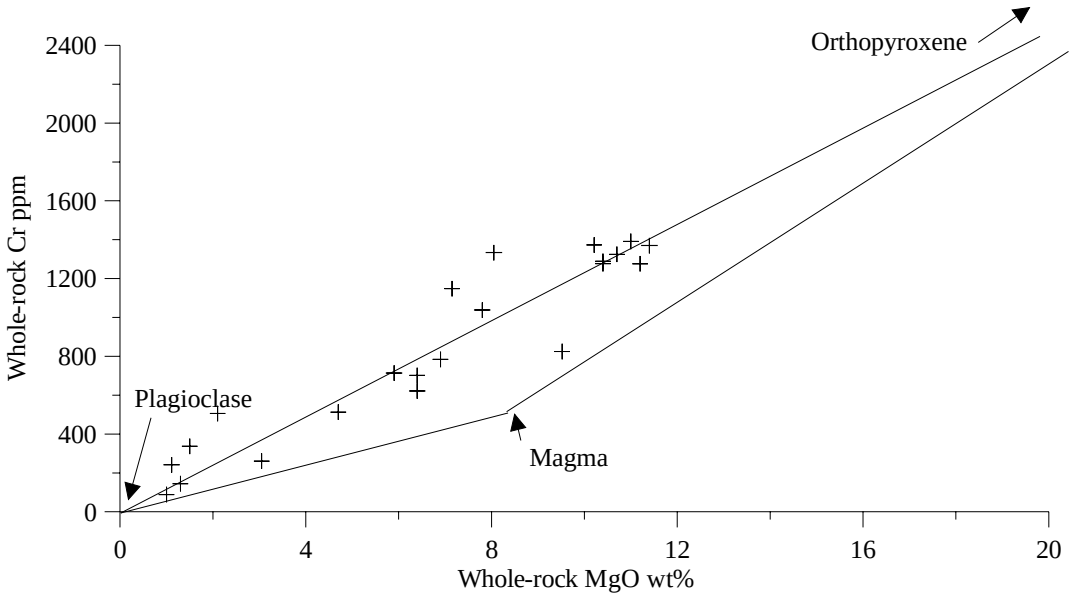


FIGURE 6.3 Plot of whole-rock Cr against MgO from RM15, showing the positive linear relationship between these two elements in orthopyroxene (based on Cawthorn 1999a), giving a Cr/MgO ratio of 120. Magma composition from Cawthorn 1999a.

The compositions of the Critical and Main Zone liquids (C_{liquid}) were determined using partition coefficients (D) from theoretical work and XRF analyses of orthopyroxene separates ($C_{mineral}$) from this study (table 6.2), using the equation $C_{liquid} = C_{mineral} / D$.

The principal of D cannot be used for an element that is a major component of the mineral, as in the case of MgO. Therefore, for the purposes of this investigation, a value was determined using $C_{mineral} / C_{liquid}$ that can be used as an enrichment factor, as in this case, but not for a Raleigh fractionation calculation. These values in table 6.2 were then used to model the Cr/MgO ratio in a range of rock types, with varying MgO content and with different trapped liquid contents.

	Opx composition		**D_{opx}**	**Liquid composition**	
	Main Zone	Critical Zone		Main Zone	Critical Zone
Cr (ppm)	938[§]	2608[§]	6.5*	91	401
MgO (wt%)	24[§]	28[§]	3.6**	6.7	7[†]
Cr/MgO	39	93		13.5	57

TABLE 6.2 Determination of liquid composition for Critical and Main Zone magmas based on the composition of orthopyroxene in this study

* Barnes (1986), based on the crystallisation of orthopyroxene and plagioclase at 1180°C

** value calculated based on $D = C_{mineral} / C_{liquid}$ (see explanation in text above)

† Cawthorn & Biggar (1993)

§ Average values from this study

Figure 6.4 shows that Cr/MgO remains largely constant where MgO > 5 wt%. Below 5 wt% MgO (rocks containing less than 15% orthopyroxene), Cr/MgO begins to decrease sharply. This is because the trapped liquid has a lower Cr/MgO value than the orthopyroxene (table 6.2). In addition, Figure 6.4 shows that theoretically, Main Zone and Critical Zone rocks have distinctly different Cr/MgO values, of approximately 35 and 90 respectively, these values decreasing slightly with an increase in trapped liquid content, or at low orthopyroxene content.

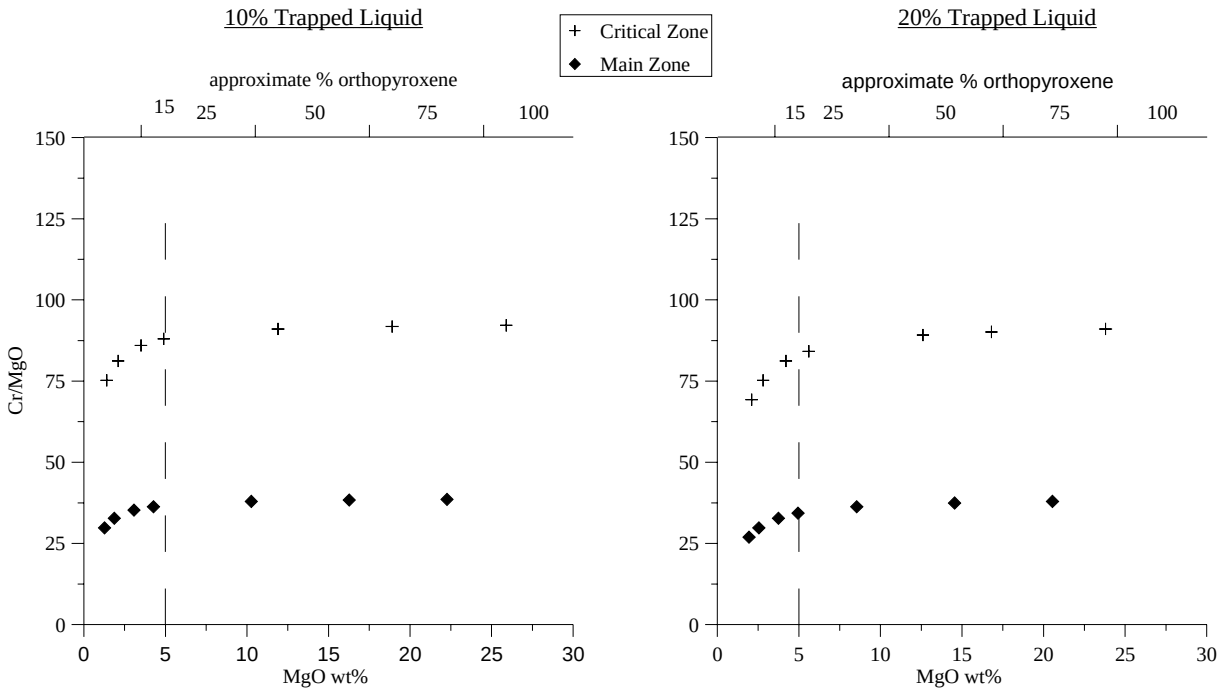


FIGURE 6.4 Calculated Cr/MgO in orthopyroxene at varying MgO content at 10% and 20% trapped liquid content, showing that the Cr/MgO remains constant with variations in lithology, except in anorthosites.

6.2 Cumulus and intercumulus minerals

It is important that the chemical differences between interstitial and cumulus minerals are clear, even though textures may no longer be definitive. Cumulus minerals are a product of fractional crystallisation of, and accumulation from, a magma. Interstitial or intercumulus minerals form from the pore liquid trapped between the cumulus framework. This intercumulus liquid may be a fractionated product of the original magma, or, where gravitational settling of cumulus crystals has occurred through a stratified magma column, may be a completely different magma. Alternatively, residual liquid may have been forced upward from deeper parts of the crystal mush. This means that cumulus and interstitial crystals in the same rock may not have formed from the same magma. This section discusses the methods of estimating trapped liquid proportions and thus the amount of interstitial material. The occurrence of cumulus plagioclase within pyroxenites is also discussed.

6.2.1 Trapped liquid estimation

Incompatible elements have been widely used to determine the amount of trapped liquid present in a rock. This principle was initiated by Henderson (1975) who suggested that it is possible to calculate the proportion of trapped liquid in cumulate rocks when the concentrations of the incompatible element in the parental magma are known. Cawthorn (1999b) used this method based on a parental magma analysed by Davies *et al*. (1980) to calculate trapped liquid content in the Upper Critical Zone. Both these studies used a single element, U and Zr respectively, in their calculations. However, it remains unclear as to how representative a single incompatible element may be for use in trapped liquid calculations. The distribution of minerals formed from incompatible elements e.g. zirconium, may be irregular throughout the portion of rock under study. For example, if a certain piece of core contains 1 zircon crystal, it must have drawn its Zr from a certain volume around it, thus depleting this volume of Zr. The rest of that specific piece of core may then be depleted in Zr. Without knowing the distribution density of such grains, it is impossible to know whether an analysis of a sample is truly representative, or conversely, how large a sample should be taken to obtain a representative analysis. In this study, and many other geochemical studies on the Bushveld Complex, bore core has been used. Typical diameter and length of half core taken are 3.5 and 20 cm respectively, producing a sample mass of approximately 300g. From this, some 20g are taken for analysis. The question is whether such methodology is valid for quantitative determination of trapped liquid content.

In order to assess the distribution of incompatible elements in any given piece of rock, multiple pellets were made for 2 samples from the same powdered rock sample. The results are given in table 6.3 and show that there is very little variation in K_2O wt% and P_2O_5 wt% for pellets from the same rock sample. This means that the crushing and milling process utilised to make XRF pellets sufficiently homogenises the material so that the presence of any incompatible element-bearing minerals is uniformly recorded in every analysis.

Sample Number	**K_2O wt%**	**P_2O_5 wt%**
RM15 31.61 A	0.156	0.038
RM15 31.61 B	0.162	0.037
RM15 31.61 C	0.160	0.038
RM15 31.61 D	0.160	0.038
RM15 31.61 E	0.158	0.037
RM15 119.18 A	0.070	0.008
RM15 119.18 B	0.071	0.009
RM15 119.18 C	0.071	0.009
RM15 119.18 D	0.072	0.009

TABLE 6.3 Repeat analyses of K_2O wt% and P_2O_5 wt% showing that homogenisation of whole-rock powders is sufficient to record uniform incompatible element abundances in each sample. Precision and accuracy for these analyses are given in Appendix II.

6.2.2 Testing the reliability of incompatible elements

In order to consider the reliability of incompatible elements to effectively demonstrate relative trapped liquid proportions, it would be necessary to show trends using more than one element, thus negating the possible effect of trace mineral distribution. Wilson *et al*. (1999) investigated two incompatible elements (Zr and P) in a sequence through the Merensky pyroxenite. In a profile of depth versus concentration, the two elements show mutual dependence in all rocks except the Merensky Unit and when plotted against each other (figure. 8, page 665, in their paper) show a positive linear correlation indicating simultaneous variations and suggesting that the ratio P/Zr is constant in any one zone, suggesting both elements give the same percentage of trapped liquid. Ideally, to fully evaluate the effectiveness of incompatible elements to demonstrate trapped liquid content, a number of elements should be used over a representative sequence.

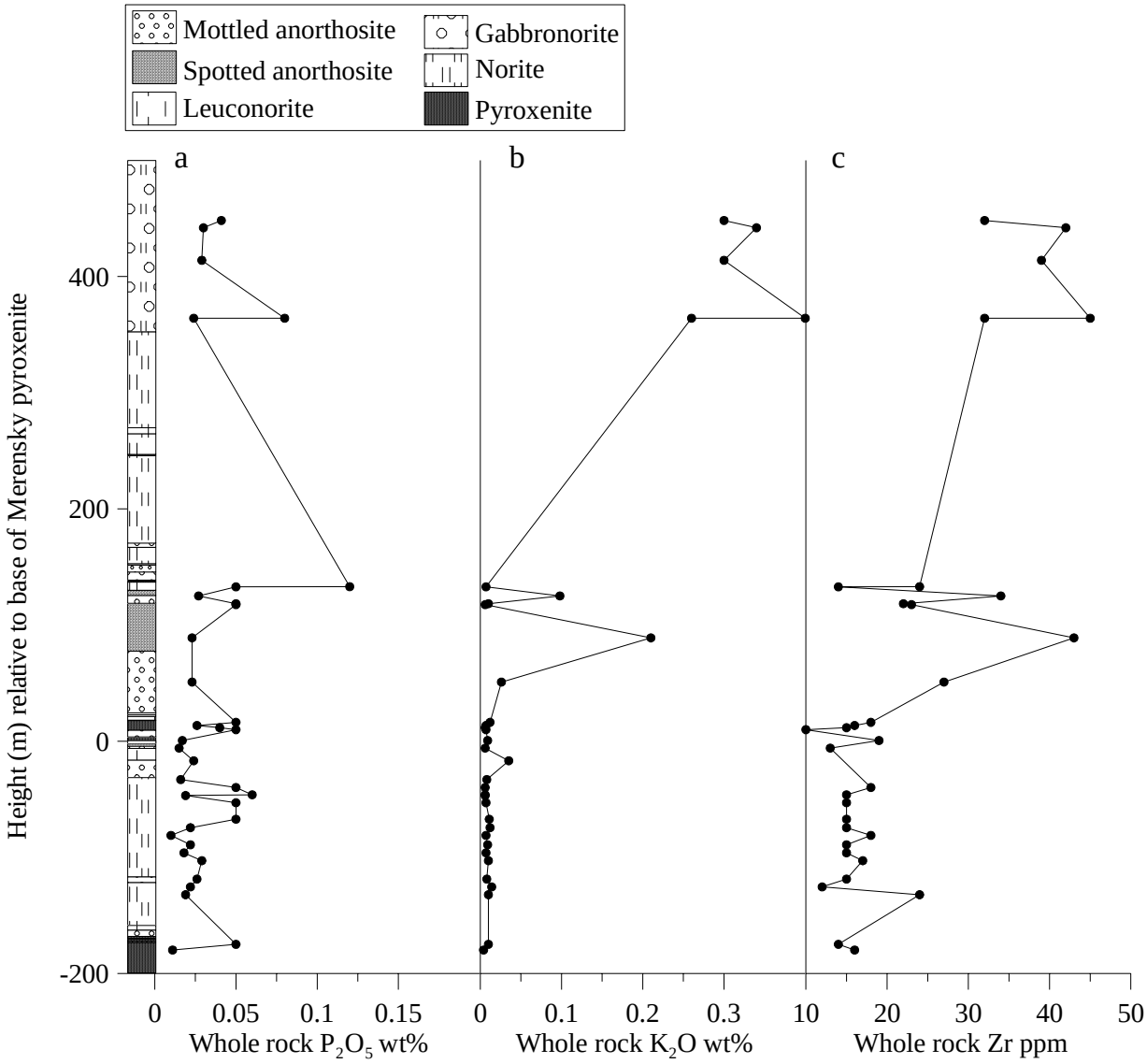


FIGURE 6.5 Whole-rock P_2O_5 (a), K_2O (b) and Zr (c) in core RM15 plotted against height. These graphs show that there is little correlation between these elements.

In this study P_2O_5, K_2O and Zr values were obtained from some RM15 samples. Precision and accuracy for these analyses are given in Appendix II. Figure 6.5 shows these elements plotted against height in core. This diagram demonstrates that these elements are not generally well coupled. This poor relationship is further demonstrated in Figure 6.6 that shows Zr, P and K plotted against each other. None of the graphs shows good positive correlation, which indicates that variations in these elements are independent of one another. Thus, using a single incompatible element to demonstrate trapped liquid proportions must be unreliable, since it is clear that these three incompatible elements do not show the same trends. The variations observed here between incompatible elements must therefore be

the result of mineral distribution and sampling, or migration of residual liquid on a scale greater than that of the sample. Larger samples should be taken before quantitative modelling of trapped liquid content can be evaluated. This study suggests that heterogeneities exist on a scale of at least a few cm.

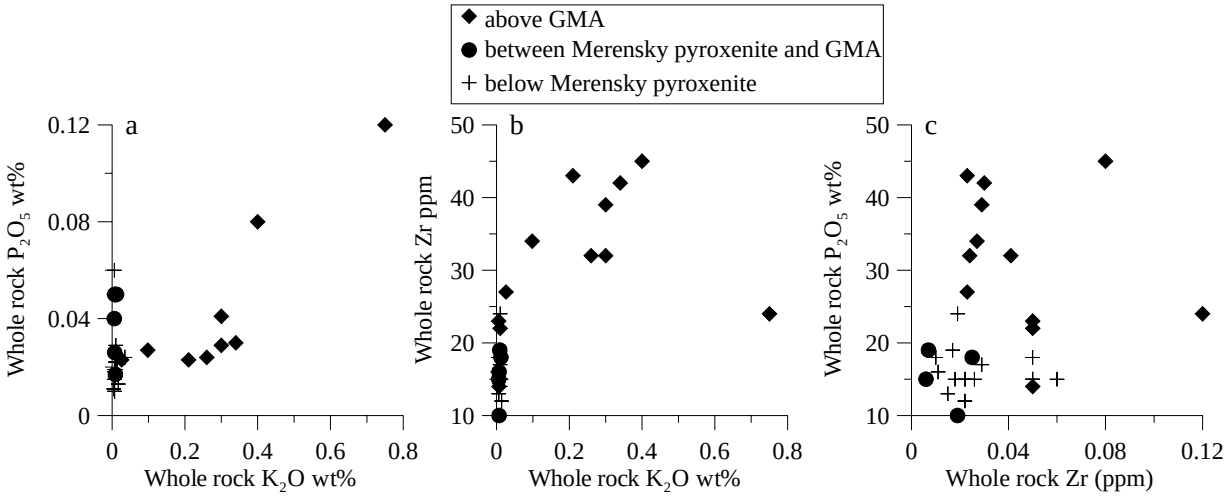


FIGURE 6.6 Whole-rock P_2O_5 (a) and Zr (b) plotted against K_2O and Zr plotted against P_2O_5 (c) for core RM15, showing little correlation.

	Parental Magma		**Average composition of rocks in this study**		**Trapped liquid fraction as %**	
	Zr ppm	K_2O wt%	Zr ppm	K_2O wt%	Zr	K_2O
Main Zone	31*	0.34*	29	0.23	94 %	68 %
Critical Zone	70†	1.03†	15	0.09	21 %	8.7 %

TABLE 6.4 – Estimations of trapped liquid content based on parental magmas and the composition of rocks in this study. P_2O_5 not included, as concentrations in parental magma are unavailable

* Maier *et al*. (2000)

† Davies *et al*. (1980)

Estimation of trapped liquid content using the data presented here (Table 6.4) shows that very different results are obtained depending on the incompatible element used. It is assumed that each element has a "D" value equal to 0. In the Critical Zone, Zr gives an average trapped liquid content of 21%, while K_2O gives 8.7%. However, since orthopyroxene does contain some Zr (approximately 15 ppm at 30%

MgO in RM15) and plagioclase does contain some K_2O (approximately 0.29 % in RM15) then the total amount of Zr or K_2O in the whole rock analyses does not purely reflect the trapped liquid component. Nevertheless, since the purpose of Table 6.4 is to emphasise the difference between trapped liquid content estimations using Zr and K_2O, this correction has not been applied. The large relative difference shown in Table 6.4 suggests that the proposed parental magma is incorrect in terms of Zr and K. Using the average trapped liquid fraction of three incompatible elements might give a better indication of overall trapped liquid proportion.

It is clear from table 6.4 that the parental magmas to the Critical and Main Zone are poorly constrained, at least in terms of incompatible elements, as the calculated trapped liquid fraction is excessively high. Compositions given in Maier *et al*. (2000) do not contain sufficiently high incompatible element concentrations. Similarly, the Main Zone magma composition suggested in Sharpe (1985), with 12 ppm Zr and 0.11 wt% K_2O, is also inaccurate. The latter value must be impossible since calculated proportions of trapped liquid would exceed 100%. The value of 0.4 wt% K_2O from Cawthorn *et al.* (1981) gives high trapped liquid contents and thus might also be inaccurate. Since the Main Zone magma is not directly represented in sills, it is not yet well defined, although a gabbronoritic marginal chill has been accepted as parental by Harmer & Sharpe (1985). However, if the Main Zone cumulates formed from a magma that was a mixture of the magma added at the base of the Main Zone (0.42 % K_2O) and a fractionated magma that formed the Upper Critical Zone (K_2O >1%), it would be difficult to constrain the exact composition of magma from which the Main Zone crystallised.

It can be concluded that quantitative estimates of the proportion of trapped liquid are largely inaccurate and should be considered unreliable, as estimations vary depending on the element used. In addition, the reliability of the parental magma composition is considered in sufficient.

6.2.3 Estimating cumulus plagioclase content with specific reference to the Merensky and Bastard units

Specific estimations of trapped liquid content and thus intercumulus minerals in the Merensky and Bastard Cyclic Units may contribute to the understanding of processes occurring in these layers. In these cyclic units, the pyroxenite contains up to approximately 30% plagioclase (e.g. Viljoen 1999 and Chapter 4, this study). It is generally considered that all plagioclase in the Merensky pyroxenite is interstitial and that plagioclase is the only interstitial mineral present (e.g. Nicholson & Mathez 1991). However, the residual liquid should crystallise approximately 60% plagioclase and 40% orthopyroxene, so that if there is 30% interstitial plagioclase, it should be accompanied by about 20% interstitial orthopyroxene. This would give a total of 50% intercumulus component, and thus only 50% of the rock would be cumulus. Such a large interstitial component seems dubious, based on incompatible trace element content, and it must therefore be considered that some plagioclase in the Merensky pyroxenite is cumulus in origin. It was shown in section 6.2.2 that estimation of trapped liquid proportion, and thus proportion of intercumulus minerals, is unreliable using incompatible element concentrations. In addition, insufficient information is available to estimate trapped liquid proportions from a Main Zone liquid. Textural observations alone are inconclusive since extensive textural annealing has occurred in these rocks (Hunter, 1996) and it is unlikely that the textures are original (section 4.6). Nevertheless, large (>1 cm) apparently interstitial plagioclase grains could easily have accommodated numerous cumulus grains, especially if they were of the small size found in orthopyroxene inclusions (section 4.4). Therefore, in order to determine whether plagioclase in the Merensky and Bastard pyroxenites is in fact cumulus or interstitial another method is investigated.

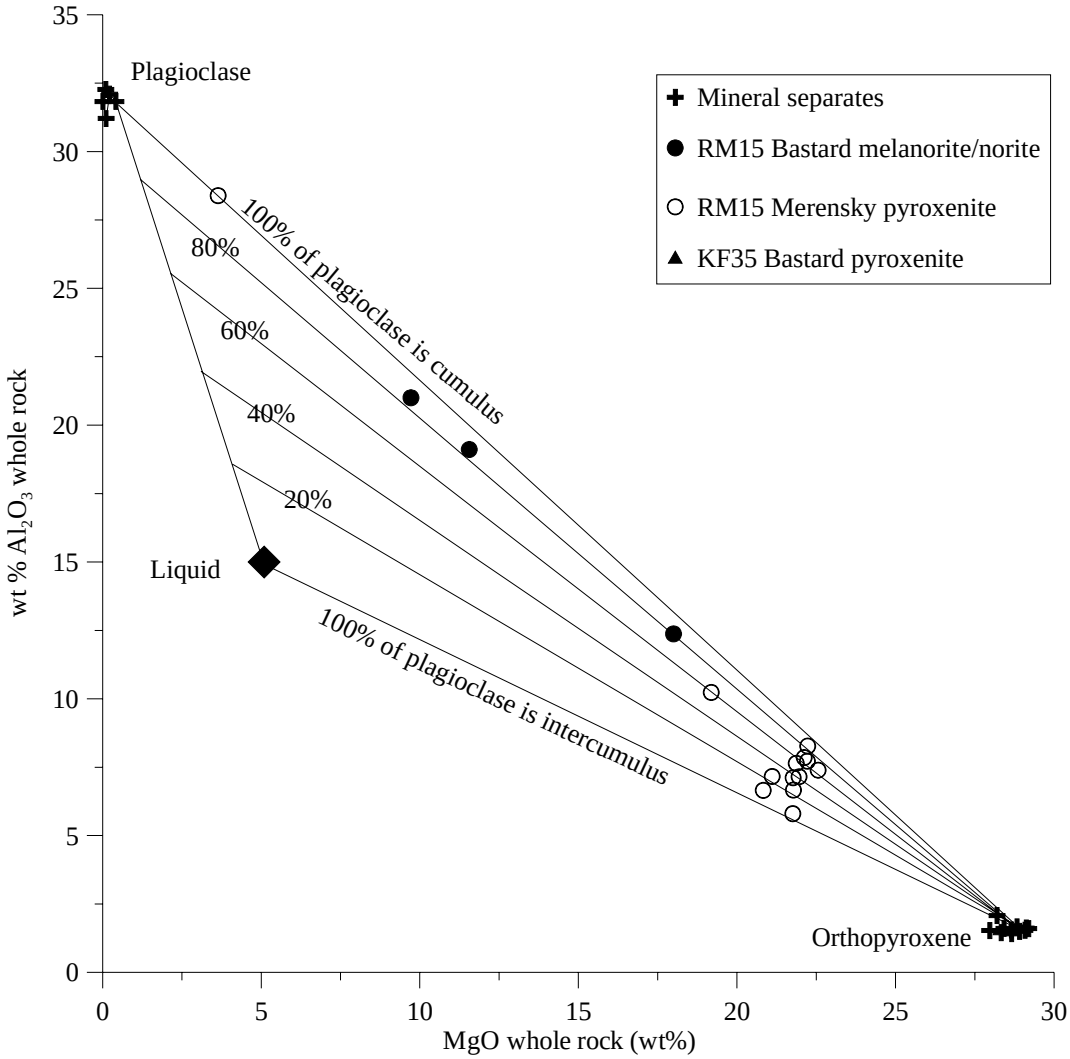


FIGURE 6.7 Diagram of whole-rock Al_2O_3 plotted against MgO and compositions of plagioclase and orthopyroxene mineral separates showing the proportion of cumulus plagioclase present in the Merensky and Bastard pyroxenites. Composition of trapped liquid is taken from Li *et al.* (2001a). From this diagram it is possible to determine the relative proportions of cumulus to interstitial plagioclase in any sample (see text for discussion).

Boerst (2001) determined that using a graph of MgO versus Al_2O_3 on which is plotted the composition of the trapped liquid, it is possible to estimate proportion of minerals and trapped liquid comprising any whole-rock composition from this section of the Bushveld Complex. Figure 6.7 shows whole-rock Al_2O_3 content plotted against MgO for the Merensky pyroxenite and Bastard melanorite/norite in RM15. The compositions of orthopyroxene and plagioclase mineral separates have also been plotted. These mineral compositions, along with the calculated composition of the trapped liquid (Li *et al.* 2001a), also determined from experimental study by Cawthorn & Biggar (1993), define a triangle that encompasses all whole-rock compositions consisting of variable proportions of cumulus orthopyroxene

and plagioclase and trapped magma. Samples that contain orthopyroxene as the only cumulus phase ought to plot along the orthopyroxene-liquid tie line. If they also contain cumulus plagioclase whole-rock compositions will lie within the triangle. The position of the liquid on the graph might vary considerably, but this would not effect the geometrical argument presented here. It is clear that in the various samples in the Merensky and Bastard pyroxenites, from 0 to over 80% of the total plagioclase content is cumulus.

In addition, a high interstitial component in the rock should be characterised by an increase in incompatible trace element concentrations. Figure 6.8 shows the proportion of plagioclase that is cumulus in samples from RM15 Merensky pyroxenite (based on Figure 6.7) plotted against the incompatible element Zr for that sample. Although there is not a clear relationship, overall, samples that have a higher cumulus component do tend to have lower Zr content and higher Zr values are observed in samples with an increased interstitial plagioclase component. Using the same graph of Al_2O_3 against MgO, as in Figure 6.7, but drawing lines of trapped liquid proportion instead of percentage of cumulus plagioclase, we can estimate % trapped liquid for each of the samples (Figure 6.9a). These results can be plotted against Zr (Figure 6.9b) to demonstrate the positive correlation between trapped liquid proportion and incompatible element content, confirming the validity of this method.

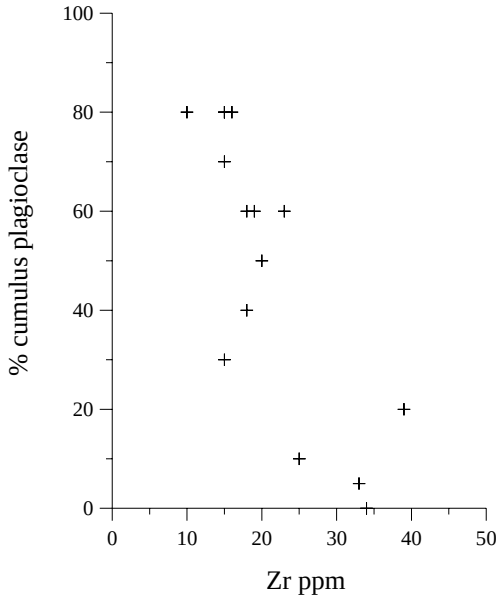


FIGURE 6.8 Proportion of cumulus plagioclase plotted against Zr ppm showing slightly higher incompatible element content where the proportion of cumulus plagioclase has been determined as low.

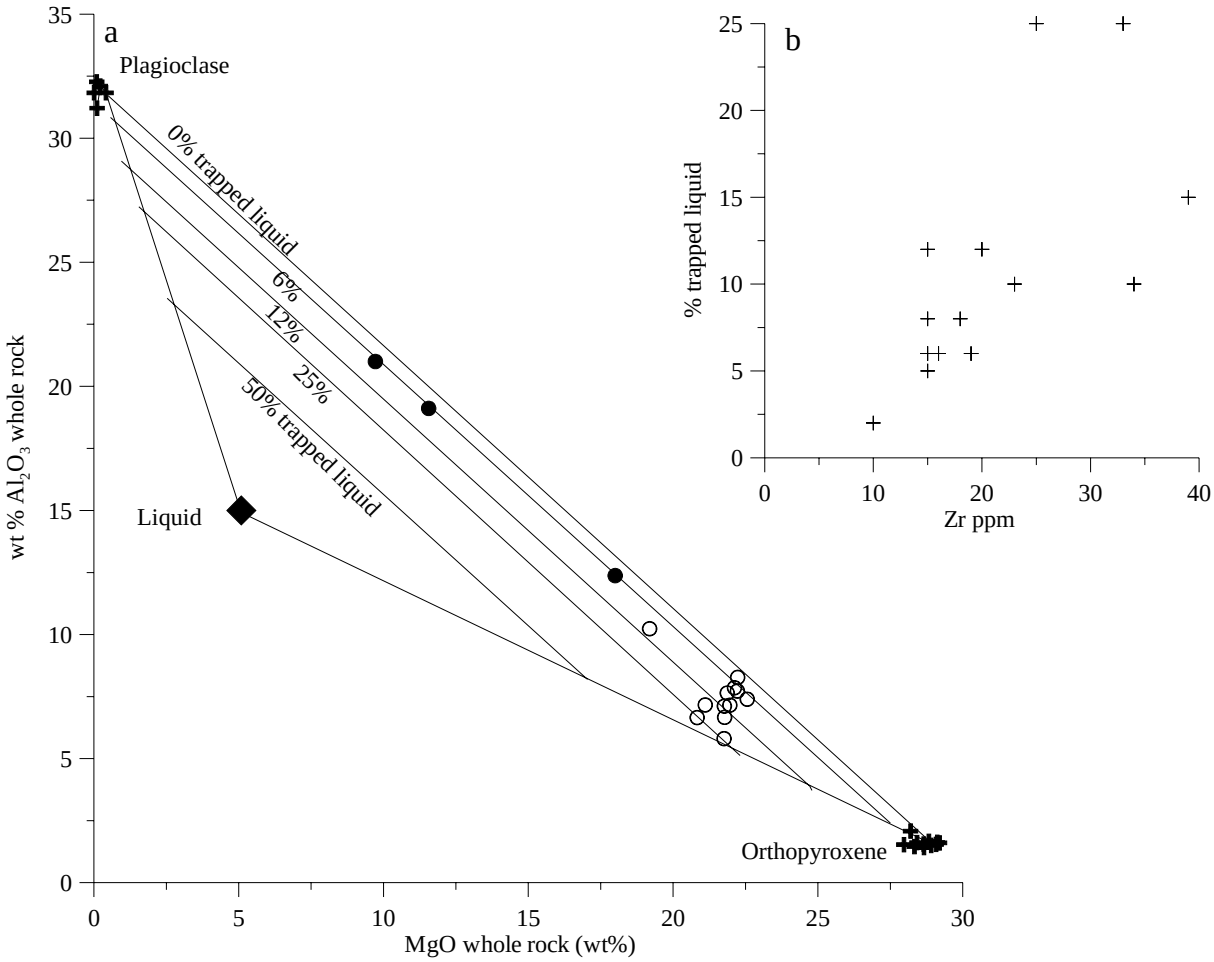


FIGURE 6.9 Diagram of a) whole-rock Al_2O_3 against MgO showing estimated proportions of trapped liquid in the Merensky and Bastard pyroxenites (symbols as in Figure 6.7) and b) trapped liquid % against Zr ppm for those samples.

6.3 Sr isotopes and their application to layered intrusions

This section provides some background information on Sr isotopes and their uses in interpreting layered intrusions. Previous work on the Bushveld Complex, specifically the Critical/Main Zone boundary, is reviewed and these ideas are initially applied to the data from this study. However, using Sr isotope data alone results in simplistic models for the origin and evolution of magmas in the Bushveld Complex. Thus, whilst this section provides information on previous isotope studies, the following chapters include detailed geochemical studies that are discussed and interpreted in combination with the isotope data.

6.3.1 Background information

The age of a rock can be obtained using the decay of ^{87}Rb to ^{87}Sr but Sr isotopes can also inform us about the geochemical history of the Sr they contain. This information can be determined because the isotopic composition of Sr is assumed to have been homogeneous in the Earth at the beginning of geologic time and has become increasingly heterogeneous ever since. Geological processes continuously destroy rock systems that formed earlier and recombine the material to form new rocks. The Sr in the newly formed rocks is derived from older rocks which themselves may have formed from still earlier generations of rocks (Faure 1986). In terms of igneous processes, this means that variations in $^{87}Sr/^{86}Sr$ are the result of integration of rocks of different ages. These variations are unaffected by fractional crystallisation and equilibrium partial melting. Thus, variations are considered to be the result of contamination from isotopically different materials, generally crustal, or mixing of isotopically different source magmas. In addition, alteration can alter the original Sr isotope ratio.

Kruger & Marsh (1982) described the change in Sr_i at the level of the Merensky Unit. They showed a pattern of variation that involves a sharp increase at the base of the Merensky Unit, which is similar to that documented in most subsequent studies (Sharpe 1985, Lee & Butcher 1990, Kruger 1992, Kruger 1994, Marcantonio & Mathez 1995 and Schoenberg *et al.* 1999), and to that observed here in KF35 and RM15 (Figure 5.20). There has been much debate over the processes involved in generating stratigraphic discontinuities in isotope ratio in layered intrusions, particularly the Bushveld Complex. The following section summarises the theories that have attempted to explain this feature.

6.3.2 Crustal Contamination

Kruger & Marsh (1982) discussed two main models to explain the increase in Sr_i at the level of the Merensky pyroxenite. Firstly, they suggested that the increase might reflect *in situ* contamination of the existing magma by its wall rocks, where contamination began at the Merensky pyroxenite and ceased in the region of the base of the Bastard Cyclic Unit and crystallisation proceeded to produce Main Zone rocks with elevated more uniform Sr_i. However, they indicated that contamination was unlikely based on the implausibility of whole-magma convection, the excessive amount of contamination needed to raise the Sr_i of the entire Main Zone and the low Sr_i of the Rooiberg felsites that form the wall rock. Using data from this study, it is possible to supply quantitative evidence against the possibility that wall rock contamination is responsible for the variations seen in the Sr_i profile (Figure 5.21). Since the RM15 and the KF35 profiles are significantly different through the Merensky and Bastard Cyclic units (Figure 5.21) then one would have to envisage different amounts of contamination, or different contaminants, in each location. To measure this possibility, Rb and K_2O concentrations in plagioclase were used as an indicator of the extent of a possible crustal component. Plagioclase separates were used because Rb is incompatible in orthopyroxene and using whole-rock content of Rb and K_2O would thus be influenced by modal proportion. Similarly, using whole-rock analyses would reflect the presence of any potassium-feldspar, increasing apparent K_2O content. An increase in Rb and K_2O in plagioclase should be indicative of an increase in crustal contamination, assuming a constant partition coefficient This should correlate with an increase in Sr_i in order to signify the introduction of crustal material at that level. Even if the contaminant is low in Rb, such as lower crustal granulite or amphibolite, a partial melt from it would contain more Rb than the magma so an increase in Rb in plagioclase would still be observed. Figure 6.10 shows Rb and K_2O in plagioclase variations with height for both cores. It is clear that variations in Rb and K_2O correlate well between each other, but when compared to the changes in Sr_i there is no convincing correlation (Figure 6.11). For RM15, where Sr_i decreases in the Bastard Cyclic Unit, Rb and K_2O increase. For KF35 there is very little variation in Rb. These data strongly indicate that wall rock contamination is not responsible for increases in Sr isotope initial ratios.

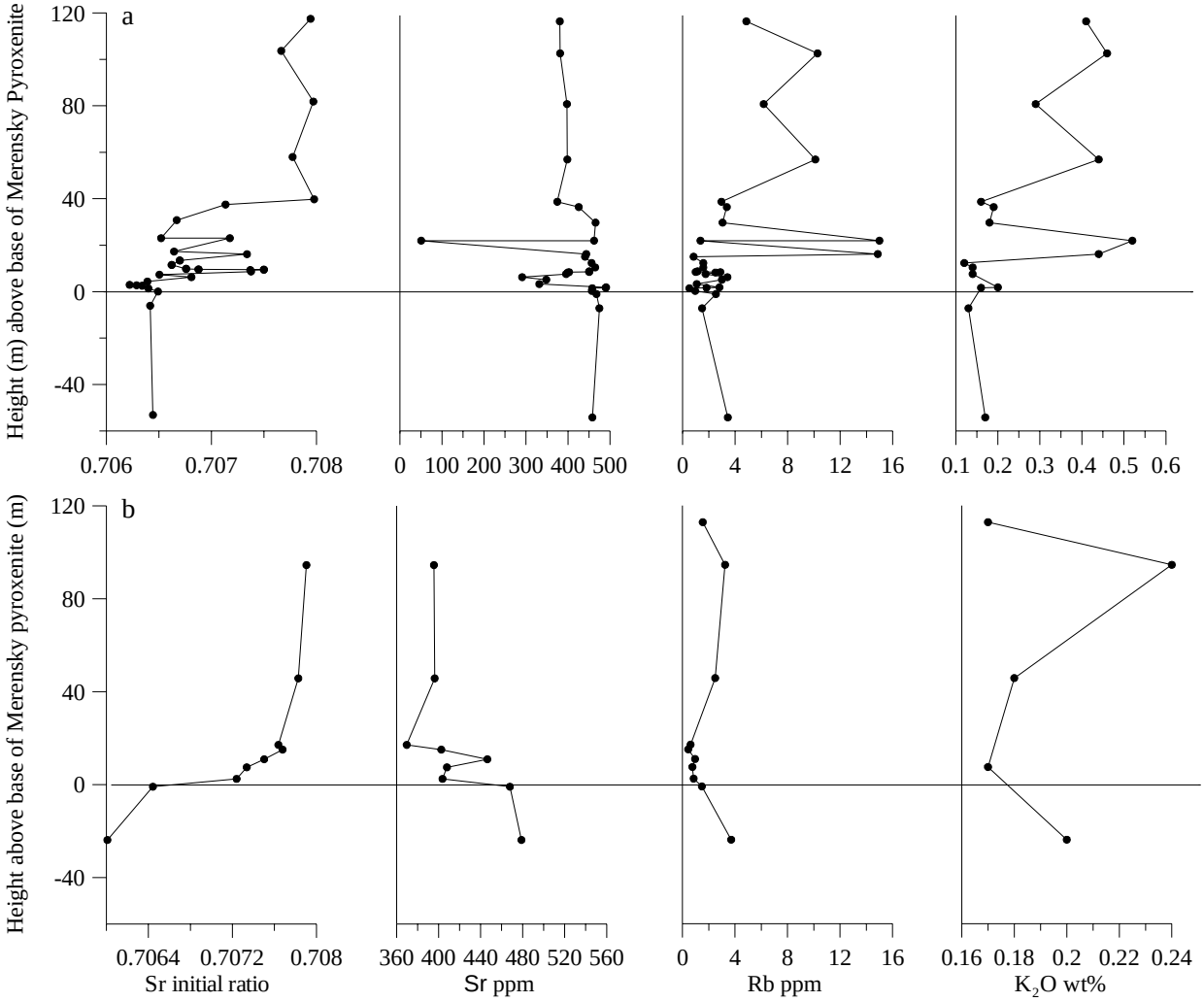


FIGURE 6.10 Sr isotopes, Sr, Rb and K_2O in plagioclase separates plotted against height for cores (a) RM15 and (b) KF35.

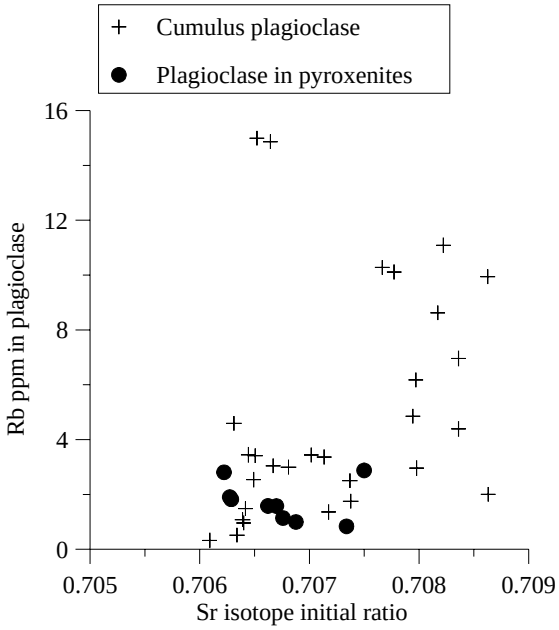


FIGURE 6.11 Rb in plagioclase plotted against Sr isotope ratios for RM15.

6.3.3 Magma Mixing

As an alternative, Kruger & Marsh (1982) indicated that the Main Zone rocks might have crystallised from an influx of new magma (with a Sr initial ratio of >0.7075) into the chamber and that the Sr_i variation observed is the result of interaction and mixing between the new and resident magma. They interpreted mixing to have occurred due to density and thermal contrasts between existing and new liquids, with turbulent or convecting mixing due to the nature of the chamber. This is however, difficult to reconcile since magmas of different densities should not mix. Although no specific mixing process was described, this model has become the most widely accepted to explain the sharp increase of Sr_i. Lee & Butcher (1990) investigated the Sr_i reversal at the level of the Bastard pyroxenite at Atok (Figure 6.12) in the eastern Bushveld. The Atok section gives a distinctly saw-tooth pattern in marked contrast to the simple pattern described by Kruger & Marsh (1982). This pattern is very similar to that observed in RM15. Lee & Butcher concur with Kruger & Marsh that processes involving more than one parental magma type formed the saw-tooth trends. They go on to propose that the new magma entering the chamber was injected into pre-existing, partly solidified, norites and anorthosites in a sill-like fashion, giving rise to the pyroxenite layers. This theory is based on data and conclusions from the Rum intrusion compiled by Bédard *et al*. (1988).

In line with previous work described above, the data presented in this study may also be interpreted as being the result of the influx of a new magma. In this case, as in KF35, the new magma would have been introduced at the base of the Merensky unit where it mixed with the residual liquid from the earlier magma, producing a large vertical interval of mixing (Figure 5.20), where Sr_i is still increasing over 400 m above the Merensky pyroxenite. This may be interpreted as either continuous mixing as 400 m of crystals accumulate, or intermittent addition of new batches of magma that mix rapidly. However, it will be shown in the following chapters that this view is simplistic.

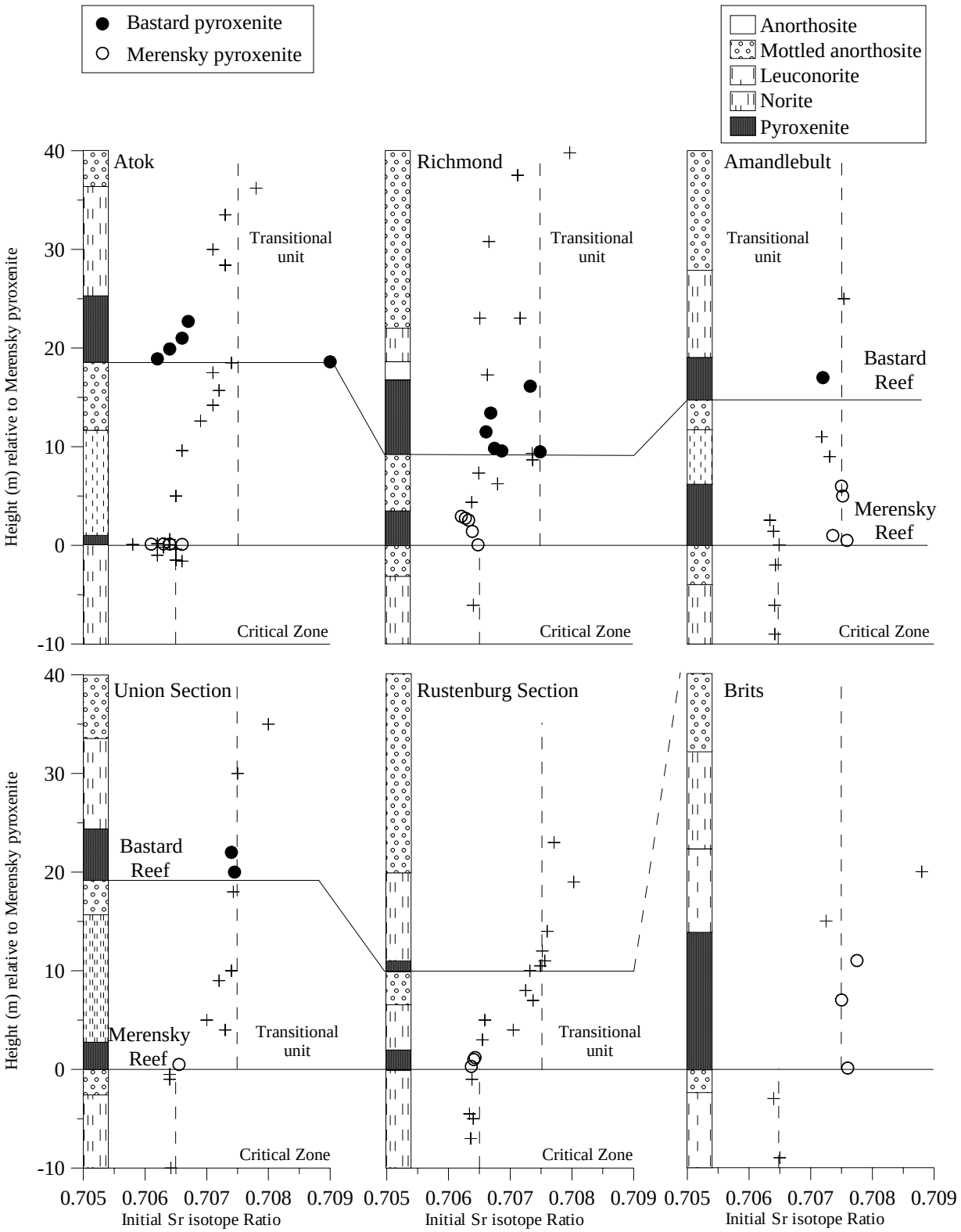


FIGURE 6.12 $^{87}Sr/^{86}Sr$ initial ratios plotted against stratigraphic height for different profiles discussed in the text (Atok - Lee & Butcher 1990; Union - Eales *et al.*, 1986; Rustenburg - Kruger & Marsh 1982; Amandelbult - Kruger 1992; Brits - Cawthorn & Kruger unpublished data).

However, in RM15 there is a return to lower Sr_i values (~0.706) at the level of the Bastard pyroxenite. It is possible that this could be interpreted as the crystallisation of the original, resident magma. This would suggest that the initial influx of new magma that formed the Merensky Unit Sr_i profile (with higher Sr_i values) was intruded somehow into a package of Critical Zone magma. The location of the new magma influx would have been determined by one or more of a number of possibilities, including significant density contrasts (Sharpe 1985), a crystal mush/residual liquid boundary (Lee & Butcher 1990) or some other form of structural or lithological control. A second influx of Main Zone magma would then mix with the residual Critical Zone magma that formed the Bastard Cyclic Unit, until chemical equilibration occurs. However, an issue that arises if one were to accept this model is that no significant change in the crystallisation sequence occurs at the point of influx of the new magma. I.e. Critical Zone-style cyclic units continue to be crystallised, in the form of the Merensky and Bastard Cyclic Units, which occur before the emergence of homogeneous Main Zone lithologies. Kruger & Marsh (1982) stated that detailed mineral and whole-rock compositions suggest the new magma was compositionally similar to the existing magma, but in the following chapters this is shown to be wrong, except for Sr. In addition, Lee & Butcher (1990) suggested that the pattern of variation within the Merensky Cyclic Unit is so similar to that in the Bastard Cyclic Unit that it indicates that the magmas involved were geochemically similar in each case. However, the extreme variation in their isotopic signatures alone indicates that they are highly unlikely to be geochemically similar. Assuming therefore, that two isotopically different magmas are present at the Critical/Main Zone boundary, one would expect to find other geochemical variations between them.

Chapter 7

The Critical / Main Zone Boundary

The exact level of the Critical/Main Zone boundary is difficult to resolve. This section deals with the characteristics of the boundary and attempts to resolve some of the problems related to its positioning. It is shown that much of the ambiguity concerning its location can be related to the introduction of the Main Zone magma and the nature of the formation of the Merensky and Bastard Cyclic Units.

7.1 The placing of boundaries

The stratigraphic division of layered intrusions is an important tool for assisting studies of such complexes and making comparisons across sometimes extensive lateral distances. Therefore the criteria upon which divisions are made must be carefully considered. Irvine (1982) set out guidelines for the division of layered igneous intrusions. These divisions were based on purely genetic classifications, rather than descriptive ones. In terms of relatively large-scale divisions, zones as opposed to say individual layers, Irvine suggested that consideration should be given to structure as well as stratigraphy. In addition, genetic features such as crystallisation relations, based on textural features and cumulus mineral sequences and compositions should be considered. Thus, he uses the term “series” to define extensive stratigraphic successions of cumulates with structural divisions. Wager *et al.* (1960) utilised the stratigraphic range of olivine to define “zones” in the Skaergaard intrusion and the cumulus appearance of other principal minerals the subsequently defined subzones. This method has been used in the Bushveld Complex, but Irvine (1982) suggested that the numerous layer repetitions make it a difficult method to be strictly applied. Irvine goes on to recommend that the essential feature for defining zones depends on the intrusion, but that the limits of the zone should be definite and where possible, mappable. With specific reference to the Bushveld Complex, Irvine suggested that the established “zones” e.g. Critical Zone and Main Zone, be renamed as “series”. However, it appears that the term “zones” was too well established to change.

7.2 The Critical/Main Zone transition

A number of positions for the boundary have been suggested using a range of criteria. Hall (1932) defined the lower boundary of the Main Zone only as the "eastern foot of the Lulu Mountains escarpment". The most common definition, particularly in industry, is based on lithological criteria and is taken to be the top of the GMA, which represents the top of the Bastard Cyclic Unit (Wager & Brown 1968). The GMA is a distinctive marker horizon, which makes it very useful for correlating in the field and between boreholes. This feature in itself however, does not necessarily make it an appropriate location for a major boundary. This is because it is a purely textural characteristic that distinguishes the GMA from other mottled anorthosites found both in the Main Zone and the Critical Zone. If the level of the GMA could not be located in the field, then there would be no other way of determining whether rocks are in the Main Zone or the Critical Zone. For this reason, it is not considered appropriate to use the GMA as the boundary between the Main and Critical Zones.

Mitchell & Manthree (2002) discussed the geochemistry of the GMA at the top of the Bastard Cyclic Unit at Impala Platinum Mines. By sampling every 5 m through the GMA they attributed chemical similarities within it to the Main Zone *and* Critical Zone. They proposed a process of partial remelting of the GMA as the result of an influx of Main Zone magma immediately above it, creating an iron-rich intercumulus melt. Their evidence for this was based on shared textural similarities between the Upper and Lower Giant Mottled, and shared geochemical similarities between the Upper Giant Mottled and the overlying Main Zone. However, the precise geochemical parameters they used are not described in the text. Subsequent percolation into the GMA of this new magma contributed to the mixed geochemical signature. They suggested therefore that the Critical/Main Zone boundary is a hybrid zone and cannot be sharply defined but occurs within the GMA. Consequently, even if one assumes that the boundary does occur somewhere around the level of the GMA, one is still at a loss as to how to determine whether an individual rock sample is part of the Critical Zone or the Main Zone. In addition, the idea of a diffuse zonal boundary contradicts the idea that zones should be clearly definable (Irvine 1982). There is one feature however that would support the use of the top of the GMA as a bounding unit. The GMA represents the top of the uppermost cyclic unit. Above this, thick sequences of homogeneous norite are observed, and pyroxenites and chromitite units become uncommon.

It has been suggested that the boundary should be placed lower in the sequence, at the base of the Merensky Cyclic Unit. The significant change in initial Sr isotope ratio at this level (Kruger & Marsh 1982, Sharpe 1985, Eales *et al*, 1986), along with the recognition of an erosional disconformity (Cousins 1964b, Viljoen *et al*. 1986, Leeb-du Toit 1986, Mossom 1986, Eales *et al*. 1988) indicates a large magma influx and a major event in the evolution of the Bushveld Complex. Kruger (1990) therefore placed the Critical/Main Zone boundary at this level. However, Mitchell & Scoon (1991) contested this location of the Main Zone boundary, preferring a return to the original definition of the Critical Zone based on the occurrence of chromitite and PGE mineralisation (Hall 1932). Mitchell & Scoon (1991) also inferred unconformable relationships at the start of every cyclic unit, which negates the importance of the Merensky unconformity. They also rejected the significance of Sr isotope ratios and preferred instead the SACS placement of the boundary at the top of the GMA, in line with Hall (1932) and Wager & Brown (1968).

Originally, the Lower Main Zone was considered petrographically homogeneous (Wager & Brown 1968), and that it represents the product of fractionation, with no new inputs of magma. However, Kruger (1990) placed the Lower Main Zone within an open system integration stage, during which crystallisation occurred concurrently with the influx of new magma into the chamber and mixing with resident magmas. Kruger suggests that closed system fractionation, where no magma is added, did not occur until the Upper Main Zone. This integration stage comprises the Lower, Critical and Lower Main Zones and is characterised by magma additions and mixing. Important criteria for placing subdivisions in a layered intrusion may include the point of an influx of magma or a mixing event, as this is intrinsic to the genesis of the intrusion (Irvine 1982). This would have created deviation away from mineralogical, petrological and geochemical trends, providing an appropriate location for placing a boundary based on definable criteria. Thus, the magma influx at the base of the Merensky Cyclic Unit provides a suitable position for the start of the Lower Main Zone. This may be a particularly attractive location for the boundary because it is easily identifiable in the field and is consistent throughout the complex. However, although the change in Sr initial ratio is distinct and well documented, the laborious and expensive process to obtain this data makes it an unappealing characteristic on which to base a

zonal boundary. Stratigraphic divisions of the Bushveld Complex do not need to coincide with the division of magma types.

The discussion above shows how difficult it has become to talk about "Main Zone rocks" or "Critical Zone rocks" since there is obviously a quite considerable section that does not clearly fit in to either category. This section occurs from the base of the Merensky pyroxenite and extends to above the GMA, and the top of the Bastard Cyclic Unit. Thus, for the purposes of this discussion "Critical Zone" will apply to rocks occurring below the Merensky pyroxenite, "Main Zone" will apply to rocks occurring above the GMA and "Transitional Unit" will apply to rocks occurring between, and including, these two units.

7.3 The boundary based on the appearance of clinopyroxene

If the methods for determining boundaries laid out in Irvine (1982) are to be followed, then the Critical/Main Zone boundary should be determined using either a structural division, if it is classed as his "series" or a mineralogical or textural boundary if it is classed as his "zone". The appearance of a new cumulus mineral has significant implications for fractionation in a layered intrusion. A tholeiitic magma, similar to the Bushveld magma, generally crystallises orthorhombic pyroxene and subsequently clinopyroxene. The major mineralogical change in the Main Zone, the first appearance of cumulus clinopyroxene, is not observed until some tens of meters above the Bastard Cyclic Unit. Although, this does appear to vary, for example, Wager & Brown (1968) noted that it first occurs intermittently about 1000ft (300m) *below* the top of the Critical Series. This change is observed towards the base of the Main Zone and can thus be used to determine height in the sequence. If the appearance of a new cumulus mineral in the sequence is to be used as a method of defining a new boundary, then a geochemical method for determining the point of its appearance would be a useful tool. Although it is possible to determine whether clinopyroxene is present in a sample using point counting in a thin section, this is a lengthy and sometimes inaccurate process. While estimation of mineral proportions in a thin section can be useful, it does not allow more precise constraints to be put on the amount of cumulus clinopyroxene present. A geochemical method is more objective and more representative.

Using whole-rock major element concentrations it is possible to distinguish between plagioclase, orthopyroxene and clinopyroxene based on the chemical formula of each mineral. Each of these minerals contains different amounts of CaO and Al_2O_3 so a simple graph of CaO against Al_2O_3 can be constructed (Figure 7.1). Figure 7.1 is plotted using data from RM15, with average cumulus orthopyroxene, clinopyroxene and plagioclase mineral separate data. Plagioclase plots at high Al_2O_3 and high CaO, orthopyroxene plots at low Al_2O_3 and low CaO and clinopyroxene at high CaO and low Al_2O_3. A likely liquid composition for Main Zone magma (Cawthorn *et al*. 1981) is also plotted. For rocks containing just cumulus plagioclase and orthopyroxene, whole-rock data should plot within the triangle defined by orthopyroxene, plagioclase and the liquid. However, where a rock contains significant proportions of cumulus clinopyroxene, the proportion of CaO to Al_2O_3 will increase. Compositions falling on the clinopyroxene side of the orthopyroxene-plagioclase tie-line must contain clinopyroxene, or more trapped liquid. It is therefore easy to recognise the presence and proportion of cumulus clinopyroxene, as these points will plot outside of the orthopyroxene – plagioclase – liquid triangle, although a rock with a small amount of interstitial clinopyroxene may still plot inside the triangle. In Figure 7.1 samples that were logged as gabbronorites in RM15 have been plotted as diamonds. Only three of these actually plot outside of the triangle. This means that while clinopyroxene was observed in the rock, it cannot have all been cumulus. Representative CIPW norms (appendix VII) show that very little clinopyroxene, at most 10%, is present in the Upper Critical Zone and Lower Main Zones. It must be assumed therefore, that in RM15 true gabbronorites were not sampled. This is a good example of the objectivity of using geochemical data, rather than thin sections to determine the presence of cumulus clinopyroxene. Point counting can be misleading due to heterogeneity in the rock and recrystallisation (chapter 4) makes textures deceptive when trying to establish proportions of cumulus minerals.

Figure 7.1 also shows Main Zone data from Mitchell (1986) around the Gabbro Marker level (approximately 300 m above the Merensky pyroxenite) at Union Section. The rock types are predominantly gabbronorites. It is clear that Mitchell's data plot further away from the triangle, than the Richmond samples, which indicates the presence of increased amounts of cumulus clinopyroxene.

Samples from closer to the Bastard Cyclic Unit plot just below the orthopyroxene-liquid tie-line, suggesting that cumulus clinopyroxene do not occur at the base of the Main Zone.

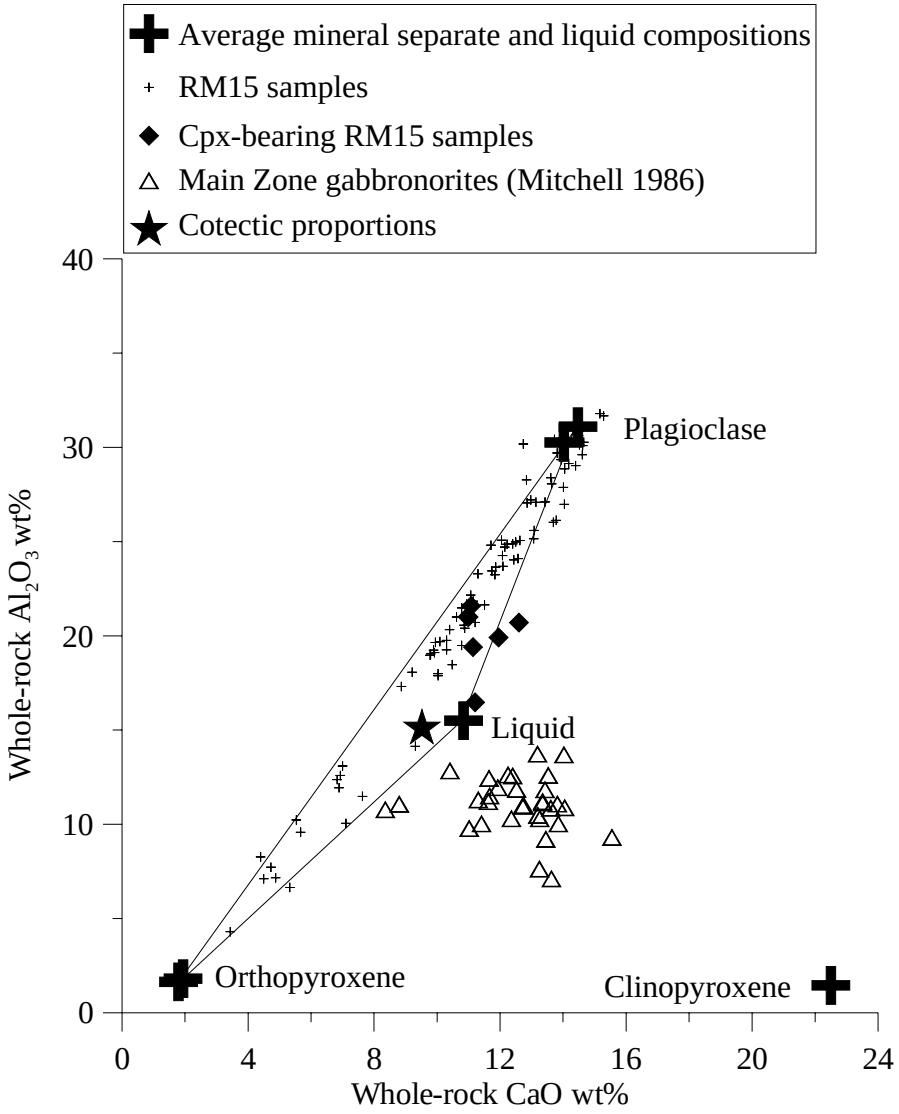


FIGURE 7.1 Diagram of whole-rock Al_2O_3 plotted against CaO and compositions of plagioclase, orthopyroxene and clinopyroxene mineral separates (from this study, Appendix IV) showing the proportion of cumulus clinopyroxene present in rocks from RM15 and gabbronorites from Mitchell (1986). Cotectic proportions taken from Cawthorn & Davies (1983).

The first appearance of cumulus clinopyroxene in the Main Zone is a recognisable horizon in the Bushveld Complex and might be considered an appropriate location for the Critical/Main Zone boundary based on Irvine's (1982) interpretation that cumulus mineral sequences should be taken into account. However, it has been shown here that cumulus clinopyroxene does not occur concurrently with

the influx of Main Zone magma and the structural break at the base of the Merensky pyroxenite. Irvine (1982) suggested that structural features should play an important role when defining zonal boundaries. Thus, it is concluded here that the first appearance of cumulus clinopyroxene is not an appropriate location for the Critical/Main Zone boundary and other geochemical parameters between Critical and Main Zone magmas are investigated.

7.4 Chemical criteria to define the Critical and Main Zones

Many discussions on the Critical/Main Zone boundary involve two separate magmas to distinguish between the zones. However, it is significant that there has been very little information provided on the exact geochemical differences between these two magmas. Compositions are difficult to constrain since the rocks are cumulates and possible mixing would have resulted in the crystallisation from varying proportions of the two magmas. The composition of Upper Critical Zone magmas that developed the cyclic units have been widely debated and summarised in Cawthorn (1996a). In this section, it is demonstrated that a number of geochemical parameters can be used to distinguish between the Critical and the Main Zone magmas.

7.4.1 Initial Sr isotope ratios

Most previous work that invoked the introduction of a different magma in the Main Zone has been based on Sr-isotope initial ratios (e.g. Kruger & Marsh 1982). In this study, additional Sr isotope data have been produced to further constrain processes at the influx of the Main Zone magma. It has been suggested that the level of this influx should be regarded as the Critical/Main Zone boundary (e.g. Kruger 1990). Figure 5.21 shows Sr initial ratios against depth for RM15 and KF35 cores, over the Transitional Unit interval. In both profiles, two populations of data can be clearly distinguished. Critical Zone rocks (below the Merensky pyroxenite) have values of around 0.706 - 0.7068 and Main Zone rocks (above the GMA) have values of around 0.707-0.708. These values are clearly consistent with other data, largely from the western Bushveld where higher ratios typical of the Lower Main Zone range from approximately 0.707 – 0.709 and Critical Zone ratios are around 0.706 (Hamilton 1977,

Kruger & Marsh 1982, Sharpe 1985, Kruger 1994). Thus, it remains clear that the isotopic break at the level of the Merensky pyroxenite is unequivocally consistent throughout the Bushveld Complex. It is this break that has been frequently used to support the introduction of a new magma at the level of the Merensky pyroxenite.

However, although both the RM15 and KF35 profiles both show a break at the Merensky pyroxenite, there are some key differences between these and previously published profiles. These differences are most significant around the level of the Merensky and Bastard pyroxenites (Figure 5.21), or the Transitional Unit between the Critical and Main Zones. The reversal at the Bastard pyroxenite in RM15, which does not occur in KF35, is similar to the profile determined at Atok in the eastern Bushveld by Lee & Butcher (1990) (Figure 6.12). These breaks, reversals and "mixed" isotopic signatures within the Transitional Unit imply processes more complicated that simple magma addition and mixing. It is clear therefore, that although Sr isotope initial ratios can be used to distinguish between Critical and Main Zone rocks, there is a certain amount of ambiguity within the Transitional Unit. In order to determine which magma rocks in the Transitional Unit formed from, it is necessary to investigate other geochemical methods of distinguishing between Critical and Main Zone rocks.

7.4.2 Sr and An# in plagioclase

Different Sr contents in plagioclase indicate that there are two magma compositions (Figure 7.2). Eales *et al*. (1986) previously demonstrated this characteristic. Sr in plagioclase in the Critical Zone is about 440 - 480 ppm, and in Main Zone plagioclase it is between 360 and 400 ppm. An anomalously low value in the Critical Zone of KF35, at 120 m below the Merensky pyroxenite, is disregarded in each graph, as this sample is directly adjacent to a replacement pegmatoid body, which may have altered geochemistry in nearby rocks. Plotting Sr against MgO (Figure 7.3) shows the expected negative correlation, whereby samples with high plagioclase content (low MgO) contain high Sr ppm. Samples containing more orthopyroxene, contain less Sr. The similarities between the two graphs shown in Figure 7.3 will be discussed first and the differences will be considered later. Two main trends emerge wherein samples below the Transitional Unit contain increased Sr, for a given MgO content, and samples from above the Transitional Unit contain lower amounts of Sr. However, this trend is not

consistent in both cores. Samples from above the Transitional Unit define a distinct linear trend in RM15, whereas those in KF35 are scattered.

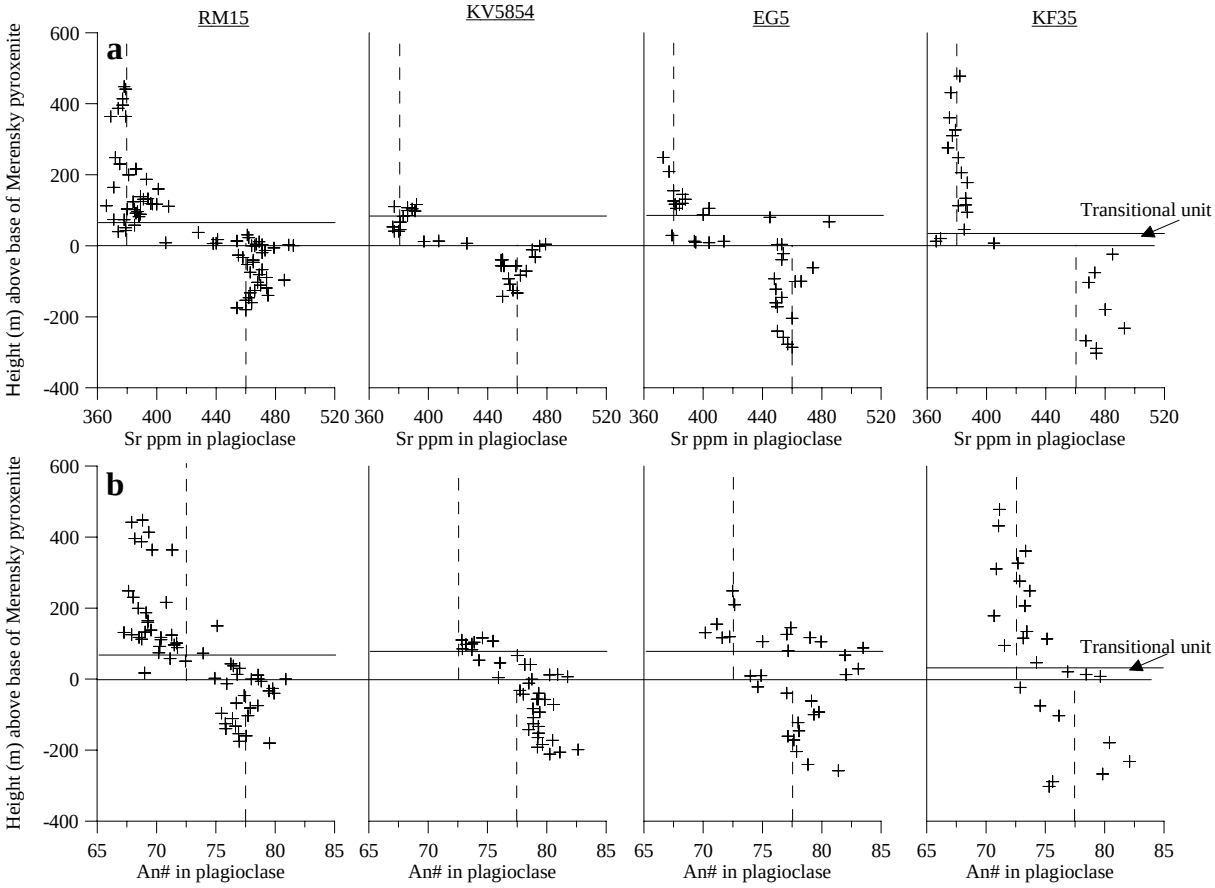


FIGURE 7.2 Sr content of plagioclase (a) and An# of plagioclase (b) plotted against height for cores RM15, KV5854, EG5 and KF35, showing the differences between Critical and Main Zone values. Vertical dashed lines show typical values for the Critical and Main Zones.

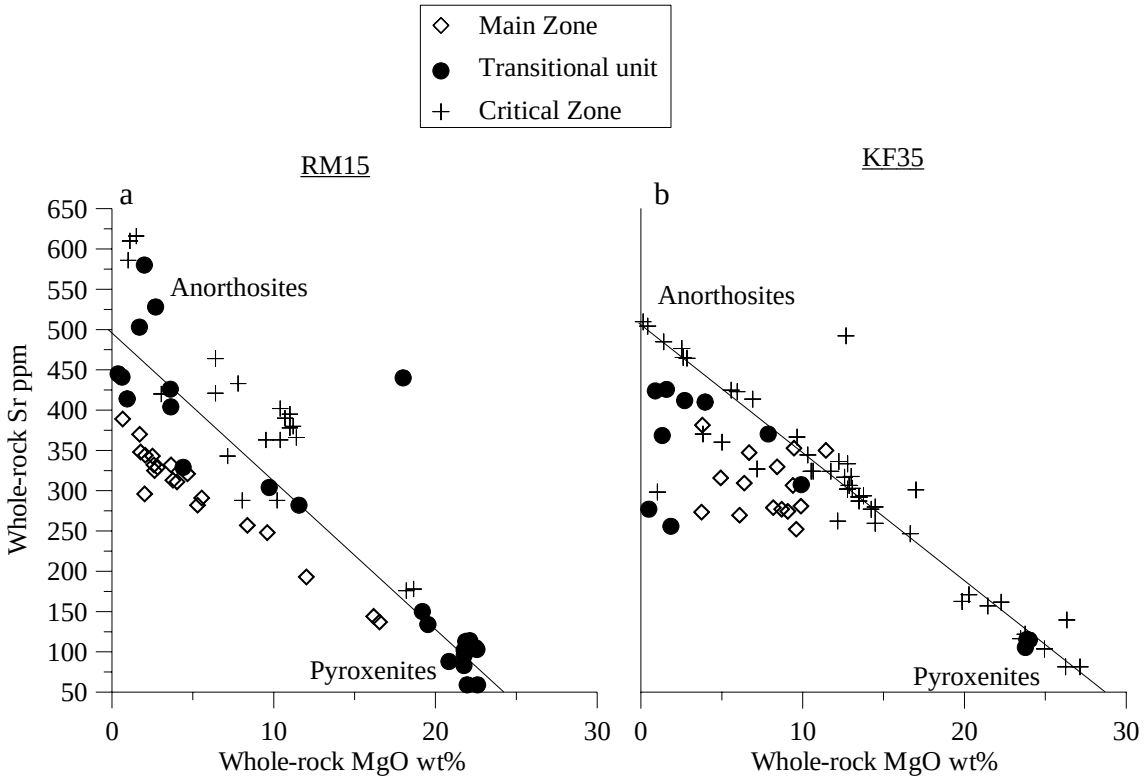


FIGURE 7.3 Plot of whole-rock Sr vs. MgO for RM15 (a) and KF35 (b) showing anorthosite-pyroxenite tie-lines.

Although the latter contain lower Sr values overall, they do not plot on a straight line as they do in RM15. Samples from below the Transitional Unit define a better linear trend in both profiles, but in both cases, some samples plot at low Sr values, away from the overall trend. Transitional Unit samples generally plot at Sr values between those of above and below, although some samples from both cores have anomalously low Sr contents. In general, therefore, this diagram shows that Sr content is fundamentally different in the Main and Critical Zones, which might suggest that the Main Zone magma had lower Sr content than the Critical Zone magma. It is also possible that the variation in Sr content is simply the result of changing D values in the magmas due to some difference in crystallisation conditions. However, it is clear that there are deviations from the trends in each core and these features will be discussed in section 7.7. Figure 7.4 further demonstrates the distinction between Main Zone and Critical Zone samples, based on Sr content in plagioclase and initial Sr isotope ratio. In this diagram Sr isotope initial ratio is plotted again $1/^{86}Sr$. Using samples containing *cumulus* plagioclase only, it is clear that there are two distinct groups. Main Zone samples with high initial ratios are depleted in Sr and Critical Zone samples that have lower initial ratios are enriched in Sr.

Transitional Unit samples in RM15 plot between the two groups. In KF35, the Transitional Unit sample plots closer to the Main Zone samples.

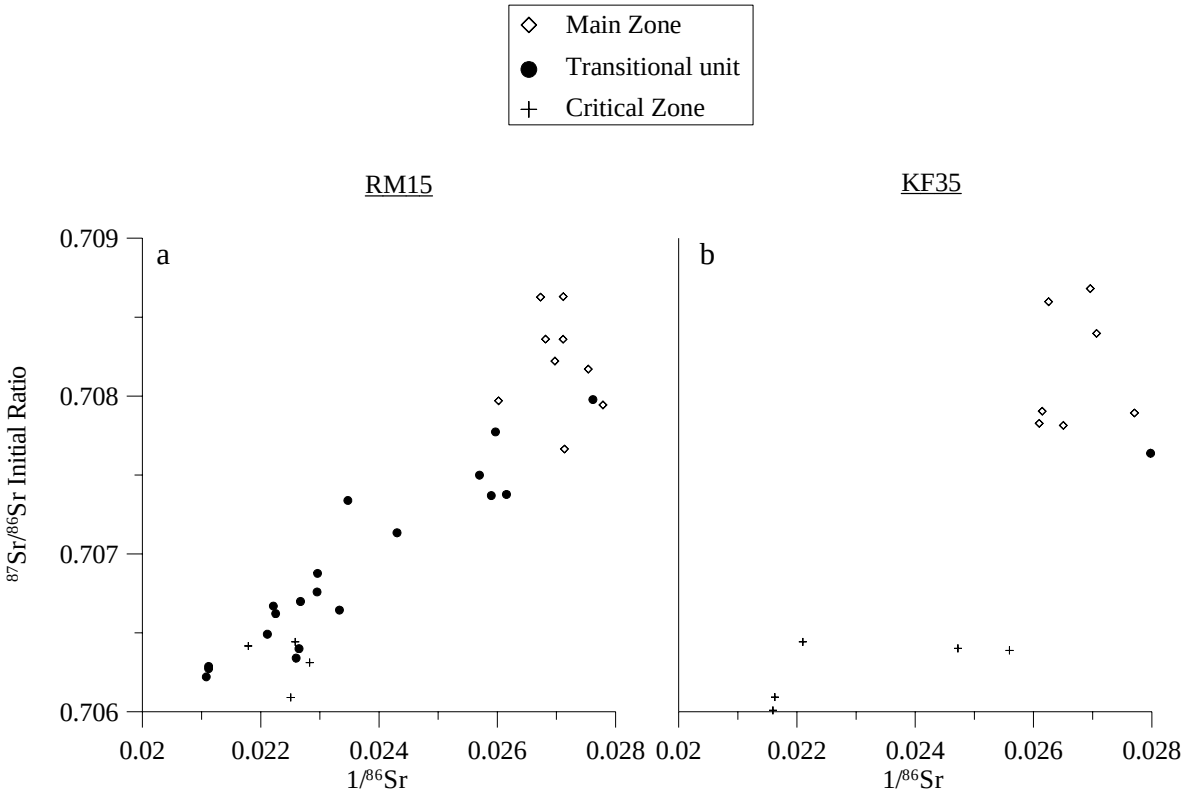


FIGURE 7.4 Plot of Sr isotope initial ratio vs. $1/^{86}Sr$ in plagioclase for RM15 (a) and KF35 (b) demonstrating two distinct groups of plagioclase, from the Critical and Main Zones.

An# in plagioclase also varies between the Critical Zone and Main Zone rocks (Figure 7.2). Again, similarities between the profiles shown will be discussed first and differences considered afterwards. In each profile, An# is greater in samples below the Transitional Unit and lower in samples above the Transitional Unit. In each core, rocks below the Transitional Unit have an An# of between 75-80. Above the Transitional Unit, cores KF35 and EG5 have An# of 70-75. However, some points plot at higher values above the Transitional Unit in EG5, and in RM15 Main Zone plagioclase has an overall lower An# than in the other cores. In general though this diagram shows that there are two distinct groups, one of Critical Zone plagioclase with higher An# and one of Main Zone plagioclase with lower An#. Another important feature of this diagram is the small variation in An# in Main Zone rocks, which is best shown in KF35 and RM15, as these samples extend furthest in to the Main Zone. This small variation suggests that little fractionation has taken place throughout the Main Zone. Large decreases in An# in the Critical/Main Zone transition, with subsequent reversals, would suggest an influx of a new

magma. It is also noted that An# in KF35 decreases systematically in the 200 m below the Merensky pyroxenite. This trend may also be present in EG5, but the other cores, from the southern sector, do not show it. This feature will be discussed in section 7.7.

7.4.3 MgO and Cr in orthopyroxene

Geochemical studies of orthopyroxene separates are also used to demonstrate differences between Critical and Main Zone magmas. Cr is highly compatible in orthopyroxene and its variation with height is shown in Figure 7.5. Two populations of values can be described, in a similar fashion to Sr in plagioclase. Eales (2000) emphasised the fundamental difference in Cr in orthopyroxene across the Critical/Main Zone boundary. In this study, Critical Zone orthopyroxenes contain significantly higher Cr values, of between approximately 2000-3000 ppm. Main Zone orthopyroxenes contain around 1000 ppm Cr. Distinct breaks are apparent in RM15 and KV5854, but are gradual in EG5 and KF35. Similar variations are also demonstrated by Mg# in orthopyroxene (Figure 7.5). Mg#'s of around 80 are typical of Critical Zone samples, whereas Main Zone samples are generally lower, around 70-75.

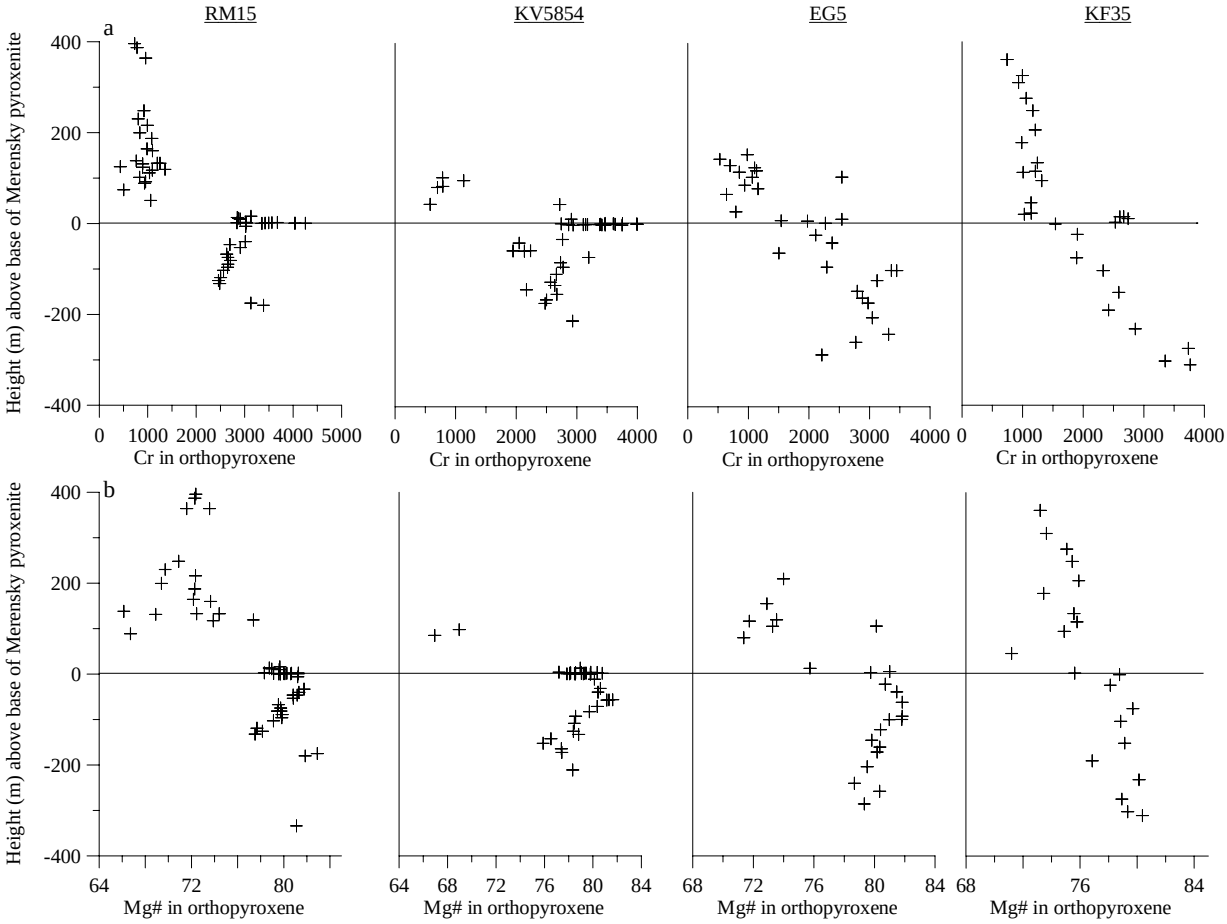


FIGURE 7.5 Cr content of orthopyroxene (a) and Mg# of orthopyroxene (b) plotted against height for cores RM15, KV5854, EG5 and KF35. These graphs emphasize distinct geochemical differences between Critical and Main Zone rocks.

These variations in Cr provide a useful tool for distinguishing between Critical and Main Zone orthopyroxenes and plotting Cr/MgO ratios, for both mineral and whole-rock compositions, will illustrate these differences. However, the modelling of this ratio in section 6.1 demonstrates that trapped liquid content will affect the ratio in anorthositic rocks and that whole-rock Cr/MgO ratios are should only be used in rocks with an MgO content greater than 5% (Figure 6.4). Thus, anorthosite samples have been disregarded for the purposes of this discussion and result in some large gaps in the data in the profile. Figure 7.6 shows Cr/MgO in orthopyroxene plotted against height for each of the cores analysed in this study. Three samples from the Bastard pyroxenite in KF35 are whole-rock data due to lack of orthopyroxene separates from this layer. This diagram demonstrates overall differences between the Critical and Main Zone ratios. In general, Critical Zone samples give values of around 80-120 and

Main Zone samples of around 40-60. However, in KF35, there is a systematic decrease in the Cr/MgO ratio in the top 200 m of the UG2 Cyclic Unit, and also possibly in EG5. This variation will be discussed in section 7.7.

In the Transitional Unit Cr/MgO ratios in orthopyroxene are generally similar to either typical Critical Zone or typical Main Zone values. In each core, the base of the Merensky Cyclic Unit displays Cr/MgO ratios of around 100. Some samples in the pyroxenite contain elevated Cr/MgO ratios, but this is due to inclusions of Cr within orthopyroxene grains (chapter 5). In the upper part of the Transitional Unit ratios decrease to around 40-60. There appears to be a distinct break between the two groups and not a gradational change, but this is not certain due to the lack of orthopyroxene separate samples from the anorthosites.

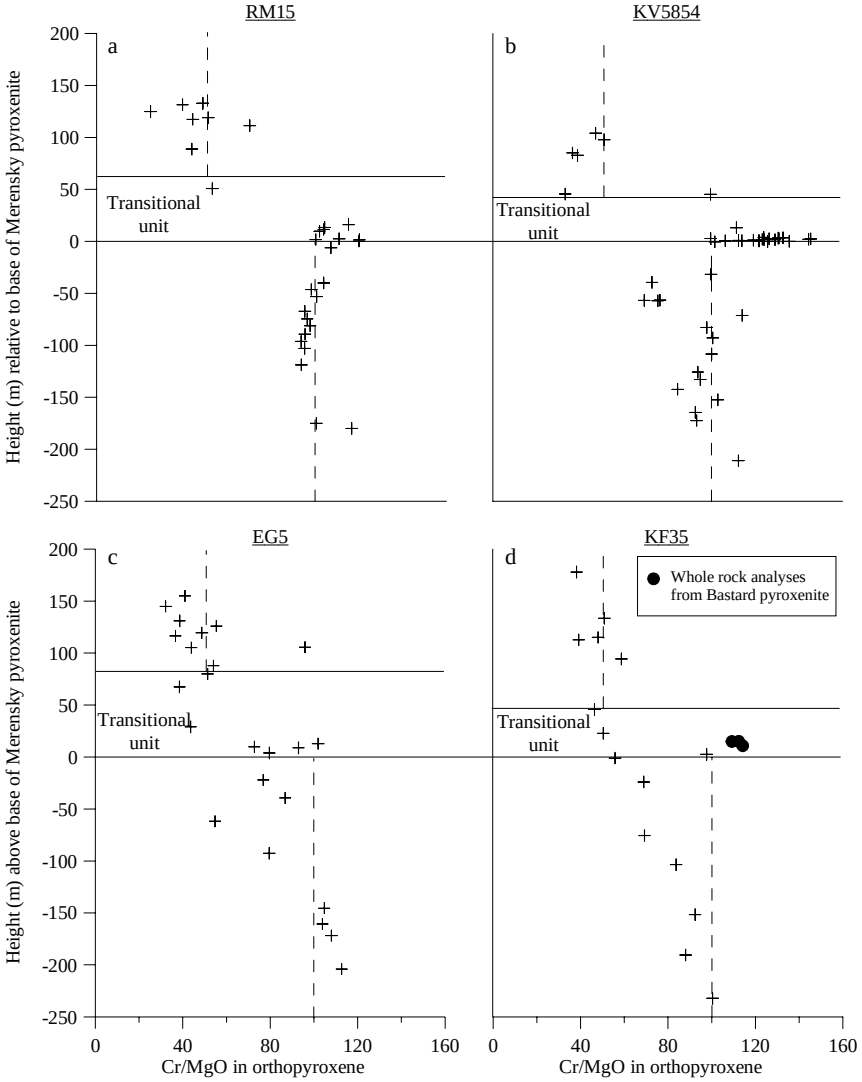


FIGURE 7.6 Cr/MgO in orthopyroxene plotted against height for cores RM15 (a), KV5854 (b), EG5 (c) and KF35 (d) demonstrating the difference in this ratio between Critical and Main Zone rocks.

7.4.4 Cr/MgO in whole-rock

Cr/MgO ratios can also be effectively used in the interpretation of whole-rock data and will give similar results to those achieved using orthopyroxene separates. This is because both Cr and MgO are highly compatible in orthopyroxene and thus, Cr/MgO ratios will be independent of modal proportions, providing MgO content is >5 wt%. Being able to use whole-rock data is beneficial as there are relatively few sources of mineral compositions for the rest of the Bushveld.

The theoretical model produced in Figure 6.4 shows that there are clear differences in Cr/MgO between Main Zone and Critical Zone rocks. Figure 7.7 shows whole-rock Cr/MgO plotted against height for the four cores investigated in this study.

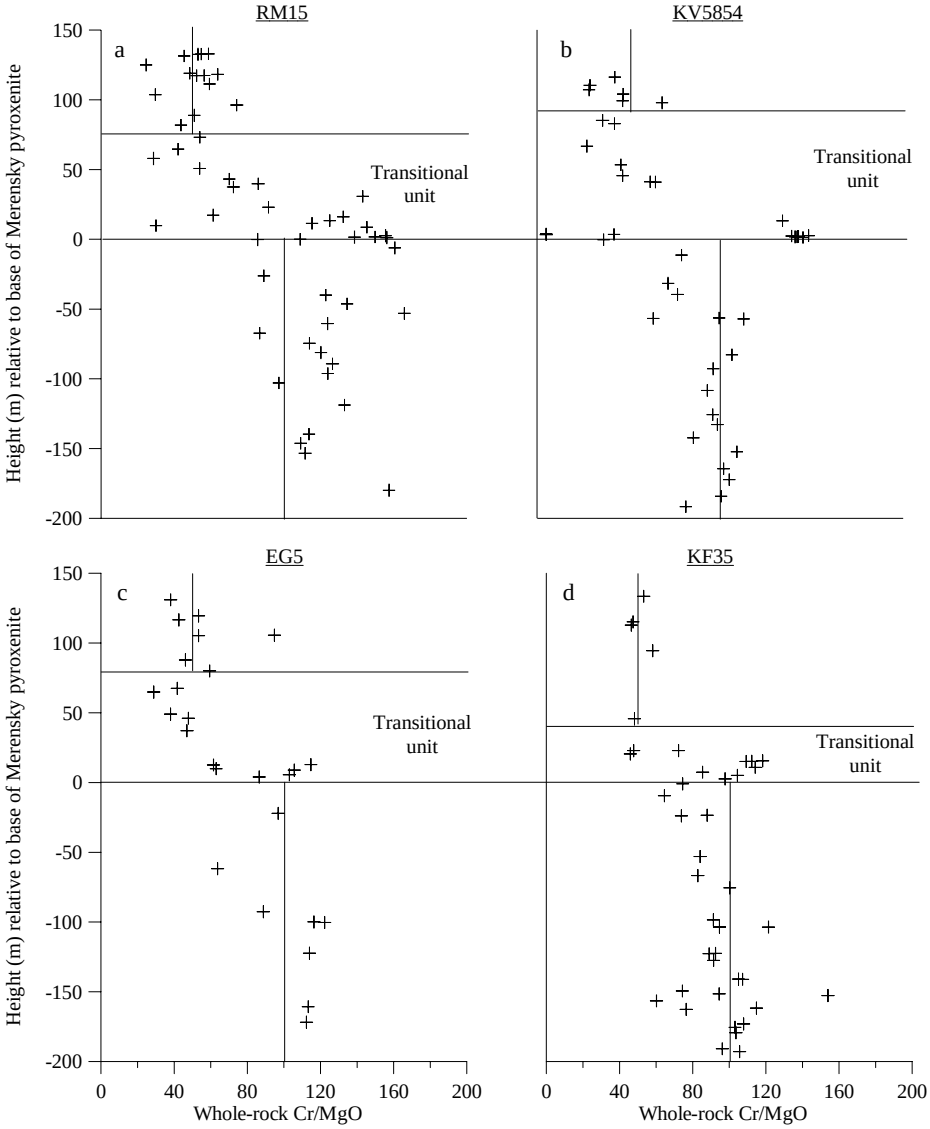


FIGURE 7.7 Whole-rock Cr/MgO plotted against height for cores RM15 (a), KV5854 (b), EG5 (c) and KF35 (d), indicating similar variations to those observed in Cr/MgO in orthopyroxene. Thus, whole-rock Cr/MgO ratios can be used to distinguish between Critical and Main Zone orthopyroxene.

Samples containing chromite grains, with anomalously high Cr values of over 3500 ppm, have been excluded (15 from RM15, 13 from KV5854, 0 from EG5 and KF35). These graphs show that Main Zone rocks tend to cluster at Cr/MgO ratios of approximately 40-60. Critical Zone rocks display consistently higher Cr/MgO values, clustering between 80 and 120. These values are in approximate agreement with the values predicted using the model in section 6.1 and because they remain constant regardless of MgO wt%, it is clear that Cr/MgO is independent of modal proportion. Thus, Cr/MgO ratios can be used to distinguish between Critical and Main Zone rocks for whole-rock samples that contain more than 5 wt% MgO. KF35 and KV5854 show a decrease in the upper section of the UG2 Cyclic Unit.

Data from elsewhere in the Bushveld show similar trends. Figure 7.8 shows Cr/MgO ratios for whole-rock data plotted against height from other locations in the Bushveld Complex. When considered collectively, these graphs show that a clear distinction can be made between Critical Zone Cr/MgO values, approximately 80-120, and Main Zone ratios, which are consistently lower, between 40 and 60. Thus, all studies across the Upper Critical to the Lower Main Zones support the fact that Cr/MgO values can be used to distinguish between Critical and Main Zone rocks. However, data for the Transitional Unit are varied. In the profiles from Amandelbult, Richmond and Rustenburg the Transitional Unit Cr/MgO values are equal to those observed in the Critical Zone. However, elsewhere, typical Main Zone Cr/MgO values are present within the Transitional Unit (Figure 7.8). At Union Section (Eales *et al*. 1986), samples from the Merensky Cyclic Unit have Main Zone Cr/MgO values, whereas the overlying Bastard Cyclic Unit has typical Critical Zone values. At Impala (Mitchell and Manthree 2002), Cr/MgO values decrease exponentially from Critical Zone values at the base of the Bastard Cyclic Unit to Main Zone.

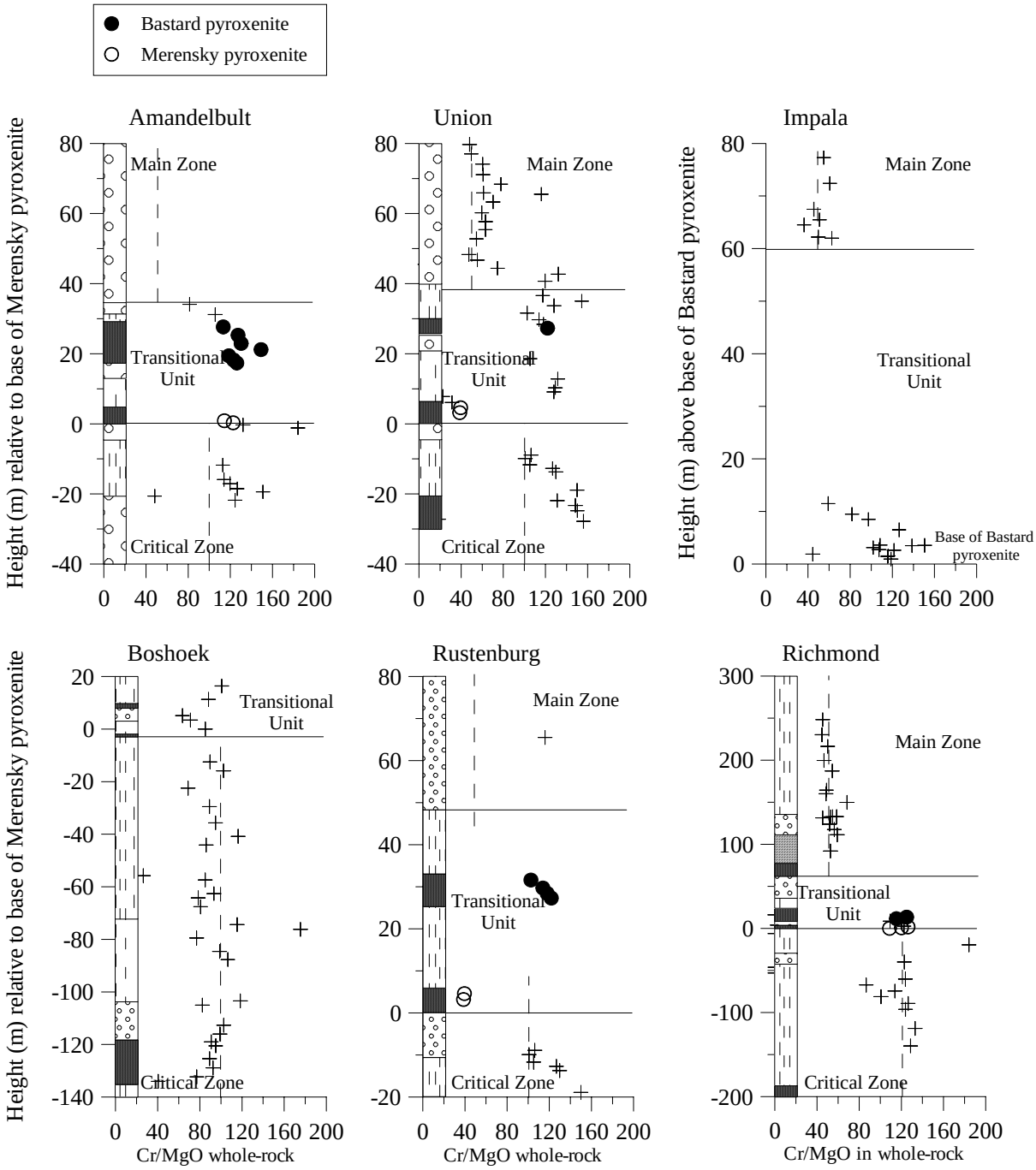


FIGURE 7.8 Cr/MgO values plotted against stratigraphic height for the different profiles discussed in the text that show that variation in Cr/MgO occurs across the Critical/Main Zone boundary in the western and eastern Bushveld. (Amandelbult - Field 1987; Union - Eales *et al.* 1986; Impala - Mitchell & Manthree 2002; Boshoek - Schürmann 1993; Rustenburg - de Klerk 1991, and Richmond - this study).

7.5 The nature of the Critical and Main Zone magmas

The geochemical parameters described in section 7.4 can be used to place constraints on the differences between the Critical and Main Zone magmas. Minerals crystallising from these magmas display distinct geochemical signatures, which can be used to determine from which magma they originated. These findings are summarized in table 7.1. K, Rb, Ba and Ti are averages of Critical and Main Zone values. It has been demonstrated that a number of criteria can be used to determine the magma of origin of plagioclase and orthopyroxene within the sequence.

Geochemical parameter	Critical Zone "signature"	Main Zone "signature"
Sr-isotope initial ratio	±0.706	>0.707
Sr in plagioclase	440-480 ppm	±380 ppm
An# in plagioclase	75-80	70-75
K in plagioclase	0.2 wt %	0.5 wt %
Rb in plagioclase	5 ppm	12 ppm
Ba in plagioclase	86 ppm	125 ppm
Cr/MgO in orthopyroxene or whole-rock (MgO >5%)	80-120	40-60
Mg# in orthopyroxene	±80	70-75
Ti in orthopyroxene	0.2 wt %	0.5 wt%

TABLE 7.1 Summary of geochemical parameters that can be used to distinguish between minerals that originated from Critical and Main Zone magmas.

Although geochemical changes over the boundary have been investigated previously e.g. Eales *et al.* (1986), modelling in section 6.1 showed that in fact some criteria used were invalid due to the effects of modal proportions. Mitchell & Manthree (2002) showed that geochemical changes occur within the GMA at Impala. K_2O in whole-rock, TiO_2 and Rb in plagioclase both display an increase at the top of HW4 (equivalent to the GMM). The K_2O, TiO_2 and Rb values in HW4 and below and those of HW5 (UGMA) and above are similar to the overall average concentrations recorded in Table 7.1 from this study. Plots of these elements in whole-rock (Figures 5.6 – 5.9) also show that a break in the GMA occurs in the rocks from this study, rather than increase at the level of the Merensky Reef. This study allows constraints to be put on previous work on the Critical/Main Zone boundary.

7.5.1 Temperature and density of Critical and Main Zone magmas

The geochemical data, specifically Fe and Mg content, do not suggest that there are great contrasts, in terms of temperature and density, between the Critical and Main Zone magmas, as variations in Mg# are not great and Fe-poor magmas are generally considered to be hotter. Lower Mg# and An# in the Main Zone, shown from this study, suggest a more evolved magma, which probably indicates a more dense liquid than the Critical Zone liquid (Kruger 1992). Density calculations by Hatton (1989) indicate that the Main Zone magma (B4) is denser that that of the Upper Critical Zone (B3), at the same temperature, which is in line with the observations of Kruger (1992). Maier *et al.* (2001) also indicated that the Main Zone magma was denser than the Critical Zone magma. These calculations were based on Bottinga *et al.* (1982). In order to more fully constrain the temperatures and densities of the magmas in this study, the composition of the magma that formed the footwall to the Merensky pyroxenite is used, based on Li *et al.* (2001a) and the composition of the Main Zone magma is based on Cawthorn *et al.* (1981). Densities were determined based on calculations adapted from Bottinga & Weill (1970) (Table 7.2). These calculations also show that the Main Zone magma was denser (ranging from 2.66-2.71 g/cm^3) than the Critical Zone magma (2.59 g/cm^3) at the compositions and temperatures given in table 7.2. These densities are similar to those calculated by Hatton (1989). Thus it can be inferred, for the purposes of this study, that the Main Zone magma was denser than the Critical Zone magma when it entered the chamber.

It should also be noted that liquidus temperatures recorded by Li *et al.* (2001a) are inconsistent with experimental data (Cawthorn & Davies 1983) that show that orthopyroxene does not start crystallising until a temperature of 1,250-1,300 °C. Li *et al.* (2001a) show it crystallising at over 1,300°C. In addition, Li *et al.* show olivine crystallising at 1,358 °C, whereas Cawthorn & Davies record that it does not appear until 1,300 °C. This indicates that the fractionation program used by Li *et al.* (MELTS, Ghioso & Sack 1995) is wrong. Although the Main Zone composition obtained by fractionating the Critical Zone magma (Li *et al.* 2001a) is not considered, as it is interpreted that a separate magma influx occurred, calculations show that the fractionated Main Zone magma would also be denser than the equivalent Critical Zone liquid.

	Main Zone (Cawthorn *et al*. 1981)		Critical Zone
	4A	**4B**	**(Li *et al*. 2001a)**
SiO_2	53.21	50.28	58.35
TiO_2	0.46	0.82	0.33
Al_2O_3	15.12	15.50	15.22
Fe_2O_3	1.07	2.72	1.03
FeO	7.48	10.07	8.17
MnO	0.16	0.19	0.25
MgO	8.59	5.88	4.55
CaO	11.26	10.84	8.67
Na_2O_3	2.28	2.87	2.35
K_2O	0.56	0.27	1.22
P_2O_5	0.80	0.09	0.11
T (^oC)	1166[†]	1166[†]	1158[§]
Density (g/cm^3)	2.66	2.71	2.59

TABLE 7.2 Composition, temperature and density of Main Zone and Critical Zone magmas. 4A and 4B are two possible Main Zone magmas from Cawthorn *et al*. (1981).

[†] Temperature based on Cawthorn & Walraven (1998)

[§] Temperature from Li *et al.* (2001a)

7.6 The Merensky and Bastard Cyclic Units in light of new information on the Critical and Main Zone magmas

While the geochemical data presented in section 7.3 show that distinctions can be made between Critical and Main Zone magmas, it also shows that there is no distinct break between them and that minerals in the Merensky and Bastard Cyclic Units have confusing affinities. This section describes these units in terms of geochemical signatures that relate to either the Critical or Main Zones.

Figure 7.9 shows some of the geochemical data presented in section 7.4, highlighting the Merensky and Bastard Cyclic Units. Based on the Critical Zone and Main Zone signatures, summarised in table 7.1, minerals in the Merensky and Bastard pyroxenites can be characterised as having originated from either the Critical or Main Zone. For RM15, plagioclase in the Merensky pyroxenite has Sr-isotope initial ratios of 0.70634 to 0.70649 and absolute Sr of around 460 ppm. Both of these

parameters show that plagioclase in the Merensky pyroxenite has a Critical Zone signature. Orthopyroxene in the Merensky pyroxenite gives Cr/MgO values of between 110 and 150, which is also a Critical Zone signature. Plagioclase in anorthosites of the rest of the Merensky Cyclic Unit shows increasing Main Zone affinities in terms of Sr isotope ratios, but orthopyroxene continues to show Critical Zone signatures. The Merensky pyroxenite in KF35 also demonstrates Critical Zone affiliation in both plagioclase and orthopyroxene, with low Sr isotope initial ratios, (approximately 0.7068, although the pyroxenite itself was not sampled, this can be inferred from the footwall and hangingwall), and high Cr/MgO of about 110. Overlying anorthosites contain plagioclase with Main Zone Sr isotope signatures. No whole-rock or orthopyroxene separates are available for the Merensky pyroxenite.

The Bastard pyroxenite however, gives conflicting signatures. In RM15, the very base of the Bastard pyroxenite gives an Sr isotope value of 0.7075, which is a Main Zone signature. The remainder of the pyroxenite however, has Critical Zone values of around 0.706. The overlying anorthosites also demonstrate Critical Zone Sr isotope values. Sr in plagioclase is ambiguous, giving a range of values. Orthopyroxene in the Bastard pyroxenite gives Critical Zone Cr/MgO values of approximately 110-120. In KF35, the Bastard pyroxenite gives Main Zone Sr-isotope values of 0.7075 - 0.7076. Sr content in plagioclase also shows a Main Zone signature of about 400 ppm. However, orthopyroxene very clearly has a Critical Zone signature, with Cr/MgO of 110-120. These observations are summarised in table 7.3.

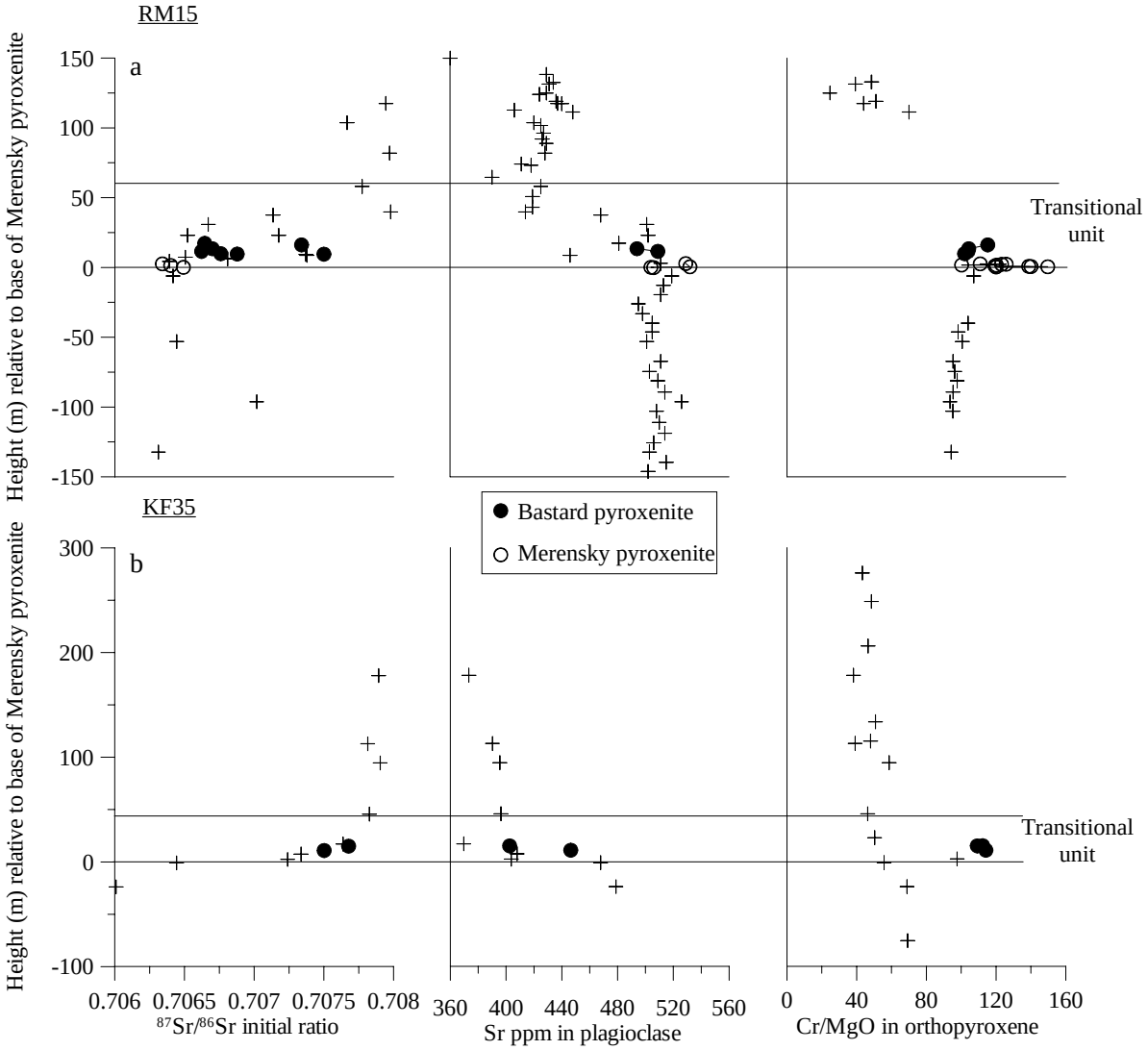


FIGURE 7.9 Comparison between Sr isotopes and Sr content of plagioclase and Cr/MgO in orthopyroxene for (a) RM15 and (b) KF35.

Using Sr isotopes and whole-rock Cr/MgO data from the literature, it is possible to compare these observations with other locations around the Bushveld. Figure 6.12 shows Sr isotope initial ratios from Rustenburg Platinum Mines (Kruger & Marsh 1982) and Union Section (Eales *et al.* 1986) in the western Bushveld and Atok in the north-eastern Bushveld (Lee & Butcher 1990) over the Transitional Unit. Both the Rustenburg profile and the Union Section profile show similar trends. Critical Zone values of around 0.7064 increase throughout the Merensky Cyclic Unit and continue to increase through the Bastard Cyclic Unit, levelling off at Main Zone values of just under 0.708. This is very similar to that recorded by Sharpe (1985) and observed in KF35 (this study). These profiles therefore are termed "normal" for the purposes of this study. Plagioclase in the Merensky pyroxenite has values

of 0.7063 in Kruger & Marsh's profile, 0.70655 in Eales *et al*. profile and 0.70684 in Sharpe's profile. These are all typical Critical Zone values. Plagioclase in the Bastard pyroxenite has values of 0.70756, 0.7075 and approximately 0.7079 respectively, which are all Main Zone values.

		Merensky pyroxenite		Merensky norite/anorth.		Bastard pyroxenite		Bastard norite/anorth.	
		plag	opx	plag	opx	plag	opx	plag	opx
West	Rustenburg[1]	CZ	MZ	-	CZ	MZ	CZ	MZ	CZ
	Amandelbult[2]	MZ	CZ	MZ	-	MZ	CZ	MZ	CZ
	Union [3]	CZ	-	MZ	CZ	MZ	-	MZ	CZ
	Boshoek[4]	-	-	-	-	-	CZ	-	CZ
	Impala[5]	-	-	-	-	-	CZ	-	CZ/MZ
	Brits[6]	MZ	-	MZ	-	-	-	MZ	-
East	Richmond [7]	CZ	CZ	CZ/MZ	CZ	CZ	CZ	CZ/MZ	MZ
	Atok[8]	CZ	-	CZ	-	CZ	-	MZ	-

TABLE 7.3 Summary of mineral affinities to Critical or Main Zone magma within the Merensky and Bastard Cyclic Units, for numerous locations around the Bushveld Complex. anorth. – anorthosite, plag – plagioclase, opx – orthopyroxene, CZ – Critical Zone, MZ – Main Zone. [1] Kruger & Marsh (1982), [2] Field (1987), [3] Eales *et al.* (1986), [4] Schürmann (1993), [5] Mitchell & Manthree, 2002, [6] Cawthorn & Kruger unpublished data, [7] This study, [8] Lee & Butcher (1990). Dash means no data available.

The Atok profile (Lee & Butcher 1990) shows a fundamentally different trend. Plagioclase in the Merensky pyroxenite shows Critical Zone values of 0.7064. The initial ratio increases through the Merensky Cyclic Unit and at the very base of the Bastard pyroxenite it jumps to 0.709, a Main Zone value. However, this is followed by a sharp break so that the overlying pyroxenite has average values of 0.7065, which is typical of Critical Zone values. This break from the trend of increasing Sr isotope initial ratio at the level of the Bastard pyroxenite characterises the profile from Atok (Lee & Butcher 1990) and RM15 (this study). At Atok and RM15 plagioclase has Critical Zone signatures in both the Merensky pyroxenite and the Bastard pyroxenite.

Cr/MgO ratios in the Union Section profile (Eales *et al*. 1986) show that orthopyroxene has Critical Zone ratios in both the Merensky and Bastard pyroxenites. Data are not available for Cr/MgO ratios in the other profiles described above, so data from the same intervals in other areas of the western

Bushveld have been used for this comparison. Figure 7.8 shows Cr/MgO for the Transitional Unit of cores from Rustenburg Platinum Mines and Amandelbult Section respectively in the western Bushveld. In both examples, orthopyroxene in the Bastard pyroxenite has Critical Zone signatures. Orthopyroxene in the Merensky pyroxenite has a Critical Zone signature at Amandelbult Section, but has a Main Zone signature at Rustenburg Platinum Mines. These data are also summarised in table 7.3.

It is clear from this table that there is a significant disequilibrium between the minerals in the pyroxenites. For example, the Merensky and Bastard pyroxenites in KF35 contain plagioclase that originated from Main Zone magma and orthopyroxene that originated from Critical Zone magma. Conversely, in RM15, both plagioclase and orthopyroxene have formed from Critical Zone magma in both pyroxenites.

7.7 Fractional crystallisation in the Critical Zone

A number of geochemical differences have been noted in this chapter that suggest that processes occurring in the Critical Zone of KF35, and possibly EG5, are different to those in other cores. These differences occur in the 200 m below the Merensky pyroxenite. Both Cr/MgO values and An# decrease systematically (but Mg# remains constant) through this section. Two explanations are considered to explain this variation; mixing between the Critical and Main Zone magmas at this level or fractional crystallisation of the Critical Zone magma

Mixing of the two magmas would result in a steady decrease, along a mixing line, of Cr/MgO values from Critical Zone values, of approximately 100, to Main Zone values of approximately 50. Similarly, An# would decrease from Critical Zone values of approximately 80, to Main Zone values of approximately 75. While both these changes do occur, other similar geochemical changes would also be expected if mixing had occurred. For example, a concurrent increase in Sr isotope ratios, from Critical to Main Zone values, would support mixing between the two magmas, as would a decrease in Sr content in plagioclase (Figure 7.2). However, neither of these trends is apparent and sharp breaks in these parameters occur at the level of the Merensky pyroxenite, not gradual ones below it. Thus, mixing is not considered a suitable solution.

These features support the hypothesis that the variations in Cr/MgO and An# in KF35 and EG5 are the result of fractionation at the top of the Critical Zone. It is unclear however, why orthopyroxene does not display a decrease in Mg# over the same interval. That fractional crystallisation apparently occurred in some areas and not others must also be considered. There are two conclusions that can be drawn. Either fractional crystallisation did not occur at this level throughout the Bushveld, or it did occur, and the rocks that recorded it have been removed by erosion. In Chapter 3, variations in thickness of the UG2-Merensky pyroxenite sequence in the eastern Bushveld were discussed. It was noted that cores in the central sector have a greater thickness of this unit than cores in the southern sector. To explain this, it is possible that erosion, related to the unconformity at the level of the Merensky pyroxenite, was more extensive in the southern sector. Both KF35 and EG5 are from the central sector. Regional potholes that extend over tens of meters into the Merensky footwall have been recorded at Impala (Leeb-du Toit 1986) and thus it may be possible for the 200 m that reflects Critical Zone fractionation in the eastern Bushveld to have been removed by erosion in the southern sector. It is considered unlikely that fractional crystallisation would have occurred in one location and not the other if the magmas were of the same source.

7.8 Implications for the positioning of the boundary

While the unconformity at the base of the Merensky pyroxenite provides a distinct stratigraphic boundary, it is geochemically unclear whether the pyroxenite itself represents the base of the Main Zone or the top of the Critical Zone. The inability to reconcile geochemical with physical changes leads to doubt in terms of the positioning of the boundary.

It remains clear that Main Zone magma was intruded at the level of the Merensky pyroxenite and that this in itself provides an appropriate location for the boundary. However, using distinctive geochemical signatures to indicate whether minerals originated in a Critical or Main Zone magma, it has been shown in this chapter that minerals from a Critical Zone magma occur in the stratigraphy above the Merensky pyroxenite, and thus above the influx of Main Zone magma. This discrepancy indicates that there is no clear geochemical boundary between the Critical and Main Zones. The data presented here do not support the hypothesis that the Merensky and Bastard Cyclic Units were simply

formed from one magma or the other or an homogenised mixture of the two, as minerals sometimes show disequilibrium, indicating that they crystallised from different magmas. Therefore, it is proposed that a "Transitional Unit" is present which extends from the base of the Merensky pyroxenite to the top of the Bastard Cyclic Unit. This was first suggested by Kruger (1990) who described a Transitional Macro unit, comprising the Merensky and Bastard units. Kruger (1990) placed this Transitional Unit at the base of the Main Zone, with the Merensky pyroxenite unconformity as the Critical/Main Zone boundary. Up until 1982, the Merensky pyroxenite was thought to be the culmination of the evolution of the Critical Zone. Detailed work by Cameron (1982) could find no predictive qualitites in the rocks preceeding the Merensky pyroxenite and he concluded that it was the result of a sudden event unrelated to the previous succession. Kruger & Marsh (1982) showed that the Merensky pyroxenite was associated with a major influx of magma with a sharply increased Sr isotope signature. This, coupled with the major disruptions at the base of the Merensky pyroxenite (potholes) is indicative of an unconformity, and evidence for a variable footwall sequence (Vermaak 1976), prompted Kruger (1990) to define the base of the Merensky pyroxenite as the base of the Main Zone. Thus, he proposed that the Merensky Reef is not a culmination of the Critical Zone, but the result of the inititation of the Main Zone. This study strengthens this view, that the Merensky and Bastard Cyclic Units would not have formed without the influx of Main Zone magma.

However, it might be considered that since the Critical Zone magma is still present, the Transitional Unit represents the *top* of the Critical Zone. This follows stratigrapic interpretations in sedimentary successions in which a zonal boundary is located where one lithology becomes predominant over another lithology, not where the second lithology first occurs as thin layers. Nevertheless, since the influx of the Main Zone magma occurred at the level of the Merensky pyroxenite, and forms the material into which Critical Zone minerals sank to form the Merensky and Bastard Cyclic Units (discussed in detail in Chaper 8), the author considers the base of the Main Zone to be the base of the Merensky Cyclic Unit, although the Transitional Unit contains minerals derived from both the Critical and Main Zone magmas. The presence and extent of the unconformity (section 7.7) supports the view that a major event in the evolution of the Bushveld magma chamber occurred at this level. In addition, the Merensky pyroxenite provides a distinct and mappable horizon in the field.

Chapter 8

The origin of the Merensky and the Bastard Cyclic Units

In Chapter 7 geochemical data from the Merensky and Bastard Cyclic Units were described. Specific attention was paid to the chemical composition of minerals forming from Critical and Main Zone magmas. It was shown in section 7.4 that it is possible to distinguish between plagioclase formed from Critical Zone magma, which has low Sr isotope initial ratios and high Sr content, and plagioclase formed from Main Zone magmas, which has high Sr-isotope initial ratios and lower Sr content. Similarly, it is possible to distinguish between orthopyroxene that crystallised from the Critical and Main Zone magmas, where Cr/MgO ratios are high and lower respectively. It was demonstrated in section 7.5 that these observations can be used to categorise plagioclase and orthopyroxene in the Merensky and Bastard Cyclic Units according to which magma the minerals formed from. It was established that in some profiles, plagioclase and orthopyroxene from these cyclic units crystallised from different magmas, but accumulated together to form the cyclic units. “Reversals” to Critical Zone Sr isotopic signatures in the Bastard pyroxenite e.g. at RM15 and Atok, suggest that Critical Zone magma was still discrete, present as an individual unit and unmixed, after the Main Zone magma was intruded.

8.1 A model for the formation of the Merensky and Bastard Cyclic Units

It is proposed that orthopyroxene in the Merensky and Bastard pyroxenites originated from Critical Zone magma and that interstitial plagioclase originated from Main Zone magma. Furthermore, the Merensky Cyclic Unit norites and anorthosites in both RM15 and KF35 cores display increasing Main Zone affinities, in the sense that Sr isotopes in plagioclase increase towards 0.707 which is typical of the Main Zone. In this section, a model is presented to explain these geochemical variations and mineral disequilibrium.

Strontium isotope data from silicate rocks indicate that the Critical Zone and Main Zone were formed from two different magmas (Sharpe 1985, Lee & Butcher 1990, Kruger 1994). Models have been proposed that

involve the mixing of these two isotopically distinct magmas to account for the gradual variation in Sr isotopes from lower values typical of the Critical Zone to higher values typical of the Main Zone, from the level of the Merensky pyroxenite upward (Kruger 1994). It is proposed that the mineral variations shown in this study are the result of the minerals crystallising and settling from two different magmas to accumulate together at a specific level, and that the geochemistry observed is *not* the result of mixing and subsequent crystallisation of the magmas, but the crystallisation of minerals from two different magmas and their subsequent mixing.

Figure 8.1 is a schematic diagram that represents the stages that formed the isotopically and geochemically distinct pyroxenites. Crystallisation had reached the footwall of the Merensky pyroxenite. In stage 1, the Main Zone magma entered the chamber as an injection, exploiting the boundary between the Critical Zone crystal pile and the liquid. This process eroded a portion of the Critical Zone crystal pile, forming the unconformity at the base of the Merensky pyroxenite. This magma was lower in SiO_2 and richer in FeO (Cawthorn *et al.* 1981) and hence denser than the Critical Zone liquid and thus intruded along the base of the chamber, as shown in section 7.5.1. This is in agreement with other observations by Hatton (1989) and Maier *et al*. (2001). This injection of new magma displaced the Critical Zone liquid upward, where it continued to crystallise orthopyroxene and plagioclase as it did to produce the Critical Zone cumulates. Crystals possibly nucleated close to the interface with the cooler, underlying Main Zone magma.

In stage 2, orthopyroxene crystallising in the Critical Zone liquid began to settle through the Main Zone injection due to its high density, in a similar fashion to that described by Kruger (1992). These orthopyroxenes collected at its base, to form the Merensky pyroxenite. The sinking of clusters of orthopyroxene crystals has previously been suggested to explain other features in the Bushveld Complex. For example, Vermaak (1976) and Campbell *et al.* (1983) suggested that orthopyroxene clusters had sunk through the Upper Critical Zone magma to form the Boulder Bed, a layer just below the Merensky pyroxenite. Vermaak (1976) also suggested that the dimpled lower surface of the Merensky pyroxenite was due to sinking of similar orthopyroxene-rich aggregates.

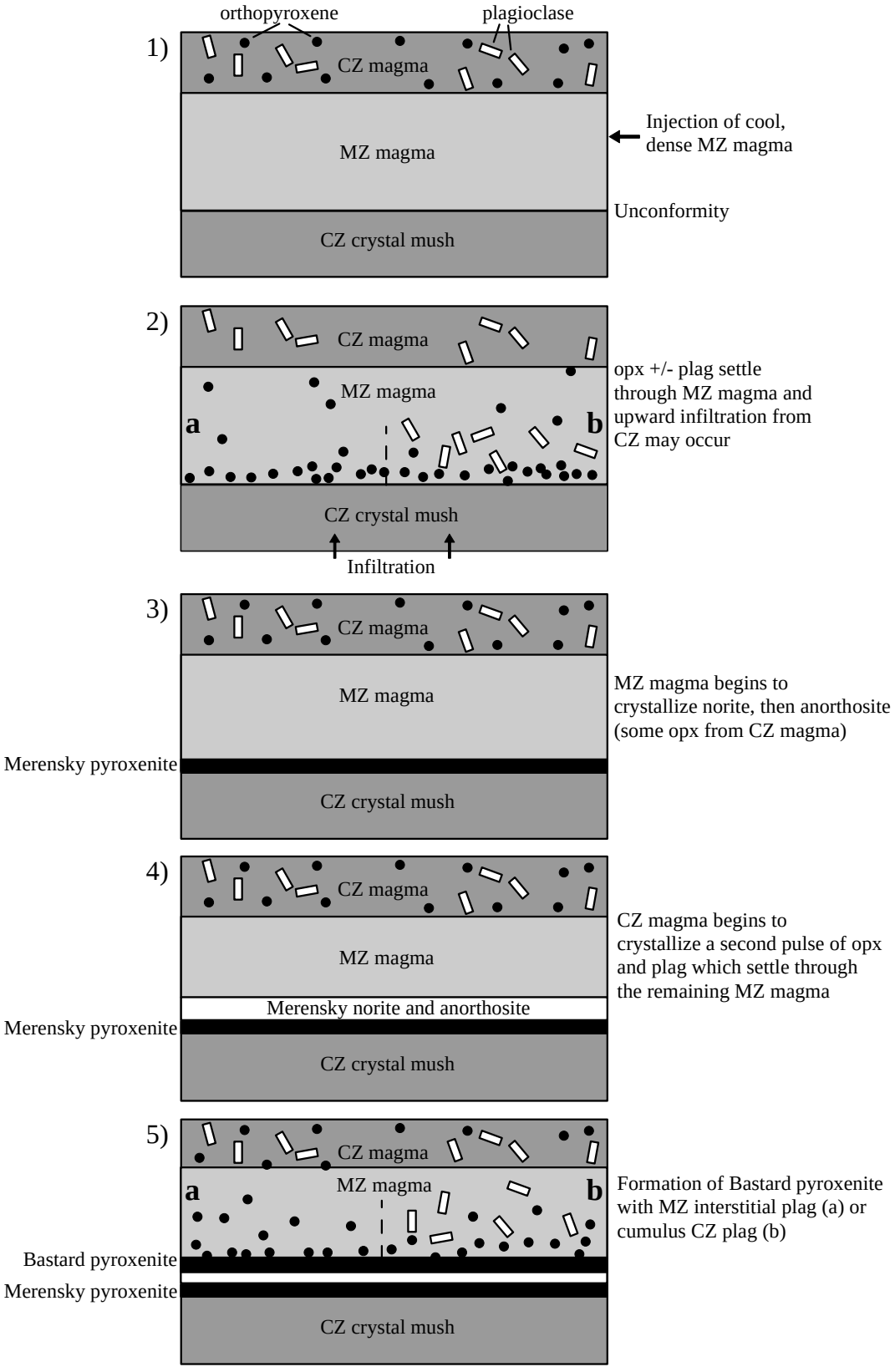


FIGURE 8.1 Schematic diagrams illustrating the development of the Merensky and Bastard Cyclic Units (see text for detailed explanation). Plag – plagioclase, opx – orthopyroxene, CZ – Critical Zone, MZ – Main Zone.

The Sr content and initial Sr isotope ratio in plagioclase provide evidence about the magma from which it formed, but not the physical processes involved. It has been shown in section 6.2.3 that not all plagioclase in the Merensky pyroxenite is interstitial as previously assumed. In fact, it is possible that up to 80% of the plagioclase can be cumulus. In the case of the Critical Zone signature of plagioclase at the base of the Merensky pyroxenite, either or both of two processes might apply. In both models some of the intercumulus plagioclase forms from the Main Zone magma. However, these pyroxenites are quite feldspathic and contain a variable proportion of cumulus and intercumulus plagioclase (section 6.2.3). Where substantial amounts of cumulus plagioclase are present, it is suggested that Critical Zone plagioclase also sank, together with orthopyroxene, through the Main Zone package (discussed in detail in section 8.3.5), contributing to a Critical Zone isotopic signature.

Alternatively, the Critical Zone signature in the Merensky pyroxenite could result from upward infiltration of residual liquid (e.g. Eales *et al.* 1986). Where there is more interstitial plagioclase, upward infiltration of Critical Zone interstitial liquid could have occurred. Eales *et al.* (1986) demonstrated that a distinct geochemical signature, in terms of whole-rock Sr/Al ratio, exists for each of the cyclic units in the Upper Critical Zone. They further showed that the signature from each unit could be traced about 1 m into the pyroxenite of the overlying cycle, which they attributed to infiltration by interstitial liquid. They identified this pattern at the base of the Merensky Cycle, where the top of the Critical Zone liquid residua infiltrated in to the cumulus base of the Merensky pyroxenite. Using their model, it could be argued that the Critical Zone signature at the base of the Merensky cycle is the result of residual Critical Zone liquid infiltrating into the lowermost part of the Merensky cycle and displacing the Main Zone liquid. Where plagioclase in the Merensky pyroxenite has Main Zone isotopic ratios, e.g. at Amandelbult, then this upward infiltration was less effective. The high (Main Zone) Sr isotopic signature at the base of the Bastard pyroxenite (Figure 5.21a) may have a similar origin. In this instance, residual Main Zone magma from the top of the Merensky Cyclic Unit may have infiltrated upward into the Bastard pyroxenite that was otherwise dominated by orthopyroxene and plagioclase, both from the Critical Zone magma. In addition, dissolution or disagregation of plagioclase from the Merensky footwall anorthosite during pothole

formation (section 8.3.6) may have contributed Critical Zone Sr isotopic signature of the plagioclase in the Merensky pyroxenite.

Above the Merensky pyroxenite, the overlying Main Zone liquid began to crystallise plagioclase that accumulated to form norite and anorthosite (section 8.2.3) of the Merensky Cyclic Unit (stage 3). However, in some areas, a significant proportion of the plagioclase in the Merensky norites and anorthosites originated from the Critical Zone. The varying proportions of Critical and Main Zone plagioclase resulted in the irregular Sr isotope ratio observed through the Merensky Cyclic Unit. In RM15, the isotope profile does not show a gradual increase through the Merensky anorthosite (Figure 5.21a), indicating that variable amounts of both Critical and Main Zone cumulus plagioclase are present. Mixing of the two magmas cannot explain this heterogeneity.

Due to some mechanism discussed below, the crystallisation of orthopyroxene from the Critical Zone magma resumed after a certain amount of mottled anorthosite had crystallised (section 8.2.3). In stage 4, this orthopyroxene then sank through the remaining Main Zone liquid to accumulate on the crystal pile, forming the Bastard pyroxenite. In most situations, interstitial plagioclase formed from the Main Zone liquid into which the orthopyroxene settled, producing a Main Zone isotopic signature (stage 5a). Figure 6.7 shows that in the "normal" profile, KF35, only 20-40% of plagioclase in the Bastard pyroxenite is cumulus, thus 60-80% is interstitial. Hence Sr isotope initial ratios largely reflect the composition of the trapped liquid, which is that of the Main Zone, even though the orthopyroxene originated from the overlying Critical Zone magma. However, in the "atypical" profiles RM15 (this study) and Atok (Lee & Butcher 1990), plagioclase in the Bastard pyroxenite has Critical Zone Sr isotope ratios. In these cases, it is proposed that plagioclase as well as orthopyroxene from the overlying Critical Zone liquid sank through the Main Zone liquid (stage 5b). This is supported by Figure 6.7, which shows that plagioclase in the Bastard melanorite in RM15 contains significant amounts of cumulus plagioclase (50-80%). Since the liquid into which the pyroxene is accumulating is considered to be a Main Zone liquid and this *cumulus* plagioclase has a Critical Zone signature, it is clear that the plagioclase must have crystallised above the level at which it has now accumulated. The plagioclase may have formed as aggregate clusters with orthopyroxene,

enabling the plagioclase to overcome neutral buoyancy. Kruger (1992) discussed a comparable process, referring to blobs of crystal-liquid slurry. However, he suggested that the liquid in this slurry, being of Critical Zone composition, could produce interstitial plagioclase of Critical Zone isotopic affinity. The difference between the present model and that of Kruger (1992) is that here, evidence is presented for the presence of cumulus plagioclase, with a Critical Zone signature, in the Bastard pyroxenite. The norites and anorthosites of the overlying Bastard Cyclic Unit overall demonstrate increasingly Main Zone affinities in plagioclase, which represent the crystallisation of the Main Zone magma in stage 5, which continues into the Lower Main Zone. At the base of the GMA, plagioclase still has a Critical Zone Sr isotopic signature, representing accumulation of cumulus plagioclase. However, interstitial clinopyroxene from the same sample (RM15 140) gives a Main Zone Sr isotope value (Figure 5.21), which supports the observation that the interstitial liquid at this level was Main Zone magma. As in the Merensky Cyclic Unit, some plagioclase in the Bastard norites and anorthosites did originated from the Critical Zone liquid, which is shown by the heterogeneous Sr isotope profile through this unit (Figure 5.21). Orthopyroxene in the Bastard pyroxenite shows typical Critical Zone Cr/MgO values indicating that orthopyroxene was still sinking from the elevated Critical Zone liquid at that stage. However, in the case of RM15, the lowest sample of pyroxenite from the Bastard Unit has a Main Zone signature. Such an observation could be consistent with the upward infiltration of magma of Main Zone affinity from the top of the Merensky Cyclic Unit. Other geochemical changes are also not observed until the level of the GMA (section 5.1.2, section 7.5, Mitchell & Manthree 2002). This indicates that significant quantities of Critical Zone minerals are present up to this level. It is unclear why Critical Zone minerals are not present above the top of the GMA, but it seems likely that the Critical Zone magma had been stopped crystallising and/or dispersed in some fashion at that point. The ultimate fate of the remaining elevated Critical Zone liquid is discussed in section 8.2.4. The constant Mg# (Figure 5.10) does not indicate that extensive fractionation occurred and this indicates that the remaining Critical Zone liquid was not exhausted and must have been removed before it had fully crystallised.

Since the Merensky and Bastard Cyclic Units contain minerals derived from both Critical Zone and Main Zone liquids, they should not be grouped with either the Critical Zone or the Main Zone, but designated as transitional Cyclic Units, as suggested by Kruger (1990), who proposed that these Cyclic Units be grouped together as the Transitional Macro-unit.

8.2 Processes within the magma chamber

While the model presented above accounts for the geochemical variations observed in this study, there remain some unresolved questions. These problems largely revolve around the physical mechanisms that result in the accumulation of crystals from two different magmas and the origin of the layering and also the relative and absolute densities of the minerals and magmas. In this section, fundamental issues are raised and discussed.

8.2.1 Sinking crystals

The model presented here depends on the ability of crystals to preserve their chemical identity when sinking through a fresh magma input. Campbell *et al*. (1978) showed that plagioclase has a density of 2700 kg/m^3 or 2650 kg/m^3 at compositions An_{90} and An_{70} respectively, at 1200^{o}C, which is close to that calculated for the Main Zone magma (section 7.5.1). Thus, if the density contrast between plagioclase crystals and Main Zone melt is insufficient, it is proposed that plagioclase may only have been able to sink as clusters with orthopyroxene (Kruger 1992). The proportions of cumulus and interstitial plagioclase vary in different areas of the Bushveld Complex giving rise to variable Sr-isotope ratios. Cawthorn & Spies (2003) showed that sinking and sorting of orthopyroxene and plagioclase grains could lead to any proportion of the two minerals being present in any specific layer. These two processes are shown in Figure 8.1. In stage 2A (Figure 8.1), no plagioclase in the Merensky pyroxenite is cumulus and its Critical Zone signature is the result of upward infiltration of residual liquid. In stage 2B, plagioclase is cumulus, and originated in the overlying Critical Zone magma. These two processes are not mutually exclusive.

Figure 8.2 demonstrates the Critical Zone characteristic of the plagioclase in the Merensky and Bastard pyroxenites from RM15. Two distinct groups of Critical and Main Zone values can be linked with a third group that represents rocks containing plagioclase of mixed affinity from both Critical and Main Zone magmas. It is clear that samples from the Merensky pyroxenite have Critical Zone Sr concentrations and Sr isotope values. Some samples from the Bastard pyroxenite also show Critical Zone affinities, but some samples plot along the mixing line (mixing of plagioclase grains from two magmas, not mixing of magmas). It is not feasible to plot the data from other studies in such a diagram as their Sr contents of plagioclase are not known, because only whole-rock isotope analyses are given.

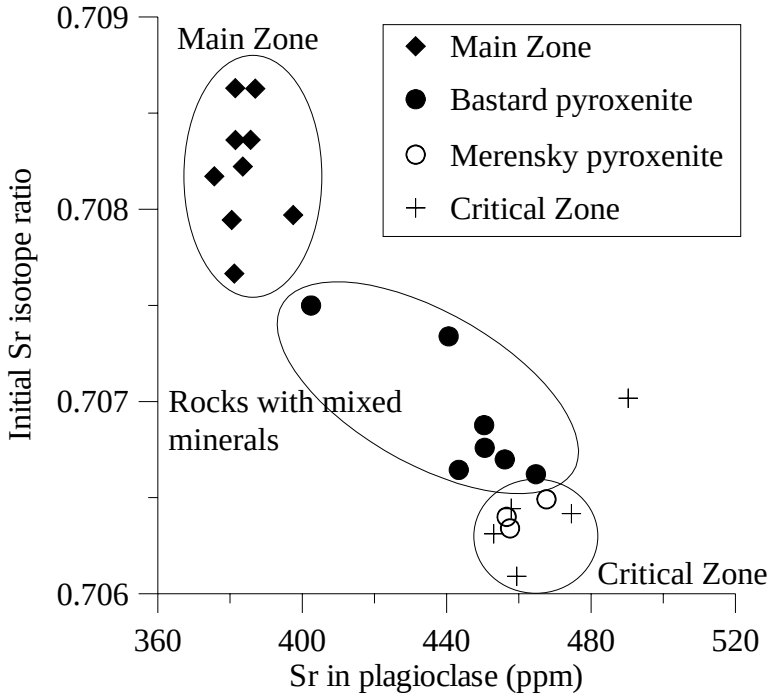


FIGURE 8.2. Graph of Sr isotope initial ratio plotted against Sr concentration in plagioclase separates, showing mixing of Critical and Main Zone plagioclase grains.

In addition, Morse (1986, 1988) described suspensions of crystals plus liquid that could have sunk much faster than individual crystals would have settled. However, there is little information as to whether the crystals would be re-melted, or partially re-melted and under what conditions this might have occurred, and whether there is a finite time a crystal might remain in magma before it is assimilated. McLeod & Sparks

(1996) undertook experiments involving the melting of wax spheres, which they used to interpret rates of xenolith assimilation in magma bodies. Although this data indicated rapid melting it shed little light on the melting of the minerals in question here. Donaldson (1985) determined that plagioclase dissolves rapidly in a basaltic melt, at a rate of 77 μm/hr at 1210^{o}C, compared to quartz and olivine at 36 and 8.7 μm/hr respectively. He also determined that these rates increase with increasing temperature. Donaldson (1993) suggested that small scale layering in intrusions might be caused by the melt from crystals rapidly recrystallising at the chamber floor, triggering abrupt changes in cumulus mineralogy. While experimental data suggests that plagioclase, and probably orthopyroxene, would be assimilated into a melt and unable to sink intact through magma, this is based on the premise that the magma through which it is sinking is not saturated in that mineral. Hence it is saturated in minerals, but the mineral composition is different. However, if the magma is saturated in that mineral and it is dense enough, then it will sink without melting. Cawthorn (2002) showed that Bushveld magma at this level in the chamber becomes plagioclase-saturated at orthopyroxene Mg# of 83. Thus, the Main Zone magma would have been saturated in both orthopyroxene and plagioclase because it does not have an Mg# of over 80 (Figure 5.10), assuming the magma was not significantly superheated. This suggests that plagioclase and orthopyroxene from the elevated Critical Zone magma would have been able to sink intact through the plagioclase- and orthopyroxene-saturated Main Zone magma, regardless of how quickly these minerals would be assimilated in an undersaturated or superheated magma.

Wager & Brown (1968) discussed rates of crystal settling in the Skaergaard Complex and indicated that pyroxene can sink at rates of up to 160 m per year, for crystals the size of those observed here. In their calculations, Wager & Brown used a viscosity of 3000 poises and a magma density of 2580. This density is a little lower than the density of the Main Zone magma calculated in section 7.5.1. Irvine (1987) presented evidence that olivine and pyroxene was carried down to the cumulate floor from the chamber roof in the Duke Island intrusion. Eales *et al*. (1991) suggested that inclusions of plagioclase in orthopyroxene (and olivine) in the Upper Critical Zone might represent crystals that settled from higher liquid layers in a stratified column. Kruger & Marsh (1985) recorded zoned plagioclase from the Merensky pyroxenite and

Merensky norite at Rustenburg Platinum Mine, western Bushveld. De Klerk (1995) recorded that cumulate plagioclase grains in the GMA show varying degrees of complex oscillatory-zonal growth and interpreted this as recording growth episodes during earlier influxes of magma. De Klerk also suggested that these plagioclase crystals escaped incorporation into the cumulate pile and were thus suspended in the magma without remelting for some time.

Tepley & Davidson (2003) recorded Sr isotopic zoning within single plagioclase grains from the Rum layered intrusion, Scotland. They ascribed this phenomenon to contamination taking place during crystal growth, which is then reflected in the crystals. Plagioclase grains that display $^{87}Sr/^{86}Sr$ zonation are proposed to have crystallised near the roof or sidewalls of the chamber, where the influence of contamination is high and wall rocks are more readily assimilated into the magma. Those grains that are not zoned are taken to have grown in situ or within a convecting magma, away from the prominent effects of contamination. These observations led Tepley & Davidson to propose that plagioclase crystals in a given layer have been transported to their present locations from elsewhere. They suggest that this was the result of gravitationally unstable currents or plumes that conveyed isotopically zoned crystals, or clots of crystals from the roof rock area to the magma chamber floor. An important factor of Tepley & Davidson's model is that crystals do not sink through the magma, but are transported by it, hence their model, and is thus slightly different to the mechanism proposed here. Nevertheless, their study suggests that it is possible for plagioclase crystals or packages of crystals to be moved around the chamber independently of the specific magma in which they were formed. However, Tepley & Davidson do indicate that the magma through which crystals are moving would have to be plagioclase saturated. Ashwal *et al*. (2004) suggested that density reversals in the Bellevue drillcore from the northern limb of the Bushveld may have resulted from dense liquid and/or crystals draining downwards from a new magma influx into the existing cumulate pile to create blending zones. Charlier *et al*. (2004) investigated microanalyses of Sr isotopes in a range of minerals, including plagioclase, in the Fish Canyon volcanics and showed that Sr isotope values vary significantly within a single grain. They interpreted this to represent open system processes within the magma by direct incorporation of xenocrystic phases from earlier periods of magmatism to produce an

isotopically heterogeneous magma at the mineral scale. Chertkoff *et al.* (2004) also determined multiple crystal populations of plagioclase within Stromboli volcanics using Sr isotopic and textural information. They suggested that the mineral populations evolved in isolated environments and were subsequently mechanically mixed prior to eruption. All these mineral-scale investigations support the model presented here that two populations of minerals, with different geochemical signatures can crystallise separately and then mix and accumulate in a single layer.

8.2.2 Intermittent sinking of plagioclase

The mechanism by which Critical Zone plagioclase sometimes managed to sink through the Main Zone magma is uncertain. In order to achieve this, plagioclase would have to overcome its neutral buoyancy. It is proposed here that plagioclase can sometimes clump together with orthopyroxene and that this combination is sufficiently dense to sink together, resulting in cumulus Critical Zone plagioclase in the Bastard pyroxenite. This process was not active in the GMA where Critical Zone plagioclase is present without orthopyroxene. Kruger (1992) postulated that orthopyroxene/liquid crystal slurries sank into the Main Zone liquid. While these slurries would account for Critical Zone signatures, it was shown in section 6.2.3 that a significant proportion of cumulus plagioclase is present in the Bastard pyroxenite, thus cumulus plagioclase crystals must also have settled from the elevated Critical Zone liquid. This is supported by the higher Al_2O_3 and Sr content in the Bastard pyroxenite at RM15, where a Sr isotope break occurs, than in KF35, where a break does not occur. Jerram *et al.* (2004) investigated clustering of olivine and plagioclase crystals in volcanic flows and determined that crystal clusters are easily formed in magmas as touching crystal frameworks. They postulated that crystals colliding and sticking together during settling would enhance crystal clustering in intrusive bodies. The investigation of Jerram *et al.* (2004) supports the crystal settling theory and implies that orthopyroxene (and plagioclase) may group together as clusters. Therefore, for the purposes of this study, it is inferred that pyroxene may form clusters with plagioclase crystals and these clusters are capable of sinking through a fresh magma input. However, in some instances plagioclase does

appear to settle independently of orthopyroxene, such as at the base of the GMA in RM15 where plagioclase has a Critical Zone signature.

It is unclear why (uncommonly) cumulus Critical Zone plagioclase is apparent in the Bastard pyroxenite in two locations (Atok and Richmond), whereas a Main Zone signature is typical in most locations. Thus far, cumulus Critical Zone plagioclase is only observed in the eastern limb, where two out of three profiles show it (RM15 and Atok). However, throughout almost every profile in the east and west, there is a gradual increase in Sr-isotope initial ratio in the Merensky and Bastard pyroxenites and the overlying succession. This suggests that plagioclase was settling from the overlying Critical Zone liquid across the whole complex, but in smaller proportions in the west.

8.2.3 The mechanics of layering

The mechanism that leads to two pulses of orthopyroxene from the Critical Zone magma to form the Merensky and Bastard pyroxenites is unclear. A number of possibilities exist. The first and most obvious suggestion is that orthopyroxene somehow stops crystallising during the period when the Merensky norites and anorthosites crystallise and subsequently resumes to form the Bastard pyroxenite. Secondly, it is possible that crystallisation of orthopyroxene does not stop, but that the crystals remain suspended and only periodically are they able to sink through the Main Zone magma. These possibilities are discussed below.

The first process requires a method of moving crystallisation into and out of the orthopyroxene field, since it is unlikely that all crystallisation of the Critical Zone magma ceases completely, although both the Critical and Main Zone magmas may have been crystallising simultaneously. Cawthorn & Spies (2003) demonstrated that the Critical Zone magma was crystallising orthopyroxene and plagioclase close to cotectic proportions. They suggested that a slight increase in pressure within the chamber would destabilise orthopyroxene. Periodic nucleation of orthopyroxene and consequent settling resulting from pressure fluctuations could contribute towards the development of layering. Pressure fluctuations to induce layering have been discussed by Naslund & McBirney (1996). Lipin (1993) used pressure changes to explain chromitite formation in the Stillwater Complex. The importance of this mechanism being that a pressure

change would affect the whole chamber simultaneously, which is expedient when explaining the lateral extent of the Merensky and Bastard layers in the Bushveld Complex.

It may also be possible that periodic orthopyroxene accumulation is simply the result of lack of deposition, not lack of formation of the crystals. In this scenario, methods for preferential suspension and subsequent deposition may invoke some form of magma current activity in the Critical Zone liquid. Convection currents acting within the magma may serve to move crystals away from the boundary with the Main Zone liquid and thus allow orthopyroxene to settle only when no current is active. However, these currents would then have to affect the entire chamber simultaneously. Fluid dynamics and thermal convection in magma chambers has been frequently invoked to explain mineral distributions in magma chambers (e.g. Sparks *et al*. 1984, Martin *et al*. 1987, Marsh 1988). In addition, the Critical Zone liquid at the top of the chamber may have crystallised against the walls and roof of the chamber.

The Critical Zone magma would have already contained crystals when it was elevated by the Main Zone influx. These would have probably have been the first to settle through the Main Zone magma. The temperatures used in Table 7.3 suggest that the Main Zone magma would have been capable of crystallising both plagioclase and orthopyroxene as soon as it entered the chamber. It is assumed that the Main Zone magma was not superheated, although crystallisation may have been interrupted at the boundary between the two magmas until equilibration, in terms of temperature, was achieved. Since the Main Zone magma is assumed, in this study, to have been warmer than the Critical Zone magma (Table 7.3) the Critical Zone magma may have been heated from below, giving rise to thermal convection. Convecting minerals may have contributed to the lag in accumulation of orthopyroxene between the deposition of the Merensky and Bastard pyroxenites in a fashion similar to that suggested by e.g. Sparks *et al*. (1984), Martin *et al*. (1987) and Marsh (1988). Intermittent spalling of crystals from the walls and roof (Parsons & Becker 1987) into the chamber may result in the observed rhythmic accumulations of crystals of orthopyroxene. Kruger (1992) suggested that a cessation in convection, the result of chilling, induced the crystallisation of orthopyroxene.

Another theory proposed here involves the possibility that orthopyroxene crystals from the elevated Critical Zone magma may not have been able to immediately pass through the boundary between the two magmas. Crystals may have collected at this boundary and once sufficient amounts had accumulated, the crystals may have sunk simultaneously, rather than settling to the base of the chamber as they formed. If subsequent crystallisation led to a second accumulation of crystals at this magma boundary, and hence a second "break through", then apparent periodic settling may be generated, accounting for the formation of the Merensky pyroxenite (first pulse) and subsequently the Bastard pyroxenite (second pulse). However, while this might explain the accumulation of two pulses of orthopyroxene, there is a great deal of doubt over the nature of the boundary and whether it would prevent crystals sinking through it until a specific mass of crystals had accumulated. This would depend on the rheology of the boundary as well as the density of the two magmas. Further work would have to be undertaken in order to attempt to constrain this model and apply it meaningfully to the situation described here.

For the purposes of this model, it is proposed that a slight pressure change, possibly the result of venting or eruption, was responsible for the intermittent crystallisation of orthopyroxene from the Critical Zone magma, as this mechanism can affect the entire magma chamber at the same time. However, it remains possible that pauses in crystallisation may be the result of a combination of the processes discussed above, active at different times and at different locations in the chamber.

Another aspect of layering that should be mentioned is the presence of significant amounts of anorthosite within the Upper Critical and Main Zones of the Bushveld Complex. Cyclic Units were initially defined by Jackson (1970) who suggested that chromite-olivine and olivine-orthopyroxene cycles are the product of differentiation. However, Cyclic Units are frequently considered to include norite and anorthosite, even though Jackson (1970) showed that anorthosites cannot form as the result of fractionation from a single magma. The origin of anorthosites in cyclic units has thus been widely discussed and various hypotheses are summarised in Cawthorn & Spies (2003). Hypotheses include crystal sorting, the presence of two discrete magmas in a density stabilised stratified succession (Irvine *et al*. 1983, Irvine & Sharpe 1986) and the retention of plagioclase in the magma from previous cycles, which is then deposited in an

overlying cycle, and the invocation of a separate plagioclase-saturated magma to form each anorthosite layer (Cawthorn & Spies 2003). In terms of this study, mechanical separation of the mafic minerals seems most appropriate.

8.2.4 The thickness of the Critical and Main Zone magmas

It is possible that there was a substantial amount of Critical Zone magma in the chamber when the Main Zone magma was intruded. While it is clear that the Critical Zone magma continued to crystallise, forming part of the Merensky and Bastard Cyclic Units, there is no evidence of a thick sequence of more evolved rocks that would have resulted from the crystallisation of a substantial volume of Critical Zone magma. A number of possibilities are envisaged for the ultimate fate of the remaining Critical Zone liquid. The most likely are that it was either erupted out of the chamber (and has subsequently been eroded) or that it eventually mixed with the Main Zone magma subsequent to the formation of the Merensky and Bastard Cyclic Units. The latter would be more likely if the Main Zone magma was introduced in pulses and not the entire volume in one go as discussed below. However, mixing would reduce the isotope ratio in the Main Zone and this is not apparent in its entire thickness (Kruger 1994). Neither eruption nor mixing provides a convincing fate for the Critical Zone magma.

In addition, the thickness of the injection of Main Zone magma is unclear. It is unlikely that the entire Main Zone was intruded at the same time. It is envisaged, for the purposes of this model, that it was introduced in stages and that the thickness through which Critical Zone minerals sank was relative small in comparison to the total volume. No textural features were observed in this study that distinguish Critical Zone plagioclase from Main Zone plagioclase, as might be expected if they had sunk through considerable amounts of magma with which they were not in equilibrium. Although textural features such as zoning, have been observed in cumulates of the Merensky and Bastard Cyclic Units (Kruger & Marsh 1985, de Klerk 1995), this also suggests that the thickness of magma through which they did sink was not great. The dissolution of anorthosite footwall during potholing (section 8.3.6) also indicates that it is likely that plagioclase grains would have dissolved if they had sunk through an extensive thickness of Main Zone

magma. However, it is observed here that there is minimal variation in An# of plagioclase in the succession overlying the Merensky pyroxenite (Figure 7.2). For any magma crystallising plagioclase, the An# will decrease systematically as the result of differentiation. The observation here, that the An# does not vary significantly through the Merensky and Bastard Cyclic Units, might indicate that a large volume of magma was present above this level. Nevertheless, after, or even during, the formation of the Merensky and Bastard Cyclic Units, the initial pulse of Main Zone magma would have been replenished repeatedly in order to eventually crystallise its entire thickness, some 3000 m. This constant replenishment would have equilibrated with Main Zone magma already in the chamber, resulting in the lack of variation observed in An#.

8.3 Comparison with other models

Although the model presented in section 8.1 accounts for the geochemical data observed in this study, an attempt must be made to compare the model with previous investigations. This section discusses the findings of a number of studies conducted over the same Transitional Unit.

8.3.1 Magma mixing

Kruger & Marsh (1982) proposed that a new magma entered the chamber and mixed with the existing liquid and that the Merensky and succeeding cyclic units formed by accumulation of crystals precipitating from the blended magmas. This theory is based on the increase in Sr isotope initial ratio at the Merensky pyroxenite. They suggest that the new magma had Sr isotope values of >0.7075 and possibly >0.7086 and that otherwise it was compositionally similar to the existing magma, based on detailed mineral and whole-rock composition data. Schoenberg *et al.* (1999) suggested that the Main Zone magma isotopic signature is the result of roof-rock contamination that occurred when the magma influx “fountained” through the chamber. Their Sr isotope data are in line with that presented here, but while some mixing between the two magmas may be a factor, it does not account for the geochemical variations in mineral separates described

here. This is supported by Wilson *et al*. (1999) who suggested that Sr isotope ratios from the Merensky pyroxenite in Rustenburg Section do not support a magma mixing model at that point. Although they do indicate that magma mixing occurred in the overlying norites, they interpret a constant Mg# in orthopyroxene of the pyroxenite to indicate formation of this layer from just one magma.

The commingling of contrasted magmas is a well-documented occurrence in granitic rocks (Wiebe 1991 and references therein). Commingling is a process that describes the interaction between two magmas where mixing is incomplete. Wiebe (1991) stated that no convincing evidence has been presented to suggest that contrasted magmas mix homogeneously and indicated that temperature, density and viscosity contrasts would inhibit complete mixing. While the model presented here does not support wholesale mixing between the Critical and Main Zones magmas, exemplified by the two geochemically distinct mineral assemblages, it remains possible that magma mingling between these two contrasting magmas may have occurred to some degree. However, the consistency of the layering does not indicate that this was a significant process.

8.3.2 Repeated magma injection

Eales *et al*. (1986, 1988) proposed that Merensky footwall, Merensky and Bastard Units formed as the result of separate injections of primitive, mafic magma. The leucocratic upper parts of these units are the result of progressive hybridisation of the liquid residua. They also proposed that rocks above the Bastard Unit represent cumulates deposited by a new influx of magma, uncontaminated by mixing or hybridisation, which was emplaced above liquids overlying the critical zone cumulates. These observations were largely supported by trace element ratios, which show the development of apparent cyclic units and it was this trend that lead to the suggestion of separate influxes of magma. However, modelling in section 6.1 shows that these geochemically defined “cyclic units” are simply the result of modal proportions and do not necessarily reflect a series magma influxes. In addition, geochemical data presented in this study indicate that in some situations cumulates and intercumulus minerals demonstrate origins from different magmas, whereas the model presented by Eales *et al*. suggests that they should form from the same liquid. Similarly,

mineral disequilibrium in a single layer indicates that the model proposed by Irvine *et al*. (1983), whereby the Pseudo, Merensky and Bastard Units are equivalent, representing deposits laid down from the same liquid re-elevated to different levels within the chamber at different times, is also inaccurate. The suggestion by Lee & Butcher (1990) that the Merensky and Bastard pyroxenites are the result of sill-like intrusions of pyroxenitic magmas also requires cumulus and intercumulus minerals to crystallise from the same liquid, which has been shown to be sometimes not the case. This study shows that minerals in these layers can be assigned to either Critical or Main Zone magma, without the need to invoke another, compositionally different magma. The minimal variation observed in An# across the Merensky Unit is also suggestive of a thicker sequence of magma, rather than thinner individual influxes.

8.3.3 Temperature and density considerations of the injected magma

Campbell *et al*. (1983) proposed injection of a hot, picritic magma to form the Merensky pyroxenite. They suggested that this magma spread out at its own density level in a density-stratified magma chamber. This hybrid layer then cooled rapidly resulting in nucleation of some orthopyroxene crystals (and sulphide and olivine), which settled to the floor of the chamber. They suggested that cooling of this magma raised its density, leading to convective overturn and brought the magma to the floor of the chamber, where *in situ* crystallisation proceeded. This model is based on the assumption that the new magma was primitive in nature. Kruger (1992) envisaged the Main Zone magma to be more evolved and of a gabbroic composition, and that the resident Critical Zone magma was noritic in composition. He also indicated that the Main Zone magma would have been compositionally and thermally denser than the resident magma, and that it remained as a stable basal layer after its influx along the interface between the crystal pile and the resident magma. This suggests that it did not rise into the chamber as suggested by Campbell *et al*. (1983). Density calculations in section 7.4 also suggest that the Main Zone magma was denser, which supports the idea of this magma forming a basal layer, with a Critical Zone liquid above. Stratification of magmas with sufficient density contrasts has been shown experimentally by Koyaguchi & Blake (1991). This study

supports the intrusion of a denser, possibly cooler, Main Zone magma, which would have ponded beneath the Critical Zone magma, and did not mix with it mechanically, to form a stratified chamber.

8.3.4 Mineral disequilibrium

Eales *et al*. (1986) noticed decoupling of trends of cryptic variation in orthopyroxene and plagioclase. They ascribed this to the positive buoyancy exhibited by plagioclase in basaltic melts (Campbell *et al*. 1978), suggesting that turbulence in the chamber led to the floating of plagioclase, above the level of the orthopyroxene with which it crystallised. Although this process has now been more thoroughly documented (e.g. Cawthorn & Spies 2003), the observations of Eales *et al*. (1986) do not equate to the disequilibrium described in this study, as they indicated that the orthopyroxenes and plagioclase both originated from Critical Zone magma. This study shows that orthopyroxene with a Critical Zone signature, as well as plagioclase, occurs above the cumulate level of the Main Zone magma influx. As orthopyroxene does not float in the magma, the process described by Eales *et al*. (1986) cannot be the only contribution to mineral disequilibrium.

Prevec *et al*. (2005, in press) described disequilibrium between feldspar and pyroxene in terms of Sm-Nd isotopic evidence in the Merensky pegmatoid and pyroxenite. These data support the observations made here. They suggested that primary magmatic orthopyroxene has an isotopic signature that indicates high degrees of contamination, whereas plagioclase shows a different signature which does not show such high amounts of contamination. They suggested that this might be the result of syn-emplacement contamination of new magma pulses, or mixtures of cumulates from already distinct magmas. The latter would be in agreement with the co-accumulation of crystals suggested here. They also discussed a secondary late-magmatic/hydrothermal process that might have contributed to the mineral disequilibrium. They suggested that later mineral overgrowths and/or overprinting might result in the disequilibrium observed. While this may apply to the minerals in this study, their geochemical similarities to typical Critical or Main Zone minerals indicates that a later process, that would have produced a completely

different geochemical signature, did not occur. There is little evidence to support secondary fluid activity where a pegmatoid is not present.

Mathez & Waight (2003) discovered systematic Pb-isotopic disequilibrium between sulphides and plagioclase in the Merensky and Bastard pyroxenites. This disequilibrium varied on the thin-section scale and they found gross isotopic variability among sulphides in some samples and small differences in plagioclase isotopic composition in adjacent lithologic layers. They noted that rocks from above and below the Merensky and Bastard pyroxenites appear to have crystallised from different magmas and suggest that this reflects mixing before or during crystallisation. Merensky footwall samples show high Pb ratios and Mathez & Waight indicated that this represents the composition of the pre-Merensky parent magma. They ascribe variations within the Merensky pyroxenite to metasomatism by late melt fluids. Sulphides reflect overprinting of different compositions from different unknown sources. The Pb isotopic data agrees with Sr isotopic data that a new influx occurs at the level of the Merensky Reef, but variations in the Merensky pyroxenite can be explained by co-accumulation of minerals from separate magmas, rather than metasomatism. The mineral disequilibrium described in this study does not support later alteration by fluids as chemical differences in the minerals are observed, rather than in whole layers or areas within the rock.

8.3.5 Crystal settling

Hatton (1989) suggested that the Merensky pyroxenite formed from Lower Zone magma that was displaced upward by the intrusion of the Main Zone magma that intruded along the base of the magma chamber. He envisaged crystallisation of B1 orthopyroxenes that increased the density of the package so that it slumped to the chamber floor to form the Merensky pyroxenite. The settling of B1 orthopyroxenes would then decrease the density of the B1 liquid, now at the base of the chamber, whereupon it would rise and mix with the Main Zone magma. Hatton attempted to explain the formation of the Bastard pyroxenite by suggesting that not all B1 orthopyroxenes slumped down with the B1 liquid and that orthopyroxenes could accumulate in sufficiently high proportions to cause a later episode of slumping from the magma at the top of the chamber and form the Bastard pyroxenite. It is significant that this study agrees with Hatton in that

orthopyroxene in the Merensky and Bastard pyroxenites formed from Critical Zone magma, but the model presented here does not support the presence of a geochemcially different Lower Zone liquid at this level, nor does it support movement of a liquid due to density changes.

Kruger (1992) proposed that the Merensky pyroxenite was formed as the result of the intrusion of a cool, dense magma. He suggests that this magma either rose into the resident (Critical Zone) magma as a fountain, or flowed along the interface between the resident liquid and the crystal pile. This new magma then thermally equilibrated with its surroundings, becoming superheated, allowing disaggregated plagioclase crystals from the underlying cumulates to become entrained and float to the upper part of the new magma layer. This model also called for remnant Critical Zone liquid to be pushed up above the new influx. Kruger envisaged orthopyroxene crystals, sulphide liquid droplets and blobs of crystal-liquid slurry from the overlying Critical Zone liquid sinking through the new influx to form the base of the Merensky Cyclic Unit. In situ crystallisation of the new magma formed the upper part of the cyclic unit. Kruger also proposed that the Bastard Cyclic Unit formed in a similar way from a second influx of Main Zone magma.

The model presented in this study clearly supports numerous aspects of the Kruger (1992) model. The influx of Main Zone magma along the crystal-pile/liquid interface and the elevation of the Critical Zone liquid is in line with the data presented here. Crystal settling through the new magma is also supported by the data from this study. However, it has been shown in this study that magma mixing need not have taken place between the new and resident magmas. A second influx to form the Bastard Cyclic Unit is not required. The minimal decrease in Mg# and An# (Figures 5.10 and 5.15) across the Merensky to Bastard interval that suggests little fractional crystallisation, indicates that the influx of Main Zone magma was much thicker than Kruger postulates. In addition, further constraints have been placed on the process of crystal settling though a magma, whereby cumulus plagioclase is envisaged to have settled from the Critical Zone liquid, rather than forming from interstitial liquid as part of droplets of slurry.

8.3.6 Plagioclase suspension

It is proposed here that Sr isotopic information, whereby Sr initial ratios typical of the Critical Zone (table 7.2) are observed above the Merensky pyroxenite, such as the isotopic break observed at the level of the Bastard pyroxenite in RM15, might be explained by the suspension of Critical Zone plagioclase above the Merensky pyroxenite. A possible explanation of this is discussed here, that plagioclase forming in the Critical Zone was taken up by and suspended in Main Zone magma influx. This plagioclase then accumulated within the Main Zone rocks. However, it is shown that this is an unlikely mechanism, as it does not account for other geochemical variations observed.

Cawthorn (2002) proposed that pyroxenites in the Upper Critical Zone are the result of mechanical separation of plagioclase and orthopyroxene from a plagioclase-orthopyroxene-saturated magma. Similarly anorthosites result from the delayed accumulation of plagioclase relative to pyroxene and not from a magma saturated only in plagioclase. Cawthorn ascribed this process to mechanical separation as the result of crystal sorting during settling. This means that plagioclase crystallising at the same time as the orthopyroxene grains that formed the Merensky pyroxenite were held in suspension while the pyroxenite accumulated. Both minerals crystallised at the same time, but appeared in the succession at different levels, with plagioclase accumulating somewhere above the pyroxenite.

In addition, the formation of potholes may play a role in redistributing plagioclase. It has generally been accepted that the input of a new magma at the level of the Merensky pyroxenite was responsible for the formation of potholes that cut across the Merensky pyroxenite footwall. Many theories describing the formation of potholes exist, most involving the removal of footwall anorthosite. Campbell (1986) ascribed potholes to thermal erosion of footwall units by a new, hot magma of a different composition or to the mechanical removal of footwall layers. In the Campbell model the new magma melted the top of the cumulate pile and thermal erosion only ceased when the products of melting become denser than the new magma. If the products of melting were less dense then they would have been swept away and replaced by the denser new magma and erosion continued. Campbell applied this theory to account for differences in thickness of plagioclase cumulates; where plagioclase cumulates are thinner, more thermochemcial erosion

has occurred. Thus he contrasted larger potholes in the northwestern limb and thinner footwall anorthosites (<20 m) with smaller potholes in the southwestern limb to thicker (>100 m) anorthosite footwall. Similarly Kruger (1992) used Campbell's model to propose that a fresh layer of magma intruded at the base of the Merensky Cyclic Unit that became superheated and was responsible for erosion of the footwall. Carr *et al.* (1994) proposed a structural control on the formation of potholes. They indicated the existence of an extensional regime during the emplacement of the Bushveld Complex. Pothole formation was the result of tectonic instability, possibly due to magma loading. They suggested depocentre subsidence and extension resulting in pull-apart ruptures and layer-parallel extension. A new input of magma is identified in both the models of Campbell and Carr *et al*. as the possible initiation for the potholing process, but the Carr *et al*. model does not necessarily require a new magma, just tectonic instability. Potholing created the possibility that plagioclase cumulates from the Merensky footwall, that crystallised from the Critical Zone magma, may be remobilised (Figure 8.3). In this fashion it is possible for anorthosite fragments or remelted material there from to be included at higher levels in the stratigraphy. If there were real, solid fragments in the Merensky and Bastard Cyclic Units an erratic Sr isotope profile, similar to the ones observed in RM15, would be expected, not a smooth trend.

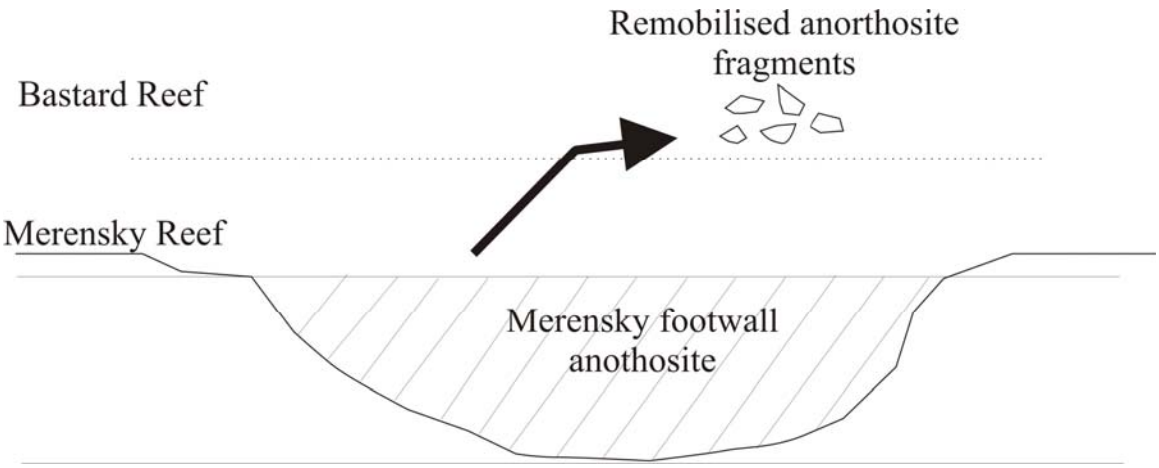


FIGURE 8.3 – Schematic representation of potholing in the Merensky Reef that may contribute to the remobilisation of plagioclase-rich footwall.

If a fresh magma impulse is envisaged entering the chamber at the level of the Merensky pyroxenite, then it is feasible to suppose that suspended plagioclase would be mixed with the new magma. Sr isotope initial ratios in plagioclase from RM15 show Critical Zone values in the Bastard pyroxenite, rocks that are thought to have originated from Main Zone magma. This might suggest that Critical Zone plagioclase is present within the new Main Zone magma. Suspension of plagioclase, by methods suggested by Cawthorn (2002) or as the result of potholing could therefore be responsible for the reversals in Sr isotope ratio observed in the Bastard Cyclic Unit.

The nature of the plagioclase in the Bastard pyroxenite is discussed in section 6.2.3, where it is shown that both interstitial and cumulus plagioclase may be present in varying proportions. If the plagioclase with Sr isotope ratios typical of the Critical Zone is interstitial, then it would indicate that the residual liquid, from which the interstitial plagioclase crystallised, also had Critical Zone values. Thus the magma at this level would have been Critical Zone magma. If all the plagioclase in the Bastard pyroxenite were interstitial, a liquid presence would be implied. However, it has been shown here that cumulus plagioclase is present in the Bastard pyroxenite (section 6.2.3). Sr isotopic signatures of this plagioclase are typical of the Critical Zone and thus it is indicated that Critical Zone plagioclase *grains* are present at the level of the Bastard pyroxenite. This indicates that these grains accumulated at this level, having been transported subsequent to crystallisation.

While the model described in section 8.1 can account for this, by orthopyroxene and plagioclase clusters descending from the elevated Critical Zone liquid, clasts ripped up by potholing from the crystallised Critical Zone beneath may also explain the Sr isotope anomaly. However, the latter model fails to account for the presence of Critical Zone orthopyroxenes in the Bastard pyroxenite. In addition, it would be expected that fragments of Merensky footwall anorthosite would be present in the norites/anorthosites of the Merensky Cyclic Unit and there is little evidence to suggest that this is so.

8.3.7 Fluids

A number of models have been proposed that suggest the Merensky pyroxenite was formed as the result of secondary fluid movement, largely based on investigations of the origins of the associated pegmatite. A number of types of late-stage magmatic fluids have been invoked. Nicholson & Mathez (1991) proposed that the pyroxenite is not cumulate at all, but that it formed in a partially molten cumulate pile by hydration and consequent isothermal melting of an initially melt-rich horizon. This melt then crystallised chromite, norite and anorthosite in the footwall. However, it has been shown here that minerals of the Merensky pyroxenite have clear affinities with either the Critical or Main Zone magmas. Mathez (1995) proposed that elevated REE concentrations of pyroxenes in the Merensky pegmatoid are the result of upward percolation of hydrated silicate melt that reacted with the crystalline cumulate pile. Sometimes pegmatoid does not occur at all in the Merensky Cyclic Unit, e.g. in RM15, so evidence for fluid activity cannot be supported.

Boudreau *et al.* (1997) proposed that layered intrusions containing elevated levels of Cl may have crystallised from magmas containing > 1 wt% water. They suggested that the presence of water would have suppressed the crystallisation of plagioclase, perhaps leading to the development of pyroxenites. Wilson *et al.* (1999) suggested interaction of the primary silicate phases with fluids that modified the minerals in the Merensky pyroxenite from their original liquidus compositions. Boudreau (1999) proposed a hydromagmatic model for the formation of the Olivine-Bearing Zone 1 in the Stillwater Complex, which hosts the PGE-rich J-M pyroxenite.

While these models involve fluids to explain the presence of the Merensky pyroxenite, few of them attempt to explain the presence of the overlying Bastard pyroxenite. In addition, it is hard to explain the disequilibrium between minerals in the same layer as the result of a fluid.

8.4 Variations between profiles

Although it is apparent that geochemical disequilibrium does occur in some layers in the Merensky and Bastard Cyclic Units, it is clear that variations are not consistent along strike (table 7.3). Variations occur within the Merensky pyroxenite. At Amandelbult and Brits, plagioclase in this layer has Main Zone signatures, whereas at other localities, plagioclase has Critical Zone signatures. This implies that at Amandelbult and Brits, the plagioclase is derived from interstitial Main Zone liquid and is not cumulus Critical Zone plagioclase from the suspended liquid. This might occur where plagioclase did not sink with orthopyroxene. Alternatively it could indicate upward infiltration of Critical Zone residual liquid (Eales *et al.* 1986) was not significant enough to alter the Main Zone signature.

Variations of signatures in the Merensky norite/anorthosite are the result of different amounts of minerals accumulating from the elevated Critical Zone liquid. At most locations, plagioclase accumulated predominantly from the Main Zone, but at Atok and Richmond, some plagioclase accumulated from the Critical Zone liquid, possibly sinking with orthopyroxene.

Distinct variations occur in the Bastard pyroxenite where plagioclase has Main Zone signatures at Rustenburg, Amandelbult and Union, but has Critical Zone signatures at Richmond and Atok. Where there is Critical Zone plagioclase, it is inferred to have sunk through the Main Zone liquid, possibly as clusters with orthopyroxene (Kruger 1992) to accumulate in the pyroxenite (section 6.2.3). It is suggested that where there is Main Zone plagioclase in the pyroxenite, less cumulus plagioclase is present and that the majority of the plagioclase is interstitial. In all profiles studied, orthopyroxene has Critical Zone signatures in the Bastard pyroxenite implying accumulation from an elevated Critical Zone liquid throughout the Bushveld Complex. In the Bastard norite and anorthosites, most locations have Critical Zone orthopyroxene, which accumulated from the elevated Critical Zone liquid. However, at Impala and Richmond, some Main Zone orthopyroxene occurs in the norites. This suggests that at these localities, orthopyroxene was not accumulating from the Critical Zone liquid, and that the Main Zone was crystallising orthopyroxene. Either the Critical Zone liquid had stopped crystallising orthopyroxene, or it was no longer sinking through the Main Zone liquid.

8.5 Summary

The data presented here places further constraints on the crystal settling model described by Kruger (1992). In this model, he envisaged an influx of a dense, cooler Main Zone magma at the level of the Merensky pyroxenite that pushed up the residual Critical Zone liquid. This is also supported by this study. In both models, orthopyroxenes crystallise in the elevated Critical Zone liquid then settle through the Main Zone influx to form the Merensky pyroxenite, creating the geochemical disequilibrium observed between orthopyroxene and plagioclase is some of the layers. This study confirms that orthopyroxenes in the Merensky and Bastard pyroxenites did originate from a Critical Zone magma and suggests that a second Main Zone influx (Kruger 1992) is not necessary in order to form the Bastard Cyclic Unit. Other models that attempt to explain geochemical variations observed at the Critical/Main Zone boundary and the Merensky Cyclic Unit cannot account for the geochemical disequilibrium observed in this study. This study does not support wholesale magma mixing.

Chapter 9

The origin of PGE in the Merensky Reef

Although PGE were not specifically investigated in this study, any model dealing with the formation of PGE-rich layers, such as the Merensky Reef, must consider the implications for PGE concentration. The origin of PGE mineralisation in the Bushveld Complex remains a point of discussion, centred on issues concerning the concentration of a minor element in the magma into an economic layer. In order to assess the implications the model in section 8.1 has for PGE mineralisation, methods of concentration of PGE must be discussed. Potential mechanisms for concentration of PGE are discussed in Campbell *et al.* (1983), Naldrett *et al.* (1986), Lee (1996), Cawthorn (1999b), Barnes & Maier (2002) and Cawthorn *et al.* (2002), and can be generally divided into three broad categories discussed below.

9.1 PGE concentration in an immiscible sulphide liquid

Mafic-ultramafic magmas are reduced magmatic systems, so, where present, excess S occurs as an immiscible sulphide liquid (e.g. Naldrett 1989) when sulphur-saturation is achieved in the magma. PGE (and Cu and Ni) readily partition into the immiscible sulphide liquid.

9.1.1 The partitioning of PGE and the Merensky Reef

Chalcophile elements fractionate according to their sulphide liquid-silicate melt partition coefficients, that is, the partitioning of elements between two phases in equilibrium, and is usually considered in terms of the Nernst distribution coefficient (D):

D_i for a metal *i*:

$$D_i^{(sul.melt/sil.magma)} = \text{wt\% of metal } i \text{ in sulphide melt / wt\% of metal } i \text{ in silicate melt}$$

Metals with high partition coefficients into sulphides will readily enter the immiscible sulphide liquid. Experimental work shows that partition coefficients for PGE into sulphides range from 10^2 to 10^6 (Stone *et*

al. 1990, Crocket *et al.* 1992, Bezman *et al*. 1994, Peach *et al*. 1994, Fleet *et al.* 1999). Depending on the amount of sulphide formed, the silicate liquid should become more depleted in highly chalcophile elements such as PGE ($D_{sil/sul}$ <10,000) relative to moderately chalcophile elements such as Cu and Ni ($D_{sil/sul}$ <1000).

The PGE-rich Merensky Reef is sulphide-poor (not more than 3 wt% disseminated sulphide). Vermaak (1976) gives values for Ni, Cu and S as 2377, 1115 and 5528 ppm respectively for the Merensky Reef, which convert to a sulphide fraction of 4.6% Cu and 10.9% Ni (Naldrett 1981). Compared to other PGE-bearing deposits, such as Sudbury, the Merensky Reef is anomalously enriched in Pt and Pd. The Merensky Reef is enriched in PGE, but not Cu and Ni. Correlation between sulphide and PGE values in the Bushveld Complex (Li *et al*. 2001a) indicates that sulphides are the collector for metals, although the exact collection mechanism remains in dispute. Models for PGE concentration in the Merensky Reef must therefore take into account the preferential enrichment of PGE over Cu and Ni.

The degree of interaction between the silicate melt and immiscible sulphide liquid can be quantified using the "R"-factor. The R-factor is the ratio of the mass of silicate to the mass of sulphide liquid. Calculations involving R assume that there is always complete equilibrium between sulphide and silicate liquids. High R-factors are the result of small amounts of sulphide liquid present in the magma system and consequently low R-factors result from increasing sulphide component. R-factors for typical reef-type PGE deposits such as the Merensky Reef are estimated to be higher than 105 (Li *et al.* 2001), whereas estimated R-factors for Ni-Cu-(PGE) deposits are as low as a few hundred (Naldrett 1989).

Modelling the Merensky and UG2 orebodies using methods described above, requires extremely high D values for PGE into the Merensky sulphides and an associated mass balance problem. This problem is based on the need of the sulphides to have equilibrated with a large amount of magma, at least 10^5 to 10^6 times their own mass, to produce high R-factors. Aggregation by shearing in convecting boundary layers has been proposed as a mechanism for creating high R-factors (Rice & von Gruenewaldt 1995).

9.1.2 Sulphur-saturation models

An immiscible sulphide liquid that can potentially concentrate PGE only forms once the silicate magma becomes saturated in sulphur. Sulphur-saturation can be triggered by a number of mechanisms: a) fractionation (e.g. Andersen *et al*. 1998, Miller & Andersen 2002), b) changing temperature and pressure (Haughton *et al.* 1974), c) magma mixing (Li *et al.* 2001a), and d) addition of S or crustal material (e.g. Ripley 1986, Naldrett 1989, 1999).

Magma mixing is commonly suggested as the mechanism for S liquid immiscibility at the level of the Merensky Reef (e.g. Naldrett & von Gruenewaldt 1989, Li *et al.* 2001a), whereby a sulphur-undersaturated magma mixes with a primitive magma in appropriate amounts to achieve sulphur-oversaturation in the resulting hybrid magma. Campbell *et al*. (1983) proposed that the high PGE content of the sulphides is related to a high magma to sulphide ratio during sulphide liquid separation and resulting high R-factors due to turbulent magma mixing. Naldrett *et al.* (1986) used density differences between a resident magma and a new influx to create a high R-factor at the time of formation of the Reef. Later density changes due to cooling of the new hybrid magma result in the crystallisation of the overlying Merensky Cyclic Unit, creating a less primitive hybrid, which crystallises orthopyroxene, followed by orthopyroxene plus plagioclase. Episodic triggering of S-saturation due to repeated replenishment of a differentiating magma chamber has been suggested by Scoon & Teigler (1994). However, Cawthorn *et al*. (2002) suggest that this model of magma mixing might be inaccurate, by demonstrating that the mixed magmas have greater sulphur solubility than the fractionated magmas and thus the mixed product is not sulphur-saturated.

Contamination by crustal rocks has been suggested to initiate sulphide saturation in numerous large magmatic Ni-Cu-(PGE) sulphide deposits. Sulphur-saturation can occur by assimilation of siliceous partial melts of country rocks, which lowers the S solubility of the magma (Irvine 1975), or by partial melting or bulk assimilation of S-rich country rock (Ripley & Alawi 1988). Sulphur-saturation can also occur due to addition of external S through devolatilisation (Buchanan & Nolan 1979). An increase in oxygen fugacity, which leads to a lowering of FeO content, decreases the sulphur carrying capacity of the magma (Elliot *et*

al. 1982), which will also lead to sulphur saturation. However, Maier *et al*. (2002) concluded that crustal contamination at depth did not trigger sulphur segregation in the Bushveld Complex. They suggested that parental magmas to the Complex show S-undersaturation, which is related to an S-poor mantle source, based on the high PGE and S-content of Bushveld sills.

The presence of sulphides in the Merensky Cyclic Units indicates that sulphide-saturation must have occurred, but it remains unclear as to which magma was saturated and the mechanism that induced the saturation.

9.1.3 S, Cu and Ni in the Merensky unit at Richmond and Kennedy's Vale

In this study, sulphur content was determined from samples, of 20 cm length, in the Merensky Reef at Richmond and Kennedy's Vale. Whole-rock Cu should reflect the proportion of sulphide present in the rock as all the Cu present is likely to be in sulphides. However, Ni also partitions into olivine and orthopyroxene. The presence of olivine is negligible in the studied cores and thus its effect on Ni content of the rocks is ignored. However, Ni does occur in significant amounts in the orthopyroxene cumulates at both Richmond and Kennedy's Vale, averaging approximately 200 ppm Ni in sulphur-free Critical Zone norite samples. Since the rocks essentially comprise orthopyroxene and plagioclase, the proportion of MgO can be taken to represent the orthopyroxene component. Thus, to calculate the amount of excess Ni contained within the sulphide component, Ni/MgO must be subtracted from the whole-rock Ni value. The average Ni/MgO ratio for sulphide-free footwall and hangingwall rocks is approximately 20 at Richmond. This is demonstrated in Figure 9.1, where extending the trend indicates that pure orthopyroxene, containing 30% MgO, would have about 600 ppm Ni. Analyses from Richmond show that orthopyroxene separates with 28 – 29% MgO contain approximately 690 ppm Ni on average.

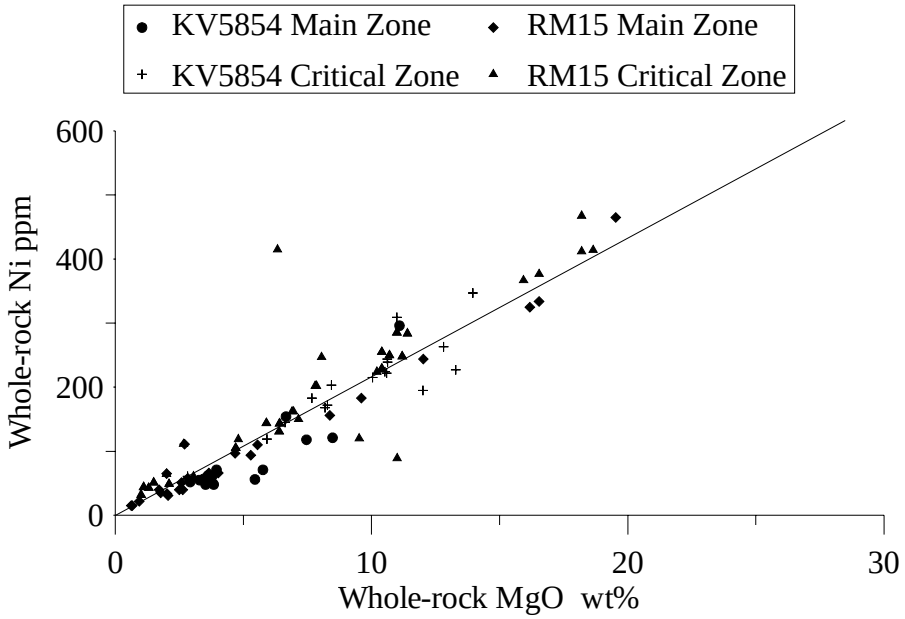


FIGURE 9.1 Plot of whole-rock MgO *versus* Ni, showing positive correlation and Ni/MgO ratio of approximately 23 at 600 ppm Ni and 30 wt% MgO.

Rocks containing only plagioclase and orthopyroxene would have a Ni/MgO ratio of 23, which is similar to that observed at Impala by Cawthorn (1999a). Actual mineral data (Figure 9.2) show that orthopyroxene separates from this study have an average Ni/MgO ratio of approximately 23 in the Critical Zone, but Main Zone hangingwall rocks have a lower average ratio of approximately 20. Since the orthopyroxene in the Merensky pyroxenite in core RM15 is derived from Critical Zone magma, 23*MgO will be used in the correction calculations. Low Ni content of some whole-rock samples results in negative values in these samples, after the correction factor has been applied. In sulphide-rich samples negative values are not likely to occur as the Ni content of these samples are generally >1000 ppm Ni.

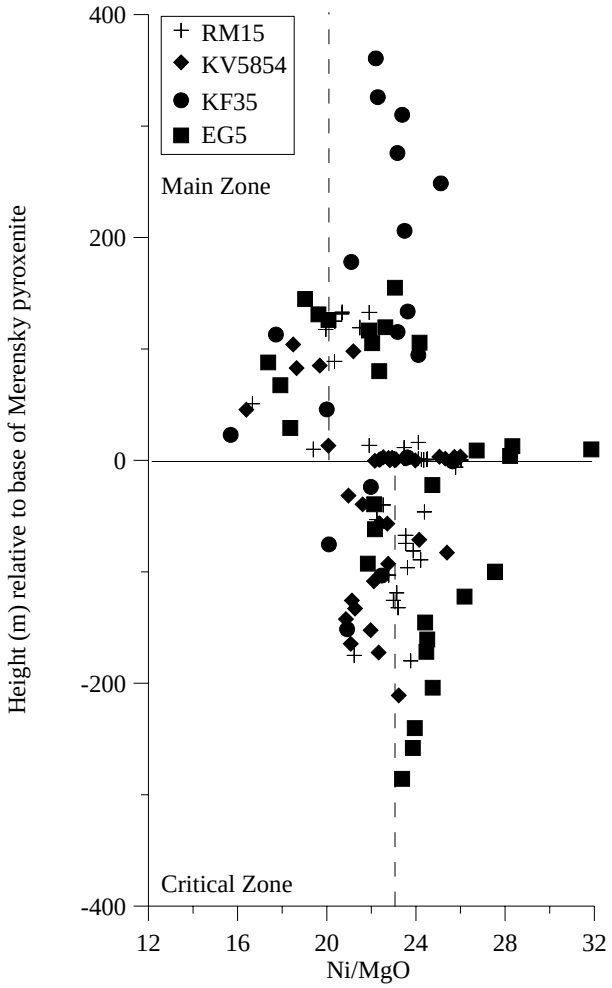


FIGURE 9.2 Plot of Ni/MgO in orthopyroxene plotted against height, showing that the average value is higher in the Critical Zone than the Main Zone.

Sulphur, Cu and corrected Ni values from the Merensky pyroxenite are combined in Figure 5.22. In general, there are two sulphur peaks in the Merensky pyroxenite of RM15. These peaks correlate well with Cu and Ni peaks in RM15, which indicates that both Cu and Ni partition into an immiscible sulphide liquid. In KV5854 however, peaks are not coincident, with S peaks occurring one sample above the peaks in Cu and Ni. This might suggest that some local remobilisation of sulphides has taken place on a 20 cm scale. In addition, peaks in S, Cu and Ni may correspond to peaks in PGE content, as noted in the western Bushveld where coincident PGE and S peaks occur at the base and towards the top of the Merensky pyroxenite (e.g. Viljoen *et al.* 1986b, Mossom 1986). Although no PGE data were determined for RM15 and KV5854, it is

observed that PGE peaks coincide with the sulphur peaks (G. Chunnett *pers. comm.* 2004). This correlation of S, Cu, Ni (and PGE) supports the theory that these elements are preferentially partitioned into an immiscible sulphide liquid.

At Richmond, it may be possible to divide the profile into three sections, delineated by S content. At the bottom of the pyroxenite is a single sample with high S content, overlying this is a series of relatively S-poor samples and an upper section of higher S content. With only a single core, it is not possible to determine if these sections can be correlated as a continuous horizon. In the Kennedy's Vale profile, sections are less defined, with a lower section of low S content and an upper section of elevated S content, with S-poor samples between.

Concentration of PGE in an immiscible sulphide liquid relies on the magma becoming S-saturated and mechanisms that can achieve this were examined in section 9.1.2. Figure 9.3 shows Cu, Ni and S ratios of sulphide-rich samples from Richmond. If sulphides in the Merensky Reef are simply the accumulation of an immiscible sulphide liquid, into which Cu and Ni have partitioned, then the S:Ni:Cu ratios might be expected to plot at the diamond in Figure 9.3. The diamond represents a calculated magmatic composition based on the magma at the level of the Merensky Reef containing 10% Ni (Naldrett 1989), 5% Cu and 30% S (Cawthorn 1999b), which indicates that any sulphide assemblage formed from an immiscible sulphide liquid should have S:Ni:Cu ratios of around 6:2:1. Samples from Kennedy's Vale contained too little sulphur to plot accurately. The Richmond sulphides plot close to the ideal magmatic sulphide. At other locations in the Bushveld Complex, e.g. Impala (Holwell 2002) S:Ni:Cu ratios are also observed to be that of the ideal magmatic sulphide, indicating that sulphides in the Reef are of magmatic origin. But at Winnarshoek, slight depletion in S and slight enrichment in Cu was observed, which may indicate interaction with a hydrothermal fluid subsequent to deposition from an immiscible sulphide liquid, which resulted in desulphidation and mobilisation of Cu (Holwell 2002).

However, there is discussion as to whether sulphide-saturation occurred at all. Maier *et al.* (1996) and Cawthorn (1999a) recorded that the Cu concentrations in the Merensky Reef hangingwall rocks were only half that expected for rocks accumulating from a sulphide-saturated magma. This suggests that

sulphide-saturation may not have occurred and was not the method that concentrated PGE in the Merensky Reef. Hoatson & Keays (1989) suggested an average S content in rocks containing intercumulus sulphide of 400 ppm (0.04%). This is very similar to the average S content of the Merensky pyroxenite in KF35, but in RM15 average S content is much higher, suggesting that sulphides in the pyroxenite are cumulus. This might indicate that sulphides (and possibly PGE) in the Merensky Reef did accumulate from and immiscible sulphide liquid formed from a S-saturated magma.

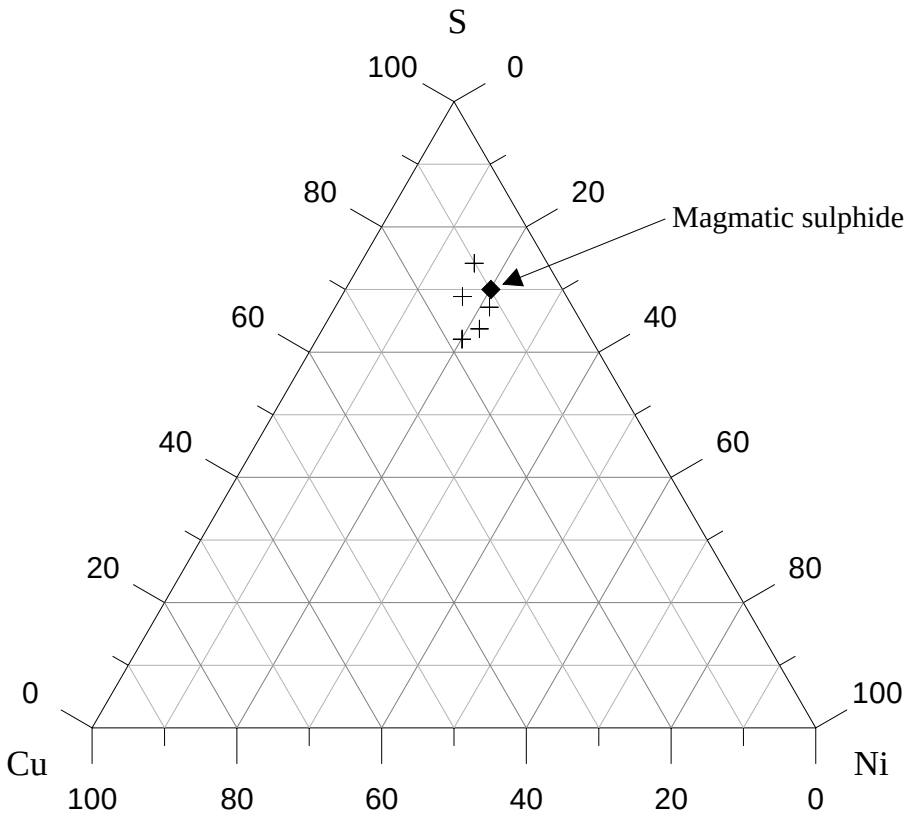


FIGURE 9.3 Ternary diagram of Cu, Ni and S ratios of sulphide-rich samples from the Merensky Reef at Richmond, showing that sulphides in RM15 plot close to the ideal composition of a magmatic sulphide.

In addition, it has been suggested that a significant volume S-saturated magma (as required by the R factor model) was not present above the Merensky Reef (Cawthorn 1999a), from which an immiscible sulphide liquid would have accumulated and scavenged PGE to mineralise the Merensky Reef. Cawthorn (1999a) suggested that if less cumulus sulphide occurred, then the residual silicate liquid would have *increased* in S content with fractionation, rather than *decreased*. Using data from Lee (1983) he showed that S contents

decrease in the Merensky hangingwall. Data from this study (Figure 5.22) support the observations of Cawthorn (1999a) that S decreases in the hangingwall to the Merensky pyroxenite and thus there was not a large volume of S-saturated magma overlying the Merensky Reef. This indicates that large volumes of S-saturated magma may not have existed. Nevertheless, Li *et al*. (2001a) maintained that once immiscible sulphides settle out of a mix of fractionated sulphide-undersaturated magma and primitive over-saturated magma, sulphide in the hybrid may remain dissolved in the magma and thus no sulphide segregation would be observed in the hangingwall rocks. Although if the magma was S-saturated, then immiscible sulphide liquid must have separated.

In addition, a magma mixing model, where an evolved, S-saturated magma resident in the chamber mixes with a new magma, requires sulphide saturation of footwall rocks to the Merensky Reef (Cawthorn 1999a). Figure 5.22 shows that the footwall anorthosite of the Merensky pyroxenite in RM15 has 6.6 ppm S, which is much lower than the average S content of the overlying pyroxenite. Thus, sulphide concentration in the footwall is not elevated, as it would be if these rocks formed from a S-saturated magma, which indicates that the evolved magma was sulphide-undersaturated. This also indicates that S-saturation did not occur at the level of the Merensky Reef. However, it has been suggested that S was partially dissolved by percolating intercumulus fluids (Willmore *et al.* 2000).

There is conflicting information as to whether the sulphide and PGE concentration in the Merensky Reef is the result of sulphide saturation of the magma. S, Cu and Ni data from this study indicate that these elements originated as an immiscible sulphide liquid. Nevertheless, if sulphide saturation was responsible for sulphide and PGE concentration, the mechanism that initiated saturation at that level remains unclear. It is possible that an immiscible sulphide liquid formed from a different magma at some level above the Merensky Reef and that PGE-enriched sulphides sank and collected at the level of the Merensky Reef. In this scenario, neither the Merensky footwall nor hangingwall rocks would indicate sulphur-saturation, but the S:Ni:Cu ratios *would* be that of an immiscible sulphide liquid, as is observed at Richmond. Where this magma was or how is became sulphur-saturated is unknown.

9.2 PGE concentration by fluids

A second type of model involves the migration of fluids that collect and concentrate PGE at a specific horizon. Late-magmatic fluids have been invoked to explain features of the Merensky Reef than cannot be simply explained by magmatic processes. Such features include the coarse-grained nature of the Reef in some areas (Barnes & Campbell 1988), the intergrowth of sulphides with late intercumulus minerals (phlogopite, amphiboles and apatite) (Ballhaus & Stumpfl 1986, Boudreau *et al*. 1986), high Cl/F ratios (Boudreau *et al*. 1986, Boudreau 2002) and sulphides associated with hydrous silicates, deuteritic alteration and aqueous fluid inclusions (Ballhaus & Stumpfl 1986). Other evidence suggests remobilisation of BMS and PGE by hydrothermal fluids in the J-M Reef, Stillwater deposit (Polovina & Hudson 2002). Single or combinations of these features have led numerous authors to suggest the presence of fluids at the level of the Merensky Reef and propose that these fluids played an intrinsic role in concentrating PGE.

Vermaak (1976) proposed the possibility that hydrothermal fluids may have concentrated PGE in the Merensky Reef. Boudreau *et al.* (1986), Ballhaus & Stumpfl (1985, 1986) and Boudreau & McCallum (1992) suggested a hydrothermal origin for Pt and Pd in the Merensky Reef. Nicholson & Mathez (1991) proposed transport of PGE in, and subsequent deposition from, a vapour that initiated hydration and melting. Mathez (1995) described decoupling of incompatible elements and suggested that metasomatic processes, which involved the upward percolation of hydrated silicate melt through, and its reaction with, the crystalline cumulate pile, was responsible for PGE enrichment in the Merensky Reef. Similarly, Mathez *et al.* (1997) discuss the upward infiltration of a residual magma. Boudreau & McCallum (1992) and Boudreau & Meurer (1999) proposed that PGE were collected and moved upwards by migrating sulphide enrichment-resorption fronts, which comprised Cl-rich fluids that exsolved from the intercumulus fluid. Boudreau (2002) proposed that separation of a volatile-rich fluid phase from interstitial liquids could transport PGE. The mechanisms for precipitation of the PGE at the level of the Reef are unclear, but centre on physical or chemical changes in the magma, such as vapour undersaturation of the magma, oxygen fugacity, sulphur fugacity, or fluid cooling (e.g. Elliot *et al.* 1982, Ballhaus & Stumpfl 1986). Hanley *et al.* (2004) analysed fluid inclusions from below the J-M Reef in the Stillwater Complex and found that some

brines yielded 0.4-4 ppm Pt and had high Cu/Pd ratios. They suggested that their studies support models of interaction of magmatic volatiles with cumulate rocks in layered intrusions to concentrate significant amounts of Cu, Pt, Bi, Ag and other metals while modifying primary silicate and sulphide compositions.

While the models described above may support the theory that fluids were responsible for concentrating PGE in the Merensky Reef, some authors have raised doubts. Barnes & Campbell (1988) argued that magmatic processes could explain most features that suggest the presence and movement of fluids. They proposed that the Merensky pegmatoid and associated volatile-bearing silicates originated from interaction between orthocumulate layers and late-magmatic fluids and that sulphides crystallised with the last of vapour-saturated intercumulus silicate melt, which led to intergrowth with amphibole and phlogopite. Thus, PGE were already present in the rock before late-stage fluid activity and although hydrothermal processes may have remobilised it to a limited extent, fluids were not responsible for their concentration. Barnes & Campbell (1988) maintained that evidence for deuteritic/hydrothermal activity is consistent with a magmatic model, interpreted as superimposed postcumulus processes. Cawthorn (1999a) pointed out that fluid models suggest that PGE and S were scavenged from the footwall to the Reef, rather than originating in an overlying magma. This creates a scenario wherein PGE and S must have been present in considerable concentrations in the footwall sequence in order for it to become dissolved and consequently transported to the Reef. In order for S to be dissolved, the percolating residual liquid would have had to have been S-undersaturated. This means that the magma would have gone from being saturated, in order to precipitate the sulphide, and then become unsaturated in order to redissolve it. One way magma can become S-undersaturated is if there had been significant iron enrichment in the magma. Cawthorn (1996b) showed that there is no evidence for this in the Merensky footwall and concluded that it is unlikely the magma became S-undersaturated after being S-oversaturated. He also concluded that the proportions of BMS in the Merensky Reef are exactly that which would be expected for an immiscible magmatic sulphide forming from a basic magma, supported in this study (section 9.1.3), which strongly indicates that sulphide composition of the Reef has not been significantly altered by migrating fluids. In addition, Cawthorn

(1999a) pointed out that the Sr isotopic break at this level would have been overprinted or moved upwards if fluids were passing through. He also noted that the Platreef occurs along the floor of the intrusion, and thus does not allow for upward migrating fluids to have concentrated the PGE. Schoenberg *et al.* (1999) suggested that similar Os-isotopes signatures in interstitial minerals and PGE-bearing cumulus chromite grains from the Merensky Reef indicate that they scavenged their Os from the same or similar sources. They concluded that PGE enrichment of interstitial sulphides in the Merensky Reef was by a primary magmatic process and considered their data not to support transport of PGE by a fluid or melt. Barnes & Maier (2002) did not support PGE transport in fluids because the rocks underlying the Reef are not depleted in PGE, whereas those overlying the Reef are, pointing out that this distribution pattern is inconsistent with a model that requires introduction of PGE by intercumulus fluid percolation from below. They also did not find high proportions of late-stage components that would support a high fluid content in the Reef. However, whole-rock incompatible trace element data from RM15 show an increase in the Merensky Reef that corresponds with the presence of sulphides (Figure 9.4a). This trend is observed in V, Y, TiO_2 and Zr (although, for simplicity, only Zr is shown in Figure 9.4). When Zr is compared to sulphur (Figure 9.4b) through the reef, peaks in one do not seem to correspond to peaks in the other. Nevertheless some relationship is apparent in which peaks in trace elements are offset to peaks in S. This is most apparent in the two uppermost S peaks where the samples immediately above these peaks show peaks in trace elements. A peak in trace elements occurs immediately below the lowest peak in S. While these observations do not prove that S was concentrated by a late-stage fluid, it does suggest that there might be some relationship between S and late-stage elements, possibly related to later remobilisation by fluids.

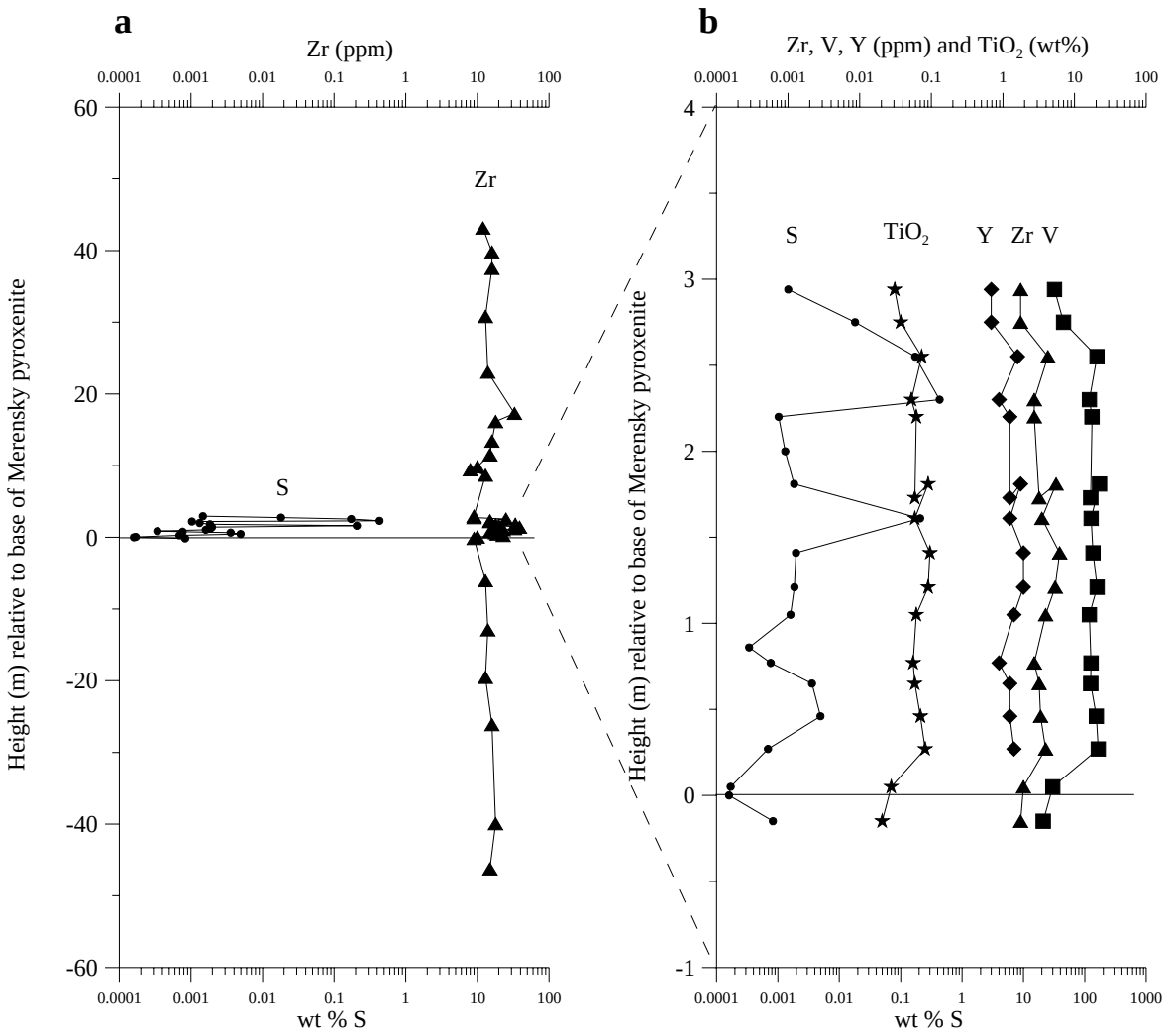


FIGURE 9.4 Data from RM15 a) S and Zr plotted against stratigraphic height, showing an increase in both these elements at the level of the Merensky Reef and b) S, Zr, Y, V and TiO_2 plotted against stratigraphic height through the Merensky Reef showing corresponding increases of these elements.

McCandless *et al*. (1999) refute PGE concentration by fluid movement, by showing the presence of PGE in chromite grains (assumed to be shielded from later processes) and inter-granular PGE in the UG2 were formed as part of the same process and unaffected by later hydrothermal fluids. In addition, Cawthorn *et al.* (2002) suggested that if chromatographic extraction (Boudreau & Meurer 1999) had occurred, PGE should have become vertically segregated as a result of different partition coefficients between sulphide and vapour. They determined, using detailed studies of Lee (1983) and Barnes & Maier (2002), that PGE do not show separation.

9.3 PGE as discrete grains

A third method that might concentrate PGE in the Merensky Reef is the process of mechanical accumulation of PGE nuclei or clusters. Tredoux *et al.* (1995) proposed a mechanical association between PGE and sulphides (and chromite), rather than a chemical one. They suggested that PGE are present in a melt initially as metallic clusters, not as single atoms or molecules, and that distribution between phases in a magmatic system does not have to depend on partitioning behaviour. This would negate the need for excessively high D values and R factors required in sulphur saturation models. This could also explain why the Cu:Ni:S ratio remains that of a magmatic sulphide. Hiemstra (1985) and Kruger *et al*. (2002) suggested that chromite grains collect PGE clusters and Merkle (1992) suggested adherence to silicate minerals as well. Finnigan & Brenan (2004) suggested that a local reduction zone around chromite grains acts to precipitate PGE alloys from a magma that is near PGE saturation. Cawthorn (1999a) proposed that PGE clusters might adhere to stable species, allowing them to accumulate at the base of the chamber to form PGE-rich layers such as the UG2 and the Merensky Reef. Cawthorn also suggested that PGE may be present as clusters in a magma chamber all the time and accumulate constantly, but are effectively diluted by the presence of large quantities of silicates. He proposed that the PGE concentration in the Merensky Reef is the result of a break in silicate crystallisation that allowed the PGE clusters to accumulate at the unconformity, having been collected by sulphides (or chromite).

Ballhaus & Sylvester (2000) suggest early-magmatic PGE saturation at liquidus temperature before sulphide saturation occurred. This led to PGM crystallising as metallic nuggets, some of which were preserved as micro-inclusions in early cumulus phases. Sulphide melt then “immobilized” the pre-existing stratiform PGE concentration. They stated, however, that irregular distribution of PGE in the sulphides in the Merensky Reef might mean that the presence of sulphides is not essential to preserve a PGE-enriched layer. Mungall (2002) proposed the development of micronuggets of PGM, specifically laurite, to explain the PGE association with chromite in magmas that do not show other evidence of being saturated with PGM. The weakness of this model is that it requires the magma to become saturated with PGM when it contains very low levels of these elements (1-10ppb) (Barnes & Maier 2002). Barnes & Maier (2002) also

proposed that PGM precipitated straight from a mixed magma rather than entering immiscible sulphides first. The magma then became S-saturated and the sulphides incorporated any clusters they encountered, becoming PGE-rich. These sulphides settled through the magma onto the crystal mush to form the PGE anomaly observed in the Merensky Reef

The existence of PGE clusters has been questioned (Mathez 1999). Barnes & Maier (2002) pointed out that the Lower Zone and much of the Critical Zone contain some cumulate sulphide. Experimental work suggests that a sulphide liquid would dissolve all the PGE in the magma and that it would not be possible to crystallise PGM from magma at the same time as segregating sulphide liquid. Thus, if PGM clusters do form, any cumulus sulphide present in the rock would have to have been somehow added to the rock after the formation of the PGM, or the PGE would have been segregated into the sulphide liquid.

There are problems associated with each of these models and consensus has yet to be reached. It is likely that PGE concentration is the result of a combination of these methods that may be active at different times. For example, Barnes and Maier (2002) argued that the distribution of PGE in the Merensky Reef does not relate to either accumulation in a sulphide liquid, or as discrete PGM. They suggest both processes must have occurred simultaneously, but in order to give the consistent PGE values observed throughout the deposit, these processes would had to have started and ended at the same time and each mechanism must have had the same influence throughout the whole chamber.

9.4 The source of the PGE

In the discussion above, numerous models invoke the mixing, or at least interaction, of two magmas to explain the PGE mineralisation in the Merensky Reef. However, it is often unclear in which magma the PGE originated. In general, the source of PGE is not often specifically mentioned and it seems to be assumed that sufficient PGE was present in whichever magma was present that the time of reef formation.

Models that invoke the scavenging of PGE by upward migrating fluids indicate that the magma that formed the footwall cumulates provided the source for the PGE.

Naldrett *et al.* (1986) indicated that PGE-rich sulphides must have accumulated from a large body of magma overlying the Reef i.e. a mixed Critical/Main Zone magma. Hatton (1989) emphasised that the B1 (Lower Zone) magma was likely to provide the source of PGE, rejecting the Main Zone magma because of its apparent low Pt content, based on low background Pt in Main Zone cumulates. But this is an invalid argument as high R factors can be invoked in order to efficiently concentrate any quantity of PGE. Kruger (1992) suggested that PGE were scavenged from an elevated Critical Zone liquid (similar to that described in the model here) by sulphide droplets that then sank through the Main Zone influx to accumulate in the Merensky Reef. Viljoen (1999) suggested that the new influx of magma at the level of the Merensky Reef brought in much of the PGE and BMS mineralisation. Mathez & Waight (2003) used Pb isotopic evidence to determine that sulphides in the Merensky Reef have much higher ratios than Main Zone sulphides. They suggested that this indicates that PGE-rich sulphides of the Merensky Reef did not accumulate from a large body of overlying magma, and thus the PGE source was not the Main Zone magma. However, they do point out that sulphides probably re-equilibrated at lower temperatures and that a percolating interstitial fluid probably imposed their S and Pb isotopes, but did not change PGE compositions. It should be considered however, that the Pb and PGE might have come from different sources.

Some authors have proposed that the source of the PGE was the Main Zone magma. Kruger (*in press*) suggested that the Main Zone magma entered the chamber to the north of the TML and that it interacted with S-rich black shales (Duitschland Formation) of the floor rocks, thus capturing Ni, Cu and PGE from the Main Zone magma and forming the Platreef. Kruger (*in press*) also inferred that the Merensky Reef got its PGE and sulphide from the Main Zone influx, once it had interacted with sediments. McDonald *et al.* (2004) suggested an injection of a new magma that had not been depleted in PGE was responsible for mineralisation in the Platreef and McDonald *et al*. (*in press*) interpreted this mineralisation to be the result of interaction between Lower Zone and Main Zone magmas.

In addition, it has been suggested that PGE concentration in the Merensky Reef is not the result of a PGE-rich magma, but that certain processes or some other feature of the magma resulted in PGE concentration. De Wit & Kruger (1990) stated that two processes are required for a Merensky-type deposit. These are an abrupt mixing event, in which there is a hiatus in crystallisation, and exsolution and deposition of a small amount of PGE-rich sulphides within a short crystallisation interval. Candless *et al.* (1999) suggested that a more contaminated magma might have increased levels of volatiles, sulphur or another component that is necessary for PGE precipitation to occur. Eales *et al.* (1993) concluded that processes active within the chamber, rather than the intrinsic properties of the liquids emplaced within it, are more significant for the occurrence of PGE mineralisation. Thus, it is possible that not one specific magma provided the source for the PGE, but that a specific event occurred that led to the concentration of PGE and that it may have occurred regardless of the magma or magmas involved.

9.5 The crystal settling model and its implications for PGE mineralisation

The model presented here (section 8.1) concentrates on the formation and genesis of the Merensky and Bastard Cyclic Units, the base of which hosts the bulk of the PGE mineralisation in the Merensky Reef. Although PGE and sulphide mineralisation was not specifically investigated in this study, any model dealing with the formation of layers, such as the Merensky Reef, must consider the implications for PGE mineralization.

Figure 9.5a shows PGE content in the Merensky Reef plotted against height for core RM15. This diagram shows that there are two peaks in PGE content through the profile, one associated with chromite and an upper peak associated with sulphides. This is apparent when PGE content is plotted against Cu (Figure 9.5b) where the positive correlation with Cu represents the PGE relationship with sulphide and the second trend, at low Cu values represents the association of PGE with chromite. A third group of points plots at elevated Cu values and is not associated with either trend. These points may be equivalent to elevated Cu values observed by Maier & Barnes (2002) at the top of the Merensky Reef. The other two

trends suggest that there were two separate mineralising events that contributed to the total PGE content of the Merensky Reef, one associated with the formation of the chromitite layer and a second associated with sulphide mineralisation. This feature suggests more than one factor contributed to the total PGE content of the Reef and that total mineralization was not the product of a single mineralising event. What is important here is that the Merensky pyroxenite is over 2 m thick (Figure. 9.5a). Elsewhere the pyroxenite, together with the pegmatite, may be very much thinner (Cawthorn *et al.* 2002) and that as the pyroxenite becomes thicker, two PGE peaks are recognisable. In the case of thin reef, these two peaks become indistinguishable and their individual identity has been overlooked.

Several models have suggested that mixing of these two magmas brought about sulphide saturation (e.g., Campbell *et al.* 1983, Naldrett *et al.* 1986, Naldrett & von Gruenewaldt 1989, Li *et al.* 2001) and the formation of an immiscible sulphide liquid into which PGE partitioned. The data from this study has shown that magma mixing did not take place between the Critical and Main Zone magmas. Thus, this suggests that models that use magma mixing to explain the PGE mineralisation are invalid. This is supported by Cawthorn *et al.* (2002) who showed that the magma mixing model does not result in sulphide saturation by demonstrating that the mixed magmas have greater sulphur solubility than the fractionated magmas and thus the mixed product is not sulphur-saturated. Alternative models must be sought in order to explain the transitory sulphide-saturation event in the Merensky Reef.

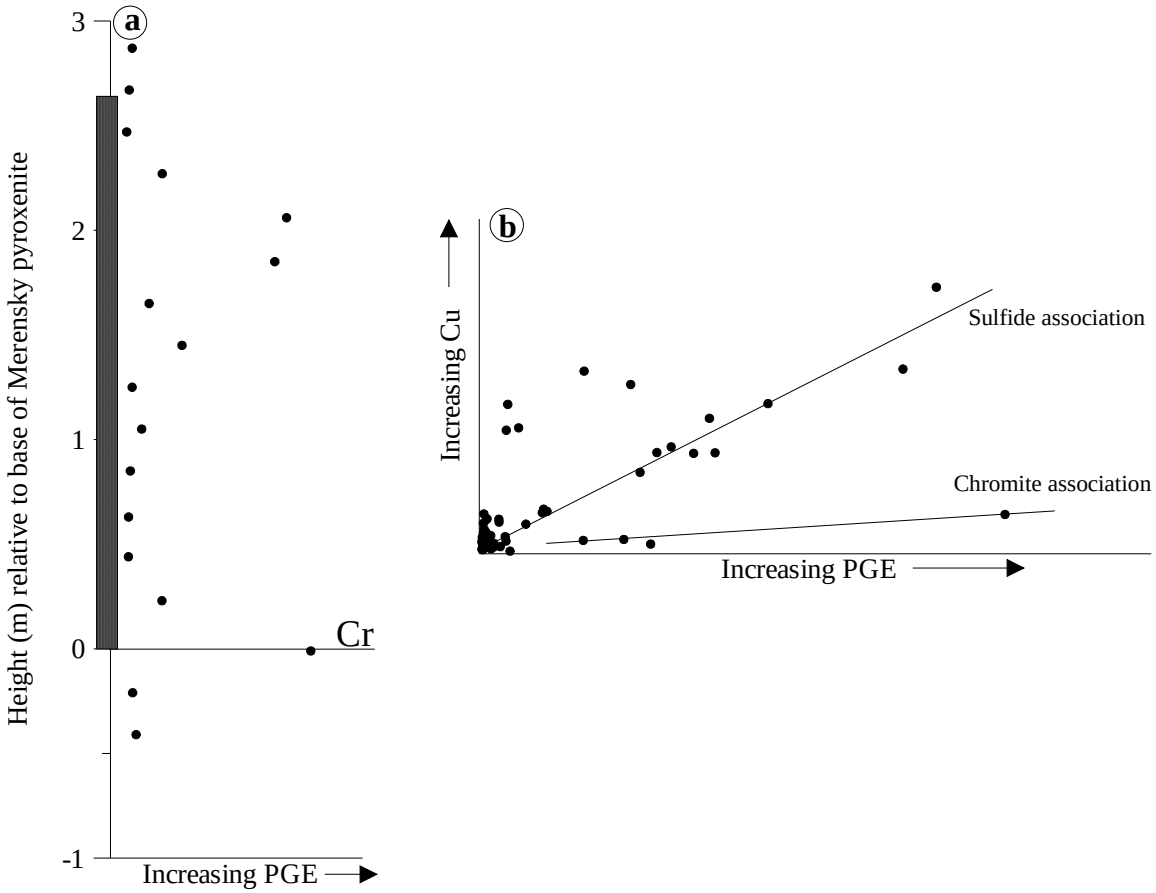


FIGURE 9.5 a) PGE content plotted against height and b) PGE content plotted against Cu for core and two deflections in RM15. PGE and Cu scales are qualitative due to confidentiality restrictions on these data.

Other authors have suggested models that support mechanical accumulation of PGE, rather than by a secondary process. Wager & Brown (1968), based on a review of others data and observations, commented that PGE mineralisation and associated sulphide minerals always occur in the same "feldspathic pyroxenite" and conclude that the PGE must have been deposited with the cumulus crystals at that particular horizon. However, this does not explain mineralisation in the footwall and top-loading. Brynard *et al.* (1976) preferred gravity settling of orthopyroxene and associated PGE to explain the sharp, undulating lower contact of the Merensky Reef and Heimstra (1986) also suggested that PGE concentration profiles in the UG2 indicated a settling mechanism.

In light of the data presented here that indicate a crystal settling model for orthopyroxenes in the Merensky Reef, it is possible to infer that PGE may have settled in the same fashion. This might suggest

that PGM formed as discrete minerals in the residual Critical Zone liquid. Kruger (1992) proposed a model that utilised the settling and accumulation of crystals and crystal slurries from an elevated Critical Zone liquid to explain the formation of the Merensky Reef. He also used this model to explain the concentration of PGE in the Reef, suggesting that sulphide droplets formed in the Critical Zone liquid, scavenging PGE and then descended through the Main Zone magma to accumulate at the level of the Reef. This model is particularly attractive in that it mimics the formation of the cumulus minerals, while invoking mechanisms that specifically relate to PGE concentration. However, Kruger (1990) stated that the sinking sulphide droplets would have to scavenge at least 80% of the PGE from only *ca* 200-300m of resident magma. This indicates that scavenging was extremely efficient, particularly in an environment with little turbulence that would allow sulphides to be brought in contact with PGE throughout the magma. It is generally assumed that little PGE was present in the Main Zone magma. The concentration of PGE from the Main Zone magma could have been more efficient if the PGE were scavenged as sulphide droplets or clusters that sank through it. However, Kruger (*in press*) suggested that sulphur was taken up by the Main Zone magma during contamination by S-rich shales in the north (Potgietersrus/Mokopane area). Partitioning of PGE into sulphides could therefore have occurred in the Main Zone magma, which is in line with deposition of the PGE at the base of the Main Zone influx, marked by the Merensky Reef. These features fit with the model presented here.

The issue of why PGE only occur in abundance at the level of the Merensky Reef has also been addressed. Observations by Lee (1996), who suggested that PGE are present in constant amounts throughout the chamber, but is normally diluted by silicates. This is also in line with the crystal settling model. He suggested that grade decreases in thicker Merensky Reef and increases as it thins. Similarly Cawthorn's (1999a) suggestion that crystallisation of silicates was temporarily terminated, allowing PGE clusters to accumulate appears to be in agreement with the proposed break in crystallisation/deposition of orthopyroxene presented here. The downward accumulation model is also supported by Os isotope data from sulphides (Schoenberg *et al.* 1999) that show Main Zone signatures in the Merensky Reef. They opposed upward filtration to concentrate PGE because it would imply that either the fluid/melt must have

undergone significant changes in its Os isotopic composition during penetration through the Reef or very radiogenic osmium must have been emplaced just within the high-PGE Reef without affecting the overlying low-PGE pyroxenites of the Bastard Reef. Sulphides may have picked up this high Os isotopic signature during their descent through the Main Zone magma injection before accumulating with orthopyroxenes in the Merensky Reef.

Cawthorn *et al.* (2004) suggested that PGE clusters might have become entrapped in an immiscible sulphide liquid that originated in an elevated and stratified Critical Zone magma. Cawthorn *et al*. (2004) suggested that these PGE clusters in sulphide liquid might sink due to density and accumulate at the crystal mush that was crystallising to form the Merensky pyroxenite. They proposed that a constant amount of PGE formed everywhere across the whole complex, but its final location in the Reef, in the footwall, or concentrated at the top, depended on how thick the Merensky pyroxenite crystal mush was. Percolation of sulphide clusters was approximately 1 m into the crystal mush, regardless of how thick the pyroxenite was.

Another important feature of the mineralisation is the lack of PGE in the Bastard pyroxenite. Previous models for the formation of the Reefs have invoked a second Main Zone influx to form the Bastard Cyclic Unit (e.g. Kruger 1992) in a manner similar to that proposed for the formation of the Merensky Reef. If this were the case, then one would expect the same mechanisms to function and PGE to be scavenged and deposited in a similar fashion, assuming the Main Zone magma was the source of PGE. However, in the present model, a second magma influx is not introduced at the level of the Bastard pyroxenite. Thus, the lack of mineralisation in the Bastard pyroxenite could be due to all the PGE already having been scavenged and accumulated in the Merensky Reef. At the time of formation of the Bastard pyroxenite, insufficient PGE remained in the Main Zone magma, having been already removed during the formation of the Merensky Reef, thus leaving the Bastard pyroxenite largely unmineralised. This is similar to the views expressed by Kruger & Marsh (1985) wherein they indicate that the Bastard unit crystallised from the same magma that formed the Merensky unit and was not the result of further influx. They suggested that this is the reason the Bastard pyroxenite is not mineralised. Similarly, if the source of the

PGE were the elevated Critical Zone magma then the PGE would have been depleted during the formation of the Merensky Reef, leaving insufficient PGE to accumulate at economic levels in the Bastard pyroxenite.

It can be concluded, therefore, that two phases of syngenetic PGE mineralisation are present in the Merensky Reef at Richmond. One associated with chromite and a second associated with sulphides. This study appears to support a cumulus syngenetic, or immediately epigenetic, model for the origin of the PGE associated with sulphides, whether by concentration in sulphide droplets originating from the Critical Zone liquid, or as PGE clusters within a sulphide liquid.

Chapter 10

Summary and Conclusions

A number of different aspects of the Upper Critical and Lower Main Zone rocks in the eastern Bushveld were investigated. A model was developed that describes the origin of the Merensky and Bastard Cyclic Units based on detailed investigation into geochemical variations in these units, and the nature of the transition from the Critical Zone to the Main Zone.

10.1 Stratigraphic variations

This study documented the stratigraphy of the Upper Critical and Lower Main Zones from four boreholes in the eastern Bushveld. Comparison with other profiles shows that there are systematic variations in the stratigraphy of the central and southern sectors of the eastern limb, north and south of the Steelpoort lineament. The most significant variations are the presence of the UG3 Cyclic Unit in the central sector only, the greater thickness of rock between the UG2 and Merensky pyroxenite in the central sector, the thicker Merensky pyroxenite in the central sector and the thicker GMA in the southern sector. It is also apparent that there are stratigraphic variations between the eastern and western limbs of the complex. The thickness of the UG2-Merensky unit in the eastern Bushveld is substantially greater than in the western Bushveld. These variations reflect differing volumes of magma present at different locations in the complex at the same time and have implications for the point of origin of the magmas and may provide information about where magmas entered the chamber. The observations in this study suggest that the Critical Zone magma intruded southwards from the TML and that the Main Zone magma was intruded to the north of the TML.

10.2 Geochemical investigations

A number of investigations into the nature and effectiveness of geochemical analysis have been undertaken. Geochemical modelling of trace elements was used to establish the effects of modal proportion on trace element ratios. Trace element ratios have commonly been used to define cyclic units and infer influxes of magma at the point where a break in the ratio trend occurs. It has been

assumed that this trend represents fractionation and that element ratios are independent of modal controls. However, the effects of modal proportion on these ratios have not previously been fully considered. A series of theoretical calculations were undertaken, based on both Upper Critical and Main Zone assemblages with constant magma compositions, and it is demonstrated that ratio variations do correspond to varying modal proportions. This modelling established that a wide range of values is obtainable based solely on changes in modal proportion. In addition, variations in ratios can also be a function of proportion of trapped liquid. It is shown that changes in the proportions of accumulating phases and trapped liquid content result in changes in trace element ratios.

Cr/MgO ratios in the Upper Critical and Main Zones were also modelled in order to determine variations in this ratio over the Critical/Main Zone boundary. The positive correlation between Cr and MgO means a ratio of these elements is independent of modal proportion and it was demonstrated that there are distinct differences between Critical and Main Zone Cr/MgO values (approximately 110 and 50 respectively) and that these values are constant regardless of lithology. It was also shown that Cr/MgO values decrease at values of 5% MgO and less due to the lack of orthopyroxene into which Cr and MgO partition.

Incompatible element abundances were investigated in order to determine their effectiveness at accurately determining trapped liquid content. Using K_2O, P_2O_5 and Zr it was shown that each of these elements does not give the same trapped liquid proportions and that compositions for the Critical and Main Zone magmas are inaccurate, at least in terms of incompatible element concentrations. In addition, it can be concluded that quantitative estimates of the proportion of trapped liquid, using a single element, are largely inaccurate and should be considered unreliable as estimations vary depending on the element used. An investigation into the presence of cumulus plagioclase in the Merensky and Bastard pyroxenites showed that from 0 to over 80% of the total plagioclase content of these rocks is cumulus and not all interstitial as previously assumed.

10.3 Mineral disequilibrium and the formation of the Merensky and Bastard Cyclic Units

Using data from the sampled cores, geochemical criteria for distinguishing between minerals of Critical Zone and Main Zone magma provenance have been established. These distinctive criteria include Sr isotope initial ratios, absolute Sr ppm and An# in plagioclase, and Cr/MgO ratios, absolute Cr ppm and Mg# in orthopyroxene. Detailed study of these minerals in the Merensky and Bastard Cyclic Units has shown that these minerals are often not in equilibrium, with orthopyroxene grains, originating from the Critical Zone magma, occurring in the same layer as plagioclase grains originating from the Main Zone magma. Comparison with other profiles from numerous locations in the western and eastern Bushveld has shown that this disequilibrium occurs at every location and that it is laterally variable.

These observations of mineral disequilibrium do not support a magma mixing theory to explain Sr isotope variations throughout the Merensky and Bastard Cyclic Units, but indicate the co-accumulation of minerals from different stratified magmas. A model has been developed that explains the geochemical variations described. It has been proposed that these mineral variations are the result of the minerals crystallising from, and settling through, two different stratified magmas (a new influx of Main Zone magma and an elevated residual Critical Zone magma), to accumulate together at a specific level (Kruger 1992). Thus, the geochemistry observed is not the result of mixing and subsequent crystallisation of the magmas. The isotopic break and return to Critical Zone Sr isotope signatures in the Bastard pyroxenite at Atok and Richmond suggest that Critical Zone magma is still chemically and physically distinct even after the Main Zone magma has been intruded. It is proposed that orthopyroxene in the Merensky and Bastard pyroxenites originated from the Critical Zone magma. The interstitial plagioclase was derived from the Main Zone magma. Any cumulus plagioclase in the pyroxenites also originated from the Critical Zone liquid. In the overlying norites and anorthosites, the plagioclase originated from the Main Zone magma, whereas the orthopyroxene continued to sink from the overlying Critical Zone liquid. Geochemical signatures of minerals in the Merensky pyroxenite do not support the influx of an additional magma that was different to the Critical or Main Zone magmas.

The origin of PGE in the Merensky Reef is also discussed. This discussion focuses on the mechanisms that concentrate PGE to economic values and the source of the PGE. Although no definite conclusion can be reached, considering the model for the formation of the Merensky pyroxenite

presented here, this study appears to support a primary, syngenetic origin for the PGE. Concentration was either in sulphide droplets originating from the Critical Zone liquid or as PGE clusters accumulating from the Main Zone magma. An association of PGE with chromite mineralization was also observed. Further mineralogical work to try and establish the magma affinities of the sulphides and PGM in the Reef should be undertaken to attempt to resolve this issue.

References

ANDERSEN J.C.Ø., RASMUSSEN H., NIELSEN T.F.D. & RØNSBO J.G., 1998, The Triple Group and the Platinova gold and palladium reefs in the Skaergaard intrusion: Stratigraphic and petrographic relations. *Econ. Geol.* **93**, 488-509

ASHWAL L.D., WEBB S.J. & KNOPER M.W., 2004, The Bellevue drillcore, northern lobe, Bushveld Complex: Continuous geophysical and mineralogical data. *Geoscience Africa 2004*, Abstract volume, University of the Witwatersrand, Johannesburg, South Africa, 26

BALHAUS C.G., 1988, Potholes of the Merensky Reef at Brakspruit Shaft, Rustenburg Platinum Mines: Primary Disturbances in the Magnetite Stratigraphy, *Econ. Geol.*, **83**, 1140-1158

BALHAUS C.G., & STUMPFL E.F., 1985, Occurrence and petrological significance of graphite in the Upper Critical Zone, western Bushveld Complex, South Africa. *Earth. Plan. Sci. Lett.* **74**, 58-68

BALHAUS C.G. & STUMPFL E.F., 1986, Sulfide and platinum mineralization in the Merensky Reef: evidence from hydrous silicates and fluid inclusions. *Contrib. Min. Pet.* **94**, 193-204

BALLHAUS C. & SYLVESTER P., 2000, Noble metal enrichment processes in the Merensky Reef, Bushveld Complex. *J. Pet.* **41** 545-561

BARNES S.J., 1986, The distribution of chromium among orthopyroxene, spinel and silicate liquid at atmospheric pressure. *Geochim. Cosmochim. Acta* **50**, 1889-1909

BARNES S.J. & CAMPBELL I.H., 1988, Role of late magmatic fluids in Merensky-type platinum deposits: A discussion. *Geology* **16**, 488-491

BARNES S-J. & MAIER W.D., 2002, Platinum-group elements and microstructures of normal Merensky Reef from Impala Platinum Mines, Bushveld Complex. *J. Pet.* **43**. 103-138

BARNES S-J., MAKOVICKY E., ROSE-HANSEN J. & KARRUP-MØLLER S., 1997, Partition coefficients for Ni, Cu, Pd, Pt, Rh and Ir between monosulfide solid solution and sulfide liquid and the formation of compositionally zoned Ni-Cu sulfide bodies by fractional crystallization of sulfide liquid. *Can. J. Earth. Sci.* **34**, 366-374

BÉDARD J.H., 1994, A procedure for calculating the equilibrium distribution of trace elements among the minerals of cumulate rocks, and the concentration of trace elements in coexisting liquids. *Chem. Geol.* **118**, 143-153

BÉDARD J.H., SPARKS R.S.J., RENNER M., CHEADLE M.J. & HALLWORTH M.A., 1988, Peridotite sills and metasomatic gabbros in the eastern layered series of the Rhum Complex. *Geol. Soc. London J.* **145**, 207-224

BEZMAN N.J., ASIF M., BRÜGMANN G. E., ROMANENKO I.M. & NALDRETT A.J., 1994, Distribution of Pd, Ru, Rh, Ir, Os and Au between sulphide and silicate melts. *Geochim. Cosmochim. Acta*. **58**, 1251-1260

BLUMBERG J., 2002, Unpublished Honours thesis, University of the Witwatersrand, South Africa, 45 pp.

BOERST K.D., 2001, Geochemistry of the Merensky Reef on Impala Platinum Mine, western Bushveld Complex. Unpublished MSc. thesis, University of the Witwatersrand, South Africa, 81 pp.

BOTTINGA, Y. & WEILL, D.F., 1970, Densities of liquid silicate systems calculated from partial molar volumes of oxide components, *Am. J. Sci*., **269**, 169-182

BOTTINGA Y., WEILL D. & RICHET P., 1982, Density calculations for silicate liquids. I. Revised method for aluminosilicate compositions. *Contrib. Min. Pet*. **97**, 417-30

BOUDREAU A., 1999, Fluid fluxing of cumulates: the J-M Reef and associated rocks of the Stillwater Complex, Montana. *J. Pet*. **40**, 755-772

BOUDREAU A.E., 2002, The Stillwater and Bushveld magmas were wet*! 9th International Platinum Symposium Abstracts*, Billings, Montana.

BOUDREAU A.E. & MCCALLUM I.S., 1992, Concentration of platinum-group elements by magmatic fluids in layered intrusions. *Econ. Geol*. **87**, 1830-1848

BOUDREAU A.E. & MEURER W.P., 1999, Chromatagraphic separation of the platinum-group elements, gold, base metals and sulfur during degassing of a compacting and solidifying igneous pile. *Contrib. Min. Pet*. **134**, 174-185

BOUDREAU A.E., MATHEZ E.A. & MCCALLUM I.S., 1986, Halogen geochemistry of the Stillwater and Bushveld Complexes: evidence for transport of the platinum-group elements by Cl-rich fluids. *J. Pet*. **24**, 967-986

BOUDREAU A.E., STEWART M.A. & SPIVACK A.J., 1997, Stable Cl isotopes and origin of high-Cl magmas of the Stillwater Complex, Montana. *Geology* **25**, 791-794

BRYNARD H.J., DE VILLIERS J.P.R. & VILJOEN E.A., 1976, A mineralogical investigation of the Merensky Reef at the Western Platinum Mine, near Marikana, South Africa. *Econ. Geol*. **71**, 1299-1307

BUCHANAN D.L. & NOLAN J., 1979, Solubility of sulfur and sulfide immiscibility in synthetic tholeiitic melts and their relevance to Bushveld Complex rocks. *Can. Mineral*. **17**, 483-494

BUICK I.S., MAAS R. & GIBSON R., 2001, Precise U-Pb titanite age constraints on the emplacement of the Bushveld Complex, South Africa. *J. Geol. Soc. London*, **158**: 3-6

CAMERON E.N., 1982, The Upper Critical Zone of the eastern Bushveld Complex – Precursor to the Merensky Reef. *Econ. Geol*. **77**, 1307-1327

CAMERON E.N., 1980, Evolution of the Lower Critical Zone, central sector, eastern Bushveld Complex, and its chromite deposits. *Econ. Geol*. **75**, 845-871

CAMERON E.N., 1978, The Lower Zone of the eastern Bushveld Complex in the Olifants River trough. *J. Pet.* **19**, 437-462

CAMERON E.N., 1964, Chromite deposits in the eastern part of the Bushveld Complex, *in* The geology of some ore deposits in southern Africa. Haughton S.H. (ed.), *Geol. Soc. S. Afr*., Pretoria, **II,** 739 p.

CAMERON E.N., 1963, Structure and rock sequences of the Critical Zone, eastern Bushveld Complex. *Mineral. Soc. Am. Spec. Paper* **1**, 93-107

CAMPBELL I.H., 1986, A fluid dynamic model for the potholes of the Merensky Reef. *Econ. Geol.* **81**, 1118-1125

CAMPBELL I.H., NALDRETT A.J., & BARNES S.J., 1983, A model for the origin of the platinum-rich sulfide horizons in the Bushveld and Stillwater Complexes. *J. Pet.* **24**, 133-165

CAMPBELL I.H., ROEDER P.L. & DIXON J.M., 1978, Plagioclase buoyancy in basaltic liquids as determined with a centrifuge furnace. *Contrib. Min. Pet.*, **67**, 369-377

CARR H.W. GROVES D.I. & CAWTHORN R.G., 1994, The importance of synmagmatic deformation in the formation of Merensky Reef potholes in the Bushveld Complex. *Econ. Geol*. **89.** 1398-1410

CARR H.W. GROVES D.I., KRUGER F.J. & CAWTHORN R.G., 1994, Petrogenesis of Merensky Reef potholes at the Western Platinum Mines: Sr-isotopic evidence for synmagmatic deformation. *Mineral. Deposit*., **34**, 335-347

CAWTHORN R.G., 2004, Origin of variation of Pt/Pd values in the UG2 chromitite layer, Bushveld Complex. G*eoscience Africa 2004*, Abstract volume, University of the Witwatersrand, Johannesburg, South Africa, 110-111

CAWTHORN R.G., 2002, Delayed accumulation of plagioclase in the Bushveld Complex. *Min. Mag*. **66**, 881-893

CAWTHORN R.G., 1999a, Permeability of the footwall cumulates to the Merensky Reef, Bushveld Complex. *S. Afr. J. Geol.* **102**, 293-310

CAWTHORN R.G., 1999b, Platinum-group element mineralization in the Bushveld Complex - a critical reassessment of geochemical models. *S. Afr. J. Geol*. **102**, 268-281

CAWTHORN R.G., 1996a, Re-evaluation of magma compositions and processes in the uppermost Critical Zone of the Bushveld Complex. *Min. Mag.* **60**, 131-148

CAWTHORN R.G., 1996b, Models for incompatible trace-element abundances in cumulus minerals and their application to plagioclase and pyroxenes in the Bushveld Complex. *Contrib. Min. Pet.* **123**. 109-115.

CAWTHORN R.G. & BIGGAR G. M., 1993 Crystallization of titaniferous chromite, magnesian ilmenite and armalcolite in tholeiitic suites in the Karoo Igneous Province. *Contrib. Min. Pet.* **114**, 221-235

CAWTHORN R.G. & DAVIES G., 1983, Experimental data at 3 Kbars pressure on parental magma to the Bushveld Complex. *Contrib. Min. Pet*. **83**, 128-135

CAWTHORN R.G. & SPIES L., 2003, Plagioclase content of cyclic units in the Bushveld Complex, South Africa. *Contrib. Min. Pet.* **145**. 47-60

CAWTHORN R.G. & WALRAVEN F., 1998, Emplacement and crystallization time for the Bushveld Complex. *J. Pet.* **39**, 1669-1687

CAWTHORN R.G., COOPER G.R.J. & WEBB S.J., 1998, Connectivity between the western and eastern limbs of the Bushveld Complex. *S. Afr. J. Geol*. **101**, 291-298

CAWTHORN R.G., DAVIES G., CLUBLEY-ARMSTRONG A. & MCCARTHY T.S., 1981, Sills associated with the Bushveld Complex, South Africa: an estimate of parental magma composition. *Lithos* **14**, 1-15

CAWTHORN R.G., LEE C.A., SCHOUWSTRA R.P. & MELLOWSHIP P., 2002a, Relationship between PGE and PGM in the Bushveld Complex. *Can. Mineral*. **40**, 311-328

CAWTHORN R.G., MERKLE K.W., & VILJOEN M.J., 2002b, Platinum-group element deposits in the Bushveld Complex, South Africa *in* The geology, geochemistry, mineralogy and mineral beneficiation of platinum-group elements. Cabri L.J. (ed.), *Canadian Institute of Mining, Metallurgy and Petroleum*, Special Volume **54**, 389-430.

CAWTHORN R.G., SLABBART M. & VAN DER MERWE J., 2004, The Full Merensky – It's lithologies and genesis. *Geoscience Africa 2004*, Abstract volume, University of the Witwatersrand, Johannesburg, South Africa, 114-115

CHARLIER B.L.A., DAVIDSON J.P., BACHMANN O. & DUNGAN M.A., 2004, Mineral-scale Sr isotopic variations as recorders of magmatic processes in the Fish Canyon system, U.S.A. Twelfth Annual V.M. Goldschmidt conference proceedings. *Geochim. Cosmochim. Acta*. **68**, A643

CHERTKOFF D.G., MORGAN D.J., FRANCALANCI L., DAVIDSON J.P., PEARSON D.G., JERRAM D.A. & NOWELL G.M., 2004, Textural and strontium isotope analysis of plagioclase phenocrysts of the Vancori Series, Stromboli volcano (Aeolian Islands). Twelfth Annual V.M. Goldschmidt conference proceedings. *Geochim. Cosmochim. Acta*. **68**, A643

COUSINS C.A., 1964a, Additional notes on the chromite deposits of the eastern part of the Bushveld Complex, *in* The geology of some ore deposits of Southern Africa. Haughton S.H. (ed.), Johannesburg, *Geol. Soc. S. Afr.* **II**, 169-182

COUSINS C.A., 1964b, The platinum deposits of the Merensky Reef, *in* The geology of some ore deposits of southern Africa. Haughton S.H. (ed.), Johannesburg, *S. Afr.* **II,** 224-237

COX K.G., BELL J.D. & PANKHURST R.J., 1981, The interpretation of igneous rocks, London, 450 pp.

CROCKET J.H., FLEET M.E. & STONE W.E., 1992, Experimental partitioning of osmium, iridium and gold between basalt melt and sulphide liquid at 1300^{o}C. *Austr. J. Earth. Sci*. **39**, 427-432

DAVEY S.R., 1992, Lateral variations within the upper Critical Zone of the Bushveld Complex on the farm Rooikoppies 297 JO, Marikana, South Africa. *S. Afr. J. Geol*. **95**, 141-149

DAVIES G., CAWTHORN R.G., BARTON J.M, & MORTON M., 1980, Parental magma to the Bushveld Complex. *Nature* **287**, 33-35

DE KLERK W.J., 1995, Textures exhibited by feldspars in the Giant Mottled Anorthosite (GMA) of the Bastard Unit in the Upper Critical Zone, western Bushveld Complex. *Min. Pet.* **54**, 25-34

DE KLERK W.J., 1991, Petrogenesis of the Upper Critical Zone in the western Bushveld Complex, with emphasis on the UG1 footwall and Bastard units. Unpublished PhD. Thesis, University of Rhodes, Grahamstown, South Africa, 294 pp.

DE WIT M.J. & KRUGER F.J., 1990, The economic potential of the Dufek Complex *in* Mineral Resources Potential of Antarctica. Splettstoesser J.F. & Dreschhoff G.A.M. (eds.) Washington D. C., *Am. Geophys. Union*. Antarctic Research Series **51,** 33-52

DONALDSON C.H., 1993, Convective fractionation during magnetite and hematite dissolution in silicate melts. *Min. Mag*. **57**, 469-488

DONALDSON C.H., 1985, The rates of dissolution of olivine, plagioclase, and quartz in a basaltic melt. *Min. Mag*. **49**, 683-693

EALES H.V., 2000, Implications of the chromium budget of the western limb of the Bushveld Complex. *S. Afr. J. Geol.* **103**, 141-150

EALES H.V. & CAWTHORN R.G., 1996, The Bushveld Complex *in* Layered Intrusions. Cawthorn R.G. (ed.) *Elsevier Science B.V.*, Amsterdam, 181-229

EALES H.V., BOTHA W.J., HATTINGH P.J., DE KLERK W.J., MAIER W.D. & ODGERS A.T.R., 1993, The mafic rocks of the Bushveld Complex: a review of emplacement and crystallization history, and mineralization, in light of recent data. *J. Afr. Earth Sci*. **16**, 121-142

EALES H. V., DE KLERK W. J., BUTCHER A. R. AND KRUGER F. J., 1990, The cyclic unit beneath the UG1 chromitite (UG1 FW unit) at RPM Union Section Platinum Mine – Rosetta Stone of the Bushveld Upper Critical Zone? *Min. Mag*. **54**, 23-43

EALES H.V., FIELD M., DE KLERK W.J. & SCOON R.N., 1988, Regional trends of chemical variation and thermal erosion in the Upper Critical Zone, Western Bushveld Complex. *Min. Mag*. **52**, 63-79

EALES H.V., MAIER W.D. & TEIGLER B., 1991, Corroded plagioclase feldspar inclusions in orthopyroxene and olivine of the Lower and Critical Zones, western Bushveld Complex. *Min. Mag.* **55**, 479-786

EALES H.V., MARSH J.S., MITCHELL A.A., DE KLERK W.D., KRUGER F.J. & FIELD M., 1986, Some geochemical constraints upon models for the crystallisation of the Upper Critical Zone - Main Zone interval, northwestern Bushveld Complex. *Min. Mag.* **50**, 567-582

EALES H.V., TEIGLER B. & MAIER W.D., 1993, Cryptic variations of minor elements Al, Cr, Ti and Mn in Lower and Critical Zone orthopyroxenes of the Western Bushveld Complex. *Min. Mag.* **57**, 257-264.

ELLIOT W.C., GRANDSTAFF D.E., ULMER G.C., BUNTIN T. & GOLD D.P., 1982, An intrinsic oxygen fugacity study of platinum-carbon associations in layered intrusives. *Econ. Geol*. **77**, 1493-1510

FAURE G., 1986, Principals of Isotope Geology, Second Edition. *John Wiley & Sons*, New York.

FIELD M., 1987, The petrology and geochemistry of the Upper Critical Zone of the Bushveld Complex at the Amandelbult Section of Rustenburg Platinum Mines Limited, Northwestern Transvaal, South Africa. Unpublished MSc. thesis, Rhodes University, Grahamstown, South Africa, 129 pp.

FINNIGAN C.S. & BRENANJ.M., 2004, Experimental evidence for the co-precipitation of PGE alloys and chromite as a result of local melt reduction during chromite crystallization. *Geoscience Africa 2004*, Abstract volume, University of the Witwatersrand, Johannesburg, South Africa, 201

FLEET M.E., CROCKET J.H., LIU MENGHUA & STONE W.E., 1999, Laboratory partitioning of platinum-group elements and (PGE) gold with application to magmatic sulfide-PGE deposits. *Lithos*, **47**, 127-142

GAIN S.B., 1985, The geologic setting on the platiniferous UG-2 chromitite layer on the farm Maandagshoek, eastern Bushveld Complex. *Econ. Geol*. **80**, 925-943

GHIORSO M.S. & SACK R.O., 1995, Chemical mass transfer in magmatic processes. IV. A revised and internally consistent thermodynamic model for the interpolation and extrapolation of liquid-solid equilibria in magmatic systems at elevated temperatures and pressures. *Contrib. Min. Pet.* **119**, 197-212.

GOUGH D.I., & VAN NIERKERK C.B., 1959, A study of the palaeomagnatism of the Bushveld Complex. *Phil. Mag*. **14**, 126-134

HALL A.L., 1932, The Bushveld Igneous Complex in the central Transvaal, *Geol. Soc. S. Afri. Mem*. **28**, 544 pp.

HAMILTON J., 1977, Sr isotope and trace element studies of the Great Dyke and Bushveld mafic phase and their relation to early Proterozoic magma genesis in Southern Africa. *J. Pet.* **18**, 24-52

HANLEY J.J., PETTKE T., MUNGALL J.E. & SPOONER E.T.C., 2004, Base and precious metal-bearing fluid inclusions of magmatic origin in the ultramafic series, Stillwater Complex, Montana. *Geoscience Africa 2004*, Abstract volume, University of the Witwatersrand, Johannesburg, South Africa, 253

HARMER R.E. & SHARPE M.R., 1985, Field relations and strontium isotope systematics of the marginal rocks of the eastern Bushveld Complex. *Econ. Geol*. **80**, 813-837

HATTINGH P.J. & WALRAVEN F., 1993, Geochronology of the Nebo Granite, Bushveld Complex, South Africa. *S. Afri. J. Geol*., **96**, 31-41

HATTON C.J., 1989, Densities and liquidus temperatures of Bushveld parental magmas as constraints on the formation of the Merensky Reef of the Bushveld Complex, South Africa. *The fifth magmatic sulphide field conference, Zimbabwe*, The Institution of Mining and Metallurgy, London, 87-93

HATTON C.J. & VON GRUENEWALDT G., 1987, The geological setting and petrogenesis of the Bushveld chromitite layers *in* Evolution of chromium ore fields, Stowe C.W. (ed.), *Van Nostrand Reinhold Co*., New York, 109-143

HAUGHTON D.R., ROEDER P.L. & SKINNER B.J., 1974, Solubility of sulfur in mafic magmas. *Econ. Geol*. **69**, 451-467

HENDERSON P., 1975, Geochemical indicator of the efficiency of fractionation of the Skaergaard intrusion, east Greenland. *Min. Mag.* **40**. 285-291

HIEMSTRA S.A., 1985, The distribution of some platinum-group elements in the UG-2 chromitite layer of the Bushveld Complex. *Econ. Geol*. **80**, 944-957

HOATSON D.M. & KEAYS R.R., 1989, Formation of platiniferous sulfide horizons by crystal fractionation and magmatic mixing in the Munni Munni layered intrusion, West Pilbara Block, Western Australia. *Econ. Geol*. **84**, 1775-1804

HOLWELL D.A., 2002, Base-metal sulphide geochemistry of the Merensky Reef, Bushveld Complex. Unpublished MSc. Thesis. University of Exeter, UK, 156 pp.

HORNSEY R.A., 2004, The geology of the UG2 chromitite layer at the Two Rivers project (Dwarsrivier 372KT, Mpumpulanga), and its stratigraphic correlation within the regional setting of the Bushveld Complex. *Geoscience Africa 2004*, Abstract volume, University of the Witwatersrand, Johannesburg, South Africa, 286-287

HUNTER R.H., 1996, Texture development in cumulate rocks *in* Layered Intrusions, Cawthorn R.G. (ed.) *Elsevier Science B.V.*, Amsterdam, 77-101

IRVINE T.N., 1975, Crystallization sequences in the Muskox Intrusion and other layered intrusions – II. Origin of chromitite layers and similar deposits of other magmatic ores. *Geochim. Cosmochim. Acta* **39**, 991-1020

IRVINE T.N., 1982, Terminology for Layered Intrusions. *J. Pet.*, **23**, 127-162

IRVINE T.N., 1987, Layering and related structures in the Duke Island and Skaergaard intrusions: similarities, differences and origins *in* Origins of Igneous Layering, Parsons I. (ed.) Dordrecht, *Reidel Publishing Company* **196,** 185-245

IRVINE T.N., KEITH D.W. & TODD S.G., 1983, The J-M platinum-palladium Reef of the Stillwater Complex, Montana: II. Origin by double diffusive convective magma mixing and implications for the Bushveld. *Econ. Geol.*, **78**, 1287-1334

IRVINE T.N. & SHARPE M.R., 1986, Magma mixing and the origin of stratiform oxide ore zones *in* the Bushveld and Stillwater Complexes in Metallogency of Basic and Ultrabasic Rocks. Gallagher M.J., Ixer R.A., Neary C.R. and Prichard H.M. (eds.) *Inst. Min. Metall*. 183 - 198

JACKSON, E.D., 1970, The Cyclic Unit in layered intrusions – A comparison of repetitive stratigraphy in the ultramafic parts of the Stillwater, Muskox, Great Dyke an Bushveld Complexes *in* Visser, D.J.L. and von Gruenewaldt, G., eds., Symposium on the Bushveld Complex and other Layered Intrusions: *The Geological Society of South Africa, Special Publication*, **1**, 3914-424

JERRAM D.A., CHEADLE M.J. & PHILPOTTS A.R., 2004, Quantifying the building blocks of igneous rocks: Are clustered crystal frameworks the foundation? *J. Pet.* **44**, 2033-2051

KINLOCH E.D., 1982, Regional trends in the platinum-group mineralogy of the Critical Zone of the Bushveld Complex, South Africa. *Econ. Geol.* **77**, 1328-1347

KINNAIRD, J.K., NEX, P.A.M., KRUGER, F.J. & CAWTHORN, R.G., 2002, Chromitite formation – a key to understanding processes of platinum enrichment: *Trans. Inst. Min. Metall.*, Section B, Applied Earth Science, **111**, B23-B35.

KOYAGUCHI T., & BLAKE S., 1991, Origin of mafic enclaves: Constraints on the magma mixing model from fluid dynamic experiments *in* Enclaves and Granite Petrology. Didier J., & Barbarin B. (eds.), Developments in Petrology **13**, *Elsevier Science B.V.*, Amsterdam Chapter 31, 415 - 430

KRUGER F.J., 1990, The stratigraphy of the Bushveld Complex: a reappraisal and the relocation of the Main Zone boundaries. *S. Afr. J. Geol.*, **93**, 376-381

KRUGER, F.J., 1992, The origin of the Merensky cyclic units: Sr-isotopic and mineralogical evidence for an alternative orthomagmatic model. *Aus. J. Earth Sci*. **39**, 255-261

KRUGER F.J, 1994, The Sr-isotopic stratigraphy of the Western Bushveld Complex. *S. Afr. J. Geol*. **97**, 393-398.

KRUGER F.J., in press, Filling the Bushveld Complex magma chamber: Lateral expansion, floor interaction, magmatic unconformities, and chromitite and PGE deposits. *Mineral. Deposita,* Fermor Meeting Papers

KRUGER F.J. & MARSH J.S., 1982, Significance of $^{87}Sr/^{86}Sr$ ratios in the Merensky cyclic unit of the Bushveld Complex. *Nature*, **298**, 53-55

KRUGER F.J. & MARSH J.S., 1985, The Mineralogy, petrology and origin of the Merensky cyclic unit in the western Bushveld Complex. *Econ. Geol*., **80**, 958-974

KRUGER F.J., KINNAIRD J.A., NEX P.A. & CAWTHORN R.G., 2002, Chromite is the key to PGE. *9th International Platinum Symposium Abstracts*, Billings, Montana.

LE MAITRE R.W., BATEMAN P., DUDEK A., KELLER J., LAMEYRE J.. LE BAS M.J., SABINE P.A., SCHMID R., SORENSEN H., STRECKEISEN A., WOOLLEY A.R. & ZANETTIN B., 1989, A Classification of Igneous Rocks and Glossary of terms: Recommendations of the International Union of Geological Sciences Subcommission on the Systematics of Igneous Rocks. *Blackwell Scientific Publications*, Oxford, U.K.

LEA S.D., 1996, The geology of the Upper Critical Zone, northeastern Bushveld Complex. *S. Afr. J. Geol.* **99**, 263-283

LEE C.A., 1983, Trace and platinum-group element geochemistry and the development of the Merensky Unit of the western Bushveld Complex. *Mineral. Deposita*, **18**, 173-190

LEE C.A., 1996, A review of mineralization in the Bushveld Complex and some other layered intrusions *in* Layered intrusions. Cawthorn R. G. (ed.). *Elsevier Science B.V.*, Amsterndam **15**, 103-145

LEE C.A & BUTCHER A.R., 1990, Cyclicity in the Sr isotope stratigraphy through the Merensky Reef and Bastard Reef units, Atok Section, Eastern Bushveld Complex. *Econ. Geol*. **85**, 877-883

LEE C.A & TREDOUX M, 1986, Platinum-group element abundances in the lower and lower critical zones of the eastern Bushveld Complex. *Econ. Geol*. **81**, 1087-1095

LEEB-DU TOIT A., 1986, The Impala Platinum Mines *in* Mineral Deposits of Southern Africa. Annhaeusser C.R.& Maske S. (eds.) *Geol. Soc. S. Afr*., **II**, 1091-1106

LI C., MAIER, W. & DE WAAL S.A., 2001a, The role of magma mixing in the genesis of PGE mineralization in the Bushveld Complex: Thermodynamic calculations and new interpretations. *Econ. Geol*. **96**, 653-662

LI C., MAIER W. & DE WAAL S.A., 2001b, Magmatic Ni-Cu versus PGE deposits: Contrasting genetic controls and exploration implications. *S. Afr. J. Geol*. **104**, 309-318

LIPIN B.R., 1993, Pressure increases, the formation of chromitite seams, and the development of the ultramafic series in the Stillwater Complex, Montana. *J. Pet*. **34**, 955-976

LOMBERG K.G., MARTIN E.S., PATTERSON M.A. & VENTER J.E., 1999, The morphology of potholes in the UG2 chromitite layer and the Merensky Reef (pothole reef facies) at Union Section, Rustenburg Platinum Mines. *S. Afr. J. Geol*. **102**, 209-220

LOMBERG K.G., CHUNNET G.K., LIONETTE M.A., MARTIN E.S., NEL J.J., RUYGROK M. & STEENEKAMP J.M.A., 2004, The geology of Bafokeng Rasimone Platinum Mine (BRPM). *Geoscience Africa 2004*, Abstract volume, University of the Witwatersrand, Johannesburg, South Africa, 393

MAIER W.D. & TEIGLER B., 1995, A facies model for the Western Bushveld Complex. *Econ. Geol*. **90**, 2343-2349

MAIER W., ARDNT N. & CURL E., 2000, Progressive crustal contamination of the Bushveld Complex: evidence from Nd isotopic analyses of the cumulate rocks. *Contrib. Min. Pet*. **140**, 316-327

MAIER W.D., BARNES S-J., & LI C., 2002, A re-evaluation in the role of crustal contamination in the formation of magmatic sulfides in the Bushveld Complex. *9th International Platinum Symposium Abstracts*, Billings, Montana.

MAIER W.D., BARNES S.J., DE KLERK W.J., TEIGLER B. & MITCHELL A.A., 1996, Cu/Pd and Cu/Pt of silicate rocks in the Bushveld Complex: Implications for platinum-group element exploration. *Econ. Geol*. **91**, 1151-1158

MAIER, W.D., BARNES, S.-J. AND VAN DER MERWE, M.J., 2001, Platinum-group elements in the Pyroxenite Marker, Bushveld Complex: Implications for the formation of the Main Zone, *South African J. Geol*. **104**, 301-308

MARCANTONIO F. & MATHEZ E.A., 1995, Sr isotopes and magma mixing in the Bushveld Complex. *EOS* Fall meeting: F641.

MARSH J.S., 1988, Crystal capture, sorting and retention in convecting magma. *Geol. Soc. Am. Bull*. **100**, 1720-1737

MARTIN D., GRIFFITHS R.W. & CAMPBELL I.H., 1987. Compositional and thermal convection in magma chambers. *Contrib. Min. Pet.* **96**. 465-475

MATHEZ E.A.,1999, On factors controlling the concentrations of platinum group elements in layered intrusions and chromitites *in* Short course notes #13 - Dynamic processes in magmatic ore deposits and their application to mineral exploration. Keays R.R., Lesher C.M., Lightfoot P.C. & Farrow C.E.G. (eds.) *Geol. Ass. Can*. Sudbury, Canada.

MATHEZ E.A., 1995, Magmatic metasomatism and formation of the Merensky Reef, Bushveld Complex. *Contrib. Min. Pet.* **119**, 277-286

MATHEZ E.A. & WAIGHT T.E., 2003, Lead isotopic disequilibrium between sulfide and plagioclase in the Bushveld Complex and the chemical evolution of large layered intrusions. *Geochim. et Cosmochim. Acta*. **67**, 1875-1888

MATHEZ E.A., HUNTER R.H. & KINZLER R., 1997, Petrologic evolution of partially molten cumulate: the Atok section of the Bushveld Complex. *Contrib. Min. Pet*. **40**, 1647-1671

MCBIRNEY A.R. & HUNTER R.H., 1995, The cumulative paradigm reconsidered. *J. Pet.* **103**, 114-122

MCCANDLESS T.E. RUIZ J., ADAIR B. & FREYDIER C., 1999, Re-Os isotope and Pd/Ru variations in chromitites from the Critical Zone, Bushveld Complex, South Africa. *Geochim. Cosmochim. Acta* **63**, 911-923

MCDONALD I., HOLWELL D.A. & ARMITAGE P.E.B., *in press*, Geochemistry and mineralogy of the Platreef and "Critical Zone" of the northern lobe of the Bushveld Complex, South Africa: implications for Bushveld stratigraphy and the development of PGE mineralisation. *Mineral. Deposita.*

MCDONALD I., HOLWELL D.A. & ARMITAGE P.E.B., 2004, Magmatic evolution of the northern limb of the Bushveld Complex and the development of Platreef-style mineralization. *Geoscience Africa 2004*, Abstract volume, University of the Witwatersrand, Johannesburg, South Africa, 440-441

MCLEOD P. & SPARKS R.S.J., 1996, The dynamics of xenolith assimilation. *Contrib. Min. pet*. **132**, 21-33

MERKLE R.K.W., 1992, Platinum-group minerals in the middle group of chromitite layers at Marikana, western Bushveld Complex: indications for collection mechanisms and post-magmatic modification. *Can. J. Earth. Sci.* **29**, 209-221

MILLER J.D. JR. & ANDERSEN J.C.Ø., 2002, Attributes of Skaergaard-type PGE reefs. *9th International Platinum Symposium Abstracts*, Billings, Montana

MITCHELL A.A., 1990, The stratigraphy, petrography and mineralogy of the Main Zone of the northwestern Bushveld Complex. *S. Afr. J. Geol.* **93**, 818-831

MITCHELL A.A., 1996, Compositional cyclicity in a pyroxenitic layer from the Main Zone of the western Bushveld Complex: evidence for repeated magma influx. *Min. Mag*. **60**, 149-161

MITCHELL A.A., 1986, The Petrology, Mineralogy and Geochemistry of the Main Zone of the Bushveld Complex, at Rustenburg Platinum Mines, Union Section. Unpublished PhD thesis, Rhodes University, Grahamstown, South Africa, 122 pp.

MITCHELL A.A. & MANTHREE R. R., 2002, The Giant Mottled Anorthosite: a transitional sequence at the top of the Upper Critical Zone of the Bushveld Complex. *S. Afr. J. Geol.* **105**, 15-24

MITCHELL A.A. & SCOON R.N.,1991, Discussion on "The stratigraphy of the Bushveld Complex: a reappraisal and the relocation of the Main Zone boundaries". *S. Afr. J. Geol*. **91**, 183-187

MITCHELL A.A., EALES H.V & KRUGER F.J., 1998, Magma replenishment and the significance of poikilitic textures in the Lower Main Zone of the western Bushveld Complex, South Africa. *Min. Mag*., **62**, 435-450

MOLYNEUX T.G., 1974, A geological investigation of the Bushveld Complex in Sekhukuneland and part of the Steelpoort Valley. *Trans. Geol. Soc. S. Afr*. **77**, 329-338

MOLYNEUX T.G., 1970, The geology of the area in the vicinity of Magnet Heights, Eastern Transvaal, with special reference to the magnetic iron ore. *Geol. Soc. S. Afr*. Spec. Publ. **1**, 228-241

MORSE S.A, 1986, Thermal structure of crystallizing magma with two-phase convection. *Geol. Mag*. **123**, 205-214

MORSE S.A, 1988, Motion of crystals, solute, and heat in layered intrusions. *Can. Min*. **26**, 209-224.

MORSE S.A, 1998, Is the cumulate paradigm at risk?: An extended discussion of the cumulate paradigm reconsidered. *J. Geol*. **106**, 367-370

MOSSOM R.J., 1986, The Atok Platinum Mine, *in* Mineral Deposits of Southern Africa. Annhaeusser C.R. & Maske S. (eds.), *Geol. Soc. of S. Afr*. **2,** 1143-1154.

MUNGALL J., 2002. A model for co-precipitation of platinum-group minerals with chromite from silicate melts. *9th International Platinum Symposium Abstracts*, Billings, Montana.

NALDRETT A.J., 1981, Nickel sulfide deposits: classification, composition and genesis. *Econ. Geol*. **75th Anniversary Volume**, 628-685

NALDRETT A.J., 1989, Magmatic Sulfide Deposits. *Clarendon Press*, New York, 177 pp.

NALDRETT A.J., 1999, World-class Ni-Cu-PGE deposits: Key factors in their genesis. *Mineral. Deposita*, **34**, 227-240

NALDRETT A.J. & VON GRUENEWALDT G., 1989, The association of PGE's with chromite in layered intrusions and ophiolite complexes. *Econ. Geol*. **84**, 180-187

NALDRETT A.J., GASPARRINI E.C., BARNES S.J., VON GRUENEWALDT G. & SHARPE M.R., 1986, The Upper Critical Zone of the Bushveld Complex and the Origin of Merensky-type ores. *Econ. Geol*. **81**, 1105-1117

NASLUND H.R. & MCBIRNEY A.R., 1996, Mechanisms of formation of igneous layering *in* Layered Intrusions, Cawthorn R.G. (ed.) *Elsevier Science*. **1,** 1-43

NEX P.A., KINNAIRD J.A., INGLE L.J., VAN DER VYVER B.A. & CAWTHORN R.G., 1998, A new stratigraphy for the Main Zone of the Bushveld Complex, in the Rustenburg area. *S. Afr. J. Geol*. **101**, 215-223

NICHOLSON D.M & MATHEZ E.A. (1991). Petrogenesis of the Merensky Reef in the Rustenburg section of the Bushveld Complex. *Contrib. Min. Pet*. **107**, 293-309

PARSONS I. & BECKER S. M., 1987, Layering, compaction and post-magmatic processes in the Klokken intrusion *in* Origins of igneous layering. Parsons I. (ed.). Dordrecht, *Reidel Publishing Company* **196,** 29-92

PEACH C.L., MATHEZ E.A., KEAYS R.R. & REEVES S.J., 1994, Experimentally determined sulfide melt-silicate melt partition coefficients for iridium and palladium. *Chem. Geol*. **117**, 361-377

POLOVINA J.S. & HUDSON D.M., 2002, Petrography and geochemistry of post-magmatic hydrothermal alteration and mineralization in the J-M Reef, Stillwater Complex, Montana. *9th International Platinum Symposium Abstracts*, Billings, Monatana.

PREVEC S.A., ASHWAL L.D. & MKAZA M.S., 2005, *in press*, Mineral disequilibrium in the Merensky Reef, western Bushveld Complex, South Africa: new Sm-Nd isotopic evidence. *Contrib. Min. Pet.*

QUADLING K. & CAWTHORN R.G., 1994, The layered gabbronorite sequence, Main Zone, eastern Bushveld Complex. *S. Afr. Tydskr. Geol*. **97**, 442-454

ROLLINSON H. R., 1993, Using Geochemical Data: Evaluation, presentation, interpretation. Longman Scientific and Technical, *John Wiley & Sons Inc*. USA, 352 pp.

RICE A. & VON GRUENEWALDT G., 1995, Shear aggregation (convective scavenging) and cascade enrichment of PGEs and chromite in mineralized layers of large layered intrusions. *Min. and Pet*. **54**, 105-117

RIPLEY E.M., 1986, Application of stable isotopic studies to problems of magmatic sulfide ore genesis with special reference to the Duluth Complex, Minnesota *in* Geology and Metallogeny of Copper Deposits. Friedrich G., Genkin A.D., Naldrett A.J., Ridge J.D., Sillitoe R.H. & Vokes E.M. (eds.). *Springer-Verlag*, Berlin, 25-42

RIPLEY E.M. & ALAWI J.A., 1988, Petrogenesis of pelitic xenoliths at the Babbit Cu-Ni deposit, Duluth Complex, Minnesota, USA. *Lithos* **21**, 143-159

SCHOENBERG R., KRUGER F.J., NAGLER T.F., MEISEL T. & KRAMERS J.D., 1999, PGE enrichment in chromitite layers and the Merensky Reef of the western Bushveld Complex; a Re-Os Rb-Sr isotope study. *Earth Plan. Sci. Lett*. **172**, 46-64

SCHÜRMANN L.W., 1993, The geochemistry and petrology of the Upper Critical Zone of the Boshoek section of the western Bushveld Complex. *Geol. Surv. S. Afr. Bull.* **113**, 88 pp.

SCHÜRMANN L.W., GRABE P-J. & STEENKAMP C.J., 1998, Chromium *in* The Mineral Resources of South Africa. Wilson M.G.C. & Anhaeusser C.R. (eds.). *Council for Geosciences*, Handbook **18**, 90-105

SCOON R.N. & TEIGLER B., 1995, New LG-6 chromitite reserve at Eerste Geluk in the Boundary Zone between the central and southern sectors of the Eastern Bushveld Complex. *Econ. Geol*. **90,** 969-982

SCOON R.N & TEIGLER B., 1994, Platinum-group element mineralization in the Critical Zone of the western Bushveld Complex: 1. Sulfide-poor chromitites below the UG2. *Econ. Geol*. **89**, 1094-1121

SHARPE M.R., 1985, Strontium isotope evidence for preserved density stratification in the Main Zone of the Bushveld Complex, South Africa. *Nature*, **316**, 119-126

SHARPE M.R., 1981, The chronology of magma influxes to the eastern compartment of the Bushveld Complex as exemplified by its marginal border groups. *J. Geol. Soc. Lon*. **138**, 307-326

SOUTH AFRICAN COMMITTEE FOR STRATIGRAPHY (SACS), 1980, Stratigraphy of South Africa. Part 1: Lithostratigrpahy of the Republic of South Africa, South West Africa/Namibia and the Republics of Bophuthatswana, Transkei and Venda. *Geol. Surv. of S. Afr*. Hand Book **8**, 690 p.

SPARKS R.S.J., HUPPERT H.E. & TURNER J.S., 1984, The fluid dynamics of evolving magma chambers. *Phil. Trans R. Soc. Lon*. **A-310**, 511-534

STONE W.E., CROCKET J.H. & FLEET M.E., 1990, Partitioning of palladium, iridium and gold between sulfide liquid and basalt melt at 1200^{o}C. *Geochim. Cosmochim. Acta*. **54**, 2341-2344

TEPLEY F.J. III & DAVIDSON J.P., 2003, Mineral-scale Sr-isotope constraints on magma evolution and chamber dynamics in the Rum layered intrusion, Scotland. *Contrib. Min. Pet*. **145**. 628-641

TEIGLER B. & EALES H.V., 1996, The Lower and Critical Zones of the Western limb of the Bushveld Complex as intersected by the Nooitgedagt boreholes. *Geol. Surv. of S. Afri. Bul.*, **111**, 206 pp.

TEIGLER B., EALES H.V. & SCOON R.N., 1992, The cumulate succession in the Critical Zone of the Rustenburg Layered Suite at Brits, western Bushveld Complex. *S. Afr. J. Geol*. **95**, 17-28

TREDOUX M., LINDSAY N.M., DAVIES G. & MCDONALD I., 1995, The fractionation of platinum-group elements in magmatic systems with the suggestion of a novel causal mechanism. *S. Afr. J. Geol.* **98**, 157-167

VILJOEN M.J., 1999, The nature and origin of the Merensky Reef of the western Bushveld Complex based on geological facies and geophysical data. *S. Afr. J. Geol*. **102**, 1-19

VILJOEN M.J. & HIEBER R., 1986, The Rustenburg Section of Rustenburg Platinum Mines Limited, with reference to the Merensky Reef, *in* Mineral Deposits of Southern Africa. Annhaeusser C.R. & Maske S. (eds.) *Geol. Soc. S. Afr*., **II,** 1107-1134

VILJOEN M.J. & SCOON R.N., 1985, The distribution and main geological features of discordant bodies of iron-rich ultramafic pegmatite in the Bushveld Complex. *Econ. Geol*., **80**, 1109-1128

VILJOEN M.J., DE KLERK W.J., COETZER P.M., HATCH N.P., KINLOCH E.D. & PEYERL W., 1986a, The Union Section of Rustenburg Platinum Mines Limited with reference to the Merensky Reef. *in* Mineral Deposits of Southern Africa. Annhaeusser C.R. & Maske S. (eds.) *Geol. Soc. S. Afr*., **II**, 1061-1090

VILJOEN M.J. THERON J., UNDERWOOD B., WALTERS B.M., WEAVER J. & PEYERL W., 1986b, The Amandelbult Section of Rustenburg Platinum Mines Limited, with reference to the Merensky Reef *in* Mineral Deposits of Southern Africa. Annhaeusser C.R. & Maske S. (eds.) *Geol. Soc. S. Afr*., **II**, 1041-1060

VERMAAK C.F., 1976, The Merensky Reef - Thoughts on it's environment and genesis. *Econ. Geol*. **71**, 1270-1298

VON GRUENEWALDT G., 1973, The Main and Upper Zones of the Bushveld Complex in the Rossenekal area, Eastern Transvaal. *Trans. Geol. Soc. S. Afr*. **76**, 207-227

WAGER L.R. & BROWN G.M., 1968, Layered Igneous Rocks. Edinburgh, Oliver & Boyd, 558 pp.

WAGER L.R., BROWN G.M. & WADSWORTH W.J., 1960, Types of igneous cumulates. *J. Pet*. **1**, 73-85.

WAGNER P.A., 1929, Platinum deposits and mines of South Africa. *Struik*, Cape Town, 358 pp.

WALRAVEN F., ARMSTRONG R.A. & KRUGER F.J., 1990, A chronostratigraphic framework for the north-central Kaapvaal Craton, the Bushveld Complex and the Vreefort structure. *Tectonophys*., **171**, 23-48

WHITE, W.M., 2001, Geochemistry. Unpublished on-line text book

WHITE, W.M., 1994, The Potgietersrus project geology and exploration history. Proceedings 15th CMMI Congress. *S. Afr. Inst. Min. Metall*., 173-182

WIEBE R.A., 1991, Commingling of contrasted magmas and generation of mafic enclaves in granitic rocks *in* Enclaves and Granite Petrology. Didier J., & Barbarin B. (eds.), Developments in Petrology **13**, *Elsevier Science B.V*., Amsterdam Chapter 29, 393 - 402

WILLMORE C.C., BOUDREAU A.E. & KRUGER J.F., 2000, The halogen geochemistry of the Bushveld Complex, Republic of South Africa: implications for chalcophile element distribution in the Lower and Critical Zones. *J. Pet.* **41**, 1517-1539

WILSON A.H., 1992, The geology of the Great Dyke, Zimbabwe: Crystallization, layering and cumulate formation in the P1 pyroxenite of Cyclic Unit 1 of the Darwendale Subchamber. *J. Pet.*, **33**, 611-663

WILSON A.H., LEE C.A. & BROWN R.T., 1999, Geochemistry of the Merensky Reef, Rustenburg Section, Bushveld Complex: controls on the silicate framework and distribution of trace elements. *Mineral. Deposita*, **34**, 657-672

WORST B.G., 1986, The chromite deposits of the Montrose and Groothoek mines, eastern Bushveld Complex *in* Mineral Deposits of Southern Africa, Anhaesseur C.R., & Maske S. (eds.), *Geol. Soc. S. Afr*. Johannesburg **II**, 1189-1195

WRIGHT C., KWADIBA M.T.O, KGASWANE E.M & NGUURI T.K., 2003, Variations in crustal thickness and uppermost mantle structure across the Kaapvaal Craton from Pn and Sn arrivals and receiver functions. *S. Afr. J. Geol*. **99**, 447-452

APPENDIX I: Core logs of RM15, KV5854, EG5 and KF35, with core descriptions and sample locations

Richmond, southern sector, eastern Bushveld Complex (RM15, RM17)

Height (m) above base of Merensky pyroxenite	Lithology and description of core	Correlation	Samples
Hand Samples			
448	medium-grained gabbronorite with poikilitic clinopyroxene	Poikilitic gabbronorite	RM15 – 5
441	medium-grained gabbronorite with poikilitic clinopyroxene	Poikilitic gabbronorite	RM15 – 3
413	medium-grained gabbronorite with poikilitic clinopyroxene	Poikilitic gabbronorite	RM15 – 4
396	medium-grained gabbronorite with poikilitic clinopyroxene	Poikilitic gabbronorite	RM15 – 2
387	medium-grained gabbronorite with poikilitic clinopyroxene	Poikilitic gabbronorite	RM15 – 1
364	medium-grained gabbronorite		RM15 – 6a
364	fine-grained gabbronorite		RM15 – 6b
RM17 core			
241.38 – 252.78	medium-grained norite		75.95
236.79 – 241.38	medium-grained lecuonorite, gradational upper contact		
221.85 – 236.79	medium-grained norite, gradational upper contact		93.94
221.60 – 221.85	medium-grained feldspathic pyroxenite		
214.72 – 221.60	medium-grained norite		107.89
172.80 – 214.72	heterogeneous medium-grained norite, some small clinopyroxene mottles and a few 2-5cm anorthosite layers		124.53, 136.98
168.99 – 172.80	very fine-grained mafic dyke intrusion		
151.50 – 168.99	fine-grained norite		159.73, 164.10
147.87 – 151.50	leuconorite, few clinopyroxene mottles towards top		174.30
140.10 – 147.87	medium-grained norite, few mottles towards base		
139.71 – 140.10	spotted anorthosite, porphyritic orthopyroxene		
134.60 – 139.71	medium-grained norite, few mottles towards top		185.92
130.81 – 134.60	mottled anorthosite, clinopyroxene mottles with some plagioclase overgrowths		
129.51 – 130.81	anorthosite, occasionally mottled, gradational upper contact		
123.62 – 129.51	medium-grained leuconorite		200.19
120.13 – 123.62	fine-grained norite, gradational upper contact		
116.41 – 120.13	medium-grained leuconorite, gradational upper contact		
110.83 – 116.41	mottled anorthosite, mottles decrease in size upwards		211.47
104.51 – 110.83	spotted anorthosite, porphyritic orthopyroxene, occasional clinopyroxene mottles		
104.05 – 104.51	mottled anorthosite		
98.59 – 104.05	spotted anorthosite, porphyritic orthopyroxene		222.45
88.13 – 98.59	medium-grained norite		232.27
67.65 – 88.13	spotted anorthosite, porhpyritic orthopyroxene, few “blotchy” orthopyroxene and clinopyroxene mottles		250.11
RM15 core			
129.46 – 129.80	medium-grained norite		30.12, 30.28
129.14 – 129.46	medium-grained melanorite		30.47
128.08 – 129.14	medium-grained norite		31.61
115.35 – 128.08	spotted anorthosite, porphyritic orthopyroxene		38.08, 44

Height (m) above base of Merensky pyroxenite	Lithology and description of core	Correlation	Samples
114.68 – 114.35	medium-grained melanorite		44.78
107.80 – 114.68	medium-grained norite		45.57, 45.72, 51.69
66.65 – 107.80	spotted anorthosite, porphyritic orthopyroxene, some faint mottles between 104 – 98.3m		59.35, 66.81, 74.18, 81.18, 89.83
39.54 – 66.65	mottled anorthosite, small, sometimes faint mottles	UGMA	98.44, 105.04, 112.23, 119.88
34.38 – 39.54	spotted anorthosite, porphyritic orthopyroxene, some leuconorites with finer grained orthopyroxene, occasional thin mottled sections	GMMA	123.24, 125.52
18.50 – 34.38	mottled anorthosite, pink tinted, with distinct large mottles, anorthositic section between 28.77 – 31.9m	LGMA	132.23, 140
16.18 – 18.50	medium-grained norite		
15.14 – 16.18	leuconorite, small patch of alteration at base		145.76
13.31 – 15.14	anorthosite, few “blotchy” mottles		
6.34 – 13.31	melanorite, increasingly feldspathic upwards, then grades back into melanorite towards the top. 1 grain thick chromitite at basal contact	Bastard pyroxenite	146.9, 149.62, 151.53, 151.53, 153.2, 153.46, 153.55
2.75 – 6.34	mottled anorthosite, disseminated-sulphide bearing, ovoid inclusions of sulphides in a patch of spotted anorthosite		153.61, 154.37 160.09, 160.28
0 – 2.75	medium-grained feldspathic pyroxenite, disseminated sulphide-bearing. 3-4mm thick chromitite at base	Merensky pyroxenite	160.48, 160.73, 160.83, 161.03, 161.22, 161.42, 161.62, 161.82, 161.98, 162.26, 162.38, 162.57, 162.76, 162.98
-4.59 – 0	medium-grained leuconorite		163.18
-5.62 – -4.59	mottled anorthosite		
-15.10 – -5.62	leuconorite, gradational upper contact		169.1
-29.48 – -15.10	mottled anorthosite, with a few small norite patches		175.94, 182.58, 189.16
-112.10 – -29.48	homogeneous, medium-grained norite		202.98, 209.28, 216.1, 223.35, 230.3, 237.58, 244.23, 252.3, 259.27, 266
-115.12 – -112.10	mottled anorthosite, few porphyritic orthopyroxene spots		274.09
-149.67 – -115.12	medium-grained norite, gradational upper contact		281.86, 288.6, 295.29, 296.14, 302.66, 309.2
-156.32 – -149.67	medium-grained leuconorite, gradational upper contact		316.43, 323
-164.39 – -156.32	mottled anorthosite, gradational upper contact		
-167.44 – -164.39	medium-grained feldspathic pyroxenite	UG2 pyroxenite	
-167.96 – -167.44	pegmatoidal feldspathic pyroxenite, olivine- and sulphide-bearing. Some alteration. 2cm chromitite at base		
-168.2 – -167.96	medium-grained feldspathic pyroxenite		
-168.26 – -168.2	feldspathic chromitite		
-169.55 – -168.26	medium-grained feldspathic pyroxenite		
-169.99 – -169.55	feldspathic chromitite	UG2 chromitite	
-170.08 – -169.99	pegmatoidal feldspathic pyroxenite		
-170.57 – -170.08	heterogeneous medium-grained norite parting		
-170.67 – -170.57	feldspathic chromitite		
-171.98 – -170.67	pegmatoidal feldspathic pyroxenite		331.47
-184.04 – -171.98	feldspathic pyroxenite, some cm-scale feldspathic layering		338, 342.92

Kennedy's Vale, southern sector, eastern Bushveld Complex (KV5854)

Height (m) above base of Merensky pyroxenite	Lithology and description of core	Correlation	Samples
KV5854 core			
113.31 – 118.05	medium-grained norite		179.94
110.37 – 118.05	mottled anorthosite, large mottles		
98.65 – 110.37	mottled anorthosite, very small mottles		185.73, 188.93, 192.00, 196.89
85.05 – 98.65	medium-grained norite, gradational upper contact with overlying mottled anorthosite		198.23, 210.93
44.53– 85.05	mottled anorthosite, small mottles, mottles less dense towards base	UGMA	213.28, 229.39, 242.74, 250.53
41.15 – 44.53	spotted anorthosite, porphyritic orthopyroxene, occasional small mottles	GMMA	254.90
26.20 – 41.15	mottled anorthosite, distinct large mottles, slight pink tint in plagioclase, sulphide patch at 38.05m	LGMA	255.07
22.10 – 26.20	medium-grained norite		
20.25 – 22.10	medium-grained feldspathic pyroxenite	Bastard pyroxenite	
12.89 – 20.25	medium-grained norite		282.88
12.86 – 12.89	feldspathic pyroxenite, disseminated sulphide-bearing	Lower Bastard pyroxenite	
7.38 – 12.86	mottled anorthosite		283.99
6.84 – 7.38	anorthosite, occasional faint mottles		
5.00 – 6.84	mottled anorthosite		289.22
4.33 – 5.00	medium-grained norite, gradational upper contact		291.71
0 – 4.33	medium-grained feldspathic pyroxenite, gradational contact with overlying norite	Merensky pyroxenite	292.25, 292.63, 292.82, 293.05, 293.28, 293.50, 293.74, 293.94, 294.13, 294.35, 294.44, 294.83, 295.05, 295.21, 295.36, 295.56, 295.75, 295.94
-0.07 – 0	pegmatoidal feldspathic pyroxenite		296.10
-31.55 – -0.07	homogeneous medium-grained norite		296.40, 307.40
-36.77 – -31.55	medium-grained leuconorite, becoming anorthositic upwards, sharp boundary with overlying norite		327.69
-39.45 – -36.77	mottled anorthosite, slightly gradational upper contact		335.50
-56.64 – -39.45	medium-grained norite, becoming increasingly mafic upwards, some felsic banding towards base		335.68, 352.53
-112.95 – -56.64	medium-grained melanorite, green alteration of plagioclase between –69.99 – -68.47m		352.85, 353.24, 367.28, 378.90, 388.85, 404.41
-172.95 – -112.95	medium-grained norite, very gradational upper contact with melanorite, green alteration of plagioclase between –115.25 – -1121.95m		421.80, 428.94, 438.41, 448.43, 460.59, 468.41
-173.09 – -172.95	Quartz		
-173.69 – -173.09	medium-grained leuconorite		
-187.36 – -173.69	medium-grained norite, gradational upper contact		480.29
-190.09 – -187.36	medium-grained leuconorite		
192.47 – -190.09	heterogeneous medium-grained norite, varying orthopyroxene content		487.78
-195.70 – -192.47	spotted anorthosite, porphyritic orthopyroxene		
-198.56 – -195.70	mottled anorthosite		494.61
-200.69 – -198.56	feldspathic pyroxenite, sulphide-bearing, highly fractured, 3-5mm chromitite stringers at -198.95 and –300.48m	UG2 pyroxenite	

Height (m) above base of Merensky pyroxenite	Lithology and description of core	Correlation	Samples
-200.77 – -200.69	feldspathic chromitite		
-200.98 – -200.77	pegmatoidal feldspathic pyroxenite		497.02
-201.69 – -200.98	feldspathic chromitite, two thin internal partings of pegmatoidal feldspathic pyroxenite	UG2 chromitite	
-203.70 – -201.69	pegmatoidal feldspathic pyroxenite, olivine- and sulphide-bearing		
-205.15 – -203.70	mottled anorthosite		
-205.27 – -205.15	pegmatoidal feldspathic pyroxenite		
-205.95 – -205.27	mottled anorthosite		502
-206.35 – -205.95	medium-grained norite		
-206.95 – -206.35	anorthosite, 2mm thick faulted Cr stringer at -206.57m		
-215.95 – -206.95	homogenous medium-grained norite		507

Eerste Geluk, central sector, eastern Bushveld Complex (EG5)

Height (m) above base of Merensky pyroxenite	Lithology and description of core	Correlation	Samples
EG5 core			
131.68 – 261.38	heterogeneous medium-grained norite of varying othopyroxene proportions		43.24, 82.47, 136.86
124.93 – 131.68	mottled anorthosite, spotted with cumulus orthopyroxene towards the base		160.83
99.82 – 124.93	medium-grained norite		172.34, 175.29, 186.22, 186.58,
98.17 – 99.82	spotted anorthosite, porhpyritic orthopyroxene		
94.28 – 98.17	medium-grained norite, occasionally spotted with porphyritic orthopyroxene and gradually becomes mottled towards the upper contact		
85.60 – 94.28	medium-grained leuconorite		203.98
75.01 – 85.60	medium-grained norite, gradational upper contact		211.83
70.07 – 75.01	pegmatoidal pyroxenite		
66.12 – 70.07	medium-grained norite		224.35
65.34 – 66.12	pegmatoidal pyroxenite, 1cm thick chromitite at 65.38m and a 1mm stringer above it		
61.00 – 65.34	medium-grained norite		
51.15 – 61.00	mottled anorthosite, small mottles, gradational upper contact with overlying norite	UGMA	EG6 147
38.33 – 51.15	pegmatoidal pyroxenite		
38.14 – 38.33	anorthosite, 1cm thick chromitite at 38.31m		
35.21 – 38.14	spotted anorthosite, occasionally mottled	GMMA	EG6 162.84, 165.85
27.93 – 35.21	mottled anorthosite, distinct large mottles	LGMA	EG6 174.75
24.56 – 27.93	pegmatoidal pyroxenite		
21.33 – 24.56	medium to coarse-grained norite		
20.34 – 21.33	medium to coarse-grained feldspathic pyroxenite		
19.53 – 20.34	pegmatoidal pyroxenite		
19.46 – 19.53	medium-grained norite		
19.45 – 19.46	chromitite		
19.35 – 19.45	pegmatoidal pyroxenite		
18.61 – 19.35	medium-grained norite		
12.57 – 18.61	feldspathic pyroxenite	Bastard pyroxenite	279.0
9.42 – 12.57	mottled anorthosite		279.25, 281.96
9.30 – 9.42	medium-grained norite		
8.51 – 9.30	feldspathic pyroxenite, becoming increasing feldspathic upwards and grades into the overlying norite	Lower Bastard pyroxenite	
8.37 – 8.51	feldspathic chromitite		
0 – 8.37	feldspathic pyroxenite, slightly pegmatitic in places, becomes increasingly feldspathic upwards	Merensky pyroxenite	286.29, 287.88
-0.04 – 0	anorthosite, occasional splotches of disseminated Cr		
-0.13 – -0.04	feldspathic pyroxenite		
-1.56 – -0.13	pegmatoidal pyroxenite		
-3.99 – -1.56	feldspathic pyroxenite		
-4.06 – -.399	medium-grained norite, gradational upper contact		
-5.7 – -4.06	pegmatoidal pyroxenite, sulphide-bearing		
-20.2 – -5.7	medium-grained norite, becoming finer-grained upwards		
-23.60 – -20.2	medium-grained melanorite		313.94
-23.76 – -23.60	medium-grained leuconorite		

Height (m) above base of Merensky pyroxenite	Lithology and description of core	Correlation	Samples
-27.04 – -23.76	medium-grained melanorite		
-55.58 – -27.04	medium-grained norite		
-64.52 – -55.58	coarse-grained norite, large amounts of interstitial clinopyroxene, giving blotchy appearance, some patches with little orthopyroxene		353.62
-100.18 – -64.52	fine-grained norite, abrupt upper contact with overlying coarse-grained norite		384.5, 391.71
-194.50 – -100.18	medium-grained norite		392.16, 414.13, 437.36, 452.5, 463.61
-194.52 – -194.50	chromitite	UG3?	
-196.12 – -194.52	medium-grained melanorite		
-273.79 – -196.12	medium-grained norite, occasional 1-5cm thick pure anorthosite bands, gradational upper contact		495.84, 532.16, 549.79
-276.36 – -273.79	mottled anorthosite, occasional mm thick Cr stringers		
-276.55 – -276.36	medium-grained norite		
-277.89 – -276.55	mottled anorthosite		568.73
-277.99 – -277.89	medium-grained norite		
-282.36 – -277.99	medium-grained feldspathic pyroxenite, becoming increasingly coarse-grained upwards		
-282.72 – -282.36	fine-grained harzburgite with serpentinised olivine		
-282.81 – -282.72	feldspathic chromitite		
-284.87 – -282.81	medium-grained feldspathic pyroxenite, several 1-5mm thick Cr stringers towards base of pyroxenite	UG2 pyroxenite	
-285.16 – -284.87	feldspathic chromitite	UG2 chromitite	
-287.51 – -285.16	medium-grained feldspathic pyroxenite		577.54

Klipfontein, central sector, eastern Bushveld Complex (KF35)

Height (m) above base of Merensky pyroxenite	Lithology and description of core	Correlation	Samples
359.70 – 520.40	medium-grained gabbronorite, poikilitic clinopyroxene	Poikilitic gabrronorite	72.06, 118.41, 188.97
358.7 – 359.7	spotted anorthosite, porphyritic orthopyroxene		
212.00 – 358.7	medium-grained norite		
314.7 – 337.7	medium-grained leuconorite, very gradational upper contact with overlying norite		223.77
123.7 – 314.7	fine-grained norite, very gradational upper contact with overlying leuconorite, "needle norite" with elongate laths of orthopyroxene (±5mm) between 269.7 - 279.7m		273.95, 301.14, 331.16, 343.73, 371.68, 416.13
116.7 – 123.7	spotted anorthosite, porphyritic orthopyroxene		
114.7 – 116.7	medium-grained norite		434.49
104.2 – 114.7	spotted anorthosite, porphyritic orthopyroxene		436.83
80.7 – 104.2	medium-grained norite		455.20
69.9 – 80.7	dolerite dyke		
507 – 69.9	medium-grained norite		503.96
28.7 – 42.7	spotted anorthosite, porphyritic orthopyroxene	UGMA?	
26.4 – 28.7	spotted anorthosite, porphyritic orthopyroxene and occasional mottles	GMMA	
16.5 – 26.4	mottled anorthosite, distinctly large mottles	LGMA	526.82, 529.17, 532.6*
15.6 – 16.5	medium-grained norite		
15.2 – 15.6	pegmatoidal feldspathic pyroxenite		534.1*
10.6 – 15.2	medium-grained feldspathic pyroxenite	Bastard pyroxenite	534.5*, 534.65*, 538.8*
7.4 – 10.6	mottled anorthosite		542.25*
1.3 – 7.4	spotted anorthosite		544.63*, 547.06*
1.1 – 1.3	pegmatoidal feldspathic pyroxenite		
0 – 1.1	medium-grained feldspathic pyroxenite	Merensky pyroxenite	
-0.87 – 0	medium-grained norite		550.6*
-9.3 – -0.87	pegmatoidal pyroxenite		
-23.4 – -9.3	medium-grained leuconorite		559.15*, 573.1*
-53.3 – -23.4	medium-grained homogeneous norite		573.55*, 602.7*
-75.3 – -53.3	medium-grained leuconorite		616.4*
-122.3 – -75.3	medium-grained homogenous norite		625.15*, 648.1*, 653.1*, 653.25*, 653.33*
-127.3 – -122.3	medium-grained melanorite		672.2*, 672.36*
-156.2 – -127.3	medium-grained homogenous norite		677.2*, 690.6*, 690.76*, 699.1*, 701.2*, 702.4*
-159.4 – -156.2	mottled anorthosite		706.2*
-162.1 – -159.4	spotted anorthosite, porphyritic orthopyroxene		711.4*
-163.3 – -162.1	medium-grained norite		712.25*
-179.2 – -163.3	medium-grained leuconorite		722.75*, 725.15*
-193.5 – -179.2	medium-grained norite		729.05*, 740.5*, 742.6*
-231.3 – -193.5	pegmatoidal feldspathic pyroxenite		
238.0 – -231.3	medium-grained norite		781.7*, 786.3*
-242.8 – 238.0	pegmatoidal feldspathic		
-268.7 – -242.8	spotted anorthosite, porphyritic orthopyroxene		792.65*, 797*, 817.12*, 817.31*
-271.3 – -268.7	medium-grained leuconorite		820.36*

Height (m) above base of Merensky pyroxenite	Lithology and description of core	Correlation	Samples
-275.3 – -271.3	porphyritic feldspathic pyroxenite		824.28*
-276.8 – -275.3	harzburgite		
-276.83 – -276.8	feldspathic chromitite	UG3A chromitite	
-277.3 – -276.83	harzburgite		826.65*
-288.6 – -277.3	porphyritic feldspathic pyroxenite		827.8*, 837.5*,
-288.67 – -288.6	feldspathic chromitite	UG3 chromitite	
-282.9 – -288.67	mottled anorthosite		838.69*, 839.43*, 839.58*
-290.9 – -289.9	medium-grained norite		
-302.4 – -290.9	medium-grained melanorite		852.1*
-312.1 – -302.4	medium-grained feldspathic pyroxenite	UG2 pyroxenite	860.5*
-312.9 – -312.1	feldspathic chromitite	UG2 chromitite	
-313.8 – -312.9	harzburgite		863.1*
-315.8 – -313.8	porphyritic feldspathic pyroxenite		
-317.8 – -315.8	mottled anorthosite		865.7*, 867.25*
-319.8 – -317.8	medium-grained norite		868.85*

* samples collected and analysed by Blumberg (2002)

APPENDIX II: Analytical techniques and standards

Sampling procedure

Core was selected on the basis of minimal weathering and faulting. Half core samples from all the boreholes were analysed, except for the section of the Merensky Reef, where only quarter core was available. The sampling interval depended on lithological characteristics and ranged from over 7m down to 20cm. Where possible, lithological contacts were sampled. The entire thickness of the Merensky Reef from boreholes RM15 and KV5854 was sampled.

Whole-rock analysis

Half-core from 4 boreholes (RM15, KV5854, EG5 and KF35) was crushed coarsely in a jaw crusher (University of the Witwatersrand) and split into two equal proportions. Half was crushed finely, to the consistency of flour, using a tima mill. The other half of the sample was retained for mineral separate analysis. Using the milled sample, pressed powder pellets were made for trace element analysis and tetraborate fusion disks were made for major element analysis. Standards used in XRF analyses and analytical precision are detailed in the following pages.

In addition, a sub-set of 10 samples (tables A and B) was sent for independent XRF analysis to ensure consistency with XRF analyses performed at the University of the Witwatersrand. Graphs of elements concentrations from the University of the Witwatersrand plotted against those from the external laboratory show a good correlation between the two data sets (figure A). These results demonstrate that element values determined in this study are accurate and repeatable. In addition, this indicates that the data presented here is comparable with that from other studies in the western Bushveld Complex.

Sample number	Fe2O3 wt %	MnO wt %	Cr2O3 wt %	V2O5 wt %	TiO2 wt %	CaO wt %	K2O wt %	P2O5 wt %	SiO2 wt %	AL2O3 wt %	MgO wt %	Na2O wt %	L.O.I wt %
RM15 30.28	10.3	0.19	0.10	0.01	0.19	7.80	0.37	<0.01	53.2	11.3	15.9	1.1	0.15
RM15 81.18	6.61	0.10	0.03	0.01	0.28	11.3	0.47	0.05	52.0	21.7	4.8	1.6	1.19
RM15 132.23	2.51	0.03	0.03	<0.01	0.12	14.1	0.25	0.01	50.3	28.6	2.0	1.8	0.45
RM15 140	3.25	0.05	0.02	0.01	0.15	14.1	0.57	<0.01	48.5	26.1	2.7	1.8	2.38
RM15 160.28	4.32	0.06	0.07	0.01	0.13	12.0	0.32	<0.01	50.6	24.1	4.4	2.1	0.55
RM15 162.76	10.7	0.18	0.66	0.02	0.22	4.38	0.41	<0.01	53.6	5.9	22.6	0.7	0.55
RM15 237.58	5.79	0.09	0.13	<0.01	0.14	10.4	0.09	0.01	53.1	20.1	11.2	1.3	0.60
RM15 244.23	5.93	0.10	0.14	0.01	0.13	9.90	0.12	<0.01	51.3	18.9	11.4	1.3	0.49
RM15 252.3	5.49	0.10	0.14	0.01	0.13	10.5	0.17	0.01	52.1	20.2	11.0	1.2	0.68
RM15 259.27	5.33	0.10	0.13	0.01	0.13	10.5	0.11	<0.01	51.6	20.4	10.4	1.3	0.54

TABLE A. Whole-rock major element XRF analyses of RM15 subset from independent laboratory.

	Co ppm	Cu ppm	Ni ppm	Zn ppm	V ppm	Cr ppm	Rb ppm	Sr ppm	Y ppm	Zr ppm
RM15 30.28	63	<18	367	74	137	950	11	159	10	<10
RM15 81.18	44	<18	119	58	90	281	23	374	11	23
RM15 132.23	13	<18	65	38	<10	286	25	580	<10	<10
RM15 140	16	<18	111	63	87	247	37	528	10	<10
RM15 160.28	28	415	472	61	77	702	94	329	<10	21
RM15 162.76	63	461	1074	83	163	6599	76	59	<10	16
RM15 237.58	39	<18	248	50	47	1276	19	380	<10	<10
RM15 244.23	46	<18	284	51	54	1370	20	366	<10	<10
RM15 252.3	48	<18	285	52	61	1391	21	378	<10	<10
RM15 259.27	47	<18	255	52	51	1289	22	402	<10	<10

TABLE B. Whole-rock trace element XRF analyses of RM15 subset from independent laboratory.

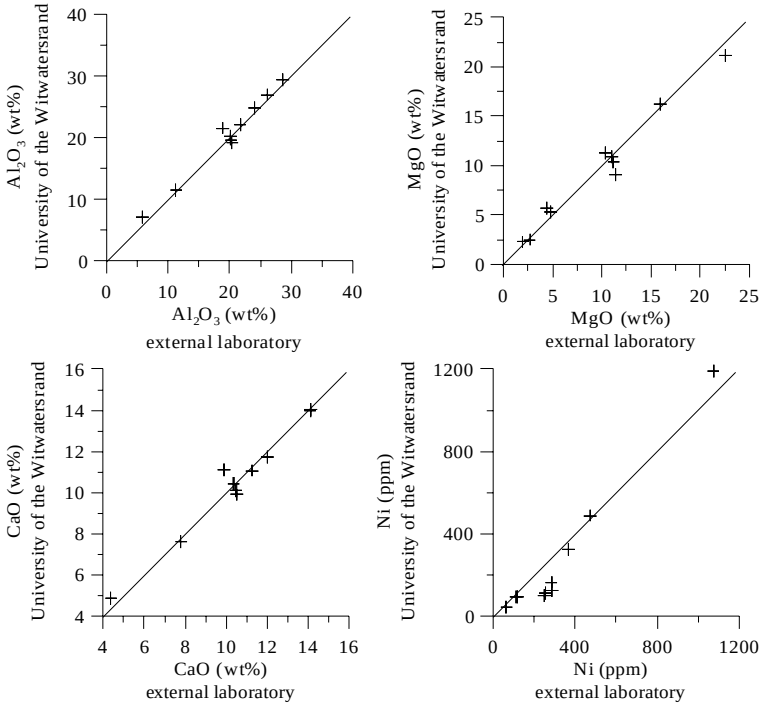


FIGURE A. Comparison of samples analysed by both the University of the Witwatersrand and an external laboratory.

Mineral separates analysis

The remaining half of the coarsely crushed samples was milled gradually and sieved to a size fraction of between 90-150μm. This material was then washed with water to remove fines and dried in pans at 100^{o}C. Magnetic material such as magnetite was removed using a hand magnet. Samples were then run through an electromagnetic separator at varying settings to obtain pure plagioclase, orthopyroxene and infrequently clinopyroxene mineral separates. Purity was established visually using a binocular microscope. Each separate was then ground to a flour-like consistency using a motorised agate mortar and pestle to prevent contamination. The separates were then analysed for major and trace elements as per the whole rock analyses.

Strontium isotope analysis

Approximately 0.1g of plagioclase grains, 90-150μm in size, was retained for strontium isotope analysis. This material was hand picked to remove cloudy, impure or composite grains and washed with acetone to remove other external contaminants.

Approximately 0.05g of the dried sample was added to a cleaned Teflon beaker to which Rb and Sr spikes were added. Spikes used were ^{84}Sr (99%) and 99% Rb. Samples were then covered and dissolved over a hot plate in a mixture of concentrated hydrofluoric acid (HF) and 8N nitric acid (HNO_3). Once the samples had totally dissolved the lids of the beakers were removed and they were returned to the hot plate to evaporate the silica. Once dry, the residue was redissolved in 2.5N hydrochloric acid (HCl) and transferred to small Teflon tubes that were placed in a centrifuge for 10 minutes at 7000 rpm. Bulk separation of Sr was achieved by standard cation-exchange chromatography techniques in quartz-glass columns with Bio-Rad AG50W 8x200-200 mesh cation exchange resin. The columns were eluted with 31ml of 2.5N HCl, of which the last 7ml was collected and dried. Sr extracted from the original samples was retained in the remaining portion. Samples of Sr and Rb were then loaded onto single and double filaments respectively. Sr was analysed using a Thermal Ionisation Mass Spectrometer (TIMS) VG354 multi-collector instrument and Rb on a MM30 solid-source mass spectrometer at the Hugh Allsopp Laboratory, University of the Witwatersrand. Sr isotopic data were normalised to ^{86}Sr/^{88}Sr = 0.1194. Runs of SRM-987 $SrCo_3$ standard yielded an ^{87}/^{86}Sr ratio of

0.7102320. Total procedural blanks were less than 1ng for Sr and <500 pg for Rb. The present day $^{87}Sr/^{86}Sr$ ratio was measured and was used to determine the initial Sr isotope ratio at the time of the intrusion using the following formula with and intrusion date of 2050.

$$^{87}Sr/^{86}Sr_{(initial)} = {}^{87}Sr/^{86}Sr_{(present)} - [(^{87}Sr/^{86}Sr) * (e\lambda^{t}-1)]$$

where: $^{87}Sr/^{86}Sr_{(initial)}$ = initial ratio

$^{87}Sr/^{86}Sr_{(present)}$ = present-day ratio (measured)

e = constant

$\lambda = 1.42*10^{-11}$

$t = 2050*10^{6}$

2 se is given for the measured $^{87}Sr/^{86}Sr$ ratio and this error is taken into consideration for calculating the initial Sr isotope ratio, from which 2 sigma is calculated.

Sulphur analysis

Sulphur analyses were undertaken on powdered whole rock samples using a LECO CS244 infra-red spectrometer and an induction furnace in an oxygen atmosphere at 1340^{o}C. Inconsistent results were obtained on blank samples where an accelerator was used, thus an accelerator was not used on the samples reported here. Standard samples of coal at 0.93% S and 1.21%S were used to calibrate the machine. Using a blank and internal sampling regime, a lower detection limit of 10 ppm (3-sigma) was calculated. Reproducibility was poor at low concentrations of sulphur and 21% at 60ppm.

Standards used for calibration of PW1400 XRFS for silicate analysis

A rhodium X-ray tube was used and was run at 50 KV and 50 mA. The method used was based on Norrish K. and Hutton J. T. "An accurate X-Ray spetrographic method for the analysis of a wide range of geological samples", Geochimica and Cosmochimica Acta, 1969, v. 33, p. 431-453, with technological improvements being implemented by the University of the Witwatersrand. Accepted values are as follows.

Standard	**%Fe_2O_3**	**%MnO**	**%TiO_2**	**%CaO**	**%K_2O**	**%P_2O_5**	**%SiO_2**	**%Al_2O_3**	**%MgO**	**%Na_2O**	**%LOI**	**Total**
NIM-G	2.02	0.02	0.00	0.79	5.03	0.01	76.31	12.18	0.06	3.39	0.45	100.42
NIM-S	1.41	0.01	0.00	0.68	15.40	0.12	63.85	17.40	0.46	0.43	0.28	99.70
NIM-N	8.96	0.18	0.20	11.49	0.25	0.03	52.57	16.48	7.49	2.46	-0.40	99.83
NIM-D	16.87	0.22	0.02	0.28	0.01	0.01	38.66	0.30	43.18	0.04	-0.93	99.42
NIM-P	12.77	0.22	0.2	2.67	0.09	0.02	51.39	4.20	25.47	0.37	-0.84	96.03
AN-G	3.39	0.04	0.22	16.03	0.13	0.01	46.67	30.04	1.81	1.64	0.65	99.84
AC-E	2.54	0.06	0.11	0.34	4.51	0.01	70.63	14.76	0.03	6.57	0.37	99.53
MA-N	0.47	0.04	0.01	0.59	3.19	1.40	66.86	17.69	0.04	5.86	1.82	97.60
AGV-1	6.79	0.10	1.06	4.96	2.91	.48	59.48	17.22	1.54	4.27	1.59	100.01
FK-N	0.09	0.01	0.02	0.11	12.88	0.02	65.37	18.71	0.01	2.59	0.54	99.82
BHVO-1	12.15	0.17	2.69	11.33	0.52	0.27	49.61	13.71	7.18	2.25	-0.71	99.82

Standards used for calibration of PW1400 XRFS for trace element analysis

A rhodium X-ray tube at 60Kv and 40mA was used for trace element analyses. The method was based on the paper by Feather C. E. and Willis J. P. entitled "A simple method for background and matrix correction of spectral peaks in trace element determination by X-Ray fluorescence spectrometry", published in X-Ray Spectrometry, 1976, v. 5, p. 41-48.

Standard	**Rb (ppm)**	**Sr (ppm)**	**Y (ppm)**	**Zr (ppm)**	**Nb (ppm)**	**Co (ppm)**	**Ni (ppm)**	**Cu (ppm)**	**Zn (ppm)**	**%TiO_2**	**V (ppm)**	**Cr (ppm)**	**Ba (ppm)**
AGV-1	67	662	21	225	15	15	17	60	88	1.06	123	12	1221
GA	175	310	21	150	12	5	7	16	80	0.38	38	12	840
GH	390	10	75	150	85	1	3	14	85	0.08	5	6	20
G-2	170	478	11	300	13	5	5	11	85	0.49	36	9	1880
NIM-G	325	10	143	300	53	0	8	12	50	0	2	12	120
NIM-S	530	62	1	20	0	3	7	19	10	0	10	12	2420
NIM-P	4	32	5	15	0	110	555	18	100	0.2	230	23950	46
NIM-N	5	260	7	14	0	58	120	14	68	0.2	220	30	102
NIM-L	190	4600	22	11000	960	2	2	13	395	0.48	81	10	450
NIM-D	0	3	0	8	0	208	2040	10	90	0.02	40	2870	10
Pcc-1	0	0	0	0	1	110	2400	10	42	0.01	30	2730	1
BR	47	1320	30	250	98	52	260	72	160	2.6	235	380	1050
BHVO-1	11	403	28	179	19	45	121	136	105	2.71	317	289	139
MAG-1	149	146	28	126	12	20	53	30	130	0.75	140	97	479
SGR-1	83	420	13	53	5	12	29	66	74	0.26	128	30	290
SCO-1	112	174	269	160	11	11	27	29	103	0.63	131	68	570
QLO-1	74	336	24	185	10	7	6	29	61	0.62	54	3	1370
STM-1	118	700	46	1210	268	1	3	5	235	0.14	9	4	560
RGM-1	149	108	25	219	9	2	4	12	32	0.27	13	4	807

SDC-1	127	183	40	290	18	18	38	30	103	1.01	102	64	630
DR-N	73	400	28	125	8	35	15	50	145	1.09	220	42	385
GS-N	185	570	19	235	21	65	34	20	48	0.68	65	55	1400
MICA-FE	2200	5	50	800	270	23	35	5	1300	2.5	135	90	150
MICA-MG	1300	27	0	20	120	24	110	4	290	1.63	90	100	4000
FK-N	860	39	0	13	0	16	3	2	10	0.02	3	5	200
BX-N	10	110	114	520	58	35	190	18	75	2.37	310	290	34
DT-N	5	27	10	370	0	12	16	9	28	1.4	150	240	130
UB-N	6	10	3	8	0	100	2000	28	85	0.11	75	2300	30
GXR-1	14	259	0	38	1	8	41	1110	760	0.06	76	13	680
GXR-2	78	160	17	269	11	9	21	76	530	0.5	52	36	2240
GXR-3	92	950	15	63	2	43	60	15	207	0.17	42	19	5000
GXR-4	160	221	14	186	10	15	42	6520	73	0.48	87	64	1640
GXR-6	90	35	14	110	8	14	27	66	118	0.83	186	96	1300
GSP-1	254	234	29	530	26	7	10	34	103	0.66	53	13	1310
MA-N	3600	84	1	27	173	1	3	140	220	0.01	5	3	42
AN-G	0	76	8	15	2	25	35	19	20	0.22	70	50	34

Analytical precision for major element analysis

The analysis is based on duplicate samples representing 5 calibrations.

Element	Standard deviation	Absolute % error
Fe_2O_3	0.07	-0.031
MnO	0.01	-0.006
TiO_2	0.07	-0.041
CaO	0.06	0.004
K_2O	0.07	-0.002
P_2O_5	0.02	-0.017
SiO_2	0.41	-0.043
Al_2O_3	0.41	-0.218
MgO	0.17	-0.050
Na_2O	0.10	0.060
LOI	0.26	-0.153
Total	0.500	-0.340

Analytical precision for trace element analyses

The analysis represents 3 calibrations.

Element	Standard deviation	Absolute % error
Rb	8	-2.6
Sr	4	-1.4
Y	2	-0.2
Zr	5	1.9
Nb	1	-2.2
V	8	4.0
Cr	15	8.1
Co	3	1.8
Ni	6	-1.8
Cu	4	0.1
Zn	2	-0.1
Ba	13	-2.3

Lower limits of detection

Element	Lower limit of detection
Rb	2
Sr	3
Y	3
Zr	6
Nb	2
V	15
Cr	12
Co	4
Ni	4
Cu	2
Zn	5
Ba	10

APPENDIX III

Whole rock major and trace element data for cores RM15, KV5854, EG5 and KF35

RM15 whole rock major element data

Sample number	Height (m) relative to base of Merensky pyroxenite	Lithology	%SiO_2	%TiO_2	%Al_2O_3	%Fe_2O_3	%MnO	%MgO	%CaO	%Na_2O	%K_2O	%P_2O_5	%LOI	Total
RM15-1	387	gabbronorite	53.19	0.25	16.47	7.08	0.14	9.58	11.21	2.06	0.33	0.04	0.08	100.43
RM15-2	396	gabbronorite	52.49	0.19	19.40	6.06	0.13	7.97	11.14	2.25	0.34	0.03	0.17	100.17
RM15-3	441.87	gabbronorite	52.62	0.20	19.91	5.32	0.15	7.24	11.95	2.25	0.34	0.03	0.24	100.25
RM15-4	413.87	gabbronorite	52.18	0.22	20.70	4.87	0.07	6.67	12.60	2.25	0.30	0.02	0.15	100.03
RM15-5	448.15	gabbronorite	52.41	0.19	21.01	5.86	0.06	7.00	10.97	2.42	0.30	0.03	0.23	100.48
RM15-6a	364	gabbronorite	52.50	0.25	21.58	5.44	0.09	6.48	11.08	2.30	0.40	0.08	0.27	100.47
RM15-6b	364	gabbronorite	51.09	0.18	21.00	5.54	0.09	7.61	11.00	2.21	0.26	0.01	0.26	99.25
RM17 75.95	248.22	norite	52.73	0.26	19.26	6.71	0.08	7.84	10.30	2.29	0.42	0.04	0.56	100.49
RM17 93.94	230.23	norite	52.89	0.23	21.00	5.68	0.09	6.47	10.97	2.57	0.35	0.04	0.28	100.57
RM17 107.89	216.28	norite	51.49	0.19	20.40	6.13	0.08	7.77	10.88	2.24	0.33	0.04	0.39	99.94
RM17 124.53	199.64	norite	52.58	0.33	20.56	5.82	0.13	6.38	10.86	2.32	0.46	0.08	0.97	100.49
RM17 136.98	187.19	norite	52.59	0.25	17.88	6.89	0.17	8.96	10.03	2.01	0.32	0.02	0.86	99.98
RM17 159.73	164.44	norite	52.55	0.24	19.76	6.35	0.09	7.96	10.30	2.21	0.30	0.03	0.67	100.46
RM17 164.10	160.07	norite	50.97	0.05	18.47	6.40	0.10	8.90	10.48	1.93	0.31	0.06	1.03	98.71
RM17 174.30	149.87	leuconorite	50.49	0.12	18.07	7.12	0.10	9.44	9.21	1.19	0.10	0.00	4.38	100.22
RM17 185.92	138.25	norite	51.68	0.25	23.24	4.98	0.06	4.76	11.84	2.52	0.41	0.04	0.40	100.18
RM17 200.19	123.98	leuconorite	51.97	0.26	19.49	6.32	0.09	7.33	10.78	2.09	0.46	0.03	1.04	99.86
RM17 211.47	112.7	mottled anorthosite	51.19	0.19	24.03	4.69	0.03	3.19	12.44	2.50	0.45	0.04	1.67	100.42
RM17 222.45	101.72	spotted anorthosite	51.21	0.24	24.10	4.51	0.09	3.75	12.57	2.27	0.36	0.05	0.92	100.07
RM17 232.27	92	norite	51.80	0.26	20.71	6.29	0.11	6.71	11.21	2.09	0.34	0.05	0.93	100.50
RM17 250.11	74.06	spotted anorthosite	51.85	0.29	23.65	5.09	0.06	3.65	11.86	2.53	0.39	0.04	0.79	100.20
RM15 30.12	132.91	norite	52.99	0.28	10.05	11.74	0.22	16.54	7.11	1.24	0.04	0.00	0.11	100.32
RM15 30.28	132.75	norite	52.25	0.22	11.48	10.82	0.20	16.18	7.63	1.36	0.01	0.00	-0.07	100.08
RM15 30.47	132.56	melanorite	52.13	0.36	21.64	5.59	0.10	5.55	11.51	2.73	0.34	0.05	0.30	100.30
RM15 31.61	131.42	norite	52.64	0.31	18.97	7.32	0.13	8.37	9.78	2.21	0.32	0.01	0.23	100.29
RM15 38.08	124.95	spotted anorthosite	51.50	0.31	23.69	5.17	0.09	4.02	12.09	2.38	0.34	0.03	0.43	100.05
RM15 44	119.03	spotted anorthosite	50.09	0.11	30.42	1.42	0.02	0.66	13.73	2.91	0.27	0.01	0.48	100.12
RM15 44.78	118.25	melanorite	50.90	0.19	28.28	2.33	0.04	1.71	12.84	3.19	0.40	0.03	0.55	100.46
RM15 45.57	117.46	norite	51.88	0.25	17.99	7.66	0.14	9.60	10.03	2.15	0.15	0.02	0.34	100.21
RM15 45.72	117.31	norite	52.17	0.24	23.29	4.55	0.08	4.67	11.30	2.79	0.34	0.02	0.94	100.39
RM15 51.69	111.34	norite	52.12	0.29	14.14	10.33	0.19	12.02	9.31	1.86	0.12	0.02	-0.04	100.36
RM15 59.35	103.68	mottled anorthosite	51.46	0.25	25.06	4.45	0.08	2.63	12.63	2.85	0.36	0.04	0.42	100.23
RM15 66.81	96.22	spotted anorthosite	50.07	0.23	26.02	3.49	0.05	2.59	13.69	2.61	0.31	0.04	1.11	100.21
RM15 74.18	88.85	spotted anorthosite	51.83	0.30	25.07	4.01	0.06	3.65	12.05	2.68	0.40	0.03	0.23	100.31
RM15 81.18	81.85	spotted anorthosite	50.78	0.31	22.16	6.21	0.10	5.29	11.07	2.16	0.20	0.06	1.19	99.53
RM15 89.83	73.2	spotted anorthosite	50.79	0.24	25.59	3.57	0.05	2.50	13.08	2.92	0.42	0.05	0.59	99.80
RM15 98.44	64.59	mottled anorthosite	49.71	0.24	26.13	3.67	0.06	2.02	13.78	2.15	0.55	0.05	1.81	100.17
RM15 105.04	57.99	mottled anorthosite	51.03	0.29	27.05	3.66	0.05	2.06	12.86	2.68	0.36	0.03	0.33	100.40
RM15 112.23	50.8	mottled anorthosite	50.81	0.23	25.15	4.49	0.08	3.77	13.07	2.37	0.24	0.04	0.23	100.48
RM15 119.88	43.15	mottled anorthosite	49.50	0.12	29.61	2.09	0.03	1.77	14.61	2.38	0.10	0.01	0.23	100.45
RM15 123.24	39.79	spotted anorthosite	49.85	0.15	27.88	2.83	0.04	2.83	14.01	2.28	0.10	0.01	0.40	100.38
RM15 125.52	37.51	spotted anorthosite	49.58	0.16	30.62	1.56	0.02	0.94	14.49	2.36	0.13	0.01	0.54	100.41
RM15 132.23	30.8	mottled anorthosite	49.23	0.15	29.34	2.31	0.04	2.26	13.94	2.46	0.10	0.02	0.46	100.31

RM15 140	23.03	mottled anorthosite	48.46	0.19	26.98	2.85	0.04	2.51	14.04	2.43	0.36	0.00	2.58	100.44
RM15 145.76	17.27	anorthosite	50.65	0.20	30.18	1.29	0.01	0.62	12.74	3.19	0.46	0.02	1.03	100.39
RM15 146.9	16.13	melanorite	53.15	0.22	9.58	10.08	0.19	19.53	5.67	0.70	0.00	0.04	1.39	100.55
RM15 149.62	13.41	melanorite	50.52	0.16	21.00	5.40	0.10	9.72	10.62	1.78	0.02	0.02	0.45	99.79
RM15 151.53	11.5	melanorite	51.41	0.18	19.11	6.24	0.12	11.56	9.92	1.60	0.01	0.01	0.23	100.39
RM15 153.2	9.83	melanorite	52.55	0.19	12.37	9.10	0.18	18.00	6.83	1.06	0.00	0.01	-0.10	100.19
RM15 153.61	9.42	mottled anorthosite	48.16	0.11	31.67	1.61	0.02	0.38	15.29	2.46	0.13	0.00	0.53	100.36
RM15 154.37	8.66	mottled anorthosite	48.32	0.13	29.03	3.16	0.04	2.26	14.40	2.10	0.11	0.02	0.55	100.12
RM15 160.09	2.94	mottled anorthosite	50.11	0.15	27.21	3.15	0.05	3.61	12.98	2.61	0.17	0.04	0.31	100.39
RM15 160.28	2.75	mottled anorthosite	50.59	0.15	24.81	4.20	0.07	5.73	11.71	2.63	0.12	0.01	0.49	100.51
RM15 160.48	2.55	pyroxenite	52.39	0.28	6.65	12.55	0.21	20.83	5.33	0.70	0.02	0.02	0.18	99.16
RM15 160.73	2.3	pyroxenite	53.39	0.19	7.39	10.98	0.20	22.56	4.24	0.80	0.00	0.01	-0.07	99.69
RM15 160.83	2.2	pyroxenite	52.26	0.23	7.11	11.60	0.20	21.77	4.50	0.81	0.00	0.01	0.06	98.55
RM15 161.03	1.73	pyroxenite	52.19	0.35	4.30	15.19	0.22	22.48	3.44	0.48	0.00	0.02	0.11	98.78
RM15 161.22	1.81	pyroxenite	52.44	0.23	7.15	10.86	0.20	21.96	4.31	0.79	0.00	0.01	0.64	98.59
RM15 161.42	1.61	pyroxenite	52.66	0.23	7.64	10.23	0.20	21.87	4.80	0.84	0.00	0.01	0.04	98.52
RM15 161.62	1.41	pyroxenite	53.27	0.33	6.66	11.23	0.21	21.78	4.27	0.88	0.06	0.02	0.25	98.96
RM15 161.82	1.21	pyroxenite	53.30	0.36	5.80	11.28	0.21	21.76	5.65	0.74	0.01	0.04	0.28	99.43
RM15 161.98	1.05	pyroxenite	53.12	0.23	10.23	9.52	0.19	19.19	5.53	1.22	0.06	0.02	-0.01	99.30
RM15 162.26	0.77	pyroxenite	53.53	0.19	8.27	10.43	0.20	22.23	4.40	0.84	0.06	0.01	-0.13	100.03
RM15 162.38	0.65	pyroxenite	53.23	0.22	7.85	10.36	0.20	22.12	4.55	0.81	0.00	0.02	-0.06	99.30
RM15 162.57	0.46	pyroxenite	53.22	0.25	7.72	10.59	0.20	22.22	4.73	0.86	0.00	0.02	0.11	99.92
RM15 162.76	0.27	pyroxenite	52.10	0.29	7.16	11.51	0.20	21.11	4.88	0.76	0.02	0.01	0.52	98.56
RM15 162.98	0.05	pyroxenite	49.12	0.12	28.39	2.40	0.04	3.64	13.61	2.07	0.08	0.00	0.89	100.36
RM15 163.18	-0.15	leuconorite	49.31	0.13	29.14	2.04	0.04	3.05	14.18	2.16	0.11	0.01	0.27	100.44
RM15 169.1	-6.07	leuconorite	50.25	0.14	24.71	3.71	0.06	7.15	12.15	1.95	0.09	0.01	0.14	100.36
RM15 175.94	-12.91	mottled anorthosite	48.50	0.12	30.09	1.83	0.02	1.11	14.62	2.40	0.09	0.02	0.27	99.07
RM15 182.58	-19.55	mottled anorthosite	48.92	0.12	30.14	2.01	0.02	1.83	14.52	2.24	0.04	0.02	0.17	100.03
RM15 189.16	-26.13	mottled anorthosite	47.98	0.10	31.79	1.28	0.01	0.64	15.17	2.22	0.15	0.01	0.64	99.99
RM15 202.98	-39.95	norite	51.42	0.16	17.31	6.39	0.12	14.24	8.87	1.34	0.01	0.01	0.06	99.93
RM15 209.28	-46.25	norite	50.84	0.14	21.48	4.94	0.09	10.21	10.78	1.79	0.04	0.02	0.16	100.49
RM15 216.1	-53.07	norite	50.14	0.14	23.44	4.24	0.07	8.05	11.74	1.96	0.06	0.00	0.07	99.91
RM15 223.35	-60.32	norite	49.09	0.13	27.10	2.99	0.06	4.90	13.43	1.77	0.50	0.01	0.14	100.12
RM15 230.3	-67.27	norite	50.75	0.16	21.67	5.01	0.10	9.52	10.93	1.73	0.08	0.01	0.13	100.09
RM15 237.58	-74.55	norite	50.50	0.15	20.33	5.33	0.10	10.38	10.40	1.81	0.08	0.01	0.38	99.47
RM15 244.23	-81.2	norite	50.49	0.17	21.58	5.07	0.09	9.10	11.09	1.66	0.06	0.02	0.13	99.46
RM15 252.3	-89.27	norite	51.49	0.17	19.69	5.68	0.11	10.87	10.09	1.69	0.04	0.02	0.43	100.28
RM15 259.27	-96.24	norite	50.96	0.17	19.24	6.13	0.12	11.26	9.89	1.61	0.05	0.01	0.35	99.79
RM15 266	-102.97	norite	51.03	0.17	19.04	5.92	0.11	11.49	9.80	1.62	0.05	0.01	1.05	100.29
RM15 274.09	-111.06	mottled anorthosite	50.84	0.17	19.65	5.77	0.10	11.00	9.95	1.96	0.09	0.00	0.61	100.14
RM15 281.86	-118.83	norite	49.88	0.16	24.98	3.53	0.06	5.96	12.50	2.43	0.16	0.01	0.44	100.11
RM15 288.6	-125.57	norite	49.92	0.16	29.70	2.03	0.03	1.93	13.81	1.87	0.17	0.02	0.31	99.95
RM15 295.29	-132.26	norite	51.04	0.19	21.84	4.96	0.09	8.57	11.15	2.15	0.10	0.02	0.28	100.39
RM15 296.14	-133.11	norite	50.38	0.16	24.86	3.92	0.07	6.33	12.22	2.00	0.12	0.01	0.34	100.41
RM15 302.66	-139.63	norite	50.05	0.16	24.88	3.81	0.07	6.09	12.40	1.98	0.13	0.01	0.58	100.16
RM15 309.2	-146.17	norite	50.31	0.16	24.26	4.17	0.07	6.52	12.08	2.12	0.15	0.01	0.54	100.39
RM15 316.43	-153.4	mottled anorthosite	49.37	0.12	27.09	3.03	0.05	4.45	13.14	2.33	0.09	0.01	0.59	100.27
RM15 323	-159.97	mottled anorthosite	49.09	0.15	30.27	1.93	0.02	1.21	14.66	2.35	0.16	0.01	0.52	100.37
RM15 331.47	-168.44	pegmatoid	48.13	0.14	28.86	2.46	0.04	2.15	14.05	0.41	0.10	0.01	2.36	98.71
RM15 338	-174.97	Pyroxenite	52.31	0.28	6.33	11.50	0.22	22.60	5.39	1.08	0.23	0.01	0.06	100.01
RM15 342.92	-179.89	Pyroxenite	52.09	0.18	13.09	7.62	0.15	18.65	7.00	0.97	0.00	0.01	-0.20	99.56

RM15 whole rock trace element data

Sample number	Height (m) relative to base of Merensky pyroxenite	Lithology	Rb ppm	Sr ppm	Y ppm	Zr ppm	Nb ppm	Co ppm	Ni ppm	Cu ppm	Zn ppm	%TiO2	V ppm	Cr ppm	Ba ppm
RM15-1	387	Gabbronorite	13	213	10	167	5	41	182	36	54	0.22	141	372	105
RM15-2	396	Gabbronorite	13	245	7	36	5	34	171	23	48	0.18	104	303	96
RM15-3	441.87	Gabbronorite	13	251	9	42	4	32	154	23	41	0.18	106	378	103
RM15-4	413.87	Gabbronorite	11	258	9	39	4	28	134	23	40	0.20	109	384	98
RM15-5	448.15	Gabbronorite	12	264	7	32	4	32	153	35	47	0.17	88	317	114
RM15-6a	364	Gabbronorite	16	267	9	45	5	30	133	32	43	0.23	86	309	120
RM15-6b	364	Gabbronorite	9	260	7	32	4	35	161	30	45	0.16	82	384	102
RM17 75.95	248.22	Norite	15	242	11	46	5	35	167	27	62	0.24	106	356	135
RM17 93.94	230.23	Norite	13	270	9	42	4	32	133	24	47	0.21	89	289	98
RM17 107.89	216.28	norite	13	257	7	32	4	36	173	24	66	0.17	87	390	90
RM17 124.53	199.64	norite	18	266	11	59	6	30	127	35	52	0.31	102	298	145
RM17 136.98	187.19	norite	14	232	10	54	5	40	202	26	56	0.25	108	488	91
RM17 159.73	164.44	norite	12	245	10	49	5	37	175	34	79	0.24	99	390	112
RM17 164.10	160.07	norite	11	244	8	36	4	42	203	21	58	0.20	88	432	94
RM17 174.30	149.87	leuconorite	8	190	4	21	3	51	307	14	58	0.12	74	646	64
RM17 185.92	138.25	norite	16	295	10	41	5	23	95	30	48	0.21	78	215	131
RM17 200.19	123.98	leuconorite	15	249	9	43	5	38	156	28	63	0.25	107	381	128
RM17 211.47	112.7	mottled anorthosite	15	286	12	47	4	19	55	21	53	0.16	92	137	113
RM17 222.45	101.72	spotted anorthosite	13	303	9	41	5	21	70	26	45	0.21	76	190	105
RM17 232.27	92	norite	13	259	10	48	5	36	133	26	54	0.25	103	354	122
RM17 250.11	74.06	spotted anorthosite	14	290	11	49	5	22	66	30	58	0.26	84	127	121
RM15 30.12	132.91	norite	13	137	7	24	5	57	334	12	74	0.23	184	970	66
RM15 30.28	132.75	norite	10	144	5	14	4	58	325	9	68	0.18	161	887	45
RM15 30.47	132.56	melanorite	17	291	9	46	5	23	110	16	35	0.29	95	294	138
RM15 31.61	131.42	norite	18	257	8	38	4	33	156	9	46	0.28	115	380	118
RM15 38.08	124.95	spotted anorthosite	14	311	9	34	4	19	66	16	36	0.22	86	99	122
RM15 44	119.03	spotted anorthosite	8	389	3	11	5	11	15	<2	13	0.07	19	32	106
RM15 44.78	118.25	melanorite	14	370	4	22	4	13	40	<2	19	0.14	35	109	145
RM15 45.57	117.46	norite	12	248	6	23	4	34	183	10	49	0.19	127	541	87
RM15 45.72	117.31	norite	16	321	6	43	6	24	97	6	32	0.21	73	244	134
RM15 51.69	111.34	norite	14	193	8	29	5	46	244	21	70	0.24	171	712	82
RM15 59.35	103.68	mottled anorthosite	17	325	10	37	5	20	40	<2	34	0.18	74	78	129
RM15 66.81	96.22	spotted anorthosite	14	332	8	29	5	17	51	<2	25	0.17	78	192	111
RM15 74.18	88.85	spotted anorthosite	16	332	8	43	5	18	66	9	28	0.22	63	186	162
RM15 81.18	81.85	spotted anorthosite	13	282	9	42	5	27	94	10	44	0.25	115	231	77
RM15 89.83	73.2	spotted anorthosite	18	343	9	37	4	18	40	2	27	0.19	81	135	183
RM15 98.44	64.59	mottled anorthosite	25	296	7	33	5	15	34	<2	29	0.2	63	85	125
RM15 105.04	57.99	mottled anorthosite	14	344	7	41	5	16	31	<2	26	0.25	56	59	130
RM15 112.23	50.8	mottled anorthosite	11	313	7	27	5	26	54	<2	29	0.18	81	203	107
RM15 119.88	43.15	mottled anorthosite	7	348	3	12	4	13	35	<2	15	0.07	32	124	80
RM15 123.24	39.79	spotted anorthosite	8	329	4	16	4	18	58	<2	19	0.1	36	243	76
RM15 125.52	37.51	spotted anorthosite	8	414	3	16	5	13	22	<2	11	0.08	19	68	80

RM15 132.23	30.8	mottled anorthosite	7	421	3	13	5	13	45	<2	16	0.08	25	204	78
RM15 140	23.03	mottled anorthosite	17	348	7	14	4	18	93	7	41	0.16	116	196	120
RM15 145.76	17.27	anorthosite	19	441	3	33	5	11	15	<2	13	0.14	c	38	123
RM15 146.9	16.13	melanorite	7	134	5	18	4	63	465	9	68	0.17	132	2586	22
RM15 149.62	13.41	melanorite	5	304	5	16	4	30	192	<2	35	0.12	67	1215	47
RM15 151.53	11.5	melanorite	8	282	4	15	4	36	214	<2	40	0.12	72	1333	46
RM15 153.2	9.83	melanorite	6	440	3	10	4	15	28	<2	13	0.06	24	54	53
RM15 153.61	9.42	mottled anorthosite	11	445	<3	8	4	12	16	<2	11	0.05	16	1905	62
RM15 154.37	8.66	mottled anorthosite	6	244	4	13	5	41	286	<2	38	0.11	84	1261	37
RM15 160.09	2.94	mottled anorthosite	9	426	3	9	4	21	288	132	22	0.08	32	724	120
RM15 160.28	2.75	mottled anorthosite	8	390	3	9	4	26	489	307	28	0.1	45	3215	95
RM15 160.48	2.55	pyroxenite	13	88	8	25	5	115	3292	1520	79	0.22	158	3239	34
RM15 160.73	2.3	pyroxenite	10	103	4	15	4	92	1784	854	71	0.15	119	3538	26
RM15 160.83	2.2	pyroxenite	9	102	6	15	3	93	2115	1436	69	0.18	131	4021	36
RM15 161.03	1.73	pyroxenite	9	105	6	18	5	78	1030	436	69	0.17	125	3366	38
RM15 161.22	1.81	pyroxenite	13	59	9	34	4	198	6648	1178	87	0.28	173	4176	31
RM15 161.42	1.61	pyroxenite	11	113	6	20	4	69	546	36	69	0.17	127	3029	33
RM15 161.62	1.41	pyroxenite	12	96	10	39	5	70	582	34	72	0.3	136	3750	50
RM15 161.82	1.21	pyroxenite	12	83	10	33	5	67	562	30	71	0.28	159	3398	45
RM15 161.98	1.05	pyroxenite	11	150	7	23	3	55	466	15	64	0.18	119	4887	43
RM15 162.26	0.77	pyroxenite	9	108	4	15	4	67	537	9	73	0.16	126	4130	29
RM15 162.38	0.65	pyroxenite	9	114	6	18	4	67	535	20	77	0.17	125	6058	35
RM15 162.57	0.46	pyroxenite	9	107	6	19	4	73	545	33	72	0.21	154	7272	30
RM15 162.76	0.27	pyroxenite	12	98	7	23	5	73	1191	407	92	0.25	166	444	35
RM15 162.98	0.05	pyroxenite	8	404	<3	10	3	17	71	2	32	0.07	30	396	66
RM15 163.18	-0.15	leuconorite	7	420	<3	9	3	18	61	<2	1	0.05	21	261	67
RM15 169.1	-6.07	leuconorite	7	343	3	13	4	28	150	<2	26	0.09	48	1148	54
RM15 175.94	-12.91	mottled anorthosite	10	321	<3	14	3	32	189	<2	30	0.11	60	1261	63
RM15 182.58	-19.55	mottled anorthosite	10	307	3	13	4	31	212	<2	32	0.11	61	1106	66
RM15 189.16	-26.13	mottled anorthosite	8	326	4	16	4	33	180	<2	30	0.14	68	1153	63
RM15 202.98	-39.95	norite	7	297	5	18	5	32	214	<2	33	0.12	62	1284	41
RM15 209.28	-46.25	norite	8	288	4	15	4	34	224	<2	36	0.12	67	1373	49
RM15 216.1	-53.07	norite	6	288	3	15	4	36	247	<2	36	0.12	68	1334	46
RM15 223.35	-60.32	norite	8	304	<3	15	4	35	225	<2	36	0.13	68	647	63
RM15 230.3	-67.27	norite	8	363	4	15	4	23	120	<2	23	0.12	53	825	63
RM15 237.58	-74.55	norite	8	436	4	15	5	15	99	10	15	0.08	21	916	95
RM15 244.23	-81.2	norite	7	328	5	18	4	31	165	<2	31	0.13	63	636	65
RM15 252.3	-89.27	norite	10	365	4	15	4	24	124	<2	24	0.12	59	1094	66
RM15 259.27	-96.24	norite	9	367	4	15	4	22	113	<2	23	0.11	49	1005	67
RM15 266	-102.97	norite	11	367	3	17	4	24	131	<2	25	0.1	37	529	72
RM15 274.09	-111.06	mottled anorthosite	8	395	3	13	5	21	89	<2	25	0.07	30	96	60
RM15 281.86	-118.83	norite	9	436	4	15	4	14	26	<2	15	0.08	28	457	76
RM15 288.6	-125.57	norite	8	425	3	12	3	14	43	<2	17	0.09	36	4609	75
RM15 295.29	-132.26	norite	14	16	8	24	4	61	578	<2	44	0.25	150	3411	35
RM15 296.14	-133.11	norite	8	177	4	13	4	52	415	<2	47	0.15	96	3842	37
RM15 302.66	-139.63	norite	8	177	3	14	4	54	414	<2	46	0.14	99	580	36
RM15 309.2	-146.17	norite	19	320	3	11	4	20	125	<2	17	0.08	38	2556	100
RM15 316.43	-153.4	mottled anorthosite	9	158	6	16	4	54	437	11	63	0.22	134	452	48
RM15 323	-159.97	mottled anorthosite	9	423	<3	9	3	20	288	131	20	0.09	36	4783	113
RM15 331.47	-168.44	pegmatoid	15	16	7	24	5	59	582	<2	45	0.25	156	2976	31
RM15 338	-174.97	pyroxenite	7	176	5	14	4	57	412	<2	48	0.13	80	3478	35
RM15 342.92	-179.89	pyroxenite	7	178	5	16	6	54	414	<2	48	0.14	77	2936	32

KV5854 whole rock major element data

Sample number	Height (m) relative to base of Merensky pyroxenite	Lithology	%SiO_2	%TiO_2	%Al_2O_3	%Fe_2O_3	%MnO	%MgO	%CaO	%Na_2O	%K_2O	%P_2O_5	%LOI	Total
KV-179.94	116.11	norite	51.28	0.20	20.58	5.52	0.10	8.48	11.17	2.39	0.19	0.03	0.25	100.19
KV-185.73	110.32	mottled anorthosite	51.81	0.26	23.36	4.31	0.07	5.45	11.75	2.70	0.42	0.04	0.31	100.48
KV-188.93	107.12	mottled anorthosite	48.78	0.25	23.61	5.20	0.08	5.76	12.06	2.63	0.28	0.03	0.26	98.94
KV-192.00	104.05	mottled anorthosite	51.22	0.23	24.52	3.63	0.07	3.52	12.61	2.49	0.35	0.04	0.18	98.86
KV-196.89	99.16	mottled anorthosite	50.15	0.28	24.18	4.18	0.07	3.62	12.44	2.50	0.45	0.04	0.64	98.55
KV-198.23	97.82	norite	51.63	0.32	20.70	6.72	0.11	6.66	11.02	2.13	0.35	0.05	0.17	99.86
KV-210.93	85.12	norite	50.59	0.29	20.91	6.71	0.12	7.46	10.53	2.20	0.31	0.04	0.67	99.83
KV-213.28	82.77	mottled anorthosite	50.41	0.26	24.22	4.29	0.08	3.80	12.22	2.53	0.42	0.05	0.48	98.76
KV-229.39	66.66	mottled anorthosite	50.81	0.26	24.24	4.70	0.08	3.84	12.28	2.46	0.35	0.05	0.35	99.42
KV-242.74	53.31	mottled anorthosite	50.20	0.18	26.18	3.72	0.07	3.46	13.34	2.13	0.20	0.04	0.47	99.99
KV-250.53	45.52	mottled anorthosite	49.95	0.50	24.85	4.69	0.08	3.28	12.89	2.43	0.34	0.02	-0.04	98.99
KV-254.90	41.15	spotted anorthosite	49.62	0.16	27.34	2.91	0.05	2.92	13.87	2.03	0.13	0.02	0.99	100.04
KV-255.07	40.98	mottled anorthosite	49.49	0.23	25.78	3.74	0.07	3.95	13.40	2.05	0.15	0.03	0.77	99.66
KV-282.88	13.17	norite	50.96	0.16	18.07	7.10	0.12	11.09	10.12	1.24	0.06	0.03	0.50	99.45
KV-283.99	12.06	mottled anorthosite	49.32	0.16	28.54	2.53	0.04	2.31	14.49	0.57	0.13	0.02	0.70	98.81
KV-289.22	6.83	mottled anorthosite	48.44	0.13	28.54	1.85	0.04	1.75	14.95	0.69	0.22	0.02	2.13	98.76
KV-291.71	4.34	norite	50.37	0.19	19.49	6.42	0.11	10.03	10.74	0.70	0.06	0.03	0.49	98.63
KV-292.25	3.8	pyroxenite	50.27	0.22	12.75	10.03	0.17	17.46	6.65	2.04	0.07	0.03	0.64	100.33
KV-292.63	3.42	pyroxenite	52.33	0.21	6.16	10.95	0.20	22.76	4.04	2.05	0.03	0.02	0.21	98.96
KV-292.82	3.23	pyroxenite	52.09	0.27	9.20	10.99	0.18	19.89	5.95	0.72	0.07	0.03	0.29	99.68
KV-293.05	3	pyroxenite	53.03	0.35	5.67	12.72	0.20	22.86	3.84	0.65	0.15	0.03	0.56	100.30
KV-293.28	2.77	pyroxenite	53.41	0.44	3.71	13.14	0.21	23.46	4.79	0.39	0.25	0.05	0.40	100.25
KV-293.50	2.55	pyroxenite	53.02	0.30	6.07	12.21	0.18	23.00	4.09	0.72	0.11	0.03	0.24	99.97
KV-293.74	2.31	pyroxenite	54.24	0.39	4.21	12.80	0.19	23.04	4.76	0.54	0.20	0.13	0.31	100.81
KV-293.94	2.11	pyroxenite	52.96	0.35	5.17	12.52	0.20	22.49	4.03	0.59	0.14	0.03	0.59	99.07
KV-294.13	1.92	pyroxenite	52.90	0.28	5.80	12.53	0.19	23.10	3.86	0.66	0.07	0.03	0.95	100.37
KV-294.35	1.7	pyroxenite	51.95	0.29	5.68	12.12	0.17	22.31	4.55	0.63	0.10	0.05	0.87	98.72
KV-294.44	1.61	pyroxenite	50.53	0.21	6.01	10.15	0.19	21.54	4.01	1.91	0.02	0.03	4.20	98.80
KV-294.83	1.22	pyroxenite	51.93	0.29	5.24	12.40	0.17	22.56	3.75	0.38	0.07	0.03	1.97	98.79
KV-295.05	1	pyroxenite	52.84	0.31	5.09	12.70	0.18	21.44	5.03	0.61	0.08	0.06	0.50	98.84
KV-295.21	0.84	pyroxenite	52.86	0.27	6.15	12.46	0.20	22.47	4.49	0.71	0.05	0.03	0.42	100.11
KV-295.36	0.69	pyroxenite	53.36	0.35	5.02	12.69	0.22	22.16	4.85	0.46	0.16	0.04	0.97	100.28
KV-295.56	0.49	pyroxenite	53.83	0.31	5.06	12.14	0.19	21.18	4.72	0.45	0.09	0.04	1.01	99.02
KV-295.75	0.3	pyroxenite	54.44	0.25	5.75	11.55	0.19	21.32	4.01	0.57	0.04	0.02	0.68	98.82
KV-295.94	0.11	pyroxenite	53.87	0.44	4.24	12.71	0.21	22.06	4.65	0.54	0.28	0.08	0.82	99.90
KV-296.10	-0.05	pegmatoid	50.56	0.30	6.83	12.51	0.21	22.54	4.54	0.56	0.04	0.03	0.86	98.98
KV-296.40	-0.35	norite	48.89	0.17	21.13	4.93	0.14	9.28	11.17	2.13	0.07	0.02	1.34	99.27
KV-307.40	-11.35	norite	51.15	0.16	17.81	6.48	0.16	13.29	9.07	1.73	0.05	0.03	0.02	99.95
KV-327.69	-31.64	leuconorite	50.45	0.18	19.17	6.22	0.13	12.01	9.41	1.78	0.07	0.03	0.25	99.70
KV-335.50	-39.45	mottled anorthosite	50.81	0.18	17.57	6.47	0.14	13.23	8.85	2.43	0.16	0.03	0.48	100.35
KV-335.68	-39.63	norite	50.01	0.17	17.59	6.10	0.13	12.81	9.85	1.50	0.07	0.02	0.54	98.79
KV-352.53	-56.48	norite	50.46	0.13	21.95	3.98	0.10	8.44	11.76	1.78	0.09	0.01	-0.06	98.64
KV-352.85	-56.8	melanorite	49.04	0.15	16.78	6.64	0.12	13.96	10.23	1.56	0.08	0.02	0.29	98.87
KV-353.24	-57.19	melanorite	54.13	0.17	18.32	5.49	0.10	10.99	9.06	1.41	0.32	0.04	-0.07	99.96
KV-367.28	-71.23	melanorite	51.02	0.13	27.67	2.27	0.08	4.07	13.14	1.20	0.21	0.03	0.47	100.29

KV-378.90	-82.85	melanorite	51.26	0.18	20.14	5.47	0.11	10.61	10.49	1.69	0.13	0.03	0.18	100.29
KV-388.85	-92.8	melanorite	50.04	0.18	20.33	5.65	0.13	10.52	10.67	1.66	0.14	0.03	0.33	99.68
KV-404.41	-108.36	melanorite	49.98	0.20	19.86	5.90	0.13	10.59	10.33	1.64	0.14	0.04	0.62	99.43
KV-421.80	-125.75	norite	49.78	0.21	19.85	6.15	0.14	10.63	10.58	1.69	0.18	0.03	0.21	99.45
KV-428.94	-132.89	norite	50.53	0.19	20.95	5.67	0.13	10.04	10.82	1.68	0.14	0.04	0.16	100.35
KV-438.41	-142.36	norite	50.89	0.21	21.85	5.19	0.12	8.18	10.97	1.72	0.14	0.05	0.72	100.04
KV-448.43	-152.38	norite	49.75	0.19	21.82	4.74	0.11	7.67	11.40	1.70	0.16	0.03	1.52	99.09
KV-460.59	-164.54	norite	50.22	0.17	22.24	5.01	0.10	8.28	11.01	1.74	0.13	0.03	0.26	99.19
KV-468.41	-172.36	norite	49.28	0.15	24.64	3.64	0.08	5.92	12.52	1.71	0.17	0.03	0.77	98.91
KV-480.29	-184.24	norite	49.26	0.15	24.13	3.94	0.10	6.62	12.29	1.65	0.11	0.02	1.54	99.81
KV-487.78	-191.73	norite	47.14	0.12	27.15	2.12	0.08	2.82	13.30	2.13	0.88	0.03	4.26	100.03
KV-494.61	-198.56	mottled anorthosite	45.30	0.11	27.19	1.88	0.08	2.45	13.99	1.85	0.24	0.02	7.16	100.27
KV-497.02	-200.97	pyroxenite	50.39	0.29	9.53	10.65	0.17	20.50	5.39	0.50	0.05	0.04	1.14	98.65
KV-502	-205.95	mottled anorthosite	48.14	0.11	30.55	1.49	0.12	1.74	15.18	2.08	0.13	0.03	0.81	100.38
KV-507	-210.95	norite	49.50	0.17	23.18	4.39	0.12	7.32	11.95	1.69	0.12	0.04	1.19	99.67

KV5854 whole rock trace element data

Sample Number	Height (m) relative to base of Merenksy pyroxenite	Lithology	Rb ppm	Sr ppm	Y ppm	Zr ppm	Nb ppm	Co ppm	Ni ppm	Cu ppm	Zn ppm	%TiO2	V ppm	Cr ppm	Ba ppm
KV-179.94	116.11	norite	9	287	4	20	5	27	121	25	44	0.16	85	359	117
KV-185.73	110.32	mottled anorthosite	17	316	7	42	6	16	56	29	37	0.23	63	157	172
KV-188.93	107.12	mottled anorthosite	13	314	4	28	5	24	71	27	42	0.17	66	163	135
KV-192.00	104.05	mottled anorthosite	12	332	7	28	5	18	48	24	35	0.17	66	165	128
KV-196.89	99.16	mottled anorthosite	19	321	6	35	5	20	62	39	37	0.22	66	169	163
KV-198.23	97.82	norite	14	249	9	37	6	28	154	39	56	0.27	112	454	145
KV-210.93	85.12	norite	14	277	6	39	6	29	118	27	51	0.25	100	266	138
KV-213.28	82.77	mottled anorthosite	14	316	6	39	5	19	62	25	39	0.20	67	162	166
KV-229.39	66.66	mottled anorthosite	15	322	8	34	6	20	48	28	40	0.21	75	103	146
KV-242.74	53.31	mottled anorthosite	8	318	4	18	4	29	57	23	39	0.12	68	158	104
KV-250.53	45.52	mottled anorthosite	13	321	6	34	6	19	55	37	40	0.40	85	153	142
KV-254.90	41.15	spotted anorthosite	8	327	3	17	4	20	52	20	32	0.10	60	180	83
KV-255.07	40.98	mottled anorthosite	6	316	3	16	5	22	71	25	34	0.11	72	255	89
KV-282.88	13.17	norite	7	208	<3	13	4	47	296	121	57	0.12	84	1486	57
KV-283.99	12.06	mottled anorthosite	10	82	5	20	4	93	1606	674	82	0.11	160	4162	59
KV-289.22	6.83	mottled anorthosite	7	95	5	16	5	75	624	104	80	0.10	155	4547	66
KV-291.71	4.34	norite	7	94	4	15	4	73	618	100	80	0.19	148	4577	58
KV-292.25	3.8	pyroxenite	5	367	<3	12	4	17	52	44	29	0.17	33	85	79
KV-292.63	3.42	pyroxenite	10	409	<3	11	5	17	85	51	22	0.16	27	111	102
KV-292.82	3.23	pyroxenite	8	86	5	18	5	74	628	95	86	0.22	164	4151	61
KV-293.05	3	pyroxenite	16	74	8	37	6	84	1167	371	90	0.30	165	3861	78
KV-293.28	2.77	pyroxenite	25	41	11	51	7	77	634	91	94	0.41	196	3479	97
KV-293.50	2.55	pyroxenite	11	85	6	27	5	76	582	67	86	0.28	140	3199	78
KV-293.74	2.31	pyroxenite	20	53	12	45	6	71	601	59	93	0.36	192	3276	89
KV-293.94	2.11	pyroxenite	17	66	8	38	6	72	597	66	91	0.30	165	3211	82
KV-294.13	1.92	pyroxenite	10	87	5	17	5	74	596	71	98	0.21	135	3255	65
KV-294.35	1.7	pyroxenite	11	88	6	19	5	75	577	63	87	0.21	137	3168	60
KV-294.44	1.61	pyroxenite	5	305	4	13	5	40	738	432	47	0.15	66	903	74
KV-294.83	1.22	pyroxenite	11	67	7	28	5	80	595	75	90	0.26	148	3277	64
KV-295.05	1	pyroxenite	12	69	9	32	5	76	580	59	89	0.27	166	3646	56
KV-295.21	0.84	pyroxenite	8	88	6	22	5	74	585	58	92	0.22	147	3899	59
KV-295.36	0.69	pyroxenite	17	57	8	42	6	75	579	68	92	0.33	184	4109	65
KV-295.56	0.49	pyroxenite	26	41	10	55	6	71	599	71	95	0.37	183	4072	86
KV-295.75	0.3	pyroxenite	7	86	6	20	5	68	591	51	90	0.20	146	4317	49
KV-295.94	0.11	pyroxenite	11	78	6	20	5	74	587	67	87	0.38	168	5188	59
KV-296.10	-0.05	pegmatoid	10	85	6	23	5	74	611	47	107	0.24	188	10393	52
KV-296.40	-0.35	norite	6	414	<3	10	4	17	77	18	24	0.10	30	336	99
KV-307.40	-11.35	norite	7	301	<3	13	5	32	227	20	43	0.09	65	1048	75
KV-327.69	-31.64	leuconorite	6	321	<3	12	5	33	195	22	38	0.10	68	858	68
KV-335.50	-39.45	mottled anorthosite	6	442	<3	10	4	13	18	13	18	0.11	17	69	69
KV-335.68	-39.63	norite	6	249	3	13	5	41	263	22	44	0.10	90	982	59
KV-352.53	-56.48	norite	6	298	<3	10	4	37	203	14	38	0.09	56	839	66
KV-352.85	-56.8	melanorite	7	277	3	11	4	51	347	11	44	0.09	61	884	65
KV-353.24	-57.19	melanorite	5	230	2	11	4	48	309	16	48	0.11	79	1240	68
KV-367.28	-71.23	melanorite	8	235	3	14	4	49	346	25	51	0.12	83	1854	72

KV-378.90	-82.85	melanorite	7	292	<3	16	5	35	244	24	45	0.13	65	1129	89
KV-388.85	-92.8	melanorite	9	295	3	19	5	34	224	39	44	0.12	61	1011	91
KV-404.41	-108.36	melanorite	8	290	4	20	4	38	222	19	45	0.15	69	984	104
KV-421.80	-125.75	norite	11	280	3	19	4	39	239	23	47	0.14	70	1020	95
KV-428.94	-132.89	norite	8	293	3	17	5	38	215	25	46	0.12	72	988	84
KV-438.41	-142.36	norite	9	314	4	24	4	30	168	24	43	0.17	68	698	110
KV-448.43	-152.38	norite	9	320	4	20	5	31	183	29	40	0.14	63	837	100
KV-460.59	-164.54	norite	7	330	3	17	5	31	172	28	39	0.11	55	843	91
KV-468.41	-172.36	norite	6	360	<3	16	4	27	119	24	31	0.11	50	621	99
KV-480.29	-184.24	norite	5	358	<3	11	4	24	145	30	35	0.10	53	665	93
KV-487.78	-191.73	norite	39	316	<3	13	5	16	61	22	24	0.09	32	229	166
KV-494.61	-198.56	mottled anorthosite	4	434	<3	8	4	19	59	20	20	0.06	32	526	67
KV-497.02	-200.97	pyroxenite	8	67	7	21	5	93	1010	98	92	0.30	223	17685	72
KV-507	-210.95	norite	7	349	<3	22	4	28	161	23	35	0.13	55	911	102

EG5 whole rock major element data

Sample number	Height (m) relative to base of Merensky pyroxenite	Lithology	%SiO_2	%TiO_2	%Al_2O_3	%Fe_2O_3	%MnO	%MgO	%CaO	%Na_2O	%K_2O	%P_2O_5	%LOI	Total
EG5 43.24	248.6	leuconorite	52.42	0.15	22.79	4.45	0.08	5.54	11.88	2.51	0.29	0.02	0.08	100.22
EG5 82.47	209.37	leuconorite	52.33	0.13	20.88	5.46	0.11	7.83	11.20	2.28	0.17	0.00	-0.04	100.36
EG5 136.86	154.98	leuconorite	52.28	0.13	23.61	4.21	0.08	5.59	11.91	2.33	0.18	0.00	0.12	100.45
EG5 160.83	131.01	mottled anorthosite	51.22	0.15	26.63	2.82	0.05	2.52	13.08	2.73	0.24	0.00	0.13	99.59
EG5 172.34	119.5	norite	52.83	0.19	20.53	5.37	0.11	7.31	11.33	2.31	0.26	0.02	0.00	100.27
EG5 175.29	116.55	norite	51.94	0.08	26.52	2.77	0.05	3.17	12.94	2.68	0.17	0.00	0.11	100.43
EG5 186.22	105.62	norite	49.51	0.09	24.26	3.70	0.08	6.93	12.42	1.85	0.10	0.00	0.54	99.47
EG5 186.58	105.26	norite	52.50	0.16	22.55	4.48	0.09	5.96	12.20	2.30	0.23	0.00	0.04	100.50
EG5 203.98	87.86	leuconorite	50.17	0.11	26.78	3.00	0.05	3.10	14.05	2.28	0.11	0.00	0.88	100.54
EG5 211.83	80.01	norite	50.20	0.15	18.53	8.20	0.14	10.40	11.13	1.11	0.03	0.00	0.54	100.46
EG5 224.35	67.49	norite	48.14	0.14	26.72	5.08	0.10	3.57	14.58	1.48	0.05	0.00	0.54	100.41
EG6 147	64.9	mottled anorthosite	51.66	0.20	26.24	3.48	0.06	2.81	13.05	2.58	0.31	0.00	0.16	100.56
EG6 162.84	49.06	mottled anorthosite	50.06	0.12	28.01	2.76	0.05	2.42	14.35	2.31	0.16	0.00	0.22	100.45
EG6 165.85	46.05	mottled anorthosite	49.48	0.11	27.43	2.66	0.05	3.12	14.60	2.30	0.13	0.00	0.40	100.30
EG6 174.75	37.15	mottled anorthosite	49.43	0.08	28.62	2.16	0.04	2.34	14.46	2.24	0.12	0.00	0.78	100.27
EG5 279.0	12.84	pyroxenite	52.25	0.21	8.12	12.42	0.22	19.67	6.18	0.49	0.01	0.00	0.49	100.07
EG5 279.25	12.59	mottled anorthosite	48.27	0.06	30.57	1.92	0.04	1.74	15.71	1.81	0.07	0.00	0.34	100.53
EG5 281.96	9.88	mottled anorthosite	48.01	0.07	30.78	1.95	0.04	1.89	15.89	1.62	0.08	0.00	0.25	100.60
EG5 282.98	8.86	pyroxenite	50.47	0.18	16.48	7.17	0.14	10.94	13.36	1.06	0.02	0.00	0.30	100.13
EG5 286.29	5.55	pyroxenite	54.08	0.24	4.90	11.86	0.23	24.01	4.71	0.37	0.00	0.00	-0.24	100.18
EG5 287.88	3.96	pyroxenite	53.43	0.17	8.48	10.04	0.20	21.57	5.85	0.80	0.02	0.00	-0.09	100.48
EG5 313 94	-22.1	melanorite	51.00	0.07	19.38	5.30	0.11	10.72	11.91	1.61	0.00	0.00	0.27	100.39
EG5 353.62	-61.78	norite	51.40	0.08	20.93	4.37	0.09	8.80	12.12	2.06	0.05	0.00	0.04	99.97
EG5 384.5	-92.66	norite	52.31	0.12	13.98	7.58	0.15	16.48	8.34	1.17	0.05	0.00	0.27	100.45
EG5 391.71	-99.87	norite	51.06	0.08	20.53	5.17	0.10	10.73	10.70	1.65	0.01	0.00	-0.09	99.94
EG5 392.16	-100.32	norite	50.33	0.07	22.85	4.32	0.08	8.35	12.17	1.67	0.04	0.00	0.30	100.18
EG5 414.13	-122.29	norite	51.22	0.11	20.10	5.41	0.11	10.71	10.80	1.58	0.05	0.00	0.36	100.47
EG5 437.36	-145.52	norite	51.93	0.12	19.44	5.60	0.11	10.85	10.47	1.62	0.07	0.00	-0.05	100.16
EG5 452.5	-160.66	norite	51.86	0.12	20.34	5.08	0.10	9.78	11.07	1.72	0.14	0.00	0.08	100.29
EG5 463.61	-171.77	norite	51.39	0.10	20.23	5.21	0.10	10.23	10.69	1.58	0.08	0.00	0.33	99.94
EG5 495.84	-204	norite	50.81	0.08	22.20	4.72	0.09	8.58	11.72	1.76	0.06	0.00	0.05	100.08
EG5 532.16	-240.32	norite	49.79	0.09	24.94	3.62	0.07	6.02	12.78	1.89	0.09	0.00	0.51	99.81
EG5 549.79	-257.95	norite	49.88	0.06	23.50	3.94	0.08	7.89	12.30	1.75	0.04	0.00	0.33	99.76
EG5 568.73	-276.89	mottled anorthosite	48.40	0.03	31.31	1.25	0.02	1.36	15.78	2.09	0.05	0.00	0.25	100.56
EG5 577.54	-285.7	pyroxenite	52.44	0.18	7.22	10.80	0.21	20.88	5.69	3.02	0.04	0.00	-0.08	100.42

EG5 whole rock trace element data

Sample number	Height (m) relative to base of Merensky pyroxenite	Lithology	Rb ppm	Sr ppm	Y ppm	Zr ppm	Nb ppm	Co ppm	Ni ppm	Cu ppm	Zn ppm	%TiO2	V ppm	Cr ppm	Ba ppm
EG5 43.24	248.6	leuconorite	11	287	6	32	5	25	115	26	43	0.14	68	245	97
EG5 82.47	209.37	leuconorite	7	262	6	22	3	31	164	23	47	0.12	78	370	79
EG5 136.86	154.98	leuconorite	7	291	6	25	3	22	121	22	46	0.13	63	248	76
EG5 160.83	131.01	mottled anorthosite	9	342	5	28	4	13	41	22	39	0.13	42	96	85
EG5 172.34	119.5	norite	10	263	7	36	4	29	160	38	49	0.18	77	390	96
EG5 175.29	116.55	norite	5	329	5	18	3	15	61	17	28	0.09	40	135	73
EG5 186.22	105.62	norite	6	312	5	18	3	20	163	20	69	0.09	42	657	68
EG5 186.58	105.26	norite	9	287	6	30	4	26	128	26	57	0.14	70	318	79
EG5 203.98	87.86	leuconorite	5	339	5	17	<3	15	60	22	42	0.09	53	143	61
EG5 211.83	80.01	norite	5	247	9	18	3	51	237	14	123	0.16	109	618	38
EG5 224.35	67.49	norite	6	391	6	19	3	15	63	17	71	0.13	39	149	58
EG6 147	144.84	mottled anorthosite	10	332	7	36	4	15	43	20	48	0.17	56	81	113
EG6 162.84	129	mottled anorthosite	7	343	5	24	4	13	39	20	44	0.10	48	92	61
EG6 165.85	125.99	mottled anorthosite	6	336	5	20	3	14	50	11	36	0.09	41	149	55
EG6 174.75	117.09	mottled anorthosite	5	349	4	17	3	10	36	14	42	0.06	36	110	51
EG5 279.0	11.94	pyroxenite	6	93	8	22	3	101	753	525	123	0.24	169	2257	<20
EG5 279.25	12.59	mottled anorthosite	4	388	3	14	3	10	64	195	54	0.06	23	107	55
EG5 281.96	9.88	mottled anorthosite	4	373	4	15	3	11	81	126	44	0.06	22	119	49
EG5 282.98	8.86	pyroxenite	5	204	10	21	<3	47	307	104	88	0.17	156	1156	48
EG5 286.29	5.55	pyroxenite	5	60	10	22	<3	110	731	126	108	0.28	153	2472	41
EG5 287.88	3.96	pyroxenite	6	117	7	22	4	92	654	66	76	0.19	136	1865	44
EG5 313 94	-22.1	melanorite	4	272	4	16	3	41	261	13	43	0.07	82	1038	<20
EG5 353.62	-61.78	norite	5	318	4	16	3	32	184	14	37	0.07	67	561	32
EG5 384.5	-92.66	norite	5	188	4	17	3	63	377	19	60	0.11	81	1462	43
EG5 391.71	-99.87	norite	5	296	3	15	3	39	277	12	64	0.07	46	1249	24
EG5 392.16	-100.32	norite	5	331	4	15	3	30	211	15	77	0.06	41	1021	39
EG5 414.13	-122.29	norite	4	296	4	19	3	35	246	17	43	0.09	57	1221	55
EG5 437.36	-145.52	norite	6	278	7	26	4	40	253	24	75	0.12	66	1187	55
EG5 452.5	-160.66	norite	7	289	7	28	4	34	230	24	55	0.11	61	1108	55
EG5 463.61	-171.47	norite	6	286	4	21	3	36	240	23	49	0.11	57	1149	51
EG5 495.84	-204	norite	6	318	5	21	4	31	200	28	39	0.09	50	1000	54
EG5 532.16	-240.32	norite	10	350	4	20	3	19	181	39	35	0.12	42	927	67
EG5 549.79	-257.95	norite	5	328	3	15	3	27	181	10	72	0.06	35	855	24
EG5 568.73	-276.89	mottled anorthosite	3	438	<3	14	3	7	32	31	23	0.03	<12	102	36
EG5 577.54	-285.7	pyroxenite	7	100	7	16	3	98	535	29	95	0.21	<12	27	58

KF35 whole rock major element data

Sample number	Height (m) relative to base of Merensky pyroxenite	Lithology	%SiO_2	%TiO_2	%Al_2O_3	%Fe_2O_3	%MnO	%MgO	%CaO	%Na_2O	%K_2O	%P_2O_5	%LOI	Total
KF35 72.06	477.64	gabbronorite	52.11	0.16	17.77	6.93	0.14	9.89	11.02	2.24	0.19	0.00	-0.09	100.38
KF35 118.41	431.29	gabbronorite	52.44	0.16	19.70	6.18	0.12	8.42	10.76	2.36	0.24	0.00	0.17	100.56
KF35 188.97	360.73	gabbronorite	51.73	0.11	24.46	3.87	0.08	4.93	12.51	2.55	0.23	0.00	0.07	100.55
KF35 223.77	315.93	leconorite	51.87	0.11	22.95	4.43	0.09	6.10	11.97	2.47	0.16	0.00	0.05	100.20
KF35 239.66	310.04	norite	52.50	0.16	18.55	6.78	0.14	9.40	10.38	2.27	0.21	0.00	-0.01	100.38
KF35 273.95	275.75	norite	52.12	0.11	22.54	4.46	0.09	6.39	11.87	2.46	0.19	0.00	0.09	100.33
KF35 301.14	248.56	norite	51.68	0.09	22.65	4.57	0.09	6.69	12.07	2.38	0.12	0.00	0.16	100.51
KF35 331.16	218.54	norite	51.23	0.09	22.19	4.03	0.09	8.18	11.76	2.07	0.08	0.00	0.20	99.93
KF35 343.73	205.97	norite	52.16	0.11	20.06	5.84	0.11	8.70	11.05	2.08	0.30	0.00	-0.05	100.39
KF35 371.68	178.02	norite	52.19	0.16	18.77	6.77	0.13	9.08	11.08	2.28	0.15	0.00	-0.04	100.58
KF35 416.13	133.57	norite	52.01	0.14	18.86	6.33	0.13	9.60	10.76	2.02	0.14	0.00	-0.05	99.97
KF35 434.49	115.21	norite	52.10	0.14	17.35	7.41	0.15	11.44	9.83	1.90	0.15	0.00	-0.08	100.40
KF35 436.83	112.87	spotted anorthosite	50.85	0.09	26.06	3.02	0.06	3.75	13.48	2.59	0.15	0.00	0.11	100.17
KF35 455.20	94.5	norite	51.76	0.15	18.92	6.40	0.12	9.46	10.62	2.08	0.17	0.00	0.21	99.90
KF35 503.96	45.74	norite	50.72	0.09	26.01	3.36	0.06	3.80	13.18	2.61	0.15	0.00	0.15	100.16
KF35 526.82	22.88	mottled anorthosite	49.45	0.04	31.21	0.96	0.01	0.49	15.21	2.47	0.11	0.00	0.33	100.29
KF35 526.82	22.88	mottled anorthosite	49.28	0.11	21.51	5.83	0.09	7.87	12.19	1.71	0.05	0.00	0.80	99.47
KF35 526.82	22.88	mottled anorthosite	49.28	0.05	29.58	1.48	0.03	1.32	14.88	2.32	0.17	0.00	0.49	99.60
KF35 529.17	20.53	mottled anorthosite	50.00	0.06	29.46	1.81	0.03	1.85	14.69	2.40	0.10	0.00	0.18	100.59
KF35 532.6*	17.1	mottled anorthosite	48.23	0.1	31.68	0.92	0.04	0.89	16.01	2.01	0.1	0.01	0.1	100.1
KF35 534.1*	15.6	pegmatoid	50.14	0.14	21.79	5.15	0.1	9.91	11.41	1.54	0.09	0.01	-0.01	100.26
KF35 534.5*	15.2	pyroxenite	52.82	0.24	5.18	12.86	0.19	23.77	4.24	0.18	0.22	0.05	0.27	100.03
KF35 534.65*	15.05	pyroxenite	53.36	0.22	5.65	12.61	0.18	23.86	4.13	0.23	0.04	0.01	0.1	100.4
KF35 538.8*	10.9	pyroxenite	52.92	0.23	5.24	12.83	0.18	24.01	4.26	0.28	0.07	0.01	-0.19	99.85
KF35 542.25*	7.45	mottled anorthosite	48.14	0.11	29.93	1.5	0.05	1.58	14.87	2.2	0.17	0.03	0.11	98.71
KF35 544.63*	5.07	spotted anorthosite	49.03	0.12	28.68	2.23	0.06	2.70	14.71	2.11	0.19	0.01	0.42	100.26
KF35 547.06*	2.64	spotted anorthosite	49.42	0.12	27.42	2.77	0.07	3.97	13.9	2.16	0.14	0.01	0.09	100.07
KF35 550.6*	-0.9	norite	51.19	0.16	18.59	5.43	0.11	10.64	12.01	1.66	0.09	0.01	0	99.78
KF35 559.15*	-9.45	leuconorite	53.72	0.23	4.98	12.97	0.2	23.75	4.25	0.49	0.02	0	-0.48	100.11
KF35 573.1*	-23.4	leuconorite	51.26	0.13	24.14	3.46	0.09	5.95	12.71	2.52	0.14	0.01	0.02	100.43
KF35 573.55*	-23.85	norite	52.78	0.19	12.64	8.76	0.16	16.65	8.02	1.29	0.07	0.01	-0.1	100.47
KF35 602.7*	-53	norite	52.02	0.14	16.38	6.78	0.12	13.07	10.11	1.67	0.13	0.02	-0.05	100.41
KF35 616.4*	-66.7	leuconorite	51.1	0.11	23.57	3.72	0.07	6.91	12.15	2.33	0.12	0.01	0.03	100.13
KF35 625.15*	-75.45	norite	51.66	0.15	17.82	4.96	0.1	10.52	12.79	1.92	0.09	0.01	0.08	100.1
KF35 648.1*	-98.4	norite	51.98	0.16	16.54	6.67	0.12	13.49	9.53	1.54	0.1	0.01	0.06	100.2
KF35 653.1*	-103.4	norite	52.15	0.16	16.28	6.83	0.13	13.48	9.47	1.56	0.14	0.02	-0.05	100.16
KF35 653.25*	-103.55	norite	49.85	0.08	31.89	0.66	0.04	0.14	14.91	2.64	0.19	0.01	0.13	100.53
KF35 653.33*	-103.63	norite	51.69	0.15	17	6.45	0.11	12.77	10.26	1.72	0.11	0.02	-0.09	100.21
KF35 672.2*	-122.5	melanorite	49.43	0.09	28.55	1.76	0.05	2.53	13.9	2.54	0.21	0.01	0.09	99.17
KF35 672.36*	-122.66	melanorite	51.91	0.14	17.98	6.43	0.11	12.59	9.37	1.73	0.12	0.01	-0.08	100.33
KF35 677.2*	-127.5	norite	51.53	0.16	15.66	7	0.1	14.23	9.15	1.45	0.11	0.02	0.74	100.16
KF35 690.6*	-140.9	norite	51.41	0.14	16.87	7.29	0.11	13.76	9.33	1.5	0.06	0.01	-0.2	100.29
KF35 690.76*	-141.06	norite	51.83	0.15	17.31	6.81	0.12	12.87	9.86	1.52	0.08	0.01	-0.11	100.45
KF35 699.1*	-149.4	norite	46.69	0.2	9.18	10.6	0.11	19.85	12.72	0.32	0.03	0.01	0.22	100.22

KF35 701.2*	-151.5	norite	50.83	0.13	16.78	7.42	0.09	14.48	9.78	0.87	0.05	0.01	-0.04	100.41
KF35 702.4*	-152.7	norite	51.76	0.33	2.45	9.08	0.19	17.04	17.82	0.09	0.07	0.01	0.47	99.31
KF35 706.2*	-156.5	mottled anorthosite	46.47	0.147	17.19	7.46	0.14	12.17	14.17	0.75	0.06	0.01	0.44	99.03
KF35 711.4*	-161.7	spotted anorthosite	47.84	0.13	27.12	2.43	0.08	3.84	16.97	1.37	0.01	0.01	0.28	100.18
KF35 712.25*	-162.55	norite	48.51	0.16	23.02	3.99	0.15	7.18	15.44	1.17	0.06	0.01	0.29	99.98
KF35 722.75*	-173.05	leuconorite	48.18	0.13	26.1	2.79	0.17	5.01	16	1.28	0.08	0.01	0.7	100.41
KF35 725.15*	-175.45	leuconorite	50.46	0.14	18.08	7.18	0.12	13.48	9.86	0.98	0.04	0.01	-0.1	100.24
KF35 729.05*	-179.35	norite	50.65	0.12	21.63	5.14	0.09	9.65	11.48	1.59	0.06	0.01	0	100.42
KF35 740.5*	-190.8	norite	50.45	0.13	18.79	6.64	0.16	11.74	10.9	1.31	0.06	0.01	-0.08	100.1
KF35 742.6*	-192.9	norite	51.78	0.15	14.78	7.62	0.13	14.48	9.89	1.38	0.04	0	-0.16	100.1
KF35 781.7*	-232	norite	50.8	0.11	19.12	5.88	0.1	12.24	10.47	1.3	0.05	0.01	-0.13	99.96
KF35 786.3*	-236.6	norite	50.04	0.11	19.09	6.06	0.11	12.78	10.76	1.23	0.04	0.01	0.21	100.43
KF35 792.65*	-242.95	spotted anorthosite	51.3	0.13	17.81	6.59	0.11	13.00	10.18	1.39	0.05	0	-0.13	100.46
KF35 797*	-247.3	spotted anorthosite	46.1	0.11	18	7.74	0.11	17.00	9.45	0.73	0.06	0	0.51	99.81
KF35 817.12*	-267.42	spotted anorthosite	49.38	0.11	29.11	1.99	0.05	2.61	14.74	2.11	0.12	0	0.12	100.35
KF35 817.31*	-267.61	spotted anorthosite	49.05	0.09	30.78	1.26	0.05	1.41	15.45	2.17	0.1	0	0.12	100.5
KF35 820.36*	-270.66	leuconorite	49.04	0.09	28.92	1.78	0.05	2.85	14.66	2.14	0.11	0.01	0.29	99.95
KF35 824.28*	-274.58	pyroxenite	53.12	0.21	5.61	12.26	0.19	23.47	5.44	0.22	0.02	0.01	-0.14	100.41
KF35 826.65*	-276.95	harzburgite	43.72	0.22	6.65	15.59	0.14	26.33	4.24	0.39	0.04	0.02	-0.1	100.18
KF35 827.8*	-278.1	pyroxenite	51.75	0.22	8.47	11.34	0.1	20.28	6.2	0.71	0.05	0.01	-0.45	100.33
KF35 837.57*	-287.87	pyroxenite	51.04	0.29	6.95	13.26	0.13	21.45	4.72	0.86	0.08	0.01	-0.42	100.39
KF35 838.69*	-288.99	mottled anorthosite	50.56	0.15	16.97	7.11	0.13	12.68	9.46	2.64	0.08	0.01	0.25	100.05
KF35 839.43*	-289.73	mottled anorthosite	49.72	0.09	30.6	1.15	0.01	1.02	15.08	1.61	0.13	0	-0.15	99.25
KF35 839.58*	-289.88	mottled anorthosite	51.12	0.13	20.33	5.74	0.06	10.32	10.56	1.93	0.1	0.01	-0.11	100.19
KF35 852.1*	-302.4	melanorite	53.66	0.17	7.73	10.97	0.17	22.27	4.97	0.66	0.02	0.01	-0.22	100.42
KF35 860.5*	-310.8	pyroxenite	53.63	0.19	3.02	12.47	0.16	27.15	3.07	0	0.3	0.01	-0.75	99
KF35 863.1*	-313.4	harzburgite	52.26	0.22	3.73	13.97	0.22	26.26	3.04	0	0.02	0.01	-0.56	100.53
KF35 865.7*	-316	mottled anorthosite	53.38	0.21	4.66	12.77	0.15	24.95	4.37	0.18	0.05	0.01	-0.57	100.15
KF35 867.25*	-317.55	mottled anorthosite	48.06	0.09	31.58	0.67	0.07	0.42	15.43	2.4	0.15	0.01	0.19	99.06
KF35 868.85*	-319.15	norite	50.09	0.14	25.91	3.49	0.05	5.58	13.01	2.05	0.16	0.01	0.06	100.57

***** data from Blumberg (2002)

KF35 whole rock trace element data

Sample Number	Height (m) relative to base of Merenksy pyroxenite	Lithology	Rb ppm	Sr ppm	Y ppm	Zr ppm	Nb ppm	Co ppm	Ni ppm	Cu ppm	Zn ppm	%TiO2	V ppm	Cr ppm	Ba ppm
KF35 72.06	477.64	gabbronorite	6	223	8	22	4	43	207	21	64	0.15	116	370	79
KF35 118.41	431.29	gabbronorite	10	250	6	28	3	38	174	21	70	0.15	94	303	87
KF35 188.97	360.73	gabbronorite	7	303	5	23	3	22	93	18	37	0.10	55	208	74
KF35 223.77	315.93	leconorite	6	288	5	20	4	24	112	15	42	0.10	63	256	62
KF35 239.66	310.04	norite	9	238	7	26	3	37	177	24	69	0.15	91	382	79
KF35 273.95	275.75	norite	7	278	5	22	3	26	137	22	45	0.11	66	327	73
KF35 301.14	248.56	norite	5	281	5	18	4	26	146	20	46	0.09	63	359	68
KF35 331.16	218.54	norite	5	322	4	20	4	31	181	20	86	0.08	50	731	44
KF35 343.73	205.97	norite	5	248	6	19	3	36	184	16	48	0.10	80	466	54
KF35 371.68	178.02	norite	8	246	7	24	3	39	174	24	61	0.15	97	434	86
KF35 416.13	133.57	norite	6	243	5	23	4	36	185	15	56	0.13	92	511	57
KF35 434.49	115.21	norite	5	219	7	20	3	46	220	21	66	0.13	111	542	62
KF35 436.83	112.87	spotted anorthosite	5	325	5	19	3	17	60.00	15.00	34.00	0.08	49.00	174.00	74.00
KF35 455.20	94.5	norite	7.00	242.00	7.00	23.00	3.00	36.00	185.00	15.00	49.00	0.14	98.00	550.00	77.00
KF35 503.96	45.74	norite	6.00	328.00	4.00	20.00	3.00	16.00	69.00	17.00	44.00	0.09	50.00	183.00	70.00
KF35 526.82	22.88	mottled anorthosite	3	359	3	15	3	<6	<6	7	44	0.04	<12	<12	41
KF35 526.82	22.88	mottled anorthosite	3	246	5	19	3	35	155	6	61	0.10	96	569	27
KF35 526.82	22.88	mottled anorthosite	5	347	3	16	<3	<6	18	8	38	0.05	18	63	52
KF35 529.17	20.53	mottled anorthosite	4	345	3	15	3	<6	21	9	20	0.05	22	85	53
KF35 532.6*	17.1	mottled anorthosite	3	405	<3	<6	4	11	17	<2	16	0.04	17	62	41
KF35 534.1*	15.6	pegmatoid	5	279	<3	7	4	35	217	46	37	0.07	62	1172	35
KF35 534.5*	15.2	pyroxenite	9	60	6	15	3	96	1079	187	81	0.17	160	2670	14
KF35 534.65*	15.05	pyroxenite	8	71	4	15	3	87	692	74	79	0.17	157	2606	5
KF35 538.8*	10.9	pyroxenite	9	70	6	16	4	96	1191	508	90	0.17	142	2741	15
KF35 542.25*	7.45	mottled anorthosite	5	407	<3	<6	4	15	92	22	15	0.06	22	135	73
KF35 544.63*	5.07	spotted anorthosite	3	392	<3	6	4	38	120	48	17	0.06	29	282	50
KF35 547.06*	2.64	spotted anorthosite	5	390	4	<6	4	37	152	58	19	0.06	38	388	49
KF35 550.6*	-0.9	norite	5	297	5	7	3	58	222	14	35	0.11	108	793	49
KF35 559.15*	-9.45	leuconorite	10	78	5	11	5	83	558	5	85	0.18	199	1533	<5
KF35 573.1*	-23.4	leuconorite	4	404	3	<6	5	20	113	6	28	0.08	60	523	58
KF35 573.55*	-23.85	norite	6	213	6	11	6	53	345	<2	56	0.13	130	1229	28
KF35 602.7*	-53	norite	4	274	4	8	4	42	263	<2	39	0.09	103	1099	32
KF35 616.4*	-66.7	leuconorite	3	394	3	6	4	28	129	<2	23	0.08	56	572	53
KF35 625.15*	-75.45	norite	5	297	4	8	5	38	219	<2	27	0.09	104	1054	34
KF35 648.1*	-98.4	norite	7	262	3	10	4	44	286	<2	44	0.10	88	1232	38
KF35 653.1*	-103.4	norite	8	263	3	9	3	46	284	<2	45	0.11	90	1276	50
KF35 653.25*	-103.55	norite	5	498	<3	<6	5	11	<9	<2	9	0.04	<15	17	65
KF35 653.33*	-103.63	norite	6	273	4	9	4	42	277	<2	43	0.10	86	1248	46
KF35 672.2*	-122.5	melanorite	4	462	<3	<6	3	14	54	<2	18	0.05	23	234	65
KF35 672.36*	-122.66	melanorite	8	289	<3	8	4	39	269	<2	44	0.10	71	1120	50
KF35 677.2*	-127.5	norite	9	246	<3	9	4	46	304	<2	45	0.11	88	1301	35
KF35 690.6*	-140.9	norite	7	264	3	8	4	45	303	<2	49	0.10	92	1445	38
KF35 690.76*	-141.06	norite	7	78	3	7	4	44	270	3	45	0.10	87	1381	36
KF35 699.1*	-149.4	norite	13	122	6	16	4	93	776	<2	60	0.13	212	1476	10

KF35 701.2*	-151.5	norite	7	227	3	9	4	48	280	<2	46	0.08	108	1368	16
KF35 702.4*	-152.7	norite	14	26	13	25	4	60	427	3	49	0.29	489	2623	19
KF35 706.2*	-156.5	mottled anorthosite	11	230	4	11	3	52	429	16	44	0.11	156	733	24
KF35 711.4*	-161.7	spotted anorthosite	6	347	4	6	3	19	72	8	21	0.07	96	441	36
KF35 712.25*	-162.55	norite	8	300	3	8	4	33	136	6	25	0.09	117	549	29
KF35 722.75*	-173.05	leuconorite	6	336	4	7	3	29	100	3	20	0.08	99	540	28
KF35 725.15*	-175.45	leuconorite	8	257	3	<6	<3	42	287	<2	45	0.09	97	1390	9
KF35 729.05*	-179.35	norite	5	343	<3	<6	3	18	203	<2	35	0.07	63	1000	32
KF35 740.5*	-190.8	norite	4	297	<3	<6	7	26	245	5	43	0.08	97	1129	25
KF35 742.6*	-192.9	norite	3	249	4	6	<3	45	303	<2	45	0.10	108	1530	25
KF35 781.7*	-232	norite	5	310	<3	<6	<3	40	257	<2	38	0.06	81	1241	15
KF35 786.3*	-236.6	norite	6	307	<3	<6	3	44	293	<2	37	0.05	79	1239	14
KF35 792.65*	-242.95	spotted anorthosite	5	290	<3	<6	<3	45	281	19	43	0.08	89	1270	19
KF35 797*	-247.3	spotted anorthosite	6	272	10	<6	<3	67	544	10	54	0.05	61	1571	22
KF35 817.12*	-267.42	spotted anorthosite	4	450	6	<6	4	19	64	23	16	0.05	28	270	50
KF35 817.31*	-267.61	spotted anorthosite	4	471	<3	<6	3	13	33	12	15	0.05	19	138	47
KF35 820.36*	-270.66	leuconorite	6	449	<3	<6	4	16	62	25	21	0.05	25	342	50
KF35 824.28*	-274.58	pyroxenite	9	72	3	12	4	85	616	17	79	0.15	152	3607	<5
KF35 826.65*	-276.95	harzburgite	13	97	3	13	3	150	1595	13	104	0.19	190	20216	416
KF35 827.8*	-278.1	pyroxenite	7	131	6	13	4	79	682	8	78	0.18	182	11250	28
KF35 837.57*	-287.87	pyroxenite	11	116	5	15	4	87	534	27	98	0.25	276	14351	35
KF35 838.69*	-288.99	mottled anorthosite	5	479	<3	<6	4	13	20	15	26	0.04	20	86	51
KF35 839.43*	-289.73	mottled anorthosite	6	269	3	8	4	45	264	9	56	0.10	118	1369	24
KF35 839.58*	-289.88	mottled anorthosite	7	319	4	6	4	35	216	<2	39	0.08	90	1020	39
KF35 852.1*	-302.4	melanorite	7	121	<3	10	3	76	524	9	79	0.13	155	2694	15
KF35 860.5*	-310.8	pyroxenite	9	34	3	12	5	98	661	26	87	0.14	148	4079	<5
KF35 863.1*	-313.4	harzburgite	7	34	5	13	4	96	776	5	93	0.19	212	9309	7
KF35 865.7*	-316	mottled anorthosite	9	54	4	13	4	87	622	<2	82	0.16	146	3531	<5
KF35 867.25*	-317.55	mottled anorthosite	3	492	<3	<6	4	10	7	<2	15	0.04	<15	91	65
KF35 868.85*	-319.15	norite	7	406	4	9	4	22	112	15	33	0.10	50	1421	82

***** data from Blumberg (2002)

APPENDIX IV

Orthopyroxene separates major and trace element data for cores RM15 (and clinopyroxene separate data), KV5854, EG5 and KF35

RM15 orthopyroxene separates major element data

Sample Number	Height (m) relative to base of Merensky pyroxenite	Lithology	%SiO_2	%TiO_2	%Al_2O_3	%Fe_2O_3	%MnO	%MgO	%CaO	%Na_2O	%K_2O	%P_2O_5	%LOI	Total	Mg#
RM15-1	387	gabbronorite	52.88	0.44	1.72	16.11	0.29	21.35	6.51	0.26	0.05	0.02	-0.41	99.22	71.7
RM15-2	396	gabbronorite	53.40	0.36	1.56	17.01	0.33	22.64	4.57	0.21	0.06	0.00	-0.45	99.69	73.1
RM15-3	441.87	gabbronorite	53.14	0.38	1.20	15.59	0.37	22.21	6.69	0.17	0.02	0.00	-0.41	99.36	73.3
RM15-4	413.87	gabbronorite	52.52	0.43	2.36	14.33	0.32	19.98	9.81	0.32	0.08	0.00	-0.18	99.97	72.4
RM15-5	448.15	gabbronorite	52.46	0.38	2.41	17.08	0.28	21.99	4.49	0.31	0.02	0.00	-0.47	98.95	72.3
RM15-6a	364	gabbronorite	52.35	0.48	1.35	17.79	0.37	22.77	3.71	0.14	0.20	0.00	-0.35	98.81	71.6
RM15-6b	364	gabbronorite	52.94	0.35	0.91	17.59	0.29	24.86	2.16	0.11	0.05	0.00	-0.56	98.70	73.6
RM17 75.95	248.22	norite	51.95	0.49	1.63	18.15	0.32	22.45	4.17	0.12	0.10	0.00	0.01	99.39	70.9
RM17 93.94	230.23	norite	52.01	0.48	1.28	19.49	0.40	22.80	2.73	0.11	0.08	0.00	-0.63	98.75	69.7
RM17 107.89	216.28	norite	52.03	0.38	1.27	17.78	0.26	23.63	3.11	0.17	0.01	0.02	-0.33	98.33	72.4
RM17 124.53	199.64	norite	50.72	0.83	2.72	18.70	0.33	21.54	3.80	0.16	0.21	0.00	0.46	99.47	69.4
RM17 136.98	187.19	norite	51.84	0.48	1.72	18.14	0.36	24.03	2.37	0.09	0.07	0.00	0.05	99.15	72.3
RM17 159.73	164.44	norite	52.56	0.56	1.66	17.87	0.28	23.54	2.50	0.09	0.04	0.00	-0.02	99.08	72.2
RM17 164.10	160.07	norite	51.49	0.40	2.43	17.12	0.30	24.31	2.46	0.13	0.03	0.00	0.76	99.43	73.7
RM17 185.92	138.25	norite	51.91	0.59	1.91	20.74	0.35	20.58	4.11	0.16	0.20	0.00	-0.25	100.30	66.1
RM17 200.19	123.98	leuconorite	51.40	0.57	2.01	19.13	0.29	22.42	2.84	0.12	0.05	0.00	0.27	99.10	69.8
RM17 222.45	101.72	spotted anorthosite	49.73	0.83	5.32	17.53	0.32	16.10	7.92	0.30	0.29	0.01	1.50	99.85	64.4
RM17 232.17	92	norite	51.19	0.67	2.67	19.55	0.35	21.49	3.42	0.12	0.10	0.00	0.59	100.15	68.4
RM17 250.11	74.06	spotted anorthosite	49.21	0.66	4.13	20.18	0.32	15.62	7.26	0.28	0.13	0.00	0.92	98.71	
RM15 30.12	132.91	norite	50.05	0.39	1.87	18.45	0.24	24.65	3.35	0	0.75	0.12	-0.58	99.29	72.5
RM15 30.28	132.75	norite	53.31	0.33	1.58	17.53	0.22	25.88	1.86	0	0	0.05	-0.33	100.43	74.4
RM15 31.61	131.42	norite	52.21	0.38	2.15	20.29	0.34	22.84	1.98	0.00	0.03	0.03	-0.64	99.61	68.9
RM15 38.01	124.95	spotted anorthosite	49.62	0.48	4.43	21.08	0.34	17.63	6.07	0.02	0.10	0.03	-0.15	99.66	62.2
RM15 44	119.03	spotted anorthosite	52.75	0.28	1.95	15.31	0.21	26.58	1.67	0.06	0	0.05	0.21	99.07	77.4
RM15 45.57	117.46	norite	51.91	0.35	1.61	17.32	0.23	24.9	2.23	0	0	0.05	1.75	100.35	73.9
RM15 51.96	111.34	norite	51.67	0.43	4.03	9.24	0.19	14.78	18.74	0.00	0.06	0.04	-0.60	98.58	75.9
RM15 74.18	88.85	spotted anorthosite	50.53	0.62	2.52	21.05	0.36	21.43	2.79	0.00	0.21	0.03	-0.37	99.17	66.7
RM15 112.23	50.8	mottled anorthosite	51.56	0.32	2.62	18.32	0.30	20.04	6.61	0.02	0.02	0.03	-0.35	99.49	68.3
RM15 146.9	16.13	melanorite	52.16	0.27	1.98	13.66	0.2	27.17	1.82	0	0	0.05	2.65	99.96	79.7
RM15 149.62	13.41	melanorite	53.30	0.26	2.28	14.51	0.25	27.30	1.81	0.00	0.00	0.03	-0.01	99.72	78.7
RM15 151.53	11.5	melanorite	52.63	0.28	1.63	14.53	0.2	27.69	1.53	0	0	0.04	1.68	100.21	79
RM15 153.2	9.83	melanorite	54.02	0.26	1.59	14.38	0.2	28.51	1.65	0	0	0.05	-0.22	100.44	79.6
RM15 160.48	2.55	pyroxenite	53.69	0.24	1.79	14.84	0.24	27.21	2.15	0.00	0.00	0.02	-0.50	99.68	78.3
RM15 160.73	2.3	pyroxenite	54.05	0.26	1.6	13.26	0.2	29.2	1.73	0	0	0.05	-0.16	100.19	81.3
RM15 160.83	2.2	pyroxenite	53.34	0.26	1.5	14.01	0.2	28.91	1.7	0	0	0.05	-0.25	99.72	80.2
RM15 161.03	1.73	pyroxenite	53.79	0.31	1.45	13.72	0.2	28.33	1.95	0	0	0.06	-0.18	99.63	80.3
RM15 161.42	1.61	pyroxenite	53.01	0.27	1.54	13.72	0.2	29.08	1.63	0	0	0.05	-0.07	99.43	80.7
RM15 161.62	1.41	pyroxenite	52.94	0.34	1.41	14.89	0.21	28.66	1.56	0	0	0.06	-0.18	99.89	79.1
RM15 161.98	1.05	pyroxenite	53.64	0.29	1.55	14.09	0.2	28.65	1.637	0	0	0.05	-0.24	99.9	80.0
RM15 162.26	0.77	pyroxenite	52.57	0.26	1.62	13.22	0.19	29.12	1.7	0	0	0.05	-0.14	99.59	81.3
RM15 162.38	0.65	pyroxenite	53.89	0.28	1.66	13.66	0.2	28.83	1.71	0	0	0.05	-0.15	100.13	80.6
RM15 162.57	0.46	pyroxenite	54.13	0.27	1.61	13.9	0.2	28.42	1.84	0	0	0.05	-0.26	100.16	80.1

RM15 162.76	0.27	pyroxenite	54.27	0.29	1.53	14.03	0.2	27.97	1.7	0	0	0.05	-0.15	98.89	79.7
RM15 169.1	-6.07	leuconorite	53.44	0.20	2.08	12.85	0.21	28.20	1.73	0.00	0.00	0.02	-0.15	98.58	81.2
RM15 175.94	-12.91	mottled anorthosite	52.12	0.35	3.09	15.22	0.27	20.23	8.03	0.17	0.03	0.03	-0.01	99.53	72.4
RM15 209.28	-39.95	norite	53.84	0.26	1.75	13.25	0.2	28.99	1.57	0	0	0.06	-0.13	99.79	81.2
RM15 209.9	-46.25	norite	53.87	0.24	1.87	12.83	0.22	27.44	1.82	0.00	0.00	0.02	0.28	98.59	80.8
RM15 216.1	-53.07	norite	53.22	0.28	1.61	13.5	0.19	28.9	1.67	0	0	0.05	-0.26	99.16	81.8
RM15 230.3	-67.27	norite	53.70	0.23	2.01	13.99	0.24	27.61	1.67	0.00	0.00	0.05	-0.20	99.30	81.2
RM15 237.58	-74.55	norite	53.41	0.25	2.30	13.80	0.26	27.57	1.83	0.00	0.02	0.03	0.15	99.62	80.8
RM15 244.23	-81.2	norite	53.00	0.22	1.79	14.12	0.26	27.72	1.76	0.00	0.00	0.01	-0.28	98.60	80.8
RM15 252.3	-89.27	Norite	52.78	0.23	2.14	13.83	0.26	27.84	1.79	0.00	0.00	0.03	0.18	99.08	79.9
RM15 259.27	-96.24	Norite	53.42	0.22	1.75	14.07	0.27	28.28	1.49	0.00	0.00	0.02	-0.09	99.43	79.8
RM15 266	-102.97	Norite	51.61	0.26	3.04	14.00	0.25	26.91	1.99	0.00	0.00	0.03	1.61	99.70	79.1
RM15 281.86	-118.83	Norite	51.95	0.28	2.10	15.13	0.28	26.75	2.13	0.00	0.00	0.03	0.01	98.67	77.7
RM15 288.6	-125.57	Norite	53.18	0.28	2.12	14.78	0.26	26.84	1.93	0.00	0.00	0.02	-0.14	99.27	78.1
RM15 295.29	-132.26	Norite	52.98	0.26	2.19	15.07	0.26	26.38	1.88	0.00	0.03	0.03	-0.14	98.94	77.5
RM15 338	-174.97	Pyroxenite	53.47	0.24	1.73	12.64	0.19	31.13	1.41	0.01	0	0.05	-0.07	99.8	82.9
RM15 342.92	-179.89	Pyroxenite	53.96	0.18	1.64	12.67	0.22	29.03	1.45	0.00	0.00	0.02	-0.35	98.82	81.9

RM15 Clinopyroxene separate major element data

Sample Number	Height (m) relative to base of Merensky pyroxenite	Lithology	%SiO_2	%TiO_2	%Al_2O_3	%Fe_2O_3	%MnO	%MgO	%CaO	%Na_2O	%K_2O	%P_2O_5	%LOI	Total
RM15 51.96	111.34	norite	51.12	0.30	1.72	20.33	0.32	23.36	1.71	0.34	0.00	0.03	0.18	99.41

RM15 orthopyroxene separates trace element data

Sample Number	Height (m) relative to base of Merensky pyroxenite	Lithology	Rb ppm	Sr ppm	Y ppm	Zr ppm	Nb ppm	Co ppm	Ni ppm	Cu ppm	Zn ppm	%TiO2	V ppm	Cr ppm	Ba ppm
RM15-1	387	gabbronorite	12	19	14	50	6	123	465	16	121	0.47	277	779	26
RM15-2	396	gabbronorite	10	19	11	36	5	139	509	13	128	0.40	237	730	26
RM15-3	441.87	gabbronorite	9	16	14	44	4	123	491	17	117	0.41	265	979	31
RM15-4	413.87	gabbronorite	11	26	18	52	4	103	432	18	105	0.45	300	1094	24
RM15-5	448.15	gabbronorite	10	29	11	35	4	129	489	22	134	0.43	220	855	37
RM15-6a	364	gabbronorite	24	12	16	41	5	138	507	22	146	0.60	235	959	65
RM15-6b	364	gabbronorite	12	9	8	29	3	155	587	27	137	0.43	210	1049	41
RM17-75.95	248.22	norite	13	10	15	39	6	138	495	17	146	0.58	247	923	50
RM17-93.94	230.23	norite	11	11	13	37	6	151	494	18	158	0.57	216	805	25
RM17-107.89	216.28	norite	8	11	10	34	4	145	554	9	146	0.44	216	992	24
RM17-124.53	199.64	norite	21	16	17	40	9	133	460	15	156	0.98	247	838	53
RM17-136.98	187.19	norite	11	8	10	31	6	149	554	9	141	0.57	223	1084	32
RM17-159.73	164.44	norite	10	11	11	39	6	140	536	12	156	0.70	220	985	26
RM17-164.10	160.07	norite	7	14	11	35	4	142	572	8	135	0.48	201	1098	28
RM17-185.92	138.25	norite	19	16	17	40	7	146	421	20	165	0.67	260	764	54
RM17-200.19	123.98	leuconorite	11	13	12	35	7	146	496	13	159	0.66	226	892	39
RM17-222.45	101.72	spotted anorthosite	20	36	23	71	9	111	343	29	148	0.89	310	835	53
RM17-232.27	92	norite	14	13	12	41	8	147	462	17	156	0.78	248	955	33
RM17-250.11	74.06	spotted anorthosite	15	24	27	69	7	130	324	24	172	0.74	309	506	40
RM15 30.12	132.91	norite	11	<5	<4	14	<2	110	510	<9	148	0.31	214	1198	22
RM15 30.28	132.75	norite	10	7	<4	7	<2	111	567	23	133	0.26	191	1253	17
RM15 31.61	131.42	norite	8	5	14	6	3	144	472	12	175	0.42	284	898	20
RM15 38.01	124.95	spotted anorthosite	10	16	21	32	5	130	359	17	176	0.52	344	435	32
RM15 44	119.03	spotted anorthosite	9	16	<4	10	<2	110	571	9	117	0.21	164	1356	22
RM15 45.57	117.46	norite	11	<5	<4	19	<2	107	497	12	147	0.33	202	1095	22
RM15 51.96	111.34	norite	6	4	8	<3	3	143	500	15	167	0.33	275	1036	27
RM15 74.18	88.85	spotted anorthosite	21	16	15	19	7	134	436	18	197	0.69	301	934	54
RM15 112.23	50.8	mottled anorthosite	7	16	17	13	3	120	334	16	146	0.31	323	1061	36
RM15 146.9	16.13	melanorite	9	7	<4	14	<2	97	655	10	102	0.22	132	3131	17
RM15 149.62	13.41	melanorite	4	9	9	5	3	111	598	<9	110	0.27	186	2848	<10
RM15 151.53	11.5	melanorite	8	8	4	15	<2	102	650	<9	95	0.22	118	2876	14
RM15 153.2	9.83	melanorite	9	7	<4	13	<2	100	553	<9	104	0.24	126	2907	17
RM15 160.48	2.55	pyroxenite	4	4	9	<3	3	113	978	73	115	0.25	189	3018	<10
RM15 160.73	2.3	pyroxenite	9	9	<4	10	<2	101	943	130	96	0.28	108	3674	17
RM15 160.83	2.2	pyroxenite	9	9	<4	13	<2	98	1000	61	100	0.21	120	3561	18
RM15 161.03	1.73	pyroxenite	10	10	<4	26	<2	96	1135	180	110	0.3	127	2840	26
RM15 161.42	1.61	pyroxenite	9	9	<4	12	<2	100	701	18	99	0.21	115	3496	22
RM15 161.62	1.41	pyroxenite	9	9	6	24	<2	99	676	13	101	0.27	124	3035	18
RM15 161.98	1.05	pyroxenite	11	11	<4	15	<2	102	702	17	106	0.24	115	3421	30
RM15 162.26	0.77	pyroxenite	9	9	<4	11	<2	98	706	16	94	0.19	112	4041	20
RM15 162.38	0.65	pyroxenite	9	9	<4	13	<2	100	706	20	96	0.21	118	4038	19

RM15 162.57	0.46	pyroxenite	9	9	<4	14	<2	96	692	10	100	0.22	117	4254	16
RM15 162.76	0.27	pyroxenite	8	8	<4	15	<2	96	728	29	95	0.24	111	3357	15
RM15 169.1	-6.07	leuconorite	4	9	6	<3	4	108	727	<9	97	0.21	163	3023	16
RM15 175.94	-12.91	mottled anorthosite	8	31	16	32	3	102	425	14	124	0.36	301	1049	29
RM15 209.28	-39.95	norite	8	8	<4	14	<2	99	653	<9	93	0.19	119	3012	22
RM15 209.9	-46.25	norite	3	6	8	<3	3	93	669	<9	99	0.27	172	2695	<10
RM15 216.1	-53.07	norite	8	9	4	14	<2	100	643	13	102	0.21	118	2909	21
RM15 230.3	-67.27	norite	5	8	7	6	4	116	650	<9	107	0.28	179	2630	14
RM15 237.58	-74.55	norite	4	9	6	5	3	112	649	<9	105	0.26	169	2656	13
RM15 244.23	-81.2	norite	4	14	6	4	3	111	662	<9	98	0.22	164	2707	17
RM15 252.3	-89.27	norite	4	9	6	<3	3	114	674	<9	98	0.24	164	2654	14
RM15 259.27	-96.24	norite	4	5	6	<3	3	120	668	10	103	0.24	165	2646	18
RM15 266	-102.97	norite	4	10	7	3	3	106	613	<9	106	0.28	171	2562	20
RM15 281.86	-118.83	norite	5	10	8	8	4	115	619	9	113	0.31	187	2505	13
RM15 288.6	-125.57	norite	5	11	7	5	3	121	617	9	115	0.29	178	2459	14
RM15 295.29	-132.26	norite	4	11	7	7	4	118	612	<9	117	0.28	180	2486	21
RM15 338	-174.97	pyroxenite	9	<5	<4	10	<2	96	661	<9	78	0.18	90	3128	20
RM15 342.92	-179.89	pyroxenite	4	4	5	<3	3	108	690	<9	88	0.18	131	3388	<10

RM15 Clinopyroxene separate trace element data

Sample Number	Height (m) relative to base of Merensky pyroxenite	Lithology	Rb ppm	Sr ppm	Y ppm	Zr ppm	Nb ppm	Co ppm	Ni ppm	Cu ppm	Zn ppm	%TiO2	V ppm	Cr ppm	Ba ppm
RM15 51.96	111.34	norite	8	42	33	19	4	52	310	29	64	0.34	385	1298	23

KV5854 orthopyroxene separates major element data

Sample Number	Height (m) relative to base of Merensky pyroxenite	Lithology	%SiO_2	%TiO_2	%Al_2O_3	%Fe_2O_3	%MnO	%MgO	%CaO	%Na_2O	%K_2O	%P_2O_5	%LOI	Total	Mg#
KV 188.93	107.12	mottled anorthosite	51.44	0.33	3.39	18.31	0.29	18.67	6.91	0.13	0.10	0.05	-0.42	99.20	66.75
KV 192	104.05	mottled anorthosite	51.07	0.38	3.56	17.60	0.30	16.71	9.68	0.13	0.31	0.04	-0.34	99.44	65.15
KV 198.23	97.82	norite	51.75	0.39	1.94	19.73	0.34	22.27	3.02	0.00	0.19	0.03	-0.45	99.21	68.97
KV 210.93	85.12	norite	51.31	0.40	2.12	21.03	0.34	21.64	2.54	0.00	0.09	0.04	-0.09	99.42	66.95
KV 218.23	82.77	mottled anorthosite	50.79	0.48	3.47	19.30	0.32	18.07	6.11	0.14	0.17	0.03	0.32	99.21	64.83
KV 250.53	45.52	mottled anorthosite	50.33	0.37	2.99	20.73	0.35	17.51	7.50	0.10	0.22	0.03	-0.42	99.71	62.45
KV 291.71	13.17	norite	52.59	0.26	2.17	15.18	0.27	26.10	2.60	0.00	0.00	0.01	0.07	99.24	77.20
KV 292.25	3.80	pyroxenite	53.72	0.28	1.65	13.91	0.19	27.96	1.82	0.00	0.00	0.01	0.85	100.39	79.83
KV 292.63	3.42	pyroxenite	54.19	0.29	1.66	13.61	0.19	28.28	1.78	0.00	0.00	0.01	0.29	100.30	80.36
KV 292.85	3.23	pyroxenite	53.63	0.32	1.72	14.38	0.2	27.58	2.16	0.00	0.00	0.01	0.4	100.40	79.06
KV 293.05	3.00	pyroxenite	53.8	0.35	1.58	14.8	0.19	27.56	1.66	0.00	0.00	0.01	0.29	100.24	78.57
KV 293.28	2.77	pyroxenite	54.04	0.38	1.36	15.17	0.2	27.51	1.69	0.00	0.00	0.01	0.04	100.40	78.12
KV 293.5	2.55	pyroxenite	54.14	0.33	2.39	13.96	0.19	27.37	1.94	0.00	0.00	0.01	-0.05	100.28	79.42
KV 293.74	2.31	pyroxenite	53.85	0.36	1.5	15.09	0.21	27.43	1.92	0.00	0.00	0.01	0.01	100.38	78.16
KV 293.94	2.11	pyroxenite	54.12	0.26	1.6	14.26	0.2	27.67	1.85	0.00	0.00	0.01	0.26	100.23	79.25
KV 294.13	1.92	pyroxenite	53.76	0.29	1.85	14.04	0.19	27.54	1.86	0.00	0.00	0.01	0.7	100.24	79.43
KV 294.35	1.70	pyroxenite	53.52	0.29	1.72	14.06	0.19	27.35	1.82	0.00	0.00	0.01	1.01	99.97	79.30
KV 294.44	1.61	pyroxenite	53.78	0.26	1.77	13.19	0.19	28.13	2	0.00	0.00	0.01	0.9	100.23	80.77
KV 294.83	1.22	pyroxenite	54.07	0.32	2.05	13.91	0.19	26.64	2.03	0.00	0.00	0.01	1.17	100.39	79.04
KV 295.05	1.00	pyroxenite	53.28	0.31	1.53	15.04	0.21	27.98	1.73	0.00	0.00	0.01	0.15	100.24	78.55
KV 295.21	0.84	pyroxenite	53.92	0.29	1.51	14.97	0.2	27.73	1.7	0.00	0.00	0.01	0.01	100.34	78.48
KV 295.36	0.69	pyroxenite	53.62	0.31	1.57	15.07	0.2	27.26	1.74	0.00	0.00	0.01	0.29	100.07	78.08
KV 295.56	0.49	pyroxenite	53.49	0.36	1.59	15.08	0.2	26.94	1.78	0.00	0.00	0.01	0.42	99.87	77.86
KV 295.75	0.30	pyroxenite	54.08	0.27	1.6	14.49	0.2	28.03	1.71	0.00	0.00	0.01	0.05	100.44	79.20
KV 295.94	0.11	pyroxenite	53.81	0.36	1.46	14.85	0.21	27.63	1.69	0.00	0.00	0.01	0.14	100.16	78.56
KV 296.1	-0.05	pegmatoid	53.49	0.29	2.12	13.75	0.2	27.57	2.34	0.00	0.00	0.01	0.59	100.36	79.79
KV 307.4	-0.35	norite	54.24	0.26	1.5	14.13	0.21	28.93	1.45	0.00	0.00	0.01	-0.31	100.42	80.12
KV 327.69	-31.64	leuconorite	53.65	0.26	2.48	13.12	0.2	27.7	2.34	0.00	0.00	0.01	0.08	99.84	80.61
KV 335.68	-39.45	mottled anorthosite	54.49	0.26	1.71	13.49	0.2	28.14	1.83	0.00	0.00	0.01	0.28	100.41	80.42
KV 352.53	-56.48	norite	54.18	0.17	1.48	12.95	0.26	29.25	1.33	0.00	0.00	0.02	-0.30	99.34	81.64
KV 352.85	-56.80	melanorite	53.66	0.25	2.42	12.7	0.2	28.09	2.8	0.00	0.00	0.00	0.13	100.25	81.32
KV 353.24	-57.19	melanorite	54.42	0.28	2.15	12.94	0.2	28.27	2.11	0.00	0.00	0.00	-0.15	100.22	81.14
KV 367.28	-71.23	melanorite	53.71	0.28	2.21	13.49	0.19	28.04	2.14	0.00	0.00	0.00	0.38	100.44	80.36
KV 378.9	-82.85	melanorite	53.66	0.23	1.78	13.99	0.25	27.92	1.61	0.00	0.00	0.01	-0.30	99.15	79.71
KV 388.85	-92.80	melanorite	53.28	0.34	1.76	14.8	0.2	27.56	1.87	0.00	0.00	0.00	0.18	99.99	78.57
KV 404.41	-108.36	melanorite	53.76	0.34	2.27	14.36	0.2	26.59	2.57	0.00	0.00	0.00	0.21	100.30	78.47
KV 421.8	-125.75	norite	54.08	0.32	1.73	14.86	0.2	27.36	1.87	0.00	0.00	0.00	-0.14	100.28	78.38
KV 428.94	-132.89	norite	54.07	0.3	1.67	14.7	0.2	27.79	1.75	0.00	0.00	0.00	-0.19	100.29	78.82
KV 438.41	-142.36	norite	52.58	0.40	2.29	15.48	0.27	25.65	2.19	0.00	0.14	0.02	0.75	99.77	76.54
KV 448.43	-152.38	norite	52.83	0.37	1.99	16.23	0.22	25.95	2.08	0.00	0.00	0	0.68	100.35	75.89
KV 460.59	-164.54	norite	53.68	0.34	1.89	15.53	0.21	27	1.8	0.00	0.00	0	-0.1	100.35	77.39
KV 468.41	-172.36	norite	52.43	0.25	2.33	15.24	0.26	26.56	1.79	0.00	0.00	0.02	0.65	99.53	77.43
KV 507	-210.95	norite	53.55	0.30	2.18	14.21	0.25	26.09	2.06	0.00	0.01	0.03	0.55	99.22	78.33

KV5854 orthopyroxene separates trace element data

Sample Number	Height (m) relative to base of Merensky pyroxenite	Lithology	Rb ppm	Sr ppm	Y ppm	Zr ppm	Nb ppm	Co ppm	Ni ppm	Cu ppm	Zn ppm	%TiO2	V ppm	Cr ppm	Ba ppm
KV 188.93	107.12	mottled anorthosite	11	29	22	35	4	114	353	21	156	0.34	297	808	44
KV 192	104.05	mottled anorthosite	23	28	25	45	4	104	309	23	151	0.39	331	786	70
KV 198.23	97.82	norite	16	7	14	19	4	136	472	16	163	0.46	287	1134	53
KV 210.93	85.12	norite	13	8	12	15	5	144	426	13	175	0.47	288	789	44
KV 218.23	82.77	mottled anorthosite	17	31	21	39	6	122	337	17	161	0.50	310	700	62
KV 250.53	45.52	mottled anorthosite	16	22	25	30	4	119	287	18	164	0.38	338	580	62
KV 291.71	13.17	norite	4	11	8	<3	2	120	893	129	118	0.27	204	2718	<10
KV 292.25	3.80	pyroxenite	10	9	4	13	<2	102	818	93	94	0.22	118	3467	34
KV 292.63	3.42	pyroxenite	9	9	7	13	2	98	735	31	94	0.21	113	3754	30
KV 292.85	3.23	pyroxenite	9	12	<4	9	<2	94	691	18	97	0.24	126	3601	27
KV 293.05	3.00	pyroxenite	10	7	4	34	2	97	709	49	107	0.28	133	3608	19
KV 293.28	2.77	pyroxenite	12	5	5	44	<2	102	620	15	107	0.33	130	2742	31
KV 293.5	2.55	pyroxenite	12	11	4	22	2	97	647	14	99	0.24	127	3459	30
KV 293.74	2.31	pyroxenite	13	7	<4	34	2	95	629	11	105	0.32	139	3989	35
KV 293.94	2.11	pyroxenite	11	6	6	42	<2	98	630	14	105	0.31	136	3998	27
KV 294.13	1.92	pyroxenite	10	13	<4	11	<2	99	646	18	102	0.24	125	3395	30
KV 294.35	1.70	pyroxenite	11	7	<4	13	<2	97	643	16	101	0.25	129	3393	31
KV 294.44	1.61	pyroxenite	9	11	<4	10	<2	97	712	16	89	0.19	118	3632	26
KV 294.83	1.22	pyroxenite	12	10	<4	18	<2	96	614	23	96	0.29	133	3177	40
KV 295.05	1.00	pyroxenite	12	<5	<4	16	<2	102	627	17	102	0.27	128	3146	29
KV 295.21	0.84	pyroxenite	9	5	<4	14	<2	102	641	22	109	0.23	126	3376	28
KV 295.36	0.69	pyroxenite	13	<5	1	17	<2	98	622	17	105	0.28	128	3106	30
KV 295.56	0.49	pyroxenite	16	6	6	37	2	96	602	15	104	0.36	137	2865	47
KV 295.75	0.30	pyroxenite	10	6	<4	12	<2	100	640	10	98	0.21	116	3415	24
KV 295.94	0.11	pyroxenite	10	7	<4	14	<2	101	637	13	95	0.36	123	3747	28
KV 296.1	-0.05	pegmatoid	11	7	<4	13	<2	96	661	15	85	0.25	117	3467	31
KV 307.4	-0.35	norite	8	5	4	13	<2	104	641	<9	101	0.19	126	2939	14
KV 327.69	-31.64	leuconorite	9	17	<4	14	<2	104	581	<9	901	0.21	149	2765	20
KV 335.68	-39.45	mottled anorthosite	8	10	<4	96	<2	106	608	<9	88	0.19	135	2049	20
KV 352.53	-56.48	norite	4	5	4	<3	3	118	654	<9	94	0.17	145	2237	<10
KV 352.85	-56.80	melanorite	9	49	<4	9	<2	97	638	<9	83	0.17	96	1946	27
KV 353.24	-57.19	melanorite	9	8	<4	7	<2	104	633	<9	86	0.17	105	2134	20
KV 367.28	-71.23	melanorite	9	14	<4	13	<2	103	677	<9	89	0.19	109	3199	23
KV 378.9	-82.85	melanorite	5	8	7	<3	3	112	709	<9	102	0.25	166	2732	18
KV 388.85	-92.80	melanorite	11	8	<4	16	<2	97	627	<9	101	0.26	124	2774	26
KV 404.41	-108.36	melanorite	14	17	<4	24	<2	93	588	<9	97	0.3	128	2662	51
KV 421.8	-125.75	norite	12	10	<4	22	<2	99	578	10	107	0.29	127	2567	37
KV 428.94	-132.89	norite	10	8	<4	13	<2	103	591	<9	106	0.25	125	2637	26
KV 438.41	-142.36	norite	12	10	9	29	4	113	535	<9	117	0.43	201	2169	67
KV 448.43	-152.38	norite	12	8	6	33	<2	97	570	15	113	0.34	149	2671	28
KV 460.59	-164.54	norite	11	10	<4	18	<2	98	569	<9	110	0.28	128	2501	30
KV 468.41	-172.36	norite	5	8	6	<3	3	115	593	<9	116	0.28	183	2477	29
KV 507	-210.95	norite	6	12	9	16	4	115	606	9	110	0.32	194	2931	26

EG5 orthopyroxene separates major element data

Sample Number	Height (m) relative to base of Merensky pyroxenite	Lithology	%SiO_2	%TiO_2	%Al_2O_3	%Fe_2O_3	%MnO	%MgO	%CaO	%Na_2O	%K_2O	%P_2O_5	%LOI	Total	Mg#
EG5 43.24	248.6	leuconorite	53.12	0.46	2.27	18.50	0.36	23.85	2.40	0.03	0.16	0.00	-0.73	100.44	71.74
EG5 136.86	154.98	leuconorite	53.47	0.35	2.23	17.53	0.34	23.94	3.02	0.05	0.13	0.00	-0.60	100.47	72.89
EG5 147	144.84	norite	51.03	0.41	4.09	18.89	0.34	16.45	8.95	0.28	0.19	0.03	-0.24	100.43	63.13
EG5 160.83	131.01	mottled anorthosite	51.38	0.44	3.68	17.18	0.32	18.09	8.98	0.22	0.33	0.00	-0.24	100.40	67.46
EG5 165.85	125.99	mottled anorthosite	51.48	0.35	4.22	16.26	0.30	19.92	7.36	0.22	0.04	0.01	0.34	100.51	70.69
EG5 172.34	119.5	norite	53.28	0.42	2.35	16.50	0.31	23.29	4.34	0.08	0.30	0.00	-0.52	100.35	73.54
EG5 175.29	116.55	norite	52.96	0.32	2.78	18.00	0.34	23.20	3.09	0.13	0.04	0.01	-0.51	100.37	71.73
EG5 186.22	105.62	norite	54.26	0.24	3.05	12.96	0.26	26.53	2.71	0.09	0.00	0.00	0.23	100.34	80.12
EG5 186.58	105.26	norite	52.96	0.37	2.15	17.40	0.34	24.23	3.30	0.04	0.12	0.02	-0.66	100.26	73.27
EG5 203.98	87.86	leuconorite	50.86	0.38	4.81	13.85	0.26	17.38	11.33	0.19	0.04	0.00	1.32	100.43	71.19
EG5 211.83	80.01	norite	52.78	0.30	3.19	17.81	0.32	22.55	3.44	0.08	0.01	0.02	-0.06	100.46	71.37
EG5 224.35	67.49	norite	50.47	0.34	4.25	21.98	0.40	16.63	6.23	0.14	0.07	0.01	-0.13	100.41	59.83
EG5 262.84	29	mottled anorthosite	51.53	0.47	4.28	16.01	0.31	18.19	9.44	0.29	0.05	0.01	-0.10	100.48	69.11
EG5 279.00	12.84	pyroxenite	54.06	0.25	2.42	15.74	0.28	24.96	2.82	0.05	0.00	0.01	-0.22	100.39	75.74
EG5 281.96	9.88	mottled anorthosite	53.16	0.37	4.15	16.53	0.32	21.18	6.24	0.12	0.04	0.01	-1.85	100.29	71.61
EG5 282.98	8.86	pyroxenite	52.60	0.29	2.80	14.47	0.27	21.25	8.10	0.12	0.00	0.01	-0.15	99.76	74.30
EG5 287.88	3.96	pyroxenite	54.90	0.19	1.68	13.17	0.26	28.52	2.10	0.00	0.00	0.02	-0.34	100.52	81.00
EG5 313.94	-22.1	melanorite	54.48	0.12	2.37	12.94	0.27	27.49	2.67	0.08	0.00	0.00	-0.41	100.03	80.70
EG5 331.16	-39.32	norite	55.03	0.19	2.16	12.29	0.26	27.43	3.56	0.06	0.00	0.00	-0.42	100.59	81.46
EG5 353.62	-61.78	norite	54.98	0.15	1.84	12.02	0.27	27.48	3.51	0.05	0.00	0.00	-0.35	99.97	81.82
EG5 384.25	-92.66	norite	54.90	0.15	1.79	12.62	0.25	28.85	2.01	0.00	0.00	0.00	-0.33	100.25	81.82
EG5 391.71	-99.87	norite	55.53	0.14	1.56	12.81	0.25	29.25	1.47	0.00	0.00	0.00	-0.57	100.47	81.80
EG5 392.16	-100.32	norite	55.09	0.17	1.63	13.17	0.26	28.47	1.98	0.00	0.00	0.02	-0.34	100.47	80.97
EG5 414.13	-122.29	norite	54.65	0.21	2.59	13.04	0.27	27.16	2.59	0.08	0.00	0.01	-0.12	100.48	80.40
EG5 437.36	-145.52	norite	54.48	0.23	2.93	13.30	0.27	26.71	3.04	0.13	0.00	0.01	-0.58	100.53	79.81
EG5 452.5	-160.66	norite	54.67	0.21	1.95	13.36	0.26	27.75	2.37	0.02	0.00	0.00	-0.51	100.09	80.35
EG5 463.61	-171.77	norite	55.12	0.22	1.95	13.42	0.26	27.55	2.24	0.01	0.00	0.01	-0.31	100.49	80.17
EG5 495.84	-204	norite	54.65	0.20	2.23	13.71	0.27	27.03	2.78	0.04	0.00	0.01	-0.51	100.41	79.52
EG5 532.16	-240.32	norite	54.06	0.23	3.49	13.42	0.26	25.14	3.48	0.13	0.00	0.00	0.25	100.48	78.67
EG5 549.79	-257.95	norite	54.30	0.16	2.30	13.25	0.27	27.49	2.51	0.03	0.00	0.01	0.04	100.36	80.33
EG5 577.54	-285.7	pyroxenite	54.37	0.21	2.74	13.37	0.27	26.05	3.46	0.17	0.00	0.00	-0.28	100.38	79.32

EG5 orthopyroxene separates trace element data

Sample Number	Height (m) relative to base of Merensky pyroxenite	Lithology	Rb ppm	Sr ppm	Y ppm	Zr ppm	Nb ppm	Co ppm	Ni ppm	Cu ppm	Zn ppm	%TiO2	V ppm	Cr ppm	Ba ppm
EG5 43.24	248.6	leuconorite	20	11	8	33	5	149	539	11	149	0.53	223	890	43
EG5 136.86	154.98	leuconorite	14	10	9	29	3	140	552	10	137	0.40	211	981	50
EG5 147	144.84	norite	20	36	25	66	5	123	313	14	158	0.44	321	529	54
EG5 160.83	131.01	mottled anorthosite	29	28	22	56	5	112	355	14	137	0.45	291	698	71
EG5 165.85	125.99	mottled anorthosite	9	36	13	32	3	117	400	9	117	0.35	283	1103	29
EG5 172.34	119.5	norite	23	13	11	34	4	135	527	19	128	0.49	239	1134	86
EG5 175.29	116.55	norite	11	19	8	25	3	149	508	13	145	0.37	207	850	40
EG5 186.22	105.62	norite	5	24	8	22	3	112	641	9	113	0.28	148	2544	22
EG5 186.58	105.26	norite	15	12	10	31	3	137	534	9	138	0.41	220	1064	43
EG5 203.98	87.86	leuconorite	8	33	17	30	3	85	302	20	105	0.35	328	939	28
EG5 211.83	80.01	norite	5	25	10	19	3	125	504	13	164	0.34	183	1158	32
EG5 224.35	67.49	norite	9	37	16	29	3	100	298	22	203	0.37	139	640	61
EG5 262.84	29	mottled anorthosite	10	43	19	51	6	105	334	14	128	0.45	319	793	30
EG5 279.00	12.84	pyroxenite	6	19	8	20	3	130	707	124	120	0.27	179	2544	<20
EG5 281.96	9.88	mottled anorthosite	7	36	11	23	3	116	675	101	126	0.39	225	1541	39
EG5 282.98	8.86	pyroxenite	5	26	13	23	4	119	568	41	124	0.31	261	1975	36
EG5 287.88	3.96	pyroxenite	5	11	6	20	3	138	805	20	91	0.23	164	2270	28
EG5 313.94	-22.1	melanorite	5	21	4	15	<3	124	680	<6	88	0.15	147	2111	<20
EG5 331.16	-39.32	norite	4	19	6	23	3	123	607	<6	104	0.22	152	2382	<20
EG5 353.62	-61.78	norite	6	17	4	17	<3	128	609	<6	83	0.19	164	1505	<20
EG5 384.25	-92.66	norite	3	8	5	17	3	122	630	<6	86	0.18	118	2295	<20
EG5 391.71	-99.87	norite	4	7	4	15	2	137	806	6	102	0.17	114	3360	<20
EG5 392.16	-100.32	norite	5	8	4	18	<3	137	784	<6	118	0.19	124	3447	<20
EG5 414.13	-122.29	norite	5	19	6	22	3	116	711	<6	93	0.22	136	3124	20
EG5 437.36	-145.52	norite	6	28	7	23	3	116	652	10	103	0.25	144	2798	31
EG5 452.5	-160.66	norite	8	13	6	25	3	123	680	9	101	0.26	141	2883	27
EG5 463.61	-171.77	norite	6	10	5	22	<3	126	674	10	101	0.25	138	2975	20
EG5 495.84	-204	norite	6	17	6	21	3	126	669	11	98	0.23	139	3046	<20
EG5 532.16	-240.32	norite	7	28	7	24	3	111	602	18	96	0.26	139	3314	23
EG5 549.79	-257.95	norite	5	15	5	17	4	121	656	<6	106	0.17	101	2773	<20
EG5 577.54	-285.7	pyroxenite	5	29	8	21	3	124	609	<6	97	0.24	178	2212	29

KF35 orthopyroxene separates major element data

Sample Number	Height (m) relative to base of Merensky pyroxenite	Lithology	%SiO_2	%TiO_2	%Al_2O_3	%Fe_2O_3	%MnO	%MgO	%CaO	%Na_2O	%K_2O	%P_2O_5	%LOI	Total	Mg#
KF35 72.06	431.29	gabbronorite	54.02	0.25	1.29	17.33	0.35	24.99	2.66	0.00	0.00	0.00	-0.65	100.26	73.95
KF35 118.41	360.73	gabbronorite	53.37	0.32	2.31	16.25	0.33	23.02	4.68	0.10	0.06	0.00	-0.53	99.90	73.61
KF35 188.97	325.93	gabbronorite	53.99	0.34	1.85	17.40	0.34	24.14	2.80	0.12	0.04	0.00	-0.52	100.52	73.20
KF35 223.77	310.04	leuconorite	53.65	0.28	2.16	16.43	0.33	23.65	4.48	0.09	0.00	0.00	-0.58	100.52	73.64
KF35 239.66	275.75	norite	54.14	0.30	1.49	17.25	0.34	24.47	3.03	0.04	0.00	0.00	-0.57	100.51	75.07
KF35 273.95	248.56	norite	54.16	0.26	3.01	15.78	0.31	24.13	3.13	0.17	0.00	0.00	-0.59	100.37	73.64
KF35 301.14	205.97	norite	54.29	0.23	1.55	16.64	0.33	25.97	2.25	0.00	0.00	0.00	-0.67	100.60	75.45
KF35 343.73	178.02	norite	54.35	0.21	2.06	16.14	0.31	25.83	2.28	0.04	0.00	0.00	-0.65	100.59	75.91
KF35 371.68	133.57	norite	53.83	0.31	1.64	17.41	0.34	24.46	3.05	0.01	0.00	0.00	-0.68	100.39	73.45
KF35 416.13	115.21	norite	54.23	0.27	1.80	16.06	0.33	25.24	3.12	0.01	0.00	0.00	-0.61	100.46	75.58
KF35 434.49	112.87	norite	54.33	0.25	1.64	16.22	0.33	25.79	2.53	0.00	0.00	0.00	-0.73	100.39	75.79
KF35 436.83	94.5	spotted anorthosite	53.39	0.31	2.39	16.28	0.33	22.44	5.69	0.08	0.00	0.00	-0.56	100.36	73.07
KF35 455.20	45.74	norite	53.69	0.28	2.09	16.21	0.31	24.55	3.31	0.10	0.00	0.00	-0.11	100.44	74.89
KF35 503.96	22.88	norite	53.21	0.31	2.42	18.07	0.33	22.69	4.10	0.06	0.00	0.00	-0.68	100.52	71.20
KF35 526.82	20.53	mottled anorthosite	51.87	0.04	30.12	0.58	0.01	0.54	13.76	0.42	0.28	0.00	1.12	97.45	64.70
KF35 529.17	477.64	mottled anorthosite	52.45	0.26	4.26	15.35	0.31	20.61	7.12	0.26	0.00	0.00	-0.46	100.17	72.55
KF35 547.06*	2.64	spotted anorthosite	53.66	0.26	2.11	16.45	0.31	25.92	2.27	0	0.02	0.06	-0.68	100.38	75.62
'KF35 550.6*	-0.9	norite	54.36	0.24	1.66	14.67	0.26	27.64	1.32	0	0.02	0.05	-0.65	99.57	78.77
'KF35 573.55*	-23.85	norite	54.3	0.23	1.36	15.23	0.28	27.62	1.59	0	0.01	0.05	-0.71	99.96	78.12
KF35 625.15*	-75.45	norite	53.33	0.19	2.14	13.7	0.27	27.32	2.17	0	0.02	0.05	-0.45	98.74	79.70
KF35 653.1*	-103.4	norite	54.17	0.23	1.64	14.7	0.27	27.83	1.41	0	0.2	0.05	-0.65	99.85	78.85
KF35 701.2*	-151.5	norite	54.2	0.2	1.74	14.55	0.26	28.02	1.62	0	0	0.06	-0.5	100.15	79.13
KF35 740.05*	-190.35	norite	51.93	0.21	1.53	16.3	0.31	27.48	1.41	0	0	0.05	-0.59	98.63	76.85
KF35 781.7*	-232	norite	54.81	0.16	1.66	13.95	0.29	28.58	1.41	0	0	0.05	-0.53	100.38	80.13
KF35 824.28*	-274.58	pyroxenite	54.02	0.21	1.97	14.56	0.25	27.71	1.69	0	0	0.05	-0.49	99.97	78.93
KF35 852.1*	-302.4	melanorite	54.57	0.21	1.58	15.53	0.27	28.34	1.15	0	0	0.05	-0.64	100.06	79.34
KF35 860.5*	-310.8	pyroxenite	53.49	0.19	2	13.65	0.26	28.40	1.48	0	0.3	0.05	-0.4	99.42	80.38

***** Data from Blumberg (2002)

KF35 orthopyroxene separates trace element data

Sample Number	Height (m) relative to base of Merensky pyroxenite	Lithology	Rb ppm	Sr ppm	Y ppm	Zr ppm	Nb ppm	Co ppm	Ni ppm	Cu ppm	Zn ppm	%TiO2	V ppm	Cr ppm	Ba ppm
KF35 72.06	431.29	gabbronorite	9	20	9	29	3	141	532	15	136	0.35	221	777	24
KF35 118.41	360.73	gabbronorite	14	16	10	21	4	139	511	14	144	0.39	217	743	42
KF35 188.97	325.93	gabbronorite	9	16	10	27	3	137	538	13	134	0.33	228	996	28
KF35 223.77	310.04	leuconorite	12	12	9	31	4	148	553	22	155	0.42	215	934	41
KF35 239.66	275.75	norite	7	26	8	23	3	142	567	13	128	0.30	191	1059	26
KF35 273.95	248.56	norite	5	9	7	18	3	149	606	9	133	0.27	191	1169	21
KF35 301.14	205.97	norite	6	11	6	19	3	150	610	11	124	0.26	189	1209	22
KF35 343.73	178.02	norite	9	8	8	25	3	152	545	18	146	0.37	210	986	36
KF35 371.68	133.57	norite	8	10	9	25	3	137	578	15	137	0.32	214	1243	24
KF35 416.13	115.21	norite	6	7	7	21	<3	149	585	19	136	0.30	207	1212	<20
KF35 434.49	112.87	norite	7	17	11	29	3	134	457	15	142	0.35	260	1009	25
KF35 436.83	94.5	spotted anorthosite	7	13	8	26	4	134	541	15	123	0.34	220	1316	33
KF35 455.20	45.74	norite	6	17	10	30	4	144	491	12	152	0.37	267	1138	22
KF35 503.96	22.88	norite	6	67	11	36	3	89	356	9	117	0.28	261	1142	<20
KF35 526.82	20.53	mottled anorthosite	5	38	10	27	3	119	362	13	115	0.29	242	1028	30
KF35 529.17	477.64	mottled anorthosite	7	6	8	35	<3	148	560	10	141	0.31	219	906	22
KF35 547.06*	2.64	spotted anorthosite	8	14	3	12	4	115	612	<2	101	0.18	178	2531	<5
'KF35 550.6*	-0.9	norite	9	13	5	15	5	112	709	36	116	0.22	200	1541	<5
'KF35 573.55*	-23.85	norite	11	9	4	12	4	115	607	<2	104	0.18	188	1903	<5
KF35 625.15*	-75.45	norite	5	20	<3	11	4	107	549	<2	79	0.15	170	1892	<5
KF35 653.1*	-103.4	norite	9	12	3	13	5	112	625	<2	96	0.18	151	2329	<5
KF35 701.2*	-151.5	norite	9	10	<3	12	4	114	586	<2	86	0.14	196	2589	<5
KF35 740.05*	-190.35	norite	9	10	3	13	5	112	628	<2	100	0.16	191	2419	<5
KF35 781.7*	-232	norite	9	10	<3	11	4	111	639	<2	90	0.11	175	2859	<5
KF35 824.28*	-274.58	pyroxenite	9	8	3	12	4	105	709	<2	94	0.15	160	3736	<5
KF35 852.1*	-302.4	melanorite	7	10	<3	11	4	112	680	<2	94	0.16	194	3352	<5
KF35 860.5*	-310.8	pyroxenite	9	10	4	12	5	106	647	<2	92	0.14	132	3767	<5

***** Data from Blumberg (2002)

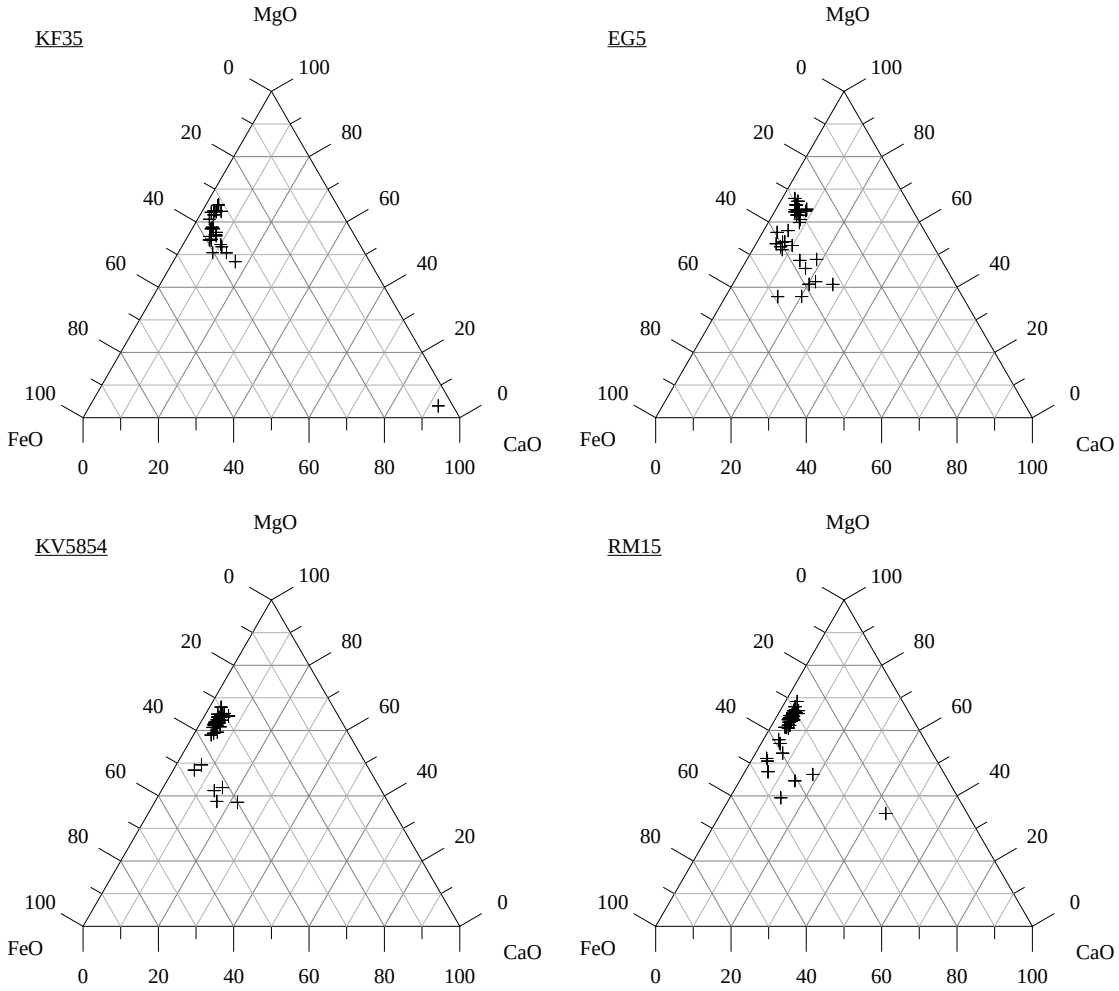


FIGURE IVa.

Ternaray diagrams showing the compositional variation of the orthopyroxene separates from KF35, EG5, KV5854 and RM15. Samples that plot at >10% CaO in this diagram, i.e. those that contain some clinopyroxene, have been excluded from diagrams and calculations within the main text.

APPENDIX V

Plagioclase separates major and trace element data for cores RM15, KV5854, EG5 and KF35

RM15 plagioclase separates major element data

Sample number	Height (m) relative to base of Merensky pyroxenite	Lithology	%SiO_2	%TiO_2	%Al_2O_3	%Fe_2O_3	%MnO	%MgO	%CaO	%Na_2O	%K_2O	%P_2O_5	%LOI	Total	An#
RM15-1	387	gabbronorite	53.32	0.06	29.78	0.25	0.00	0.24	12.81	3.22	0.47	0.02	0.26	100.43	68.73
RM15-2	396	gabbronorite	52.04	0.05	29.91	0.24	0.02	0.14	13.02	3.36	0.40	0.00	0.31	99.49	68.17
RM15-3	441	gabbronorite	51.27	0.06	29.52	0.39	0.02	0.10	12.86	3.36	0.44	0.00	1.25	99.27	67.90
RM15-4	413	gabbronorite	52.36	0.06	30.22	0.30	0.00	0.18	13.22	3.23	0.38	0.02	0.24	100.21	69.34
RM15-5	448	gabbronorite	51.84	0.06	30.05	0.26	0.00	0.17	13.02	3.26	0.38	0.02	0.69	99.75	68.82
RM15-6a	364	gabbronorite	53.02	0.06	28.84	0.27	0.00	0.12	12.82	3.09	0.40	0.04	0.24	98.90	69.63
RM15-6b	364	gabbronorite	50.75	0.05	30.58	0.14	0.00	0.14	13.41	2.98	0.33	0.00	0.23	98.61	71.32
RM17-75.95	248.22	norite	53.30	0.06	28.93	0.37	0.00	0.27	12.48	3.30	0.56	0.04	0.59	99.90	67.64
RM17-93.94	230.23	norite	53.29	0.06	29.58	0.32	0.00	0.20	12.63	3.28	0.41	0.04	0.40	100.21	68.03
RM17-107.89	216.28	norite	51.52	0.06	30.23	0.40	0.00	0.32	13.35	3.04	0.48	0.02	0.60	100.02	70.82
RM17-124.53	199.64	norite	53.45	0.06	28.10	0.66	0.00	0.44	12.33	3.14	0.59	0.05	0.77	99.59	68.45
RM17-136.98	187.19	norite	53.11	0.06	28.73	0.66	0.01	0.50	12.72	3.14	0.50	0.04	0.81	100.28	69.12
RM17-159.73	164.44	norite	52.22	0.07	29.45	0.59	0.00	0.45	12.97	3.18	0.39	0.00	0.50	99.82	69.27
RM17-164.10	160.07	norite	51.79	0.06	29.38	0.66	0.01	0.63	13.17	3.23	0.39	0.00	0.85	100.17	69.26
RM17-174.30	149.87	leuconorite	56.33	0.05	25.79	0.90	0.00	1.02	12.29	2.25	0.26	0.00	1.50	100.39	75.11
RM17-185.92	138.25	norite	52.11	0.06	30.01	0.32	0.00	0.17	13.05	3.16	0.50	0.01	0.51	99.90	69.53
RM17-200.19	123.98	leuconorite	52.39	0.06	29.02	0.68	0.00	0.50	13.02	2.90	0.55	0.00	0.82	99.94	71.27
RM17-211.47	112.7	mottled anorthosite	52.30	0.05	29.17	0.79	0.00	0.35	12.90	3.24	0.56	0.02	1.03	100.41	68.75
RM17-222.45	101.72	spotted anorthosite	51.85	0.06	29.28	0.76	0.00	0.43	13.29	2.90	0.41	0.02	0.65	99.65	71.69
RM17-232.27	92	norite	51.96	0.06	29.27	0.64	0.00	0.50	13.00	3.04	0.49	0.03	0.69	99.68	70.27
RM17-250.11	74.06	spotted anorthosite	52.55	0.06	29.44	0.53	0.00	0.29	12.95	3.04	0.47	0.04	0.50	99.87	70.19
RM15 30.47	132.56	melanorite	52.56	0.11	29.25	0.47	0.01	0.19	12.83	3.18	0.46	0.06	0.50	99.62	69.04
RM15 31.61	131.42	norite	52.81	0.10	28.56	0.77	0.01	0.27	12.53	3.37	0.45	0.03	0.35	99.25	67.26
RM15 38.08	124.95	spotted anorthosite	51.48	0.10	29.29	1.16	0.01	0.23	12.90	3.37	0.42	0.06	0.42	99.44	67.90
RM15 44	119.03	spotted anorthosite	50.68	0.10	29.39	0.90	0.01	0.19	13.42	3.14	0.39	0.02	0.29	98.53	70.25
RM15 45.57	117.46	norite	53.36	0.11	29.00	0.49	0.01	0.28	13.00	3.30	0.41	0.04	0.33	100.33	68.52
RM15 45.72	117.31	norite	50.50	0.16	29.97	0.84	0.02	0.25	12.98	3.02	0.32	0.03	0.68	98.77	70.37
RM15 51.96	111.34	norite	51.48	0.10	30.27	0.48	0.02	0.27	13.32	3.10	0.34	0.04	0.40	99.82	70.37
RM15 59.35	103.68	mottled anorthosite	52.66	0.11	29.32	0.56	0.01	0.20	13.03	2.95	0.46	0.06	0.48	99.84	70.94
RM15 66.81	96.22	spotted anorthosite	50.90	0.10	29.64	0.87	0.01	0.28	13.75	3.03	0.38	0.03	0.77	99.76	71.49
RM15 74.18	88.85	spotted anorthosite	52.10	0.11	29.82	0.39	0.01	0.15	13.29	2.89	0.43	0.04	0.26	99.49	71.76
RM15 81.18	81.89	spotted anorthosite	52.22	0.10	28.81	1.15	0.02	0.45	12.59	3.27	0.29	0.07	0.44	99.41	68.03
RM15 89.83	73.24	spotted anorthosite	51.02	0.10	28.91	0.40	0.01	0.16	14.98	2.92	0.96	0.03	0.41	99.90	73.92
RM15 98.44	64.63	mottled anorthosite	50.55	0.09	28.73	0.60	0.01	0.25	14.15	2.58	0.64	0.07	1.07	98.74	75.19
RM15 105.04	57.99	mottled anorthosite	51.19	0.10	29.81	0.81	0.01	0.16	13.25	2.97	0.44	0.04	0.34	99.12	71.14
RM15 112.23	50.8	mottled anorthosite	50.98	0.09	30.71	0.79	0.01	0.16	13.80	2.90	0.34	0.04	0.25	100.07	72.45
RM15 119.88	43.15	mottled anorthosite	49.27	0.10	32.13	0.70	0.01	0.17	14.95	2.57	0.19	0.02	0.12	100.23	76.27
RM15 123.24	39.79	spotted anorthosite	48.94	0.09	31.28	0.42	0.01	0.20	14.85	2.37	0.16	0.02	0.25	98.59	77.59

RM15 125.52	37.51	spotted anorthosite	49.45	0.10	31.67	0.88	0.01	0.20	14.99	2.55	0.19	0.03	0.39	100.46	76.46
RM15 132.23	30.8	mottled anorthosite	49.13	0.11	31.12	0.47	0.01	0.22	14.97	2.47	0.18	0.03	0.34	99.05	77.01
RM15 140	23.03	mottled anorthosite	49.75	0.11	30.23	0.75	0.01	0.36	14.09	2.75	0.52	0.02	1.37	99.96	73.90
RM15 145.76	17.27	anorthosite	51.15	0.10	30.07	0.83	0.01	0.28	13.09	3.25	0.44	0.02	0.67	99.91	69.00
RM15 149.62	13.41	melanorite	48.56	0.10	31.26	0.95	0.02	0.70	14.91	2.49	0.12	0.03	0.55	99.69	76.79
RM15 151.53	11.5	melanorite	49.07	0.10	32.03	0.44	0.01	0.34	15.57	2.35	0.14	0.03	0.35	100.43	78.55
RM15 154.37	8.66	mottled anorthosite	48.31	0.09	32.14	0.66	0.01	0.15	15.37	2.26	0.14	0.03	0.29	99.45	78.98
RM15 160.09	2.75	mottled anorthosite	50.08	0.11	31.21	0.43	0.04	0.11	14.00	2.59	0.16	0.02	0.39	99.14	73.65
RM15 160.28	0.44	mottled anorthosite	48.27	0.09	32.10	0.37	0.01	0.22	15.07	2.27	0.18	0.02	0.29	98.89	74.92
RM15 162.95	0.08	pyroxenite	49.05	0.1	32.27	0.37	0.06	0.1	15.17	1.98	0.13	0.02	0.05	99.32	80.89
RM15 163.18	-0.15	leuconorite	48.66	0.11	31.83	0.82	0.01	0.42	15.32	2.39	0.14	0.01	0.26	99.97	77.98
RM15 169.1	-6.07	leuconorite	48.46	0.09	31.85	0.44	0.01	0.47	15.09	2.24	0.13	0.03	0.24	99.05	78.83
RM15 175.94	-12.91	mottled anorthosite	49.15	0.09	32.14	0.89	0.01	0.19	15.01	2.63	0.15	0.02	0.18	100.47	75.93
RM15 189.16	-26.13	mottled anorthosite	48.31	0.08	31.56	0.56	0.03	0.72	15.07	2.11	0.56	0.02	0.43	99.45	79.78
RM15 196.14	-33.11	norite	49.37	0.09	31.27	0.55	0.01	0.28	14.92	2.13	0.15	0.01	0.54	99.32	79.47
RM15 202.98	-39.95	norite	48.55	0.09	32.66	0.26	0.01	0.35	15.97	2.22	0.07	0.02	0.36	100.56	79.90
RM15 209.28	-46.25	norite	48.73	0.09	32.11	0.78	0.01	0.24	15.35	2.48	0.15	0.02	0.51	100.47	77.38
RM15 216.1	-53.07	norite	49.13	0.10	31.27	1.03	0.02	0.80	15.07	2.47	0.17	0.02	0.26	100.34	77.12
RM15 230.3	-67.27	norite	49.45	0.10	31.62	0.73	0.01	0.32	14.92	2.50	0.14	0.02	0.23	100.04	76.73
RM15 237.58	-74.55	norite	48.35	0.09	31.25	0.59	0.01	0.71	15.36	2.32	0.11	0.01	0.43	99.23	78.53
RM15 244.23	-81.2	norite	49.21	0.09	31.93	0.45	0.01	0.44	15.12	2.37	0.14	0.02	0.32	100.10	77.90
RM15 252.3	-89.27	norite	49.10	0.10	31.34	1.04	0.02	0.55	14.89	2.68	0.14	0.03	0.52	100.41	75.43
RM15 259.27	-96.24	norite	49.25	0.09	31.18	0.84	0.01	0.45	14.98	2.69	0.19	0.02	0.37	100.07	75.47
RM15 266	-102.97	norite	49.78	0.10	31.37	0.45	0.01	0.34	14.88	2.36	0.23	0.02	0.50	100.04	77.70
RM15 274.09	-111.06	mottled anorthosite	50.14	0.11	31.46	0.45	0.01	0.29	14.53	2.48	0.19	0.03	0.35	100.04	76.40
RM15 281.86	-118.83	norite	48.36	0.10	31.38	0.58	0.08	0.95	15.16	2.49	0.55	0.04	0.42	100.12	77.09
RM15 288.6	-125.57	norite	49.37	0.10	31.65	0.70	0.01	0.30	14.90	2.63	0.23	0.02	0.50	100.41	75.79
RM15 295.28	-132.25	norite	49.52	0.09	31.54	0.77	0.01	0.37	14.98	2.52	0.19	0.02	0.49	100.50	76.66
RM15 302.66	-139.63	norite	48.69	0.10	30.90	1.00	0.02	0.47	14.71	2.59	0.26	0.02	0.62	99.38	75.84
RM15 309.2	-146.17	norite	48.60	0.10	32.33	0.52	0.01	0.23	15.64	2.23	0.22	0.02	0.50	100.40	79.49
RM15 316.43	-153.4	mottled anorthosite	49.44	0.10	31.68	0.92	0.01	0.27	14.89	2.47	0.24	0.02	0.41	100.45	76.91
RM15 323	-159.97	mottled anorthosite	49.71	0.11	31.05	0.64	0.08	0.60	14.88	2.38	0.17	0.02	0.37	100.01	77.55
RM15 338	-174.97	pyroxenite	48.50	0.08	32.41	0.81	0.01	0.51	15.24	2.52	0.04	0.03	0.26	100.42	76.97
RM15 342.92	-179.89	pyroxenite	49.96	0.10	31.24	0.46	0.01	0.29	14.83	2.11	0.25	0.02	0.20	99.47	79.52

RM15 plagioclase separates trace element data

Sample Number	Height (m) relative to base of Merenksy pyroxenite	Lithology	Rb ppm	Sr ppm	Y ppm	Zr ppm	Nb ppm	Co ppm	Ni ppm	Cu ppm	Zn ppm	%TiO2	V ppm	Cr ppm	Ba ppm
RM15-1	387	gabbronorite	12	374	3	22	3	<6	<6	15	12	0.04	<12	12	128
RM15-2	396	gabbronorite	11	377	3	17	3	<6	<6	16	13	0.04	<12	14	117
RM15-3	441.87	gabbronorite	12	379	3	16	3	<6	8	10	14	0.04	<12	13	119
RM15-4	413.87	gabbronorite	10	377	3	17	3	<6	6	14	13	0.04	<12	14	120
RM15-5	448.15	gabbronorite	9	378	3	17	3	<6	<6	14	12	0.04	12	12	110
RM15-6a	364	gabbronorite	11	369	4	30	3	<6	6	12	13	0.04	<12	13	125
RM15-6b	364	gabbronorite	6	379	3	15	3	<6	6	12	11	0.04	<12	<12	97
RM17-75.95	248.22	norite	14	372	3	28	3	<6	6	21	16	0.04	<12	12	148
RM17-93.94	230.23	norite	11	375	3	22	3	<6	<6	12	13	0.04	<12	15	131
RM17-107.89	216.28	norite	14	386	3	17	4	<6	8	17	17	0.04	<12	17	117
RM17-124.53	199.64	norite	16	381	4	40	3	<6	9	29	16	0.04	<12	16	153
RM17-136.98	187.19	norite	14	393	4	26	3	<6	14	23	16	0.04	12	20	126
RM17-159.73	164.44	norite	9	371	3	23	3	<6	7	19	20	0.05	<12	18	123
RM17-164.10	160.07	norite	10	401	3	18	3	<6	13	19	15	0.05	<12	29	117
RM17-174.30	149.87	leuconorite	8	320	3	18	3	6	24	10	15	0.03	<12	37	77
RM17-185.92	138.25	norite	14	389	4	30	3	<6	<6	13	15	0.04	<12	12	147
RM17-200.19	123.98	leuconorite	15	384	4	24	4	<6	8	23	17	0.05	<12	16	139
RM17-211.47	112.7	mottled anorthosite	17	366	5	36	3	<6	<6	10	21	0.04	<12	<12	151
RM17-222.45	101.72	spotted anorthosite	12	385	4	24	3	<6	6	15	18	0.04	12	12	115
RM17-232.27	92	norite	12	386	3	31	3	<6	7	19	17	0.04	12	<12	136
RM17-250.11	74.06	spotted anorthosite	14	371	4	28	3	<6	<6	17	18	0.04	<12	<12	132
RM15 30.47	132.56	melanorite	12	394	<3	41	4	15	<9	20	20	0.06	<15	55	194
RM15 31.61	131.42	norite	10	391	<3	58	4	11	<9	25	20	0.05	<15	23	176
RM15 38.08	124.95	spotted anorthosite	11	389	<3	20	4	12	<9	25	21	0.05	<15	48	160
RM15 44	119.03	spotted anorthosite	7	396	<3	9	4	14	<9	15	19	0.05	<15	53	131
RM15 45.57	117.46	norite	8	397	<3	13	5	12	<9	26	19	0.13	18	42	147
RM15 45.72	117.31	norite	9	400	3	30	5	14	<9	18	18	0.05	<15	26	171
RM15 51.96	111.34	norite	7	408	<3	15	4	14	<9	28	19	0.05	<15	35	157
RM15 59.35	103.68	mottled anorthosite	13	380	4	68	4	13	<9	17	20	0.05	<15	32	153
RM15 66.81	96.22	spotted anorthosite	12	387	<3	16	4	13	<9	19	20	0.05	<15	25	152
RM15 74.18	88.85	spotted anorthosite	10	389	<3	22	4	14	9	19	20	0.05	<15	35	164
RM15 81.18	81.89	spotted anorthosite	9	388	<3	21	4	15	10	18	24	0.05	<15	21	121
RM15 89.83	73.24	spotted anorthosite	10	378	<3	19	4	15	<9	17	20	0.04	<15	67	184
RM15 98.44	64.63	mottled anorthosite	21	350	3	25	5	14	<9	13	22	0.05	<15	54	154
RM15 105.04	57.99	mottled anorthosite	11	385	<3	36	4	13	<9	25	21	0.04	<15	31	149
RM15 112.23	50.8	mottled anorthosite	11	379	<3	31	4	12	<9	22	21	0.04	<15	51	144
RM15 119.88	43.15	mottled anorthosite	5	379	<3	10	4	14	<9	16	18	0.03	<15	59	113
RM15 123.24	39.79	spotted anorthosite	6	374	<3	10	4	14	<9	18	16	0.04	<15	61	109

RM15 125.52	37.51	spotted anorthosite	6	428	<3	13	4	13	<9	15	17	0.05	<15	210	103
RM15 132.23	30.8	mottled anorthosite	6	461	<3	11	4	14	<9	8	16	0.06	<15	33	105
RM15 140	23.03	mottled anorthosite	17	462	<3	8	4	19	13	30	36	0.05	<15	31	150
RM15 145.76	17.27	anorthosite	17	441	<3	23	4	15	<9	18	18	0.06	<15	21	147
RM15 149.62	13.41	melanorite	4	454	<3	10	5	16	29	23	19	0.05	<15	81	100
RM15 151.53	11.5	melanorite	6	469	<3	9	5	16	9	17	16	0.05	<15	36	114
RM15 154.37	8.66	mottled anorthosite	5	406	<3	8	4	15	43	60	15	0.04	<15	29	93
RM15 160.09	2.75	mottled anorthosite	7	489	<3	8	<3	<9	24	48	13	0.04	<15	<9	116
RM15 160.28	0.44	mottled anorthosite	5	492	<3	6	<3	<9	22	80	13	0.04	<15	9	121
RM15 162.95	0.08	pyroxenite	7	464	<3	8	<3	<9	12	11	13	0.04	<15	<9	75
RM15 163.18	-0.15	leuconorite	7	466	<3	10	5	14	10	21	17	0.04	<15	47	98
RM15 169.1	-6.07	leuconorite	4	479	<3	8	4	11	15	19	16	0.04	<15	288	101
RM15 175.94	-12.91	mottled anorthosite	5	473	<3	9	4	13	<9	12	21	0.05	<15	26	102
RM15 182.58	-19.55	mottled anorthosite	6	471	<3	9	4	11	9	24	17	0.04	<15	110	76
RM15 189.16	-26.13	mottled anorthosite	10	455	<3	9	5	15	<9	10	17	0.04	<15	171	92
RM15 196.14	-33.11	norite	4	458	<3	10	4	15	13	15	17	0.04	<15	94	91
RM15 202.98	-39.95	norite	6	465	<3	10	5	15	9	14	16	0.04	<15	88	100
RM15 209.28	-46.25	norite	6	465	<3	9	4	15	<9	12	23	0.04	<15	71	103
RM15 216.1	-53.07	norite	8	461	<3	11	4	14	17	14	17	0.04	<15	149	110
RM15 230.3	-67.27	norite	4	471	<3	9	4	14	10	16	14	0.04	<15	52	110
RM15 237.58	-74.55	norite	6	463	<3	10	4	13	9	20	16	0.04	<15	61	111
RM15 244.23	-81.2	norite	4	469	<3	9	4	14	11	16	15	0.04	<15	264	107
RM15 252.3	-89.27	norite	4	474	<3	9	4	12	12	18	17	0.04	<15	64	110
RM15 259.27	-96.24	norite	7	486	<3	9	4	13	11	15	17	0.04	<15	40	120
RM15 266	-102.97	norite	7	468	<3	10	5	16	<9	12	15	0.04	<15	16	114
RM15 274.09	-111.06	mottled anorthosite	7	470	<3	11	5	14	11	18	17	0.06	<15	15	136
RM15 281.86	-118.83	norite	7	474	<3	9	4	15	9	16	15	0.05	<15	24	129
RM15 288.6	-125.57	norite	8	466	<3	10	4	13	<9	19	16	0.05	<15	25	119
RM15 295.28	-132.25	norite	7	463	<3	9	4	10	11	16	16	0.05	<15	47	126
RM15 302.66	-139.63	norite	9	475	<3	10	5	12	16	19	22	0.05	<15	270	124
RM15 309.2	-146.17	norite	6	462	<3	10	5	12	10	19	18	0.04	<15	40	108
RM15 316.43	-153.4	mottled anorthosite	8	460	<3	11	4	15	<9	14	18	0.05	<15	147	108
RM15 323	-159.97	mottled anorthosite	6	464	<3	10	4	15	9	19	18	0.05	<15	471	99
RM15 338	-174.97	pyroxenite	3	454	<3	8	4	14	14	19	16	0.03	<15	82	101
RM15 342.92	-179.89	pyroxenite	4	460	<3	7	4	13	11	20	15	0.03	<15	157	88

KV5854 plagioclase separates major element data

Sample number	Height (m) relative to base of Merensky pyroxenite	Lithology	%SiO_2	%TiO_2	%Al_2O_3	%Fe_2O_3	%MnO	%MgO	%CaO	%Na_2O	%K_2O	%P_2O_5	%LOI	Total	An#
KV 179.94	116.11	Norite	51.08	0.12	30.98	0.36	0.07	0.07	13.91	2.62	0.25	0.02	0.30	99.76	74.58
KV 185.73	110.32	mottled anorthosite	51.82	0.11	30.36	0.38	0.05	0.05	13.64	2.81	0.40	0.04	0.36	100.02	72.84
KV 188.93	107.12	mottled anorthosite	51.21	0.12	30.70	0.39	0.04	0.10	13.86	2.49	0.29	0.03	0.15	99.40	75.47
KV 192	104.05	mottled anorthosite	50.72	0.11	30.53	0.35	0.05	0.00	13.77	2.69	0.33	0.05	0.17	98.78	73.88
KV 196.89	99.16	mottled anorthosite	51.92	0.12	30.12	0.51	0.06	0.22	13.58	2.68	0.50	0.04	0.45	100.21	73.69
KV 198.23	97.82	Norite	52.43	0.12	30.30	0.41	0.07	0.15	13.39	2.71	0.45	0.04	0.09	100.17	73.19
KV 210.93	85.12	Norite	52.37	0.13	30.00	0.49	0.05	0.05	13.28	2.73	0.45	0.02	0.14	99.72	72.89
KV 213.28	82.77	mottled anorthosite	52.13	0.12	30.65	0.45	0.05	0.11	13.48	2.66	0.39	0.04	0.24	100.33	73.69
KV 229.36	66.69	mottled anorthosite	51.08	0.11	31.35	0.47	0.05	0.08	14.53	2.33	0.24	0.03	0.07	100.34	77.51
KV 242.74	53.31	mottled anorthosite	51.44	0.12	30.84	0.54	0.07	0.30	13.54	2.59	0.56	0.06	0.35	100.40	74.29
KV 250.53	45.52	mottled anorthosite	51.26	0.10	31.11	0.43	0.08	0.05	14.37	2.50	0.34	0.03	0.19	100.44	76.06
KV 254.9	41.15	spotted anorthosite	50.66	0.11	31.28	0.57	0.07	0.22	14.56	2.25	0.22	0.03	0.39	100.37	78.15
KV 255.07	40.98	mottled anorthosite	50.20	0.13	31.18	0.60	0.05	0.28	14.57	2.19	0.16	0.03	0.38	99.77	78.62
KV 282.88	13.17	norite	50.01	0.11	31.76	0.57	0.05	0.29	15.12	1.97	0.21	0.03	0.31	100.44	80.92
KV 283.99	12.06	mottled anorthosite	49.06	0.11	31.94	0.57	0.05	0.20	15.21	2.07	0.12	0.02	0.19	99.53	80.24
KV 289.22	6.83	mottled anorthosite	48.53	0.13	29.74	1.23	0.09	0.92	15.32	1.89	0.21	0.02	1.97	100.05	81.75
KV 291.71	4.34	norite	50.12	0.11	31.86	0.41	0.07	0.13	14.49	2.54	0.15	0.02	0.22	100.12	75.92
KV 296.4	-0.35	norite	49.75	0.11	31.21	0.74	0.07	0.70	14.81	2.21	0.13	0.02	0.78	100.53	78.74
KV 307.4	-11.35	norite	50.66	0.12	31.51	0.43	0.05	0.28	14.66	2.22	0.19	0.03	0.16	100.31	78.49
KV 327.69	-31.64	leuconorite	48.97	0.11	31.24	0.44	0.06	0.38	14.72	2.33	0.13	0.02	0.22	98.61	77.73
KV 335.56	-39.51	mottled anorthosite	48.78	0.11	31.48	0.42	0.06	0.16	14.93	2.15	0.11	0.02	0.33	98.57	79.33
KV 338.68	-42.63	norite	50.19	0.11	31.26	0.46	0.05	0.43	14.70	2.29	0.22	0.02	0.41	100.15	78.01
KV 352.53	-56.48	norite	50.09	0.11	31.40	0.41	0.05	0.39	15.20	2.21	0.14	0.03	0.13	100.16	79.17
KV 352.85	-56.8	melanorite	50.80	0.10	31.40	0.39	0.04	0.28	14.11	2.04	0.22	0.02	0.16	99.56	79.26
KV 353.24	-57.19	melanorite	51.51	0.09	30.90	0.38	0.05	0.30	13.90	1.94	0.18	0.03	0.14	99.42	79.84
KV 367.28	-71.23	melanorite	48.59	0.10	32.13	0.41	0.07	0.31	15.00	2.00	0.10	0.01	0.33	99.06	80.56
KV 378.9	-82.85	melanorite	50.44	0.11	30.98	0.53	0.07	0.42	14.16	2.10	0.15	0.05	0.20	99.20	78.84
KV 388.85	-92.8	melanorite	50.05	0.11	31.44	0.65	0.05	0.55	14.73	2.11	0.15	0.04	0.31	100.20	79.41
KV 404.41	-108.36	melanorite	50.42	0.11	31.24	0.51	0.05	0.45	14.79	2.19	0.15	0.04	0.36	100.32	78.87
KV 421.8	-125.75	norite	49.88	0.11	30.78	0.52	0.05	0.44	14.59	2.16	0.15	0.04	0.29	99.01	78.87
KV 428.94	-132.89	norite	50.14	0.12	31.99	0.42	0.08	0.27	14.75	2.13	0.14	0.03	0.27	100.33	79.28
KV 438.41	-142.36	norite	50.23	0.11	31.44	0.56	0.07	0.40	14.84	2.25	0.16	0.05	0.31	100.42	78.47
KV 448.43	-152.38	norite	50.24	0.12	31.72	0.63	0.05	0.54	14.36	2.07	0.19	0.04	0.47	100.43	79.31
KV 460.59	-164.54	norite	50.17	0.11	31.88	0.45	0.04	0.23	14.85	2.15	0.14	0.04	0.24	100.30	79.24
KV 468.41	-172.36	norite	50.46	0.12	31.18	0.65	0.04	0.47	15.01	2.01	0.22	0.03	0.39	100.57	80.49
KV 480.29	-184.24	norite	49.60	0.11	31.51	0.77	0.04	0.82	14.65	2.07	0.13	0.02	0.64	100.37	79.64
KV 487.78	-191.73	norite	47.53	0.12	28.61	1.20	0.07	1.33	14.00	2.03	0.76	0.03	3.55	99.22	79.21
KV 494.61	-198.56	mottled anorthosite	48.07	0.10	31.61	0.69	0.09	0.63	15.50	1.80	0.12	0.02	0.69	99.33	82.63
KV 502	-205.95	mottled anorthosite	49.21	0.12	31.43	0.70	0.11	0.62	15.38	1.98	0.26	0.02	0.44	100.27	81.11
KV 507	-210.95	norite	49.76	0.11	31.02	0.64	0.03	0.44	14.63	1.99	0.14	0.03	0.70	99.50	80.25

KV5854 plagioclase separates trace element data

Sample Number	Height (m) relative to base of Merenksy pyroxenite	Lithology	Rb ppm	Sr ppm	Y ppm	Zr ppm	Nb ppm	Co ppm	Ni ppm	Cu ppm	Zn ppm	%TiO2	V ppm	Cr ppm	Ba ppm
KV 179.94	116.11	norite	8	392	<3	8	<3	<9	<9	14	15	0.04	<15	<9	111
KV 185.73	110.32	mottled anorthosite	15	377	<3	22	<3	<9	<9	11	16	0.04	<15	<9	142
KV 188.93	107.12	mottled anorthosite	11	386	<3	17	<3	<9	10	16	13	0.04	<15	<9	117
KV 192	104.05	mottled anorthosite	10	389	<3	12	<3	<9	<9	14	15	0.04	<15	<9	112
KV 196.89	99.16	mottled anorthosite	17	386	<3	18	<3	<9	<9	14	15	0.04	<15	<9	143
KV 198.23	97.82	norite	11	391	<3	14	<3	<9	10	20	13	0.04	<15	<9	148
KV 210.93	85.12	norite	11	386	<3	22	<3	<9	11	20	16	0.04	<15	<9	150
KV 213.28	82.77	mottled anorthosite	13	383	<3	17	<3	<9	9	13	15	0.04	<15	<9	130
KV 229.36	66.69	mottled anorthosite	7	381	<3	12	<3	<9	9	13	16	0.03	<15	<9	76
KV 242.74	53.31	mottled anorthosite	13	376	<3	17	<3	<9	<9	13	16	0.04	<15	<9	133
KV 250.53	45.52	mottled anorthosite	11	381	<3	13	<3	<9	9	13	15	0.03	<15	<9	125
KV 254.9	41.15	spotted anorthosite	6	377	<3	12	<3	<9	15	10	14	0.04	<15	<9	77
KV 255.07	40.98	mottled anorthosite	6	380	<3	10	<3	<9	13	10	14	0.04	<15	<9	74
KV 282.88	13.17	norite	5	407	<3	7	<3	<9	20	58	12	0.03	<15	13	69
KV 283.99	12.06	mottled anorthosite	6	397	<3	7	<3	<9	11	23	14	0.03	<15	<9	72
KV 289.22	6.83	mottled anorthosite	10	426	<3	11	<3	<9	71	37	18	0.06	19	71	95
KV 291.71	4.34	norite	5	479	<3	6	<3	<9	23	81	16	0.04	<15	<9	97
KV 296.4	-0.35	norite	6	475	<3	7	<3	<9	17	11	12	0.03	<15	16	86
KV 307.4	-11.35	norite	6	470	<3	8	<3	<9	13	9	11	0.03	<15	21	70
KV 327.69	-31.64	leuconorite	6	472	<3	6	<3	<9	14	7	11	0.03	<15	15	72
KV 335.56	-39.51	mottled anorthosite	8	450	<3	7	<3	<9	<9	5	12	0.03	<15	<9	61
KV 338.68	-42.63	norite	5	449	<3	7	<3	<9	13	6	12	0.03	<15	11	74
KV 352.53	-56.48	norite	6	449	<3	7	<3	<9	14	5	10	0.03	<15	40	66
KV 352.85	-56.8	melanorite	6	459	<3	7	<3	<9	9	6	9	0.03	<15	10	71
KV 353.24	-57.19	melanorite	5	451	<3	5	<3	<9	9	6	11	0.03	<15	20	74
KV 367.28	-71.23	melanorite	6	466	<3	6	<3	<9	10	8	12	0.03	<15	13	77
KV 378.9	-82.85	melanorite	7	462	<3	8	<3	<9	10	8	12	0.04	<15	15	84
KV 388.85	-92.8	melanorite	7	454	<3	11	<3	<9	23	14	13	0.04	<15	41	91
KV 404.41	-108.36	melanorite	7	455	<3	8	<3	<9	18	13	12	0.04	<15	29	95
KV 421.8	-125.75	norite	7	457	<3	8	<3	<9	16	10	11	0.04	<15	32	92
KV 428.94	-132.89	norite	6	460	<3	6	<3	<9	13	10	13	0.04	<15	12	87
KV 438.41	-142.36	norite	5	450	3	10	<3	<9	20	14	14	0.04	<15	15	95

EG5 plagioclase separates major element data

Sample number	Height (m) relative to base of Merensky pyroxenite	Lithology	%SiO_2	%TiO_2	%Al_2O_3	%Fe_2O_3	%MnO	%MgO	%CaO	%Na_2O	%K_2O	%P_2O_5	%LOI	Total	An#
EG5 43.24	248.6	leuconorite	52.58	0.04	29.11	0.54	0.02	0.64	13.76	3.03	0.30	0.05	0.22	100.29	71.51
EG5 82.47	209.37	leuconorite	51.76	0.05	29.23	0.63	0.02	0.86	14.26	3.24	0.22	0.00	0.18	100.47	70.86
EG5 136.86	154.98	leuconorite	51.36	0.04	29.95	0.52	0.02	0.62	14.54	3.05	0.18	0.01	0.16	100.46	72.48
EG5 160.83	131.01	mottled anorthosite	51.77	0.05	29.57	0.58	0.02	0.60	14.15	3.17	0.23	0.04	0.28	100.47	71.15
EG5 172.34	119.5	norite	52.73	0.05	28.89	0.44	0.02	0.63	13.88	3.26	0.26	0.03	0.17	100.37	70.17
EG5 175.29	116.55	norite	52.19	0.05	30.18	0.50	0.02	0.58	14.64	3.11	0.18	0.02	-1.36	100.10	72.23
EG5 186.22	105.62	norite	49.57	0.05	30.88	0.61	0.02	0.80	15.86	2.33	0.12	0.00	0.33	100.59	79.00
EG5 186.58	105.26	norite	51.83	0.05	29.51	0.50	0.02	0.65	14.19	3.11	0.22	0.00	0.18	100.29	71.60
EG5 203.98	87.86	leuconorite	50.31	0.04	30.46	0.56	0.02	0.64	15.05	2.77	0.08	0.02	0.32	100.26	75.02
EG5 211.83	80.01	norite	45.40	0.03	29.29	0.56	0.02	0.64	15.57	2.16	0.00	0.01	6.67	100.37	79.93
EG5 224.35	67.49	norite	47.80	0.04	30.69	0.72	0.02	0.64	16.18	1.77	0.04	0.11	0.61	97.22	83.48
EG6 147	64.9	mottled anorthosite	51.92	0.05	29.48	0.62	0.02	0.59	14.23	2.96	0.32	0.03	0.20	100.42	72.65
EG6 162.84	49.06	mottled anorthosite	50.14	0.05	30.68	0.60	0.02	0.54	15.22	2.49	0.18	0.02	0.21	100.16	77.16
EG6 165.85	46.05	mottled anorthosite	49.82	0.05	30.63	0.62	0.02	0.75	15.42	2.49	0.13	0.01	0.26	100.22	77.39
EG5 174.75	37.15	mottled anorthosite	50.60	0.05	30.23	0.70	0.02	0.70	15.07	2.48	0.18	0.01	0.36	100.40	77.05
EG5 279.09	12.84	pyroxenite	47.62	0.04	32.26	0.58	0.02	0.52	16.85	2.05	0.02	0.04	0.36	100.38	81.96
EG5 279.25	12.59	mottled anorthosite	48.35	0.03	32.17	0.54	0.02	0.51	16.70	1.88	0.05	0.00	0.21	100.46	83.03
EG5 281.96	9.88	mottled anorthosite	47.71	0.05	32.35	0.54	0.02	0.46	17.15	1.81	0.03	0.00	0.23	100.38	83.96
EG5 282.98	8.86	pyroxenite	48.46	0.04	31.79	0.61	0.02	0.62	16.37	1.98	0.04	0.02	0.26	100.21	82.04
EG5 287.88	3.96	pyroxenite	49.88	0.04	30.55	0.51	0.02	0.72	15.05	2.79	0.10	0.07	0.68	100.43	74.88
EG5 288.29	3.55	pyroxenite	50.61	0.04	30.38	0.51	0.02	0.79	14.76	2.87	0.10	0.11	0.31	100.51	73.97
EG5 313.94	-22.1	melanorite	50.09	0.03	30.73	0.47	0.02	0.75	15.41	2.56	0.04	0.00	0.28	110.49	76.89
EG5 331.16	-39.32	norite	50.23	0.05	30.76	0.44	0.02	0.62	15.27	2.67	0.13	0.00	0.19	100.38	75.69
EG5 353.62	-61.78	norite	50.42	0.04	30.40	0.40	0.02	0.64	15.10	2.84	0.10	0.01	0.18	100.16	74.61
EG5 384.25	-92.66	norite	49.71	0.03	30.91	0.46	0.02	0.79	15.55	2.56	0.11	0.01	0.24	100.38	77.05
EG5 391.71	-99.87	norite	49.70	0.03	31.15	0.42	0.02	0.66	16.05	2.34	0.07	0.00	0.13	100.58	79.12
EG5 392.16	-100.32	norite	49.16	0.03	31.19	0.50	0.02	0.83	16.11	2.26	0.07	0.01	0.20	100.40	79.75
EG5 414.13	-122.29	norite	49.63	0.05	30.99	0.58	0.02	0.89	15.77	2.27	0.10	0.01	0.29	100.58	79.33
EG5 437.36	-145.52	norite	50.15	0.04	30.74	0.50	0.02	0.73	15.53	2.42	0.13	0.02	0.15	100.44	78.00
EG5 452.5	-160.66	norite	50.18	0.04	30.78	0.46	0.02	0.62	15.53	2.41	0.14	0.02	0.18	100.37	78.07
EG5 463.61	-171.77	norite	49.46	0.05	31.50	0.51	0.01	0.58	15.15	2.48	0.22	0.00	0.27	100.23	77.15
EG5 495.84	-204	norite	49.70	0.03	31.67	0.47	0.01	0.44	15.27	2.43	0.13	0.00	0.17	100.34	77.64
EG5 532.16	-240.32	norite	49.52	0.03	31.58	0.57	0.01	0.56	15.29	2.40	0.08	0.00	0.26	100.32	77.88
EG5 549.79	-257.95	norite	49.18	0.04	31.50	0.45	0.01	0.46	15.50	2.30	0.12	0.00	0.23	99.79	78.83
EG5 568.73	-276.89	mottled anorthosite	48.36	0.02	32.28	0.48	0.01	0.39	16.15	2.04	0.05	0.00	0.19	99.99	81.39
EG5 577.54	-285.7	pyroxenite	52.03	0.02	30.45	0.48	0.01	0.66	13.94	0.77	0.20	0.02	0.40	97.98	90.91

EG5 plagioclase separates trace element data

Sample Number	Height (m) relative to base of Merenksy pyroxenite	Lithology	Rb ppm	Sr ppm	Y ppm	Zr ppm	Nb ppm	Co ppm	Ni ppm	Cu ppm	Zn ppm	%TiO2	V ppm	Cr ppm	Ba ppm
EG5 43.24	248.6	leuconorite	6	373	3	17	3	<6	<6	10	14	0.04	<12	14	90
EG5 82.47	209.37	leuconorite	4	377	3	15	3	<6	12	12	13	0.04	<12	33	89
EG5 136.86	154.98	leuconorite	3	380	3	15	<3	<6	<6	8	13	0.03	<12	15	74
EG5 160.83	131.01	mottled anorthosite	5	388	3	17	3	<6	<6	6	13	0.03	<12	<12	78
EG5 172.34	119.5	norite	4	386	3	18	3	<6	<6	8	12	0.04	<12	12	100
EG5 175.29	116.55	norite	4	384	<3	14	3	<6	<6	<6	11	0.03	<12	<12	69
EG5 186.22	105.62	norite	5	404	3	15	4	<6	8	11	18	0.03	<12	27	68
EG5 186.58	105.26	norite	4	382	<3	16	3	<6	<6	<6	14	0.04	<12	18	72
EG5 203.98	87.86	leuconorite	4	400	3	14	3	<6	<6	<6	15	0.02	<12	12	61
EG5 211.83	80.01	norite	3	445	3	14	<3	<6	<6	<6	18	0.02	<12	<12	63
EG5 224.35	67.49	norite	3	485	3	15	3	<6	<6	<6	18	0.02	<12	<12	63
EG6 147	64.9	mottled anorthosite	7	386	3	22	3	<6	<6	8	16	0.03	<12	<12	107
EG6 162.84	49.06	mottled anorthosite	5	379	3	17	3	<6	<6	7	15	0.03	<12	<12	77
EG6 165.85	46.05	mottled anorthosite	4	380	3	16	3	<6	<6	6	15	0.03	<12	<12	60
EG5 174.75	37.15	mottled anorthosite	4	381	<3	14	3	<6	<6	<6	14	0.03	<12	<12	47
EG5 279.09	12.84	pyroxenite	3	394	3	23	3	6	75	56	14	0.02	<12	22	50
EG5 279.25	12.59	mottled anorthosite	3	414	2	14	3	<6	<6	23	17	0.02	<12	<12	38
EG5 281.96	9.88	mottled anorthosite	3	395	3	14	3	<6	<6	15	14	0.02	<12	<12	43
EG5 282.98	8.86	pyroxenite	3	404	<3	13	<3	<6	<6	10	19	0.02	<12	20	56
EG5 287.88	3.96	pyroxenite	3	453	3	17	3	<6	<6	<6	7	0.02	<12	22	61
EG5 288.29	3.55	pyroxenite	<3	450	4	15	3	<6	<6	7	10	0.02	<12	25	73
EG5 313.94	-22.1	melanorite	3	454	3	13	3	<6	<6	<6	11	0.02	<12	39	32
EG5 331.16	-39.32	norite	3	453	<3	15	3	<6	<6	<6	14	0.02	<12	21	38
EG5 353.62	-61.78	norite	4	474	3	13	3	<6	<6	<6	10	0.02	<12	<12	50
EG5 384.25	-92.66	norite	3	448	3	14	3	<6	<6	<6	10	0.02	<12	22	70
EG5 391.71	-99.87	norite	3	466	<3	14	3	<6	<6	<6	13	0.02	<12	<12	50
EG5 392.16	-100.32	norite	3	462	<3	13	3	<6	7	<6	18	0.02	<12	34	42
EG5 414.13	-122.29	norite	4	449	<3	14	3	<6	7	6	11	0.03	<12	29	56
EG5 437.36	-145.52	norite	4	453	<3	14	3	<6	<6	6	14	0.03	<12	23	65
EG5 452.5	-160.66	norite	4	449	3	15	3	<6	<6	5	11	0.03	<12	19	74
EG5 463.61	-171.77	norite	4	450	3	14	3	<6	<6	<6	12	0.03	<12	39	61
EG5 495.84	-204	norite	4	460	<3	14	3	<6	<6	10	11	0.03	<12	31	75
EG5 532.16	-240.32	norite	4	450	3	14	<3	<6	13	10	11	0.03	<12	30	64
EG5 549.79	-257.95	norite	3	454	<3	13	3	<6	<6	<6	15	0.02	<12	18	37
EG5 568.73	-276.89	mottled anorthosite	4	457	3	13	3	<6	<6	9	13	0.02	<12	<12	32
EG5 577.54	-285.7	pyroxenite	<3	460	<3	23	3	<6	17	15	15	0.02	182	2240	123

KF35 plagioclase separates major element data

Sample number	Height (m) relative to base of Merensky pyroxenite	Lithology	%SiO_2	%TiO_2	%Al_2O_3	%Fe_2O_3	%MnO	%MgO	%CaO	%Na_2O	%K_2O	%P_2O_5	%LOI	Total	An#
KF35 72.06	477.64	Gabbronorite	52.09	0.05	30.22	0.44	0.01	0.41	13.73	3.08	0.24	0.00	0.18	100.46	71.13
KF35 118.41	431.29	Gabbronorite	53.10	0.06	28.05	0.61	0.02	1.29	13.64	3.07	0.35	0.06	0.23	100.49	71.06
KF35 188.97	360.73	Gabbronorite	51.29	0.05	28.28	0.55	0.02	1.25	14.28	2.87	0.31	0.05	0.33	99.30	73.33
KF35 223.77	325.93	Leuconorite	52.13	0.06	28.67	0.52	0.02	1.22	14.16	2.94	0.21	0.05	0.16	100.15	72.69
KF35 239.66	310.04	Norite	52.90	0.06	28.39	0.51	0.02	1.07	13.78	3.13	0.28	0.05	0.18	100.37	70.87
KF35 273.95	275.75	Norite	51.96	0.06	28.91	0.49	0.02	1.21	14.46	2.98	0.23	0.04	0.16	100.53	72.84
KF35 301.44	248.26	Norite	51.67	0.04	29.05	0.63	0.02	1.30	14.55	2.87	0.22	0.04	0.17	100.56	73.69
KF35 343.73	205.97	Norite	51.08	0.04	29.47	0.47	0.02	1.01	14.59	2.94	0.19	0.01	0.13	99.98	73.28
KF35 371.68	178.02	Norite	51.93	0.06	28.63	0.52	0.02	1.12	13.82	3.17	0.29	0.04	0.15	99.75	70.67
KF35 416.13	133.57	Norite	51.71	0.06	29.27	0.44	0.02	0.99	14.36	2.87	0.21	0.03	0.39	100.36	73.44
KF35 434.49	115.21	Norite	51.60	0.05	29.54	0.51	0.02	0.91	14.33	2.91	0.23	0.03	0.16	100.30	73.13
KF35 436.83	112.87	spotted anorthosite	51.46	0.06	29.69	0.38	0.02	0.95	14.82	2.71	0.17	0.01	0.15	100.42	75.14
KF35 455.20	94.5	Norite	51.98	0.05	29.16	0.51	0.02	0.98	14.11	3.10	0.24	0.02	0.24	100.41	71.55
KF35 503.96	45.74	Norite	51.04	0.05	30.13	0.40	0.02	0.77	14.82	2.84	0.18	0.01	0.19	100.46	74.25
KF35 526.82	12.88	mottled anorthosite	49.56	0.05	30.52	0.53	0.03	1.00	15.60	2.37	0.11	0.02	0.28	100.09	78.44
KF35 529.17	20.53	mottled anorthosite	49.95	0.06	29.53	1.20	0.03	1.63	15.17	2.52	0.09	0.00	0.20	100.40	76.89
KF35 542.25*	7.45	mottled anorthosite	48.67	0.1	31.32	0.68	0	0.68	15.78	2.23	0.17	0.06	0.12	99.81	79.63
KF35 573.55*	-23.85	Leuconorite	50.02	0.1	30.16	0.24	0	0.66	14.35	2.95	0.2	0.05	0.13	98.86	72.89
KF35 625.15*	-75.45	Norite	49.58	0.09	29.96	0.35	0	0.86	14.85	2.8	0.14	0.05	0.12	98.8	74.56
KF35 653.1*	-103.4	Norite	49.44	0.01	30.31	0.31	0	0.72	14.96	2.59	0.22	0.05	0.15	98.76	76.14
KF35 729.05*	-179.35	Norite	48.23	0.09	31.58	0.2	0	0.62	16.11	2.17	0.08	0.04	0.12	99.24	80.40
KF35 781.7*	-232	Norite	47.42	0.08	31.89	0.17	0	0.64	16.35	1.97	0.07	0.04	0.11	98.74	82.10
KF35 817.05*	-267.35	spotted anorthosite	47.9	0.09	31.5	0.23	0	0.58	16.04	2.24	0.11	0.04	0.14	98.87	79.83
KF35 838.69*	-288.99	mottled anorthosite	48.67	0.09	30.96	0.33	0	0.62	15.1	2.69	0.17	0.05	0.17	98.85	75.62
KF35 852.1*	-302.4	Melanorite	49.28	0.09	30.76	0.26	0	0.75	14.85	2.69	0.14	0.06	0.14	99.02	75.31

***** data from Blumberg (2002)

KF35 plagioclase separates trace element data

Sample Number	Height (m) relative to base of Merenksy pyroxenite	Lithology	Rb ppm	Sr ppm	Y ppm	Zr ppm	Nb ppm	Co ppm	Ni ppm	Cu ppm	Zn ppm	%TiO2	V ppm	Cr ppm	Ba ppm
KF35 72.06	477.64	Gabbronorite	5	382	<3	14	3	<6	<6	13	16	0.04	<12	13	93
KF35 118.41	431.29	Gabbronorite	6	376	3	16	3	<6	<6	9	19	0.04	<12	12	85
KF35 188.97	360.73	Gabbronorite	6	375	<3	16	3	<6	<6	7	13	0.04	<12	14	77
KF35 223.77	325.93	Leuconorite	4	379	<3	13	3	<6	<6	9	13	0.03	<12	<12	74
KF35 239.66	310.04	Norite	5	377	3	16	4	<6	<6	11	20	0.04	<12	<12	99
KF35 273.95	275.75	Norite	4	374	3	14	3	<6	<6	7	13	0.04	<12	31	76
KF35 301.44	248.26	Norite	4	381	<3	13	3	<6	<6	9	13	0.03	<12	18	67
KF35 343.73	205.97	Norite	4	383	3	14	3	<6	6	8	14	0.03	<12	16	77
KF35 371.68	178.02	Norite	4	387	<3	15	3	<6	<6	11	14	0.04	<12	15	86
KF35 416.13	133.57	Norite	5	386	3	14	3	<6	<6	10	16	0.04	<12	20	70
KF35 434.49	115.21	Norite	4	386	<3	14	3	<6	<6	10	14	0.04	13	<12	89
KF35 436.83	112.87	spotted anorthosite	4	381	<3	15	3	<6	<6	7	15	0.04	<12	15	66
KF35 455.20	94.5	Norite	6	387	3	14	3	<6	<6	9	13	0.04	<12	14	91
KF35 503.96	45.74	norite	4	385	3	15	3	<6	<6	<6	16	0.04	<12	<12	77
KF35 526.82	12.88	mottled anorthosite	4	366	3	14	3	<6	<6	<6	16	0.03	<12	<12	42
KF35 529.17	20.53	mottled anorthosite	4	369	3	15	3	<6	<6	<6	13	0.03	<12	<12	51
KF35 542.25*	7.45	mottled anorthosite	5	405	<3	<6	4	9	<9	<2	12	0.04	<15	<9	76
KF35 573.55*	-23.85	leuconorite	6	485	<3	<6	4	10	<9	<2	14	0.03	<15	14	76
KF35 625.15*	-75.45	norite	5	473	<3	<6	5	12	<9	<2	10	0.03	<15	61	65
KF35 653.1*	-103.4	norite	5	469	<3	<6	5	11	<9	<2	<9	0.03	<15	34	86
KF35 729.05*	-179.35	norite	6	480	<3	<6	4	10	<9	<2	<9	0.03	<15	16	54
KF35 781.7*	-232	norite	5	493	<3	<6	4	11	<9	<2	10	0.03	<15	<9	36
KF35 817.05*	-267.35	spotted anorthosite	5	467	<3	<6	4	11	<9	<2	9	0.04	<15	10	58
KF35 838.69*	-288.99	mottled anorthosite	5	474	<3	<6	4	11	<9	<2	13	0.04	<15	<9	57
KF35 852.1*	-302.4	melanorite	5	474	<3	<6	4	9	<9	<2	13	0.03	<15	35	79

* data from Blumberg (2002)

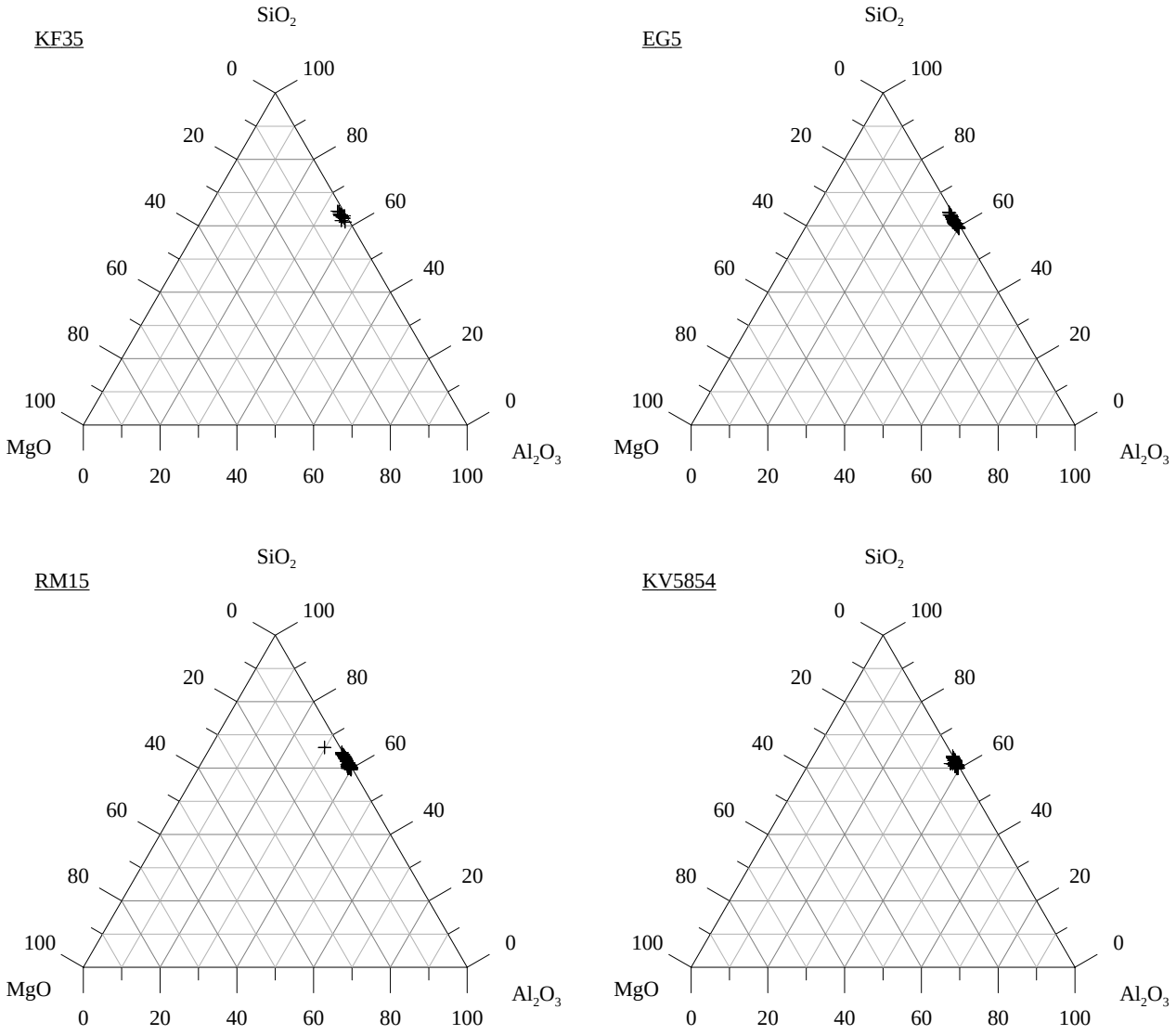


FIGURE Va.

Ternaray diagrams showing the compositional variation of the plagioclase separates from KF35, EG5, KV5854 and RM15. All samples plot at the expected composition for pure plagioclase, apart from one sample in RM15 with slightly elevated SiO_2. This sample may contain some quartz. When plotted against K2O instead of MgO, all samples plot in similar clusters, indicating that there is no orthoclase feldspar present.

APPENDIX VII

Sulphur content in the Merensky Reef, cores RM15 and KV5854

RM15

Sample number	Height (m) relative to base of Merensky pyroxenite	Lithology	wt% sulphur
RM15 160.09	2.94	mottled anorthosite	0.0968
RM15 160.28	2.75	mottled anorthosite	0.147
RM15 160.48	2.55	pyroxenite	0.887
RM15 160.68	2.35	pyroxenite	0.424
RM15 160.73	2.3	pyroxenite	0.372
RM15 160.83	2.2	pyroxenite	0.499
RM15 161.03	2	pyroxenite	1.8
RM15 161.22	1.81	pyroxenite	0.182
RM15 161.42	1.61	pyroxenite	0.00046
RM15 161.62	1.41	pyroxenite	0.0022
RM15 161.82	1.21	pyroxenite	0.00206
RM15 161.98	1.05	pyroxenite	0.00188
RM15 162.17	0.86	pyroxenite	0.0008
RM15 162.26	0.77	pyroxenite	0.00023
RM15 162.38	0.65	pyroxenite	0.0007
RM15 162.57	0.46	pyroxenite	0.00105
RM15 162.76	0.27	pyroxenite	0.263
RM15 162.98	0.05	pyroxenite	0.00026
RM15 163.18	-0.15	mottled anorthosite	0.00066

KV5854

Sample number	Height (m) relative to base of Meresnky pyroxenite	Lithology	wt% sulphur
KV5854 282.88	13.17	mottled anorthosite	0.00147
KV5854 283.99	12.06	mottled anorthosite	0.0181
KV5854 289.22	6.83	mottled anorthosite	0.00027
KV5854 291.71	4.34	mottled anorthosite	0.173
KV5854 292.25	3.8	pyroxenite	0.432
KV5854 292.44	3.61	pyroxenite	0.00103
KV5854 292.63	3.42	pyroxenite	0.00132
KV5854 292.82	3.23	pyroxenite	0.00184
KV5854 293.05	3	pyroxenite	0.208
KV5854 293.28	2.77	pyroxenite	0.00197
KV5854 293.5	2.55	pyroxenite	0.00186
KV5854 293.74	2.31	pyroxenite	0.00161
KV5854 293.94	2.11	pyroxenite	0.00034
KV5854 294.13	1.92	pyroxenite	0.000765
KV5854 294.35	1.7	pyroxenite	0.00359
KV5854 294.83	1.22	pyroxenite	0.00494
KV5854 295.05	1	pyroxenite	0.00069
KV5854 295.21	0.84	pyroxenite	0.00017
KV5854 295.36	0.69	pyroxenite	0.00016
KV5854 295.56	0.49	pyroxenite	0.00083
KV5854 295.75	0.3	pyroxenite	0.00079

Appendix VII
Representative CIPW norms for RM15

Relative to base of Merensky pyroxenite	Apatite	Illmenite	Ortho-clase	Albite	Anorthite	Corrun-dum	Magnetite	Enstatite	Ferrosillite	Diopside	Hede-bergite	Quartz	Forsterite	Fayalite	Total	total plag	total opx	total cpx
132.91	0.00	0.53	0.24	10.49	21.72	0.00	0.73	37.49	17.47	7.88	3.02	0.42	0.00	0.00	99.99	32.21	54.96	10.90
132.75	0.00	0.42	0.59	11.52	25.20	0.00	0.68	34.16	15.05	7.49	2.71	0.00	1.87	0.86	100.53	36.71	49.21	10.20
132.56	0.12	0.69	2.01	23.14	45.85	0.00	0.35	11.11	7.02	5.89	3.06	0.78	0.00	0.00	100.00	68.99	18.12	8.95
124.95	0.70	0.59	2.02	20.24	53.21	0.00	0.32	8.49	6.88	3.38	2.25	2.54	0.00	0.00	100.63	73.45	15.37	5.63
118.25	0.70	0.36	2.37	27.05	61.76	0.00	0.15	3.22	2.70	0.89	0.62	0.00	0.44	0.38	100.63	88.80	5.92	1.51
117.31	0.05	0.46	2.02	23.77	50.33	0.00	0.29	10.22	6.32	3.20	1.63	1.72	0.00	0.00	100.00	74.10	16.54	4.83
103.68	0.93	0.48	2.14	24.20	54.69	0.00	0.28	4.96	5.31	3.48	3.06	1.32	0.00	0.00	100.84	78.89	10.27	6.54
88.85	0.40	0.57	2.37	22.68	55.19	0.00	0.25	8.02	5.44	2.30	1.28	1.83	0.00	0.00	100.33	77.87	13.47	3.58
73.20	0.12	0.46	2.51	24.95	55.99	0.00	0.23	4.26	3.79	4.36	3.18	0.17	0.00	0.00	100.00	80.93	8.05	7.54
43.15	0.12	0.46	3.31	18.53	61.10	0.00	0.23	3.50	3.98	3.50	3.27	2.01	0.00	0.00	100.00	79.63	7.47	6.76
37.51	0.02	0.30	0.77	20.01	71.92	0.28	0.98	2.34	2.32	0.00	0.00	1.94	0.00	0.00	100.88	91.92	4.66	0.00
23.03	0.00	0.37	2.18	21.06	63.11	0.00	0.18	2.06	1.45	4.23	2.46	0.00	1.67	1.23	100.00	84.18	3.51	6.69
16.13	0.09	0.42	0.00	5.98	23.20	0.00	0.64	47.64	16.18	3.07	0.86	1.91	0.00	0.00	100.00	29.18	63.82	3.93
11.50	0.02	0.31	0.06	13.53	44.88	0.00	0.39	27.54	9.71	2.61	0.76	0.16	0.00	0.00	99.97	58.41	37.25	3.37
9.42	0.00	0.21	0.44	20.59	75.23	0.00	0.10	0.00	0.00	2.61	0.76	0.16	0.00	0.00	100.10	95.82	0.00	3.37
2.94	0.93	0.29	1.01	22.09	62.02	0.00	0.20	7.33	4.04	0.23	0.50	0.00	0.59	1.61	100.96	84.11	11.36	0.74
2.55	0.05	0.54	0.12	6.00	15.12	0.00	0.79	47.89	18.92	6.97	2.27	0.00	0.95	0.39	100.00	21.11	66.81	9.24
2.20	0.02	0.44	0.00	6.97	16.03	0.00	0.74	49.76	17.45	4.11	1.18	0.00	2.42	0.88	100.00	23.00	67.21	5.29
1.73	0.02	0.45	0.00	6.83	16.31	0.00	0.69	52.68	17.14	3.45	0.92	0.00	1.12	0.38	100.00	23.14	69.82	4.37
1.41	0.05	0.64	0.36	7.55	14.24	0.00	0.71	52.92	17.80	4.45	1.23	0.05	0.00	0.00	100.00	21.79	70.72	5.69
1.05	0.05	0.44	0.36	10.41	22.43	0.00	0.60	46.12	15.03	3.21	0.86	0.00	0.38	0.13	100.00	32.83	61.15	4.06
0.65	0.05	0.42	0.00	6.91	17.91	0.00	0.65	52.90	16.32	2.99	0.76	0.00	0.84	0.27	100.00	24.82	69.22	3.75
0.46	0.02	0.23	0.65	17.91	66.96	0.00	0.17	8.90	3.80	0.50	0.17	0.00	0.48	0.21	100.00	84.87	12.70	0.67
0.05	0.00	0.23	0.48	17.62	67.88	0.16	0.15	9.11	3.82	0.00	0.00	0.55	0.00	0.00	100.00	85.50	12.94	0.00
-6.07	0.02	0.27	0.53	16.48	58.30	0.00	0.23	16.52	5.53	1.13	0.31	0.00	0.51	0.18	100.00	74.77	22.05	1.44
-19.55	0.05	0.23	0.24	18.99	72.01	0.06	0.13	4.56	3.13	0.00	0.00	0.61	0.00	0.00	100.00	91.00	7.69	0.00
-39.95	0.02	0.30	0.06	11.36	41.26	0.00	0.40	33.32	9.80	1.77	0.43	0.00	0.97	0.30	100.00	52.63	43.12	2.20
-46.25	0.02	0.35	0.00	16.63	26.51	0.00	0.50	25.66	7.23	5.68	1.32	0.00	12.47	3.65	100.00	43.13	32.89	7.00
-53.07	0.00	0.27	0.36	16.63	55.11	0.00	0.27	16.78	5.73	2.04	0.57	0.00	1.66	0.59	100.00	71.74	22.51	2.61
-67.27	0.02	0.30	0.47	14.66	51.16	0.00	0.31	22.74	7.80	1.89	0.53	0.00	0.07	0.03	100.00	65.82	30.54	2.43

opx – orthopyroxene, cpx – clinopyroxene, plag - plagioclase